JPL Publication 91-8

An Atlas of Monthly Mean Distributions of GEOSAT Sea Surface Height, SSMI Surface Wind Speed, AVHRR/2 Sea Surface Temperature, and ECMWF Surface Wind Components During 1988

D. Halpern
V. Zlotnicki
J. Newman
Jet Propulsion Laboratory

O. Brown
University of Miami
Miami, Florida

F. Wentz
Remote Sensing Systems
Santa Rosa, California

February 1991

National Aeronautics and
Space Administration

Jet Propulsion Laboratory
California Institute of Technology
Pasadena, California

The research described in this publication was carried out, in part, by the Jet Propulsion Laboratory, California Institute of Technology, under a contract with the National Aeronautics and Space Administration.

FOREWORD

This report is an experimental version of a possible series of atlases of global oceanographic data products. Please communicate to Dr. D. Halpern (Earth and Space Sciences Division, Jet Propulsion Laboratory, Pasadena, CA 91109, U.S.A.; OMNET Telemail, D.HALPERN; Fax, 818-393-6720) any comments and suggestions you have to make the atlas more useful.

Data presented in Appendices A1, A4 and A8 are available as binary integer, direct access files on a single 6250-bpi magnetic tape produced on a Sun™-4 computer. To receive a tape copy, contact Dr. Halpern.

ACKNOWLEDGEMENTS

Many people contributed to the preparation of the data sets displayed in the atlas, and we thank them for their tremendous support. Brian Beckley (STX), Lee Fu (JPL), Akiko Hayashi (JPL), and Chester Koblinsky (GSFC) helped with the GEOSAT data. James Brown (RSMAS) and Joan Splain (RSMAS) participated in processing the MCSST data set. Paul McClain (NESDIS) and Guillermo Podesta (RSMAS) reviewed sections of the report. Elena Lobl (Hughes Aircraft) and Michael Cummings (GE Aerospace) provided photographs of the DMSP and NOAA spacecrafts. We are extremely grateful to NASA (NAWG-273 (OB), RTOP-578-22-26 (DH, JN), NAS8-38075 (FW), RTOP-578-22-25 (VZ), TOPEX Project (VZ)) and ONR (N00014-89-J-1144 (OB)) for their continued support of our research.

CONTENTS

ABSTRACT

The following monthly mean global distributions for 1988 are presented with a common color scale and geographical map: sea surface height variation estimated from the U.S. Navy geodetic satellite GEOSAT; surface wind speed estimated from the special sensor microwave imager (SSMI) on a U.S. Air Force Defense Meteorological Satellite Program (DMSP) spacecraft; sea surface temperature estimated from the advanced very high resolution radiometer (AVHRR/2) on U.S. National Oceanic and Administration (NOAA) spacecrafts; and the Cartesian components of the 10-m height wind vector computed by the European Center for Medium-Range Weather Forecasting (ECMWF). Charts of monthly mean value, sampling distribution, and standard deviation value are displayed. Annual mean distributions are displayed.

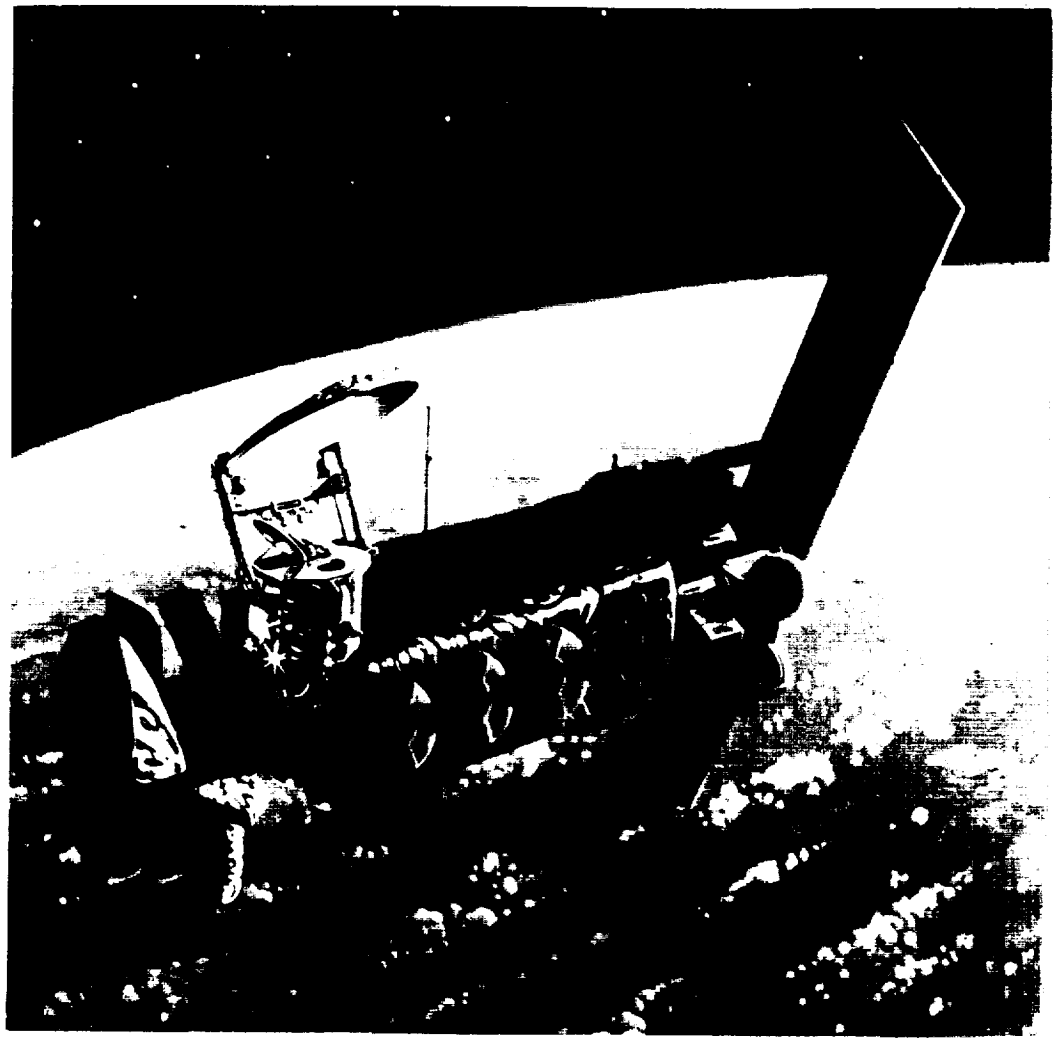

Plate 1. Defense Meteorological Satellite Program (DMSP) satellite with special sensor microwave imager (SSMI) located at the upper left. (Courtesy of Hughes Aircraft Company, Los Angeles.)

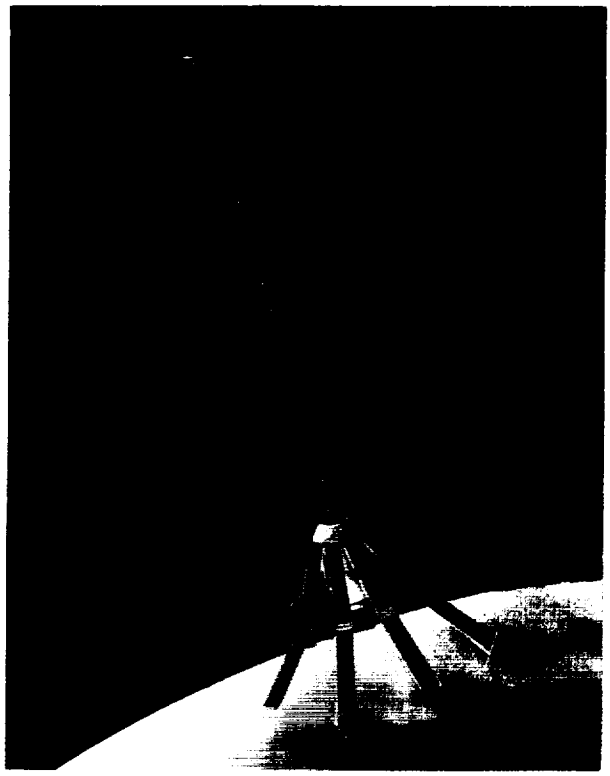

Plate 2. GEOSAT radar altimeter spacecraft. (Reproduced from Frain *et al.*, 1987.)

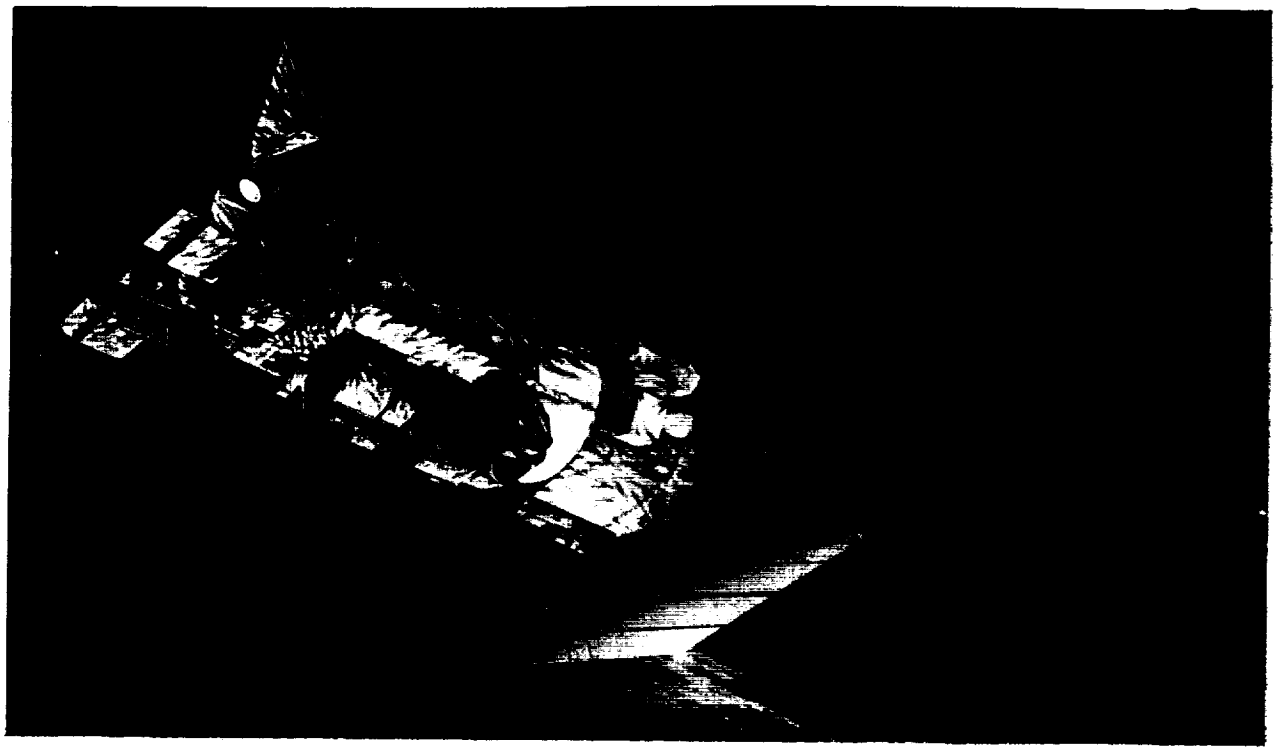

Plate 3. NOAA-9 or TIROS-I spacecraft. (Courtesy of GE Aerospace, Princeton.)

1 INTRODUCTION

Progress in climate research will depend on the availability of a variety of geophysical data sets to describe the boundary conditions and forcing functions of the climate system. The importance of long-period global data sets is highlighted in the U.S. National Aeronautics and Space Administration (NASA) Earth Observing System and the U.S. Committee on Earth Sciences Global Change Research Program. The unique perspective from space provides the opportunity for observations well suited for the global ocean, which is an essential component of the climatic system. Ocean circulation, ocean heat flux, ocean-atmosphere interactions, and ocean biogeochemical processes are considered prime subjects for immediate studies to understand the uncertainties associated with prediction of global change. All ocean science subjects require data to improve understanding of the ocean.

Stommel and Fieux (1978), in their guide to oceanographic atlases, stated that "the oceanographic atlas is one of the main tools of the oceanographer". Because of the scarcity of oceanographic data, very few atlases cover the world ocean, and none provide monthly mean distributions for a particular year. Several years of monthly mean data are necessary to analyze the seasonal cycle and interannual variations.

Since about ten years ago, substantial advances in remote and *in situ* techniques to record temperature, sea level, horizontal current and surface wind have helped oceanographers define annual cycles and interannual variations. Innovative ideas of how the ocean and atmosphere are coupled together occurred in parallel with new instrumentation. Three examples are El Niño Southern Oscillation (Philander, 1989), the ocean-atmosphere flux of carbon (Oeschger, 1988), and the relationship between global sea surface temperature and precipitation over Africa (Palmer, 1986). Monthly mean distributions of geophysical variables, which cover the globe or a large-scale region like an ocean basin, are becoming *de rigueur*.

Although both satellite- and ground-based recording systems provide essential information for global change studies, satellite-borne instrumentation yields unprecedented spatial and temporal coverage of the global ocean. This report contains monthly mean distributions of satellite measurements of surface wind speed, sea surface temperature, and sea surface height variation from January to December 1988. The year 1988 was chosen because it is the first occasion when an annual cycle of simultaneous satellite observations of these variables was recorded.

The report displays observations from three different satellites, each operated by a different agency. Very little averaging or interpolation of the data was made to retain the fundamental sampling characteristics of each data set. Deficiencies of current remote sensing systems are easily seen in maps of data sampling density, which should be especially interesting to developers of new and innovative satellite-borne instrumentation.

The report also displays surface wind vector components, which were computed by a numerical forecast-analysis system with assimilation of atmospheric observations.

2 DATA PROCESSING

2.1 GEOSAT Sea Surface Height

The U.S. Navy's *geo*detic *sat*ellite (GEOSAT) primary mission for improving the description of the geoid began shortly after its launch on 12 March 1985. On 1 October 1986 the spacecraft was maneuvered into an exact repeat orbit for oceanographic studies, now known as the Exact Repeat Mission (ERM). Each GEOSAT ERM orbit repeats within 1 km every 17.0505 days. The ground track separation at the equator is about 164 km. Global ERM data exists from 8 November 1986 until September 1989 when both tape recorders on GEOSAT ceased to operate; however, global data coverage was very poor after March 1989.

The GEOSAT sea surface height data set used in this report was prepared by V. Zlotnicki and is based on the Zlotnicki *et al.* (1990) data product, which is a resampled, edited and condensed version of the Cheney *et al.* (1987) geophysical data record (GDR).

The technique is complex to convert a radar altimeter's travel time measurement between the satellite and the sea surface into a meaningful estimate of the elevation of the sea surface relative to a reference surface, which becomes the oceanographic signal of interest. Numerous algorithms are involved (Cheney *et al.*, 1987; Chelton, 1988). No universal set of algorithms exists and the exact model functions and magnitudes are issues of current investigations.

2.1.1 Altimeter Measurement

Electronic noise of the GEOSAT altimeter is about 3 cm root-mean-square (rms). This is about one-half the noise of the SEASAT altimeter and about 10% of the GEOS-3 altimeter (Sailor and LeSchack, 1987).

The Cheney *et al.* (1987) GDR contains 10 altimeter height measurements per s and a 1-s averaged altimeter height value obtained by an iterative linear fit with outlier rejections. The 1-s averaged altimeter height measurement is here called H_{alt}. A H_{alt} value was deleted when the standard deviation of the 0.1-s altimeter heights was greater than 15 cm (2% rejected), or when it was not within 30 cm of the second degree polynomial fitted to the data 4 s before and after the time of H_{alt} (0.1% rejected), or when the location was on land (7.5% rejected) (Zlotnicki *et al.*, 1990). H_{alt}, which depends upon sea state, is representative of circular areas with diameters between 3 and 12 km. H_{alt} forms the basic data set for subsequent data processing.

2.1.2 Orbit Height

The satellite orbit height above the reference ellipsoid, H_{orbit}, in the Cheney *et al.* (1987) GDR had been supplied by the U.S. Navy Astronautics Group (NAG). The NAG orbit is based on the Goddard Space Flight Center's (GSFC's) Goddard Earth Model 10 (GEM-10) of the gravity field and on Doppler tracking observations of GEOSAT's position by the U.S. Navy's Operational Network (OPNET), which consists of three sites within the continental U.S. and one site in Hawaii. The NAG radial orbit error was about 2.2 m rms worldwide (Zlotnicki *et al.*, 1990), but 4.5 m systematic differences occurred at high latitudes with the 1984 world geodetic system reference frame (Shum *et al.*, 1990).

In this report we used a new H_{orbit} called GEM-T2. The GEM-T2 H_{orbit}, which was computed by GSFC's Space Geodesy Branch, combined the Marsh *et al.* (1989) GEM-T2 satellite-only gravitational model with Doppler tracking measurements of GEOSAT's position by the Defense Mapping Agency's (DMA's) 48-station Transit Network (TRANET). The preliminary radial orbit error of GEM-T2 H_{orbit} for GEOSAT is about 35 cm rms (Haines *et al.*, 1990).

2.1.3 Environmental Corrections

GEOSAT's altitude was approximately 800 km and the round-trip travel time of the radar altimeter electromagnetic pulse between the sea surface and the satellite is affected by atmospheric and ionospheric conditions. Also, ocean surface waves complicate the interpretation of the returned radar pulse. In addition, the sea surface height relative to the reference ellipsoid,

$$SSH = H_{orbit} - H_{alt},$$

is influenced by vertical displacements caused by earth tides, ocean tides, and the static response of the sea surface to atmospheric pressure load (*i. e.*, the inverse barometer effect). Atmospheric and ionospheric effects on travel time produce an apparent lowering of the sea surface height.

The largest environmental corrections affecting the altimeter pulse are the travel-time delays or path lengthening caused by air molecules within the troposphere (*i. e.*, dry troposphere correction, H_{dry}) and by water vapor within the troposphere (*i. e.*, wet troposphere correction, H_{wet}). The global average of H_{dry} is about 225 cm (Chelton, 1988); H_{wet} is about 15 cm (Monaldo, 1990). The geographical variability of H_{wet} is 5-45 cm with highest values in tropical regions (Emery *et al.*, 1990).

For H_{dry}, we used the Cheney *et al.* (1987) GDR values, $H_{dry\text{-}FNOC}$, which were computed from the surface atmospheric pressure, p_o, computed by the U.S. Navy's Fleet Numerical

Oceanography Center (FNOC) 12-hour, 2.5°-latitude x 2.5°-longitude global atmosphere general circulation model. A 4.4 hPa (or 4.4 mbar) uncertainty in p_o produces an error in H_{dry} of about 1.0 cm (Chelton, 1988).

H_{wet} was estimated from vertically integrated water vapor (also called precipitable water) measurements recorded globally at 25-km resolution since July 1987 by the special sensor microwave imager (SSMI) on board a polar-orbiting Defense Meteorological Satellite Program (DMSP) spacecraft. Thus, $H_{wet} = H_{wet\text{-}SSMI}$. The 1394-km wide swath scan of SSMI yielded global coverage in 3.5 days. The SSMI water vapor data set used herein was processed by Wentz (1989a) from a nonlinear combination of brightness temperatures or radiances measured at 22 and 37 GHz; the accuracy is about 3.0 kg m^{-2}. $H_{wet\text{-}SSMI}$ in cm was equal to the SSMI water vapor measurements in kg m^{-2} multiplied by 6.55×10^{-3} m^3 kg^{-1} (Wentz, 1988). Thus, a global estimate of the uncertainty of $H_{wet\text{-}SSMI}$ is about 2.0 cm.

$H_{wet\text{-}SSMI}$ is considered an improvement over the H_{wet} used by Cheney *et al.* (1987) and Zlotnicki *et al.* (1990), who used the values (called $H_{wet\text{-}FNOC}$) estimated from surface air temperature and surface water vapor pressure derived from the FNOC 2.5°-latitute x 2.5°-longitude atmospheric general circulation model at 12-hour intervals. $H_{wet\text{-}SSMI}$ was computed from total water vapor measured throughout the atmosphere, unlike $H_{wet\text{-}FNOC}$, which used only the water vapor at the surface predicted by the model with poor data coverage. The 25-km resolution of $H_{wet\text{-}SSMI}$ was one-tenth the spatial scale of $H_{wet\text{-}FNOC}$ and, consequently, provided more realistic estimates of H_{wet} in narrow regions of large atmospheric moisture, such as the Intertropical Convergence Zone. However, $H_{wet\text{-}SSMI}$ will continue to underestimate the true H_{wet} in narrow areas of high moisture. Of all corrections, H_{wet} is the most troublesome because its magnitude changes by about 10-15 cm over spatial scales which closely match mesoscale oceanographic phenomena (Emery *et al.*, 1990). Research on alternate methods to estimate integrated water vapor is an active subject (Lybanon and Crout, 1987; Emery *et al.*, 1990).

Free electrons in the ionosphere reduce the speed of the altimeter signal compared to the speed of light in a vacuum; the range correction caused by refraction from ionospheric electrons is denoted H_{ion}. On a typical orbit in 1986, H_{ion} varies from 1-2 cm over large latitudinal distances (Cheney *et al.*, 1987). This report uses H_{ion} values provided by Cheney *et al.* (1987) on the GDR, which were computed from Klobuchar's semiempirical ionospheric model (Musman *et al.*, 1990). H_{ion} has annual and interannual fluctuations. By June 1988 when the solar flux activity was two times greater than at the time of the beginning of the ERM, H_{ion} reached 7 cm (Cheney *et al.*, 1988) and continued to increase because of the 11-year sun spot cycle.

Ocean waves complicate the interpretation of the measurement of the 2-way travel time of the radar altimeter pulse. Sea state bias has three components which, to a first approximation, are proportional to local wave height. First, the corrugated sea surface degrades the returned pulse waveform so that the uncertainty in travel time produced by the onboard tracker's discrete digitization interval is about 0.7 cm (Chelton *et al.*, 1989); this correction is called $H_{tracker}$. Second, because an ocean wave signature is generally skewed with a flat trough and peaked crest, the returned power of the radar pulse is biased towards wave troughs. This error is called electromagnetic (em) bias, H_{em}, and is expressed as a percentage of significant wave height for Gaussian distributed heights. For this report, H_{em} = 1% of GEOSAT measurements of significant wave height, which are listed on the Cheney *et al.* (1987) GDR. The uncertainty of H_{em} could be two or even three times greater than the magnitude of H_{em} used herein (Chelton *et al.*, 1989; Walsh *et al.*, 1989; Zlotnicki *et al.*, 1989), and caution is advised in interpretation of sea surface height where ocean wave heights change by a large amount. No additional correction to H_{em} was made for wave age (Fu and Glazman, 1991). A third source of error caused by ocean waves is related to the non-Gaussian nature of the skewed sea surface height distribution, $H_{skewness}$. Estimates of $H_{skewness}$ are very uncertain and range from 20-100% of H_{em} (Chelton *et al.*, 1989). For this report, $H_{skewness} = 0$.

Tide corrections used in this report were provided on the GDR by Cheney *et al.* (1987). The solid-earth tide height, $H_{solid\ tide}$, was determined from the tide generating potential and its gradient over a 30-s interval along the groundtrack (Cartwright and Tayler, 1971). The ocean tide height at

the sea surface, $H_{ocean\ tide}$, was based on Schwiderski's (1980) 1°-latitude x 1°-longitude global gridded model of 11 tidal constituents.

The inverted barometer correction, $H_{barom\ pressure}$, produced by atmospheric pressure was not included in the Cheney *et al.* (1987) GDR. For this report, we used the Zlotnicki *et al.* (1990) values of $H_{barom\ pressure}$, which is defined by

$$H_{barom\ pressure} = -9.948\ (H_{dry\text{-}FNOC}/(-2.277)(1+(0.0026 \cdot \mathrm{Cos}(2 \cdot \mathrm{latitude})))-1013.3).$$

$H_{dry\text{-}FNOC}$ values were on the Cheney *et al.* (1987) GDR.

2.1.4 Corrected Sea Surface Height

The environmentally corrected GEOSAT sea surface height relative to the reference ellipsoid is defined by

$$SSH_{corrected} = H_{orbit} - H_{alt} - H_{solid\ tide} - H_{ocean\ tide} - H_{barom\ pressure} - H_{dry} - H_{wet} - H_{ion} - H_{em}$$

Table 1 summarizes the evolution of the corrections applied to the GEOSAT altimeter data.

2.1.5 Alongtrack Sea Surface Height Residual

Along each groundtrack, the $SSH_{corrected}$ values were resampled at fixed latitudes at about every 7 km using a cubic spline. No interpolation was made over a data gap larger than 3 s.

During each ERM year, the groundtrack was repeated approximately 22 times. For each series of 22 groundtracks, the groundtrack with the most resampled $SSH_{corrected}$ values was defined as a reference groundtrack and then $SSH_{corrected}$ differences or residuals, called SSH', were computed between the reference groundtrack and all other groundtracks within the series. This deleted a 25 m rms uncertainty caused by the geoid (Zlotnicki, 1991). The orbit error was further reduced from 35 cm rms (§2.1.2) to less than 5 cm rms by fitting a once per revolution (≈ 101 minutes) sine wave to resampled SSH'. The resampled, edited, environmentally corrected, GEOSAT residual sea surface heights are called SSH".

2.1.6 1/3° x 1/3° Gridded Monthly Data Set

An annual arithmetic mean SSH" value, <SSH">, was computed at each location where 11 or more SSH" values existed. SSH" values at sites where an annual mean had not been computed because of insufficient data were deleted from further data processing. The sea surface height variation relative to the annual mean, SSH"' = SSH" - <SSH">, was then computed. All SSH"' with positions occurring within nonoverlapping 1/3° x 1/3° squares were arithmetically averaged in 30.5-day intervals to form the basic monthly data set for this report. The origin of our global 1/3° x 1/3° grid is 90°N and 0° longitude.

Table 1
Heritage of GEOSAT sea surface height, $SSH_{corrected}$, described in this report.

Parameter	Cheney *et al.* (1987)	Zlotnicki *et al.* (1990)	This report
H_{orbit}	NAG/OPNET	NAG/OPNET	GEM-T2/TRANET
H_{alt}	outliers	§ 2.1.1 (this report)	§ 2.1.1
$H_{solid\ tide}$	Cartwright/Tayler	Cartwright/Tayler	Cartwright/Tayler
$H_{ocean\ tide}$	Schwiderski	Schwiderski	Schwiderski
$H_{barom\ pressure}$	none	FNOC p_o	FNOC p_o
H_{dry}	FNOC	FNOC	FNOC
H_{wet}	FNOC	FNOC	SSMI
H_{ion}	Klobucher	Klobucher	Klobucher
H_{em}	none	none	1% SWH
$H_{skewness}$	none	none	none

The data loss near the northern hemisphere continents is caused primarily by off-nadir spacecraft attitude angles greater than 1.1°. This situation is particularly severe when the GEOSAT spacecraft passes from land to water because the altimeter is unable to "lock on" to the return radar pulse (Cheney *et al.*, 1988).

2.1.7 Sea Surface Height Accuracy

The accuracy of satellite altimeter estimates of sea surface height depends very much on the data processing procedures (Cheney and Miller, 1990). The data contained in this report should be subjected to continuous ground-truth studies (Wyrtki and Mitchum, 1990).

2.2 SSMI Surface Wind Speed

The special sensor microwave imager (SSMI) is a 7-channel, 4-frequency, linearly polarized, passive microwave radiometer flown on the U.S. Air Force's Defense Meteorological Satellite Program (DMSP) F8 spacecraft in a circular sun-synchronous near-polar orbit at an altitude of approximately 860 km and an orbit period of 102.0 min. The orbit has an ascending (south-to-north) equatorial crossing at 0613 local time. This SSMI, which has provided data since July 1987, is the first of a series of about ten; the second SSMI was launched on a DMSP satellite in December 1990. The nearly 1400-km swath of SSMI produces complete coverage between 87°36'S to 87°36'N every 3 days. Each of the 7 separate passive radiometers measures naturally occurring microwave emissions from land, water and ice surfaces and from the intervening atmosphere. The SSMI receives both vertical and horizontal linearly polarized radiation at 19.3, 37.0 and 85.5 GHz and vertical only at 22.2 GHz.

2.2.1 Microwave Radiometer Measurement

The emitted microwave radiometer at the ocean surface is affected by roughness of the sea surface, which is correlated with the near-surface wind speed. Wentz (1989b) prepared the SSMI surface wind speed data product used in this report. Attenuation of 37 GHz radiation propagating from the sea surface to the satellite is very small, except when an appreciable amount of rain in the atmosphere scatters the 37 GHz radiation. The Wentz (1989b) algorithm relates wind speed (w, m s^{-1}) at 19.5 m height to the 37 GHz brightness temperatures, which are computed from the SSMI 37 GHz horizontal and vertical polarized radiance measurements, and to the radiative transfer and absorption between the sea surface and SSMI. The horizontal and vertical polarized (denoted by superscript "h" and "v" for horizontal and vertical, respectively) 37 GHz brightness temperatures (T_B^h, T_B^v) are defined by (Wentz, 1983)

$$T_B^h = T_{Bu} + \tau(E^h T_s + (1-E^h)(1+\omega^h w)(T_{Bd} + \tau T_{B\text{-cold}})) \quad (1a)$$

$$T_B^v = T_{Bu} + \tau(E^v T_s + (1-E^v)(1+\omega^v w)(T_{Bd} + \tau T_{B\text{-cold}})), \quad (1b)$$

where T_{Bu} is the upwelling brightness temperature (°K) caused by atmospheric emission and absorption, T_{Bd} is the downwelling brightness temperature (°K) produced by atmospheric emission and absorption, (E^h, E^v) are the emissivities of the sea surface for 37 GHz electromagnetic radiation, (ω^h, ω^v) are coefficients (Table 2) describing the intensities of electromagnetic radiation scattering at the sea surface, τ is atmospheric transmittance along the viewing path between the sea surface and SSMI, $T_{B\text{-cold}}$ is the 37 GHz cold brightness temperature of cosmic background radiation and equals 2.8 °K, and T_s is the sea surface temperature (°K).

The upward and downward atmospheric brightness temperatures for a non-scattering atmosphere are (Wentz, 1991)

$$T_{Bu} = (1 - \tau)(T_a - 14.6)$$

$$T_{Bd} = (1 - \tau)(T_a - 13.0),$$

where T_a is the surface air temperature (°K). Let the air temperature at the sea surface equal the sea surface temperature, *i. e.*, $T_a = T_s$, and let T_s be specified by Reynolds' (1982) climatological-mean monthly, 1°-latitude x 1°-longitude sea surface temperature analysis.

Sea surface emissivities (E^h, E^v) are given by

$$(E^h, E^v) = (E_o^h, E_o^h) + (\Delta E_o^h, \Delta E_o^h) + (b^h, b^v)[w\ (\theta - 49)],$$

where (E_o^h, E_o^v) are emissivities for a specular or perfectly flat sea surface, (ΔE_o^h, ΔE_o^v) account for changes in emissivities because of occurrences of surface roughness and foam, (b^h, b^v)[w (θ - 49)] account for changes in incidence angle θ of the SSMI radiometer, and (b^h, b^v) are wind-induced emissivity coefficients. Table 2 contains values of (b^h, b^v). Microwave radiation at frequencies above 10 GHz is only weakly sensitive to salinity changes (Maul, 1985), and the specular emissivity for an ocean surface of constant salinity of 35 PSU is (Wentz, 1991)

$$E_o^h = (s_o^h + s_1^h t + s_2^h t^2 + s_3^h t^3 + s_4^h u + s_5^h tu + s_6^h u^2 + s_7^h t^2 u)/T_s$$
$$E_o^v = (s_o^v + s_1^v t + s_2^v t^2 + s_3^v t^3 + s_4^v u + s_5^v tu + s_6^v u^2 + s_7^v t^2 u)/T_s$$

and

$$t = T_s - 273.16$$
$$u = \theta - 51.$$

Table 2 contains values of (s_i^h, s_i^v), where i = 0 to 7. The incidence angle is computed from the geometry of the DMSP/SSMI orbit. Wind-forced variations of emissivities are given by (Wentz *et al.*, 1986)

$$(\Delta E_o^h, \Delta E_o^v) = (m_1^h, m_1^v)\ w, \qquad \text{for } w \le 7 \text{ m s}^{-1},$$
$$(\Delta E_o^h, \Delta E_o^v) = (m_1^h, m_1^v)\ w + c^{-1}\ [(m_2^h, m_2^v) - (m_1^h, m_1^v)]\ (w - 7)^2, \qquad \text{for } 7 < w < 17 \text{ m s}^{-1},$$
$$(\Delta E_o^h, \Delta E_o^v) = (m_2^h, m_2^v)\ w - d\ [(m_2^h, m_2^v) - (m_1^h, m_1^v)], \qquad \text{for } w \ge 17 \text{ m s}^{-1}.$$

The constants c (= 20 m s^{-1}) and d (= 12 m s^{-1}) provide continuity between the segments of (ΔE_o^h, ΔE_o^v). The coefficients (m_1^h, m_1^v) and (m_2^h, m_2^v) are listed in Table 2.

The two unknowns, w and τ, in equations (1a) and (1b) are determined by Newton's iteration method. "First-guess" values for w and τ are 8 m s^{-1} and 0.8, respectively, which represent typical values over the ocean. Convergence is defined when the difference between successive iterations of w becomes less than 0.05 m s^{-1}. Convergence is usually found after 3 to 5

Table 2
Parameters used by Wentz (1989b) to calculate SSMI surface wind speed from 37 GHz horizontal and vertical polarized radiance measurements.

Symbol	Parameter	Unit	V-polarization	H-polarization
b	Wind-induced emissivity coefficient	s m^{-1} degree^{-1}	-1.193x10^{-4}	1.052x10^{-4}
m_1	Wind-induced emissivity coefficient	s m^{-1}	0.70x10^{-3}	4.10x10^{-3}
m_2	Wind-induced emissivity coefficient	s m^{-1}	2.50x10^{-3}	7.30x10^{-3}
ω	Surface scattering coefficient	s m^{-1}	3.52x10^{-3}	8.55x10^{-3}
s_1	Specular emissivity coefficient	none	-5.637x10^{-1}	-6.171x10^{-1}
s_2	Specular emissivity coefficient	°K^{-1}	1.481x10^{-2}	1.437x10^{-2}
s_3	Specular emissivity coefficient	°K^{-2}	-2.96x10^{-5}	-7.07x10^{-5}
s_4	Specular emissivity coefficient	°K degree^{-1}	2.123	-1.701
s_5	Specular emissivity coefficient	degree^{-1}	1.17x10^{-2}	0.55x10^{-2}
s_6	Specular emissivity coefficient	°K degree^{-2}	4.1x10^{-2}	-1.9x10^{-2}
s_7	Specular emissivity coefficient	°K^{-1} degree^{-1}	-0.71x10^{-4}	-1.27x10^{-4}

iterations. If convergence is not reached after 10 iterations, then the measured brightness temperatures (T_B^h, T_B^v) are considered erroneous or caused by heavy rain.

SSMI wind speeds referenced to 10-m height, which are equal to 94.3% of w (Wentz, 1989b), are used in this report.

2.2.2 Environmental Corrections

Environmental conditions reduce the amount of emitted radiation measured at the satellite. At 37 GHz, microwave emission from the ocean surface is masked by the emission and attenuation characteristics of rain. If the integrated liquid water content throughout the atmosphere is greater than 0.25 kg m^{-2}, then the Wentz (1989b) algorithm is considered invalid because there would be too much radiative scattering from water droplets. Brightness temperatures measured within about 100 km of land, which is defined with a geographical data base, are not used to estimate surface wind speed because the emissivity of land is very different than that of water. For the same reason, surface wind speed within 200 km of the climatological-mean monthly position of the ice edge was not used in this report.

2.2.3 1/3° x 1/3° Gridded Monthly Data Set

The Wentz (1989b) GDR contains wind speed values in nonoverlapping areas of 25 km x 25 km, which are arrayed across the 1394-km SSMI swath width. Geographical coordinates are provided at the center of each 25-km x 25-km region. All SSMI wind speeds within nonoverlapping 1/3° x 1/3° squares were arithmetically averaged to form the basic data set for this report. The origin of our global 1/3° x 1/3° grid is 90°N and 0° longitude.

The January 1988 data set began on 13 January because of a 40-day off-period to avoid possible damage of the SSMI by increased heating of the bearing and power transfer assembly (Hollinger *et al.*, 1990). During the winters of 1988 and 1989, the DMSP spacecraft solar arrays were repositioned so that the SSMI was not turned off.

Most of the 1/3° x 1/3° areas contained at least 50 SSMI wind speed values per month, or about 1-2 values per day. For each month, the standard deviation of daily averaged SSMI surface wind speeds was computed for 1/3° x 1/3° areas containing 10 or more daily values per month.

2.2.4 Surface Wind Speed Accuracy

The SSMI accuracy specification for wind speed retrievals under rain-free conditions is ± 2 m s^{-1} rms over the range 3-25 m s^{-1}. Wentz (1991) compared SSMI wind speeds presented in this report with a NOAA National Data Buoy Center moored buoy wind data set prepared by Goodberlet *et al.* (1990), and found differences of zero bias and 1.6 m s^{-1} rms. Model functions different than Wentz' (1989b) physically-based algorithm exist. The Environmental Research and Technology (ERT) algorithm for SSMI surface wind speed did not meet the accuracy specification (Goodberlet *et al.*, 1990). Bates' (1991) statistical algorithm with brightness temperatures from five SSMI channels had a 1.1 m s^{-1} bias and a 1.8 m s^{-1} rms difference with moored buoy wind measurements at four sites from 5° to 5°N along 165°E.

2.3 AVHRR/2 Sea Surface Temperature

The U.S. National Oceanic and Atmospheric Administration (NOAA) satellite platforms (called NOAA-j where j is an integer) are in sun-synchronous orbits at altitudes of 833 or 870 km with ascending equatorial crossings at 0730 or 1400 local time. Since the 1981 launch of NOAA-7, odd-numbered NOAA satellites have a five-channel advanced very high resolution radiometer, which is called AVHRR/2. (Even-numbered NOAA satellites have a four-channel advanced very high resolution radiometer, called AVHRR.) During 1988, NOAA-9 was

operational until 17 November and thereafter NOAA-11 was operational; both platforms had similar AVHRR/2 instruments.

The AVHRR/2 scan rate is 360 swaths per min with a total field of view of ± 55.4° from nadir and with an effective ground resolution of 1.1 km at nadir in five co-registered spectral bands. Two spectral channels are in the visible range (0.58-0.68 and 0.725-1.1 μm) and three in the infrared range (3.55-3.93 (*i. e.*, 3.7) μm, 10.3-11.3 (*i. e.*, 11) μm, 11.5-12.5 (*i. e.*, 12) μm).

2.3.1 Infrared Radiometer Measurement

Infrared radiation received by a satellite radiometer is determined primarily by the sea surface emissivity and temperature and by atmospheric transmittance. Infrared radiation emitted from the ocean surface at wavelengths of about 3.5-4.0 μm and 10-12.5 μm propagates virtually unattenuated through a dry atmosphere (Maul, 1985). In these spectral regions the ocean emissivity is approximately constant and close to unity, so that the amount of radiation emitted at the surface is proportional to the sea surface temperature. Only 30% of the emitted radiation at 10-12 μm is transmitted through a wet atmosphere with 5.5 cm precipitable water (Njoku, 1990).

Atmospheric absorption of emitted radiation at the AVHRR/2 infrared wavelengths is primarily by water vapor, which occurs in the lower levels of the atmosphere so that the atmosphere is perceived to be optically thin. The transmission of emitted radiation through the atmosphere differs for each AVHRR/2 wavelength so that the difference of satellite-measured radiances at two or more wavelengths is independent of atmospheric absorber concentration. For small cumulative amounts of water vapor in the atmosphere, a linear combination of AVHRR/2 infrared radiation measurements recorded at the satellite yields an estimate of sea surface temperature, which is known as multi-channel sea surface temperature (MCSST).

This report uses daytime MCSST data produced operationally by NOAA's National Environmental Satellite and Data Information Service (NESDIS). The procedure is described by McClain *et al.* (1985). The NOAA-9 daytime MCSST algorithm is (P. McClain, personal communication, 1991)

$$\text{MCSST (NOAA-9)} = 3.4317T_{11} - 2.5062T_{12} - 251.24,$$

where MCSST (NOAA-9) is the sea surface temperature in °C, and T_{11} and T_{12} are the brightness temperatures in °K computed from NOAA-9 radiance measurements at 11 μm (AVHRR/2 channel 4) and 12 μm (AVHRR/2 channel 5), respectively. The NOAA-11 daytime MCSST (°C) algorithm is (P. McClain, personal communication, 1991)

$$\text{MCSST (NOAA-11)} = 0.9712T_{11} + 2.0663\,(T_{11} - T_{12}) +$$
$$1.8983\,(T_{11} - T_{12})\,(\text{SEC}\,\alpha - 1) - 1.9790\,(\text{SEC}\,\alpha - 1) - 264.79,$$

where α is the satellite zenith angle. On 11 August 1988 the threshold for rejection of outliers was modified. The MCSST value was rejected if the difference between a MCSST value and a climatological-mean value was greater than 10°C; the previous threshold for blunders was 7°C (P. McClain, personal communication, 1991).

2.3.2 Environmental Corrections

Major sources of error are water vapor absorption in the lower atmosphere and aerosol absorption. Radiance measurements from only cloud-free areas are processed by NOAA into MCSSTs. Very conservative cloud tests, which involve various combinations of the visible and infrared AVHRR/2 data, detect clouds so that cloud-free MCSSTs are computed (McClain *et al.*, 1985); on a typical day, less than 2% of the maximum possible number of MCSSTs are retained.

2.3.3 1/3° x 1/3° Gridded 28-Day Data Set

The 1.1-km AVHRR/2 observations are available only within areas containing a downlink ground station to receive high-resolution data transmission. Global AVHRR/2 measurements have an effective ground resolution of 4 km. A computer on board the NOAA spacecraft generates an

average radiance for each channel from four 1.1-km elements within each nonoverlapping group of five consecutive 1.1-km measurements along a scan. The day-time MCSSTs archived on NESDIS global retrieval tapes represent the average sea surface temperatures within 8 km x 8 km areas, which would occur at 25-km intervals in a cloud-free environment. The 8-km x 8-km MCSSTs are mapped at the University of Miami's Rosenstiel School of Marine and Atmospheric Sciences (RSMAS) onto a cyclindrical equi-rectangular grid of 2048 (longitude) x 1024 (latitude) space-elements (Olson *et al.*, 1988). Dimension of each space-element is approximately 18 km x 18 km, and geographical coordinates are assigned to the center of the element. The origin of the grid is 90°N, 180°W. RSMAS produces MCSSTs averaged over 7 days. For this report, four consecutive 7-day values are arithmetically averaged to form 28-day mean MCSST values. The arithmetic mean of four 18-km x 18-km MCSSTs adjacent to each other in a 2-dimensional array was computed. The average MCSSTs of 4-element groups, which were independent of each other, represent a 1/3° x 1/3° gridded MCSST data set.

2.3.4 Sea Surface Temperature Accuracy

The coefficients used in the NOAA MCSST algorithm change only as the operational satellite is replaced and on rare occasions when the continuous validation procedure indicates a need for a change. NOAA continuously monitors the performance of the MCSST data product with satellite-tracked drifting buoy sea surface temperature measurements, which are recorded within 25 km and 4 h of the location of the MCSST. During 1988, the MCSST was 0.06°C less than the *in situ* data and the rms difference was 0.7°C for an average of 245 matchups per month throughout the global ocean (Table 3).

Table 3
Monthly mean bias and root-mean-square (rms) difference between day-time MCSST and drifting buoy sea surface temperature (DRIBU SST) global matchups during 1988.
Bias = DRIBU SST - MCSST.
(Courtesy of P. McClain, NOAA NESDIS)

Month	Number of Matchups	Bias °C	RMS Difference °C
Jan	283	0.28	0.70
Feb	213	0.16	0.57
Mar	129	0.08	0.62
Apr	222	-0.17	0.69
May	33	-0.05	0.86
Jun	203	-0.23	0.74
Jul	181	-0.28	0.64
Aug	260	-0.23	0.53
Sep	338	-0.17	0.62
Oct	357	-0.09	0.78
Nov	347	0.00	0.70
Dec	371	0.01	0.68

2.4 ECMWF Surface Wind Components

Month-to-month variations of upper ocean circulation are primarily caused by spatial and temporal changes in the surface wind vector: both east-west (u; positive eastward) and north-south (v; positive northward) wind components are important. To augment the SSMI scalar surface wind speed data (§2.2), this report contains the Cartesian components of the surface wind field

computed by the European Center for Medium-Range Weather Forecasting (ECMWF). The ECMWF forecast-analysis system, like all operational atmospheric general circulation models, is complex and continually being improved. During 1988, five changes (two in January; one in July, September and November) were made to the ECMWF analysis-forecast system (Hoskins *et al.*, 1989); the effect of these changes upon the surface wind is not known.

ECMWF analyses, instead of other model-generated results, are used in this report because they are considered superior. Kalnay *et al.* (1990) showed that ECMWF northern hemisphere daily 1000- and 500-hPa rms height errors of the 1-, 3-, and 5-day forecasts during August 1989 were slighly smaller than National Meteorological Center (NMC) results.

The area of each element of the ECMWF global 144-zonal x 73-meridional grid was approximately 2.5° x 2.5°. ECMWF forecast-analyses of surface wind components at 10-m height were issued twice a day, at 0000 and 1200 GMT. Wind speed, s, was computed at 12-h intervals: $s = (u^2 + v^2)^{1/2}$.

3 DATA PRESENTATION

All data are presented in the form of color-coded maps. To ease interpretation of features among different parameters, a common color code is used: blues represent low values, reds are high values, yellow and green are in the middle range, white means no data, and black represents land. Data are linearly scaled for color and an incremental color scale represents a contour interval. A single geographical scale is used for all maps. The land mask, which was prepared by O. Brown from the U.S. Central Intelligence Agency (CIA) World Data Base II, is the same throughout this report.

The color maps were generated on a Sun™-4 computer using IDL®, which prepared the PostScript® files. Each PostScript® file was transferred to an Apple Macintosh™ IIci then printed with PostScript® Dumper on a Tektronix™ Phaser CP Color Printer. All data values are retained in the PostScript® image files. The GEOSAT and SSMI images contain 1080 x 540 pixels (picture elements) and the AVHRR images contain 1024 x 512 pixels. All images are plotted on a 5.75-in x 2.875-in map. The PostScript® interpreter linearly transforms the size of each pixel within the user image file into a source-image coordinate system, which is compatible with the 300 dot-per-in resolution of the Tektronix™, to achieve the maximum rendition of the image within the specified dimensions (Adobe Systems, 1985).

4 REFERENCES

Adobe Systems, Inc. (1985) *PostScript® Language Reference Manual.* Addison-Wesley, 321 pp.

Bates, J.J. (1991) High frequency variability of SSMI-derived wind speed and moisture during an intraseasonal oscillation. *Journal of Geophysical Research, 96*, in press.

Cartwright, D.E., and R.J. Tayler (1971) New computations of the tide generating potential. *Geophysical Journal of the Royal Society, 23*, 45-74.

Chelton, D.B. (1988) WOCE/NASA altimeter algorithm workshop. U.S. WOCE Technical Report No. 2, U.S. Planning Office for WOCE, Texas A&M University, College Station, 70 pp.

Chelton, D.B., E.J. Walsh and J.L. MacArthur (1989) Pulse compression and sea level tracking in satellite altimetry. *Journal of Atmospheric and Oceanic Technology, 6*, 407-438.

Cheney, R.E., and L.L. Miller (1990) Recovery of the sea level signal in the western tropical Pacific from GEOSAT altimetry. *Journal of Geophysical Research, 95*, 2977-2984.

Cheney, R.E., B.C. Douglas, R.W. Agreen, L.L. Miller, D.L. Porter and N.S. Doyle (1987) GEOSAT altimeter geophysical data record user handbook. NOAA Technical Memorandum NOS-NGS-46, National Oceanic and Atmospheric Administration, U.S. Department of Commerce, Washington, 32 pp.

Cheney, R.E., B.C. Douglas, R.W. Agreen, L. Miller and N. Doyle (1988) The NOAA GEOSAT geophysical data records: Summary of the first year of the Exact Repeat Mission. NOAA Technical Memorandum NOS-NGS-48, National Oceanic and Atmospheric Administration, U.S. Department of Commerce, Washington, 20 pp.

Emery, W.J., G.H. Born, D.G. Baldwin and C.L. Norris (1990) Satellite-derived water vapor corrections for GEOSAT altimetry. *Journal of Geophysical Research, 95*, 2953-2964.

Frain, W.E., M.H. Barbagallo and R.J. Harvey (1987) The design and operation of GEOSAT. *Johns Hopkins APL Technical Digest, 8*, 184-189.

Fu, L.-L., and R. Glazman (1991) The effect of the degree of wave development on the sea-state bias in radar altimetry measurements. *Journal of Geophysical Research, 96*, 829-834.

Goodberlet, M.A., C.T. Swift and J.C. Wilkerson (1990) Ocean surface wind speed measurements of the special sensor microwave imager (SSMI). *IEEE Transactions on Geoscience and Remote Sensing, 28*, 823-828.

Haines, B.J., G.H. Born, G.W. Rosborough, J.G. Marsh and R.G. Williamson (1990) Precise orbit computation for the GEOSAT Exact Repeat Mission. *Journal of Geophysical Research, 95*, 2871-2885.

Hollinger, J.P., J.L. Pierce and G.A. Poe (1990) SSMI instrument evaluation. *IEEE Transactions on Geoscience and Remote Sensing, 28*, 781-790.

Hoskins, B.J, H.H. Hsu, I.N. James, M. Masutani, P.D. Sardeshmukh and G..H. White (1989) Diagnostics of the global atmospheric general circulation based on ECMWF analyses 1979-1989. WCRP-27, WMO/TD-No. 326, World Climate Research Program, World Meteorological Organization, Geneva, 217 pp.

Kalnay, E., M. Kanamitsu and W.E. Baker (1990) Global numerical weather prediction at the National Meteorological Center. *Bulletin of the American Meteorological Society, 71*, 1410-1428.

Lybanon, M., and R.L. Crout (1987) The NORDA GEOSAT ocean applications program. *Johns Hopkins APL Technical Digest, 8*, 212-218.

Marsh, J.G., F.J. Lerch *et al.* (1989) The GEM-T2 gravitational model. NASA Technical Memorandum 100746, Goddard Space Flight Center, Greenbelt, Maryland, 91 pp.

Maul, G.A. (1985) *Introduction to Satellite Oceanography*. Matinus Nijhoff, Dordrecht, 606 pp.

McClain, E.P., W.G. Pichel and C.C. Walton (1985) Comparative performance of AVHRR-based multichannel sea surface temperatures. *Journal of Geophysical Research, 90*, 11587-11601.

Monaldo, F. (1990) Path length variations caused by atmospheric water vapor and their effects on the measurement of mesoscale ocean circulation features by a radar altimeter. *Journal of Geophysical Research, 95*, 2923-2932.

Musman, S., A. Drew and B. Douglas (1990) Ionospheric effects on GEOSAT altimeter observations. *Journal of Geophysical Research, 95*, 2965-2967.

Njoku, E.G. (1990) Satellite remote sensing of sea surface temperature. In: *Surface Waves and Fluxes, II*, edited by G.L. Geernaert and W.J. Plant, Kluwer Academic, Dordrecht, 311-338.

Oeschger, H. (1988) The ocean system - ocean/climate and ocean/CO_2 interactions. In: *Scales and Global Change*, edited by T. Rosswall, R.G. Woodmansee and P.G. Risser, John Wiley & Sons, New York, 319-352.

Olson, D.B., G.P. Podesta, R.H. Evans and O.B. Brown (1988) Temporal variations in the separation of Brazil and Malvinas Currents. *Deep-Sea Research, 35*, 1971-1990.

Palmer, T.N. (1986) Influence of the Atlantic, Pacific and Indian Oceans on sahel rainfall. *Nature, 322*, 251-253.

Philander, S.G.H. (1989) *El Niño, La Niña, and the Southern Oscillation*. Academic Press, San Diego, 293 pp.

Reynolds, R.W. (1982) A monthly averaged climatology of sea surface temperature. NOAA Technical Report NWS 31, National Oceanic and Atmospheric Administration, Silver Springs, Maryland, 35 pp.

Sailor, R.V., and LeSchack (1987) Preliminary determination of the GEOSAT radar altimeter noise spectrum. *Johns Hopkins APL Technical Digest, 8*, 182-183.

Schwiderski, E.W. (1980) On charting global tides. *Reviews of Geophysics and Space Physics, 18*, 243-268.

Shum, C.K., D.N. Yuan, J.C. Ries, J.C. Smith, B.E. Shutz and B.D. Tapley (1990) Precision orbit determination for the GEOSAT exact repeat mission. *Journal of Geophysical Research, 95*, 2887-2898.

Stommel, H., and M. Fieux (1978) *Oceanographic Atlases*. Woods Hole Press, Woods Hole, Massachusetts, 6 pp + 97 charts.

Walsh, E.J., F.C. Jackson, E.A. Uliana and R.N. Swift (1989) Observations on electromagnetic bias in radar altimeter sea surface measurements. *Journal of Geophysical Research, 94*, 14575-14584.

Wentz, F. (1983) A model function for ocean microwave brightness temperatures. *Journal of Geophysical Research, 88*, 1892-1908.

Wentz, F.J. (1988) Water vapor path length correction for altimeters. In: Appendix to U.S. WOCE Technical Report No. 2, edited by D.B. Chelton, U.S. Planning Office for WOCE, Texas A&M University, College Station, 5 pp.

Wentz, F.J. (1989a) User's manual for the collocated GEOSAT SSMI tape. RSS Technical Report 100190, Remote Sensing Systems, Santa Rosa, California, 3 pp.

Wentz, F.J. (1989b) User's manual SSMI geophysical tapes. RSS Technical Report 060989, Remote Sensing Systems, Santa Rosa, California, 16 pp.

Wentz, F. (1991) Measurement of oceanic wind vector using satellite microwave radiometers. Submitted to *Journal of Geophysical Research.*

Wentz, F.J., L.A. Mattox and S. Peteherych (1986) New algorithms for microwave measurements of ocean winds: Applications to SEASAT and the special sensor microwave imager. *Journal of Geophysical Research, 91*, 2289-2307.

Wyrtki, K., and G. Mitchum (1990) Interannual differences of GEOSAT altimeter heights and sea level: The importance of a datum. *Journal of Geophysical Research, 95*, 2969-2975.

Zlotnicki, V. (1991) Sea level differences across the Gulf Stream and Kuroshio Extension. *Journal of Physical Oceanography, 21*, in press.

Zlotnicki, V., L.-L. Fu and W. Patzert (1989) Seasonal variability in global sea level observed with GEOSAT altimetry. *Journal of Geophysical Research, 94*, 17959-17969.

Zlotnicki, V., A. Hayashi and L.-L. Fu (1990) The JPL-Oceans-8902 version of GEOSAT altimetry data. JPL Internal Document D-6939, Jet Propulsion Laboratory, Pasadena, 17 pp + 60 charts.

Appendix A

Atlas of Monthly Mean Distributions

A1

Monthly Mean GEOSAT Sea Surface Height Variation

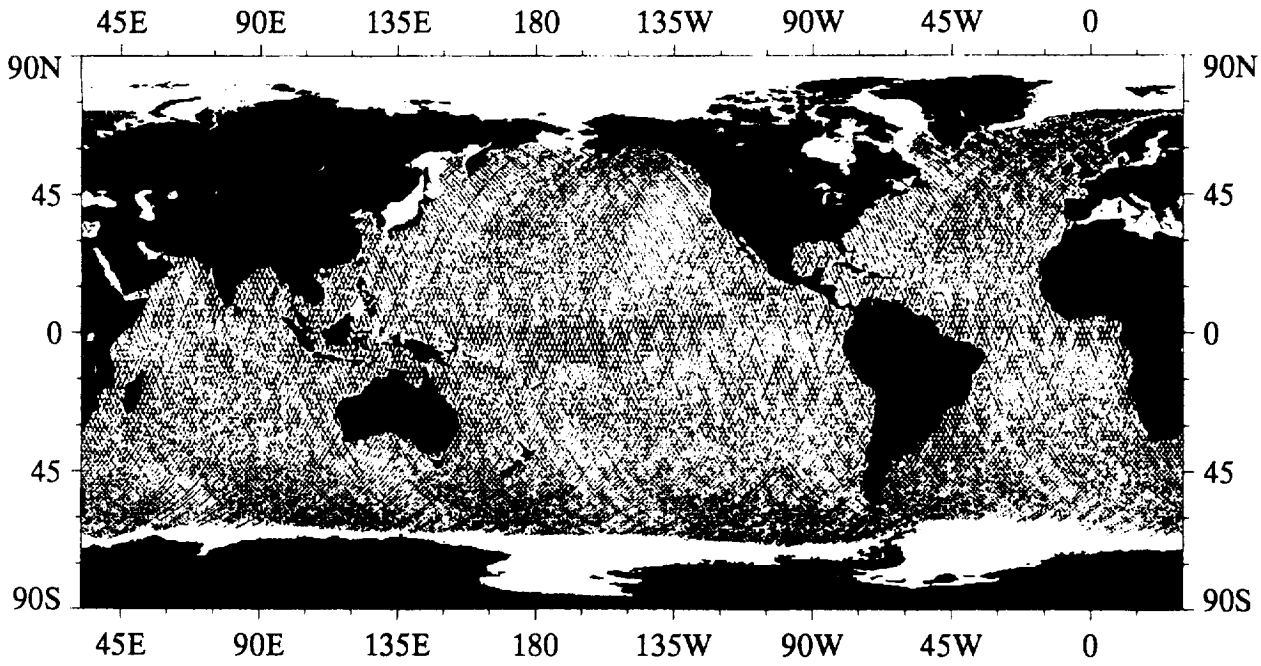

January 1988

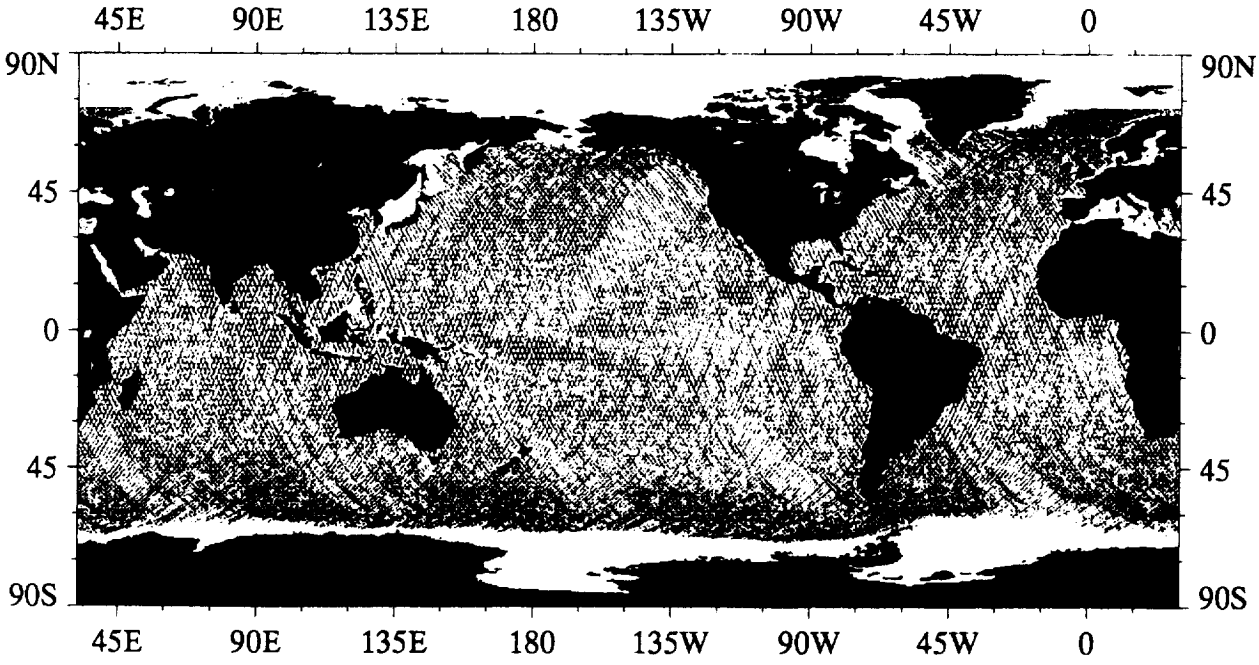

February 1988

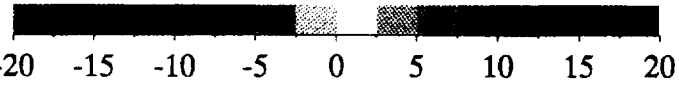

GEOSAT Sea Surface Height Variation Referenced to 1988 Mean, cm

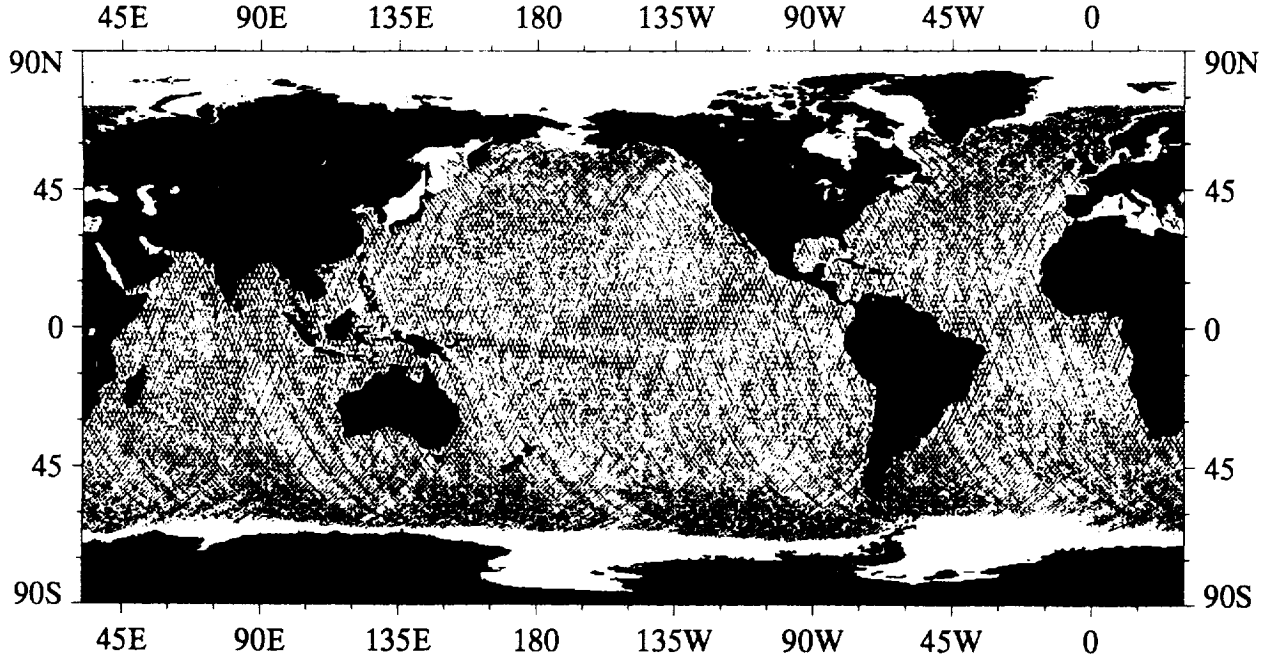

March 1988

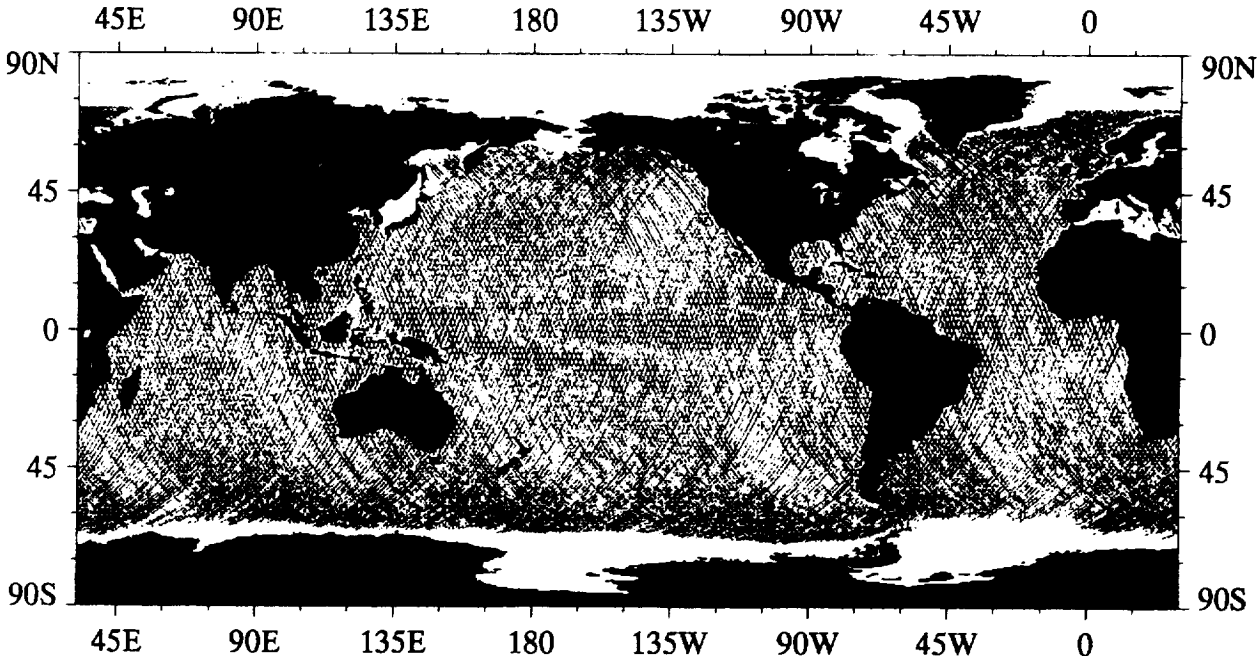

April 1988

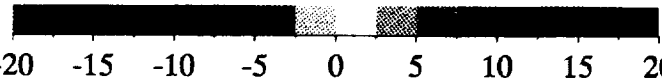

GEOSAT Sea Surface Height Variation Referenced to 1988 Mean, cm

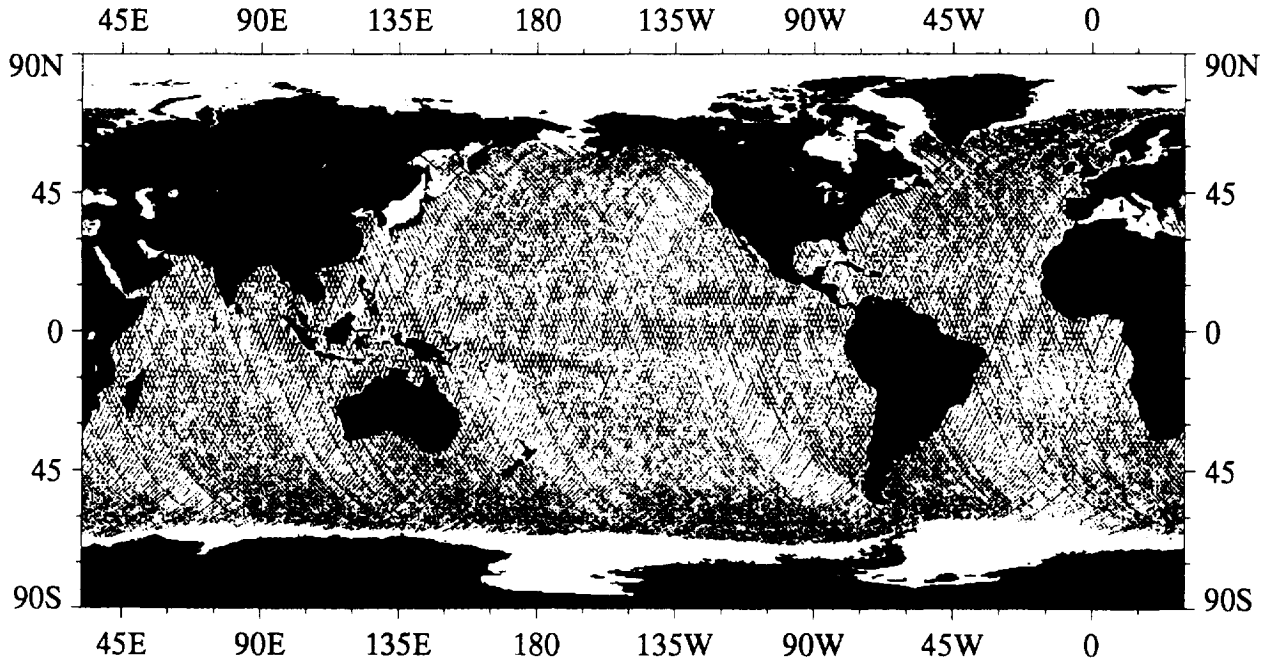

May 1988

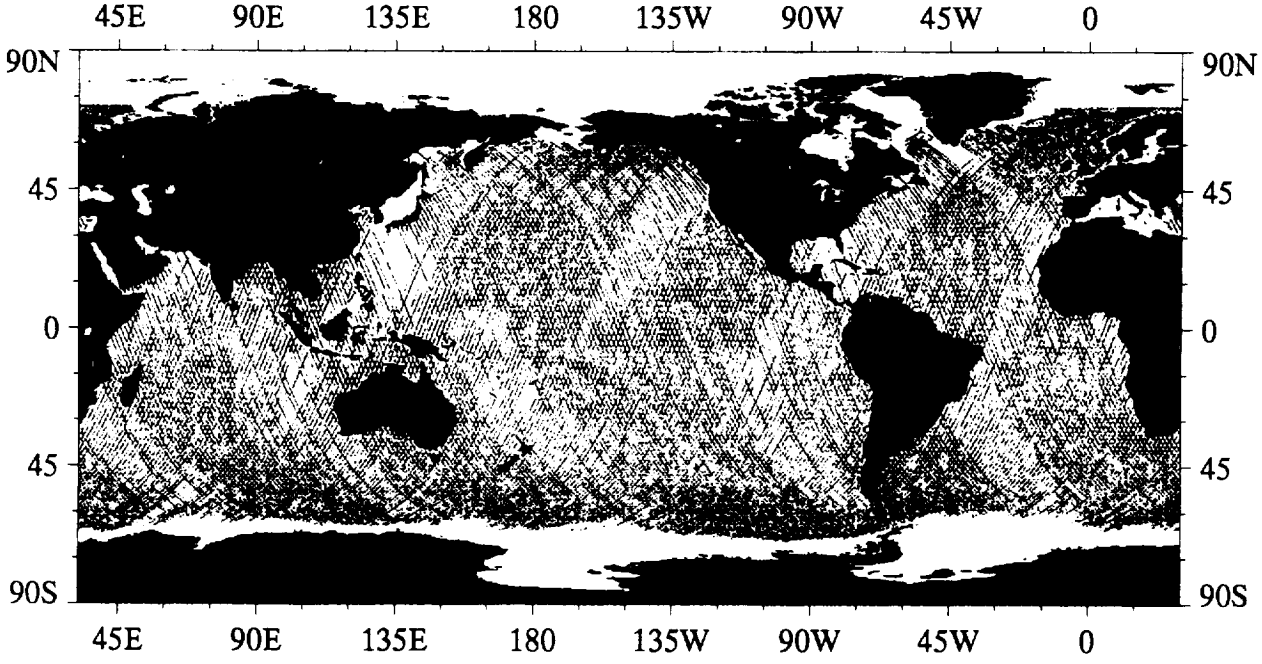

June 1988

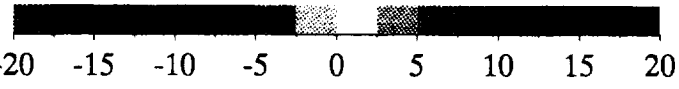

GEOSAT Sea Surface Height Variation Referenced to 1988 Mean, cm

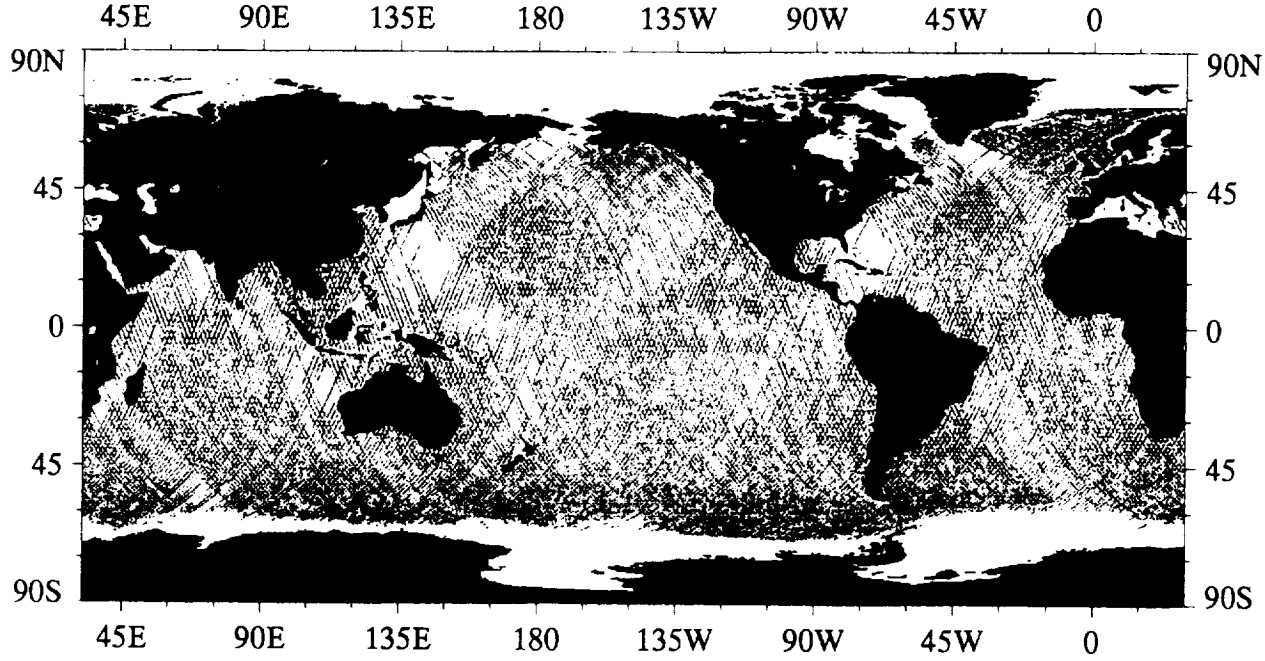

July 1988

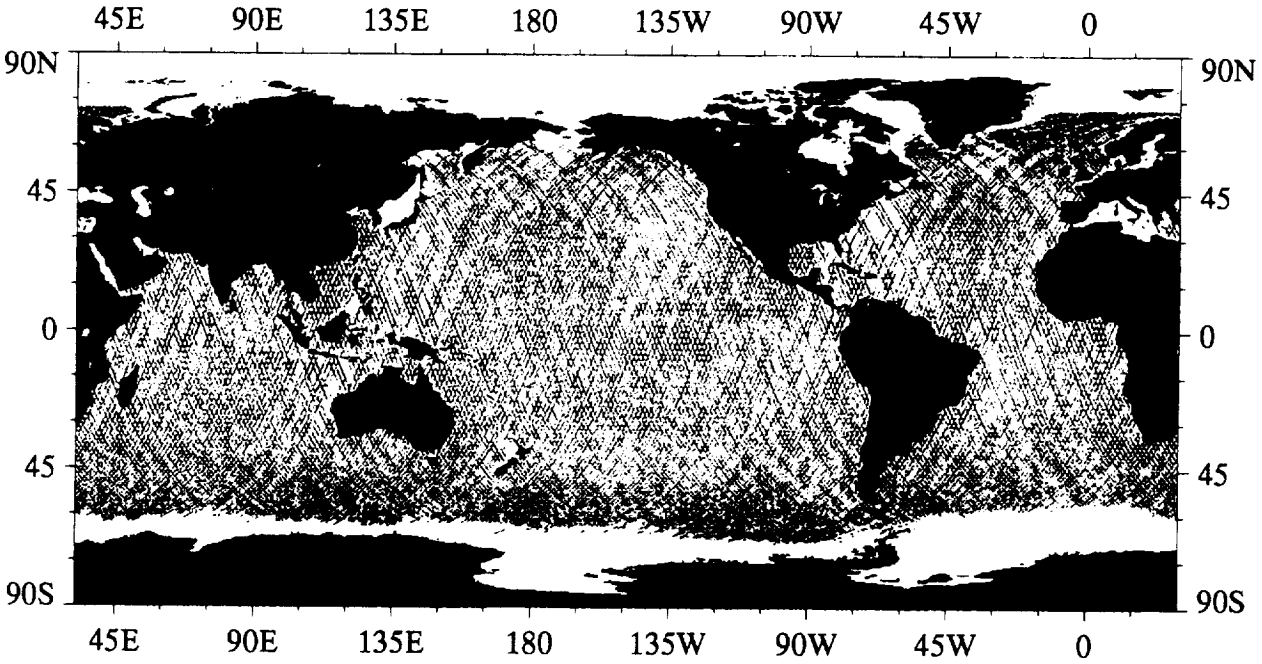

August 1988

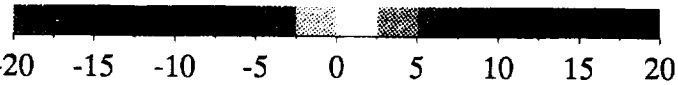

GEOSAT Sea Surface Height Variation Referenced to 1988 Mean, cm

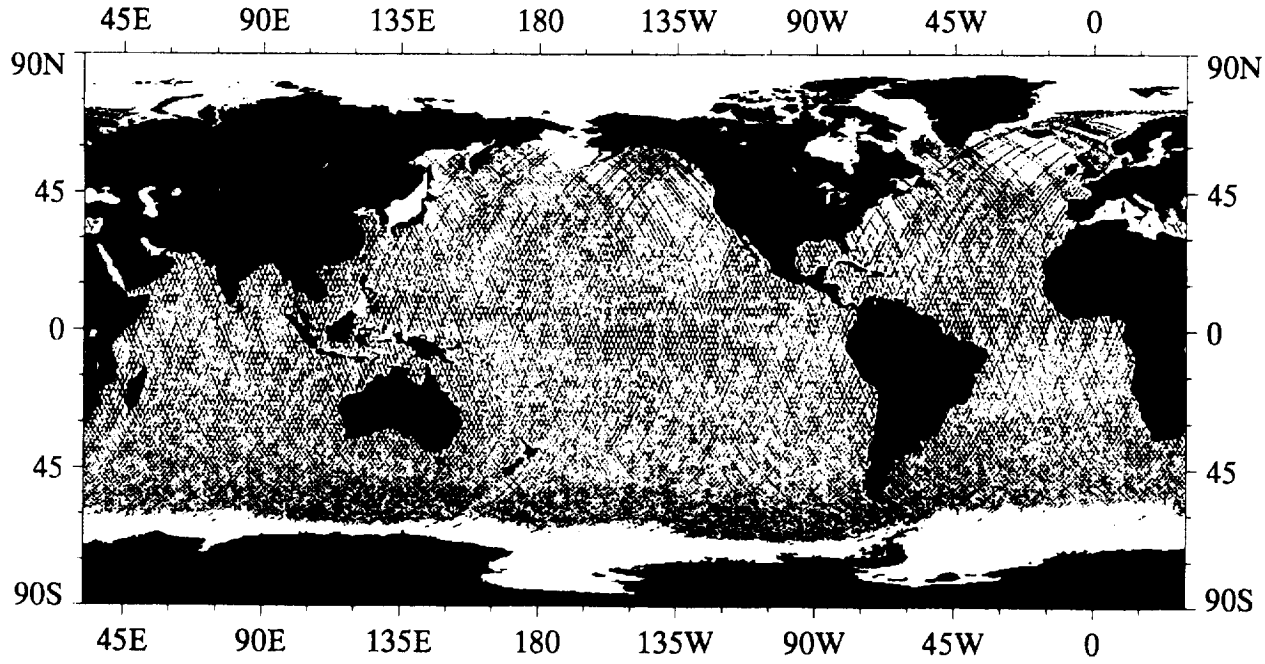

September 1988

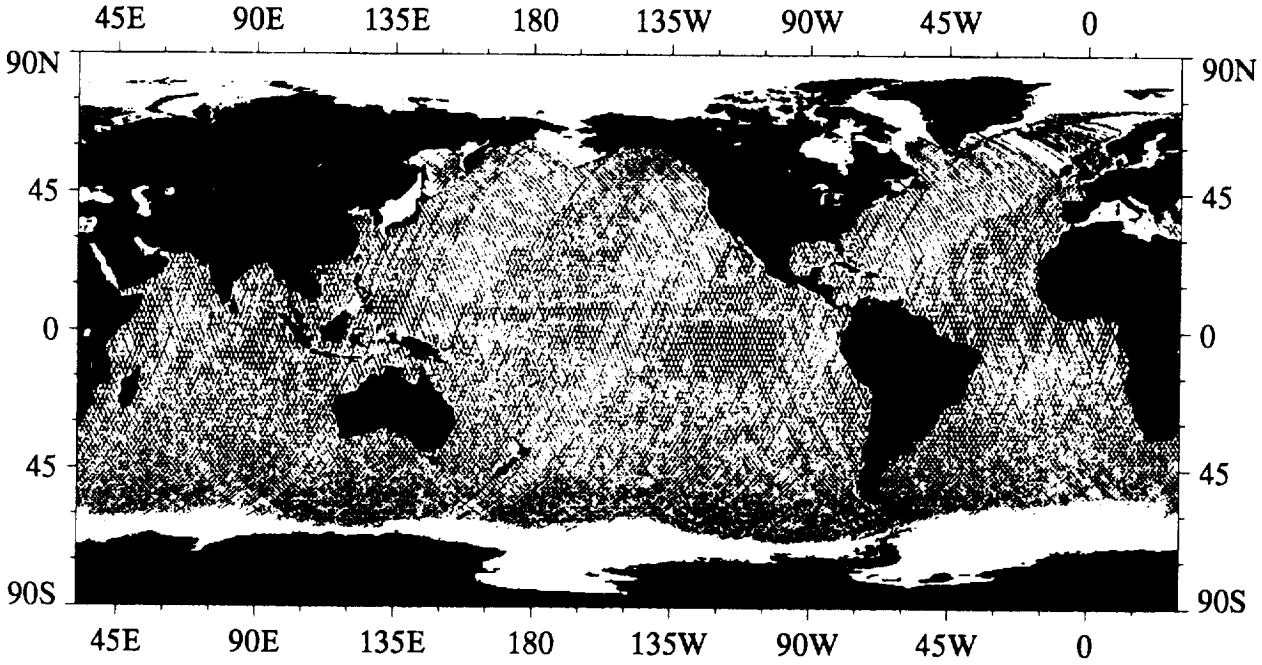

October 1988

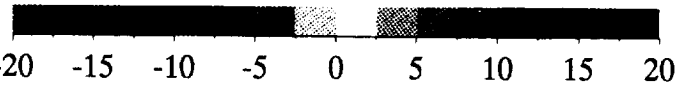

GEOSAT Sea Surface Height Variation Referenced to 1988 Mean, cm

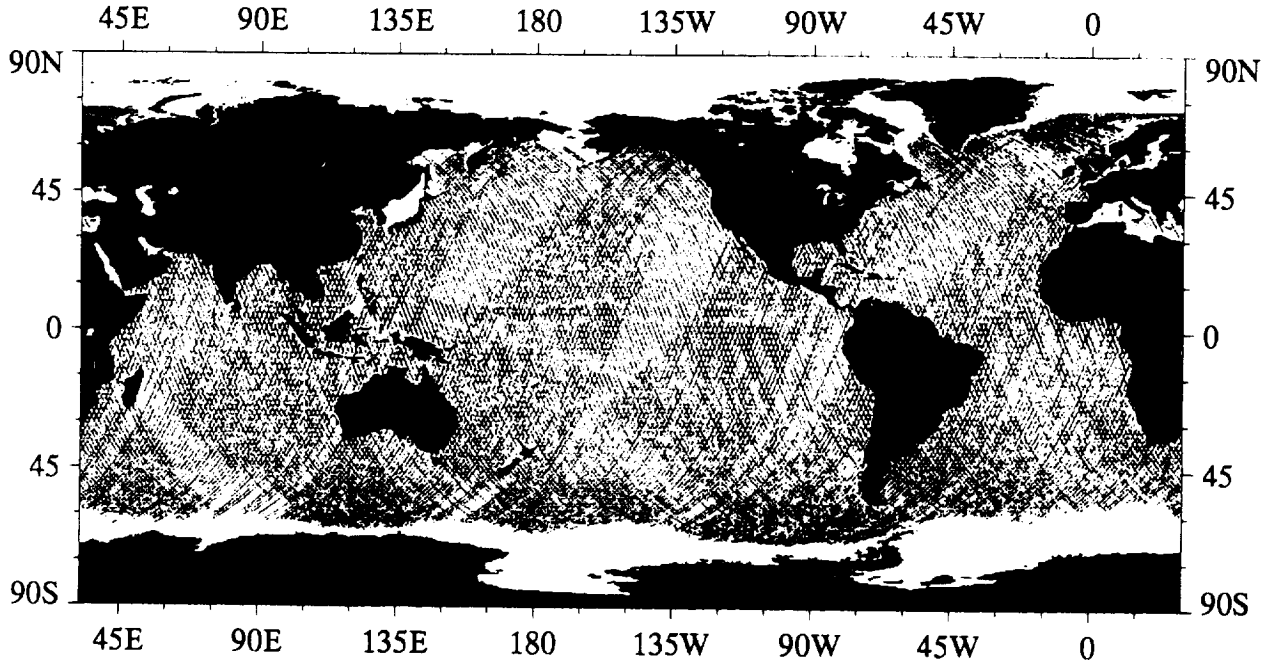

November 1988

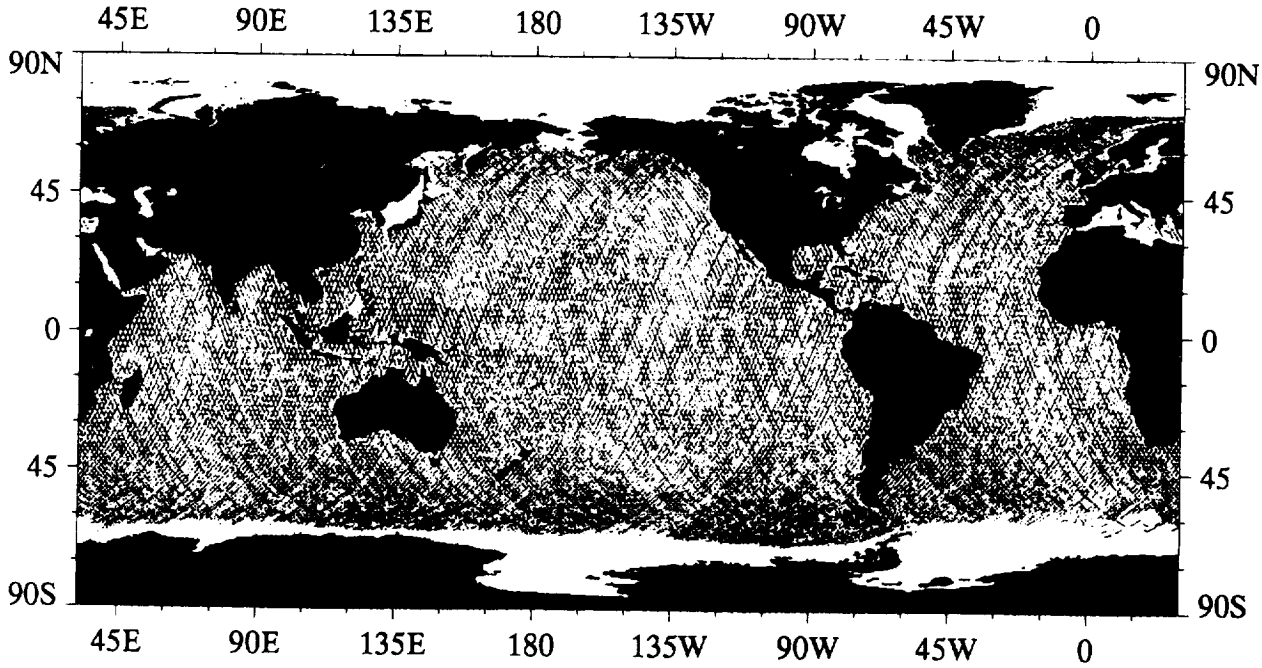

December 1988

GEOSAT Sea Surface Height Variation Referenced to 1988 Mean, cm

A2

Monthly GEOSAT Sampling Distribution

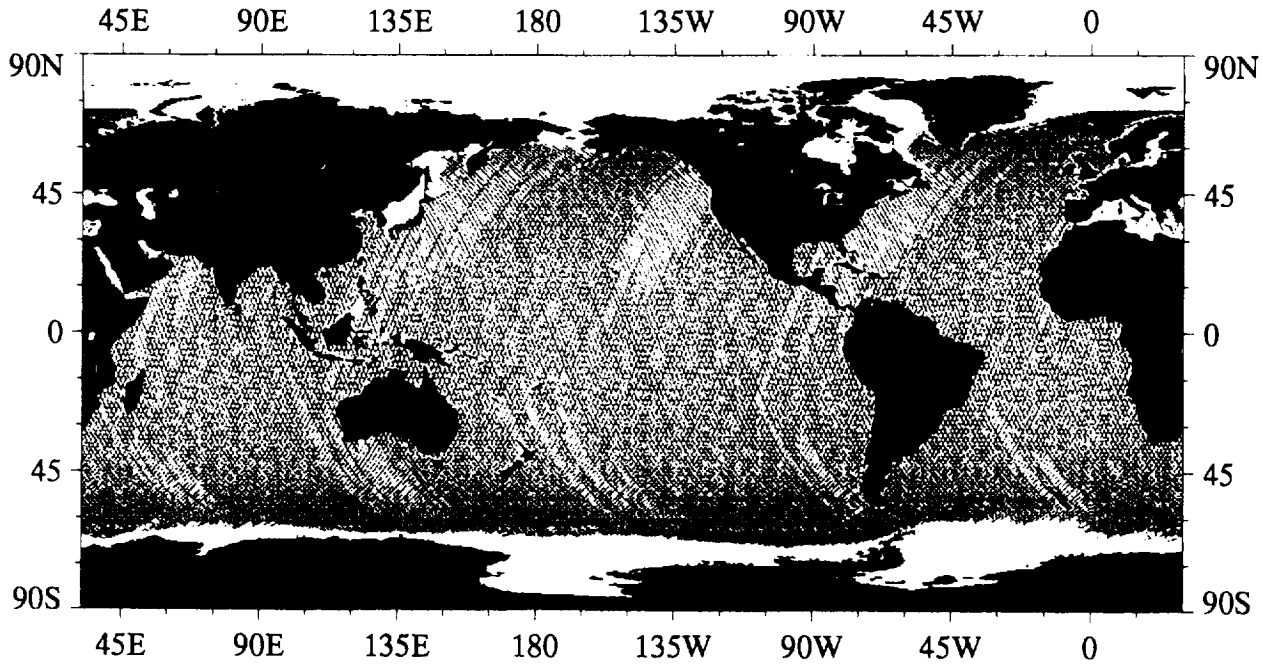

January 1988, max = 35

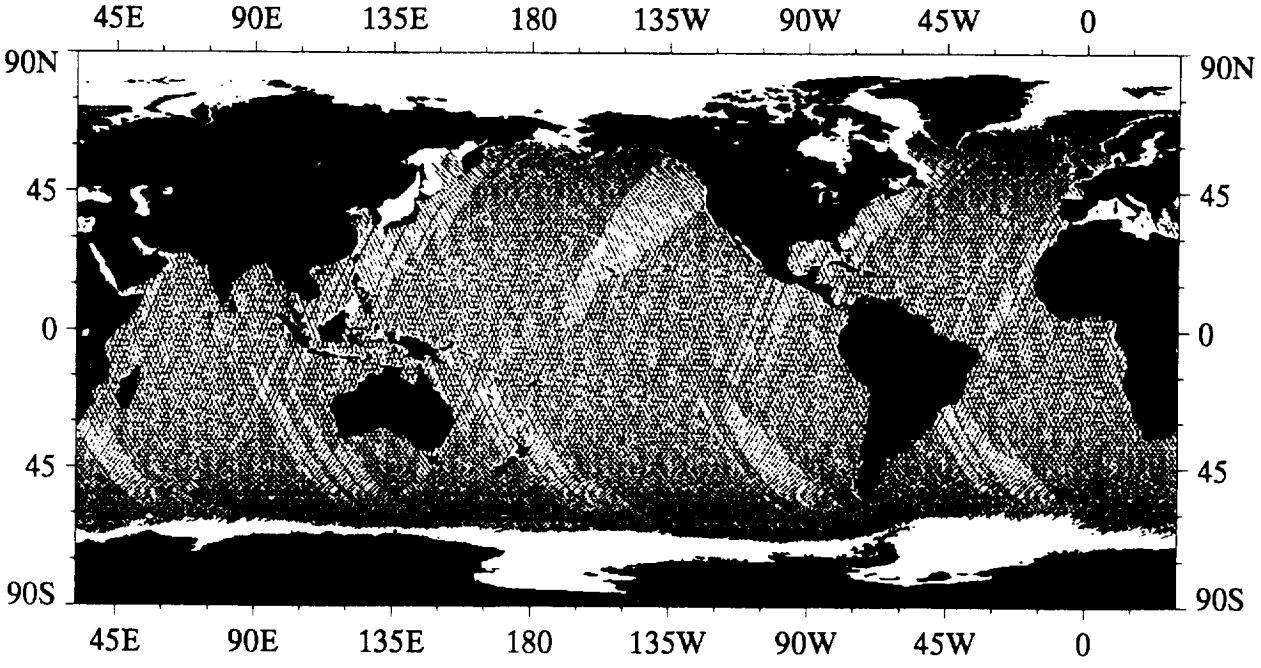

February 1988, max = 35

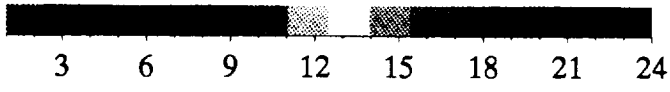

Number of GEOSAT Sea Surface Height Values per Pixel

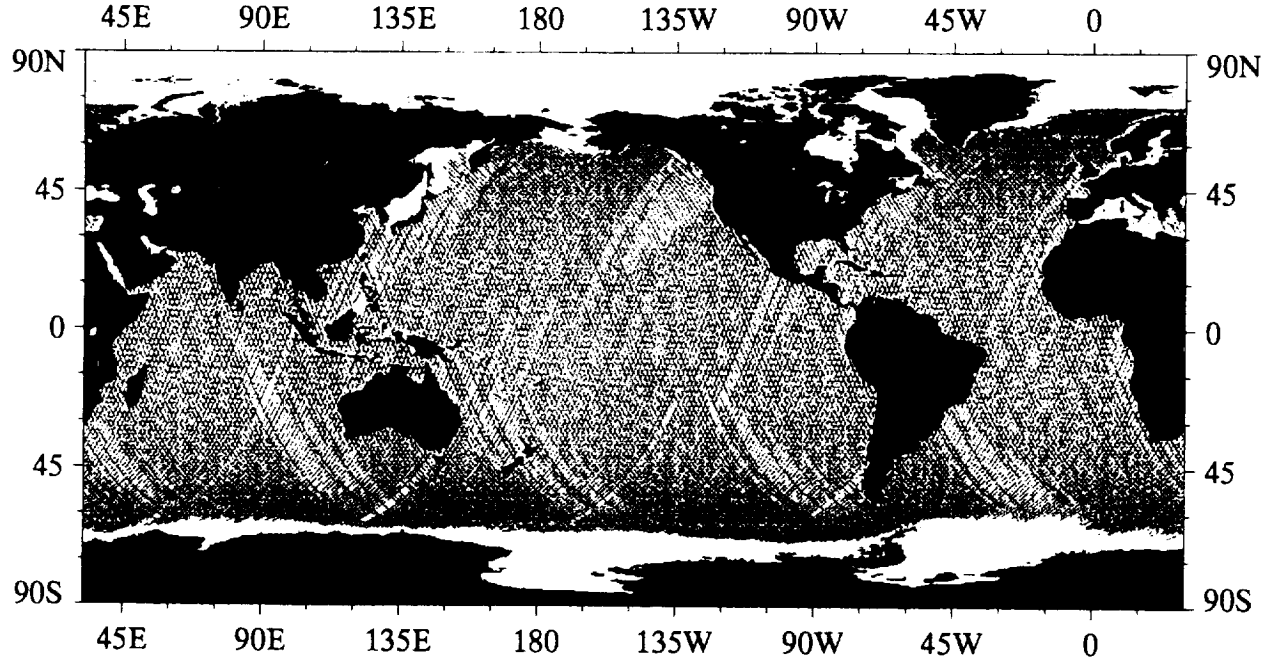

March 1988, max = 37

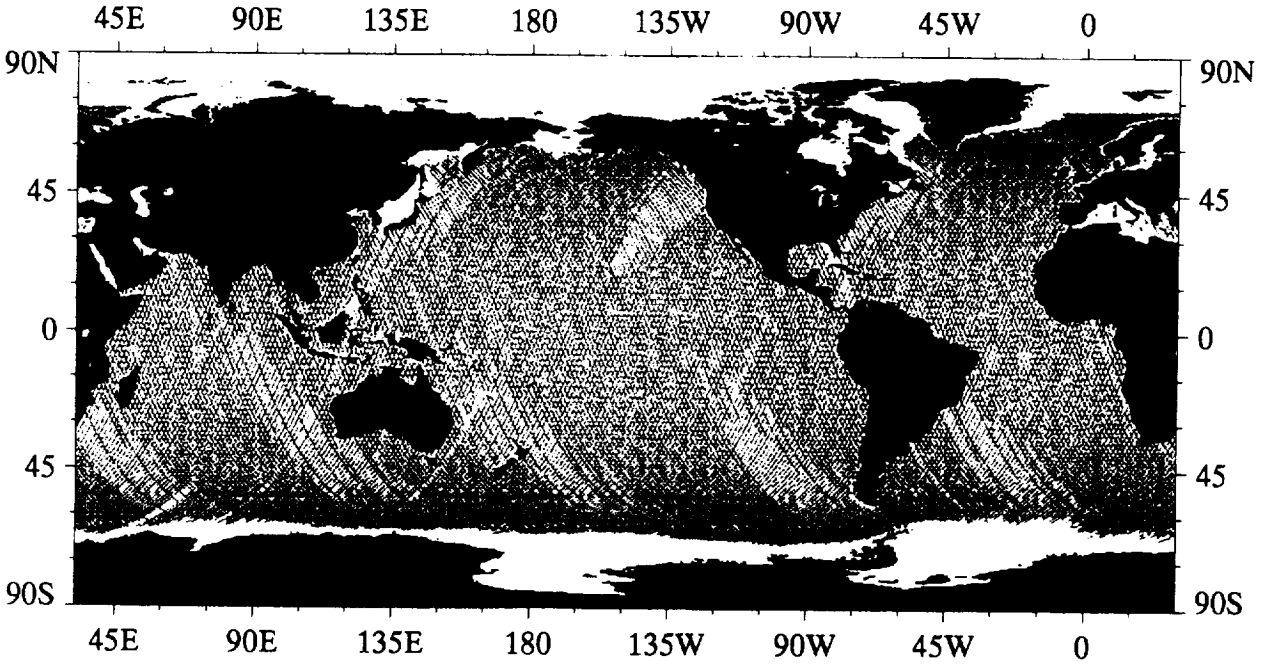

April 1988, max = 36

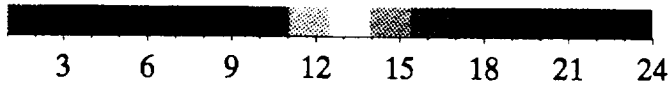

Number of GEOSAT Sea Surface Height Values per Pixel

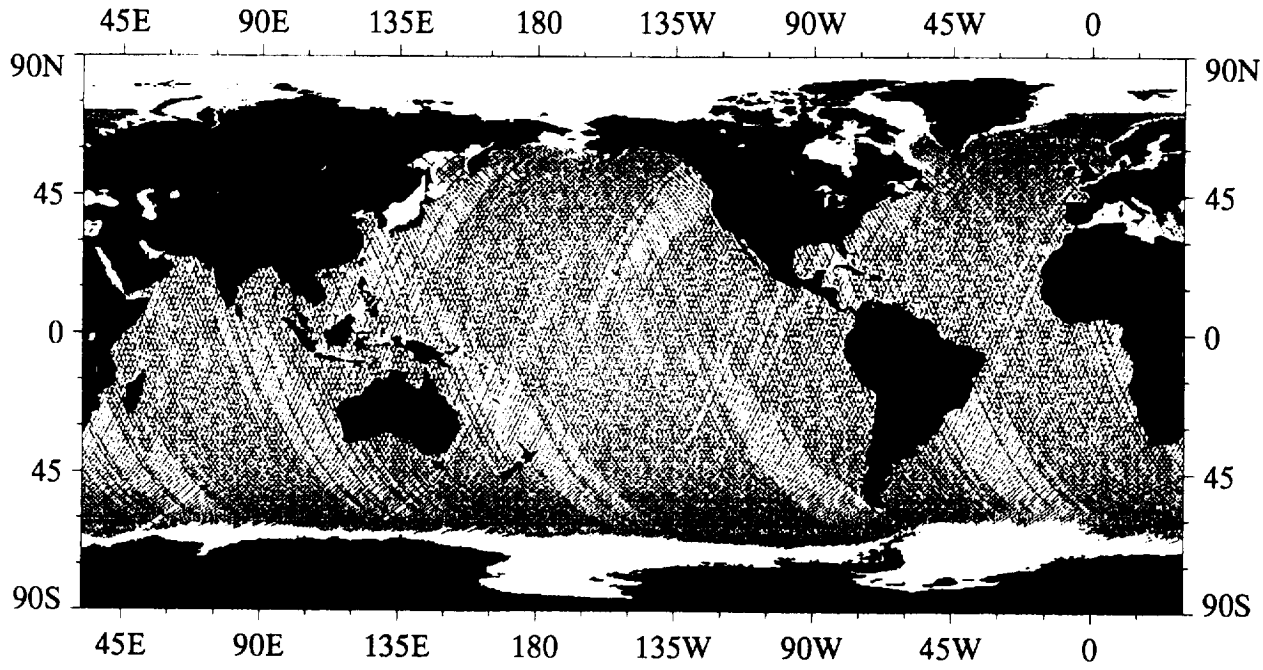

May 1988, max = 35

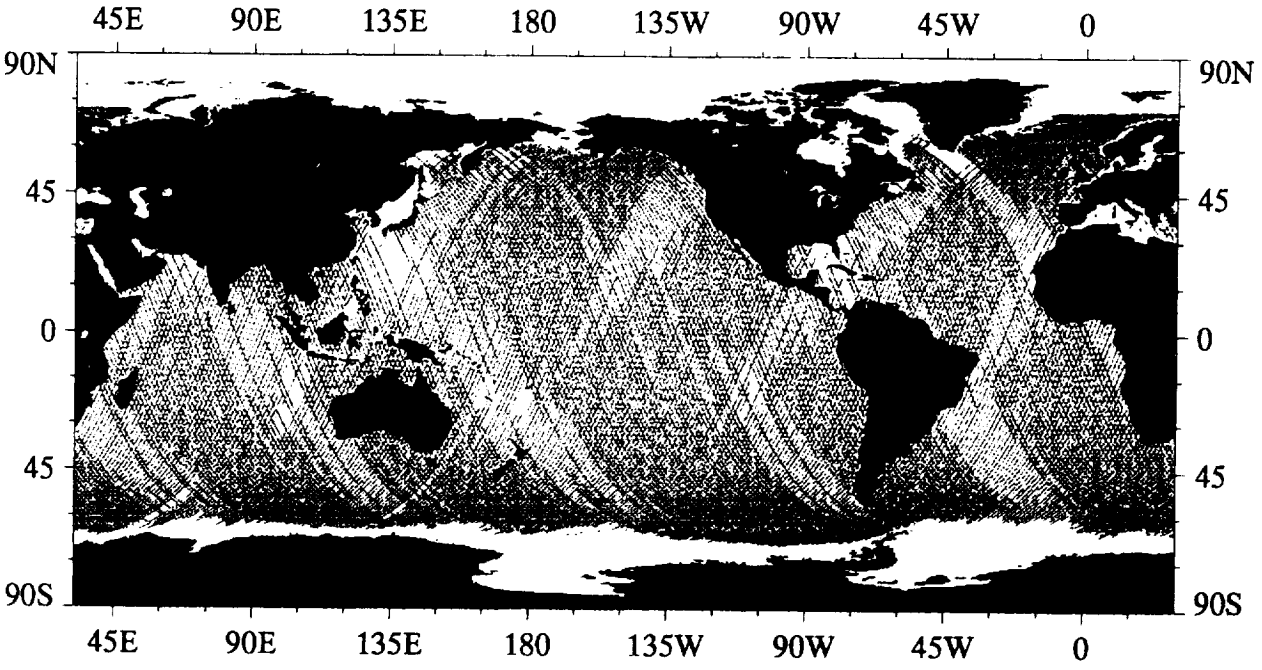

June 1988, max = 34

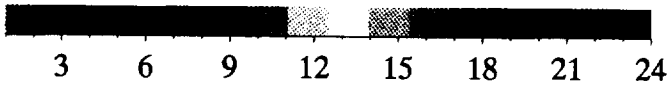

Number of GEOSAT Sea Surface Height Values per Pixel

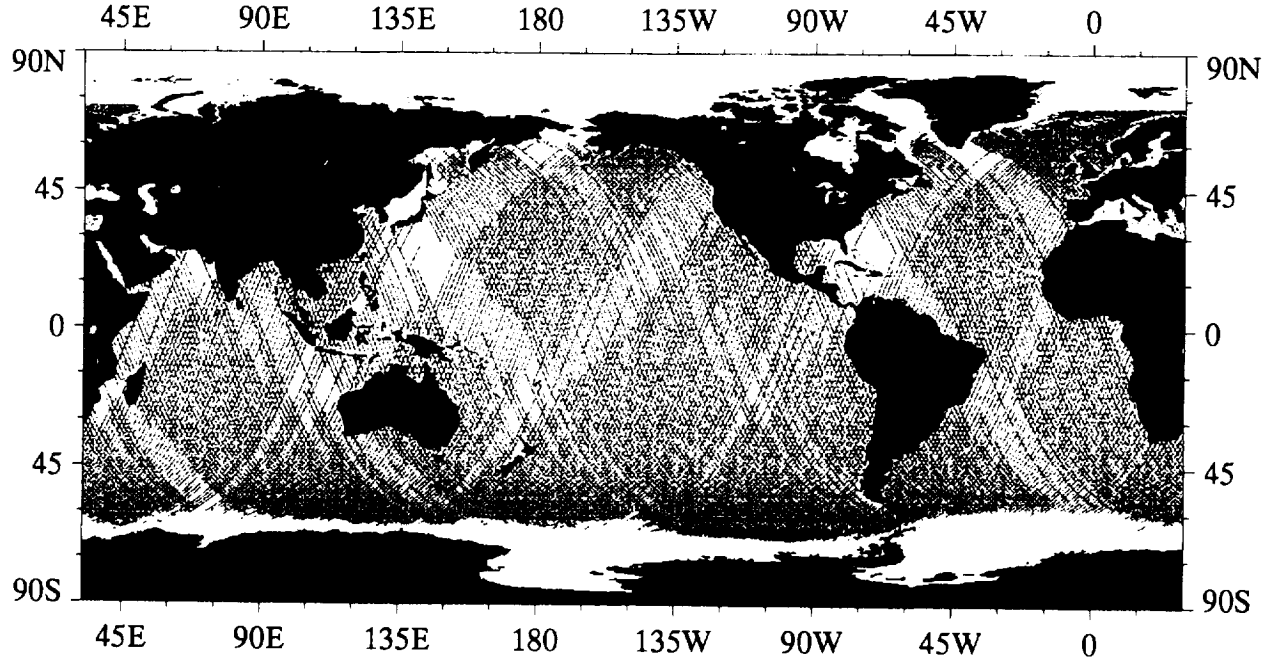

July 1988, max = 33

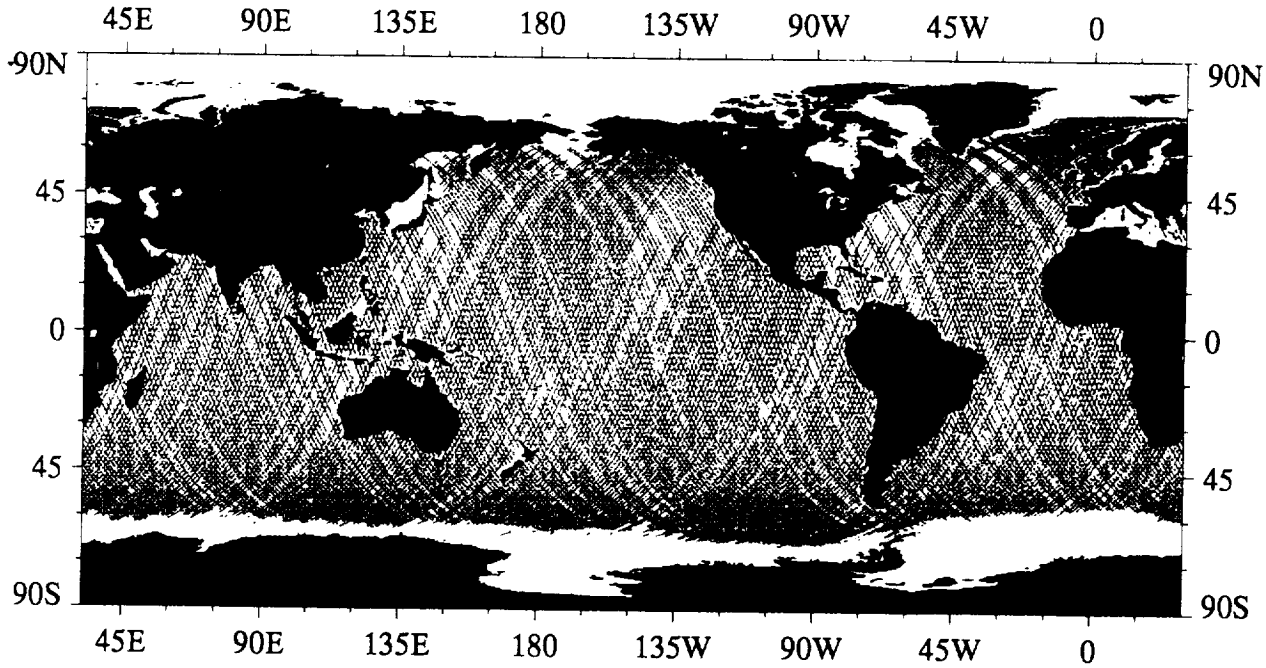

August 1988, max = 26

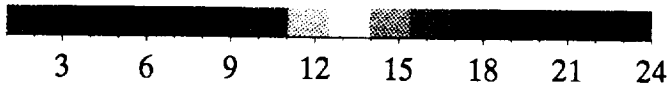

Number of GEOSAT Sea Surface Height Values per Pixel

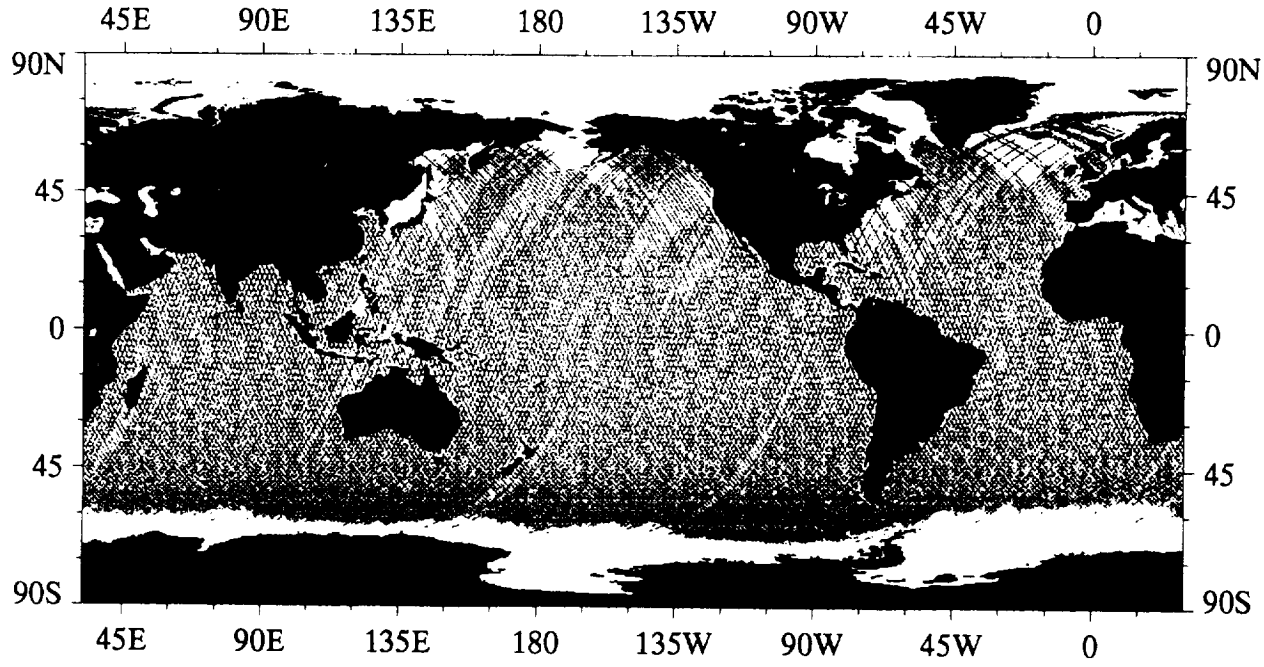

September 1988, max = 24

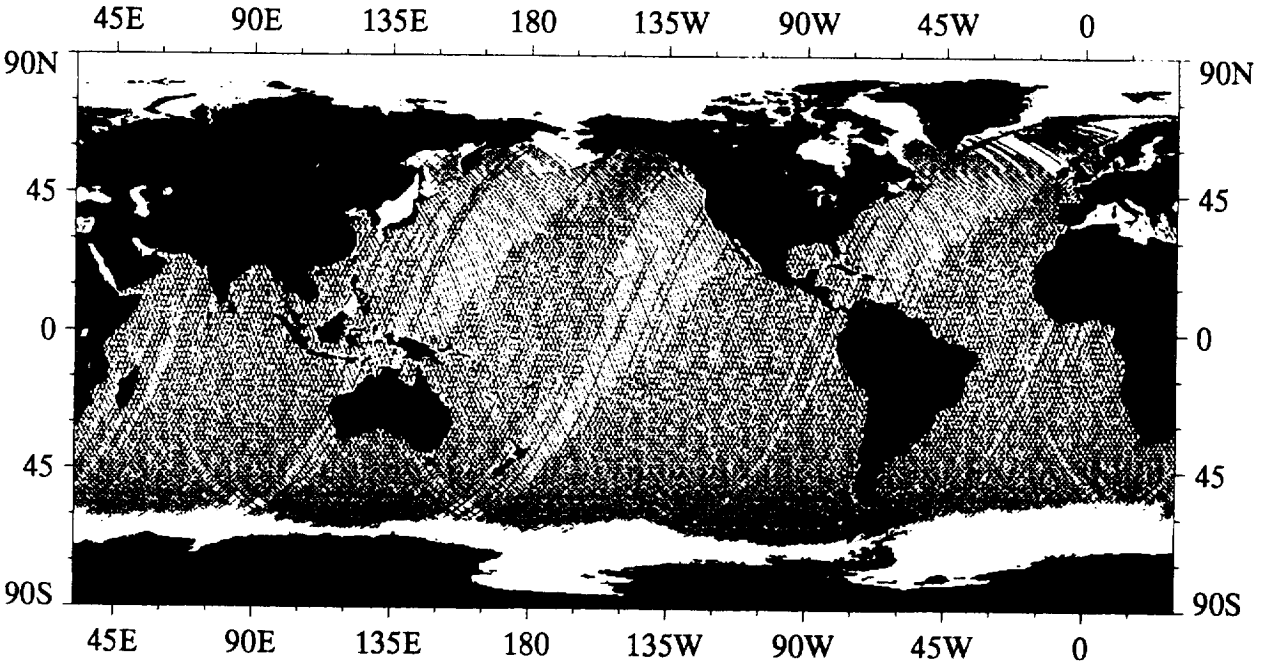

October 1988, max = 33

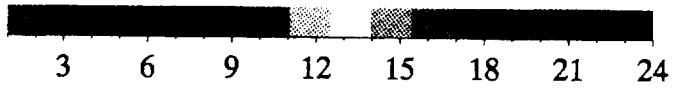

Number of GEOSAT Sea Surface Height Values per Pixel

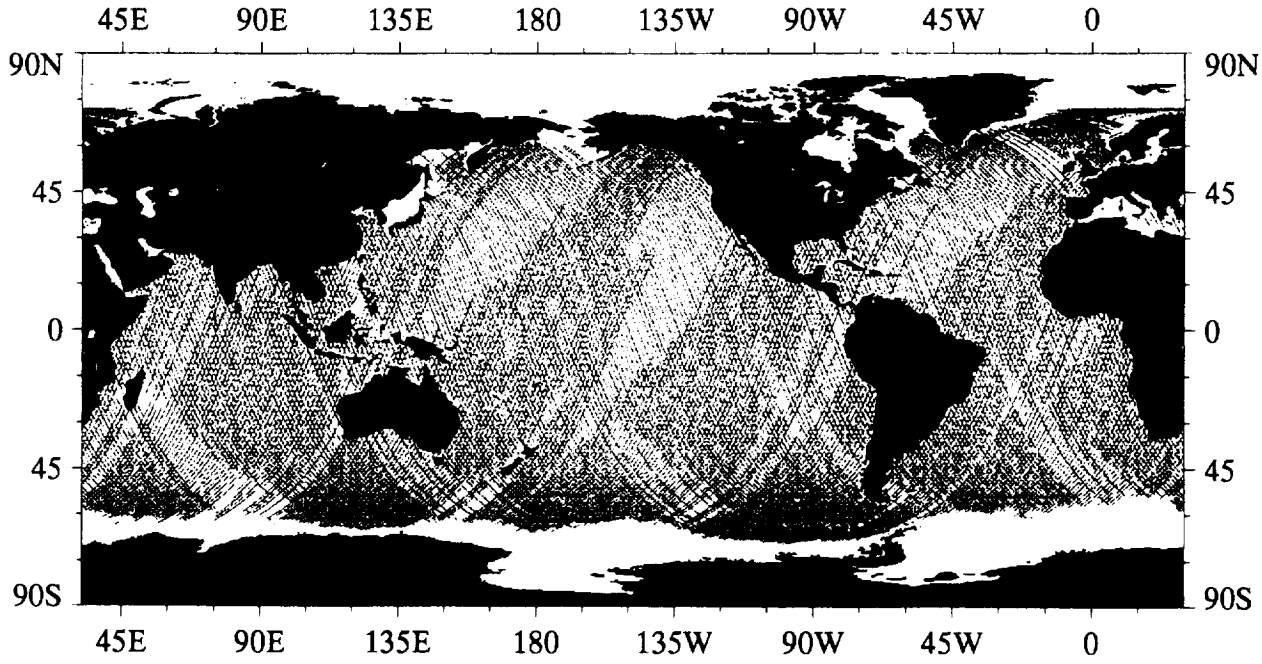

November 1988, max = 36

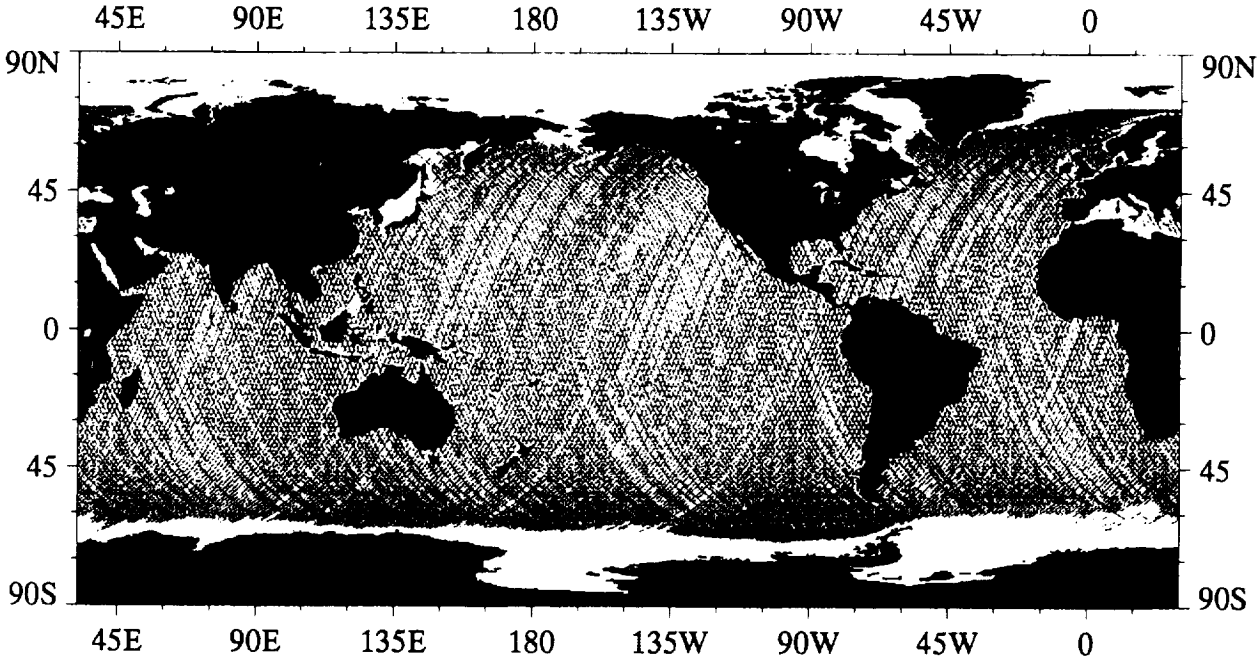

December 1988, max = 37

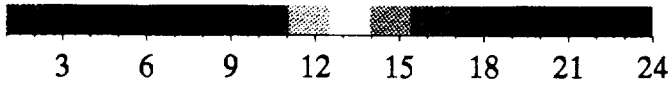

Number of GEOSAT Sea Surface Height Values per Pixel

A3

Annual Mean and Sampling Distribution of SSMI Surface Wind Speed

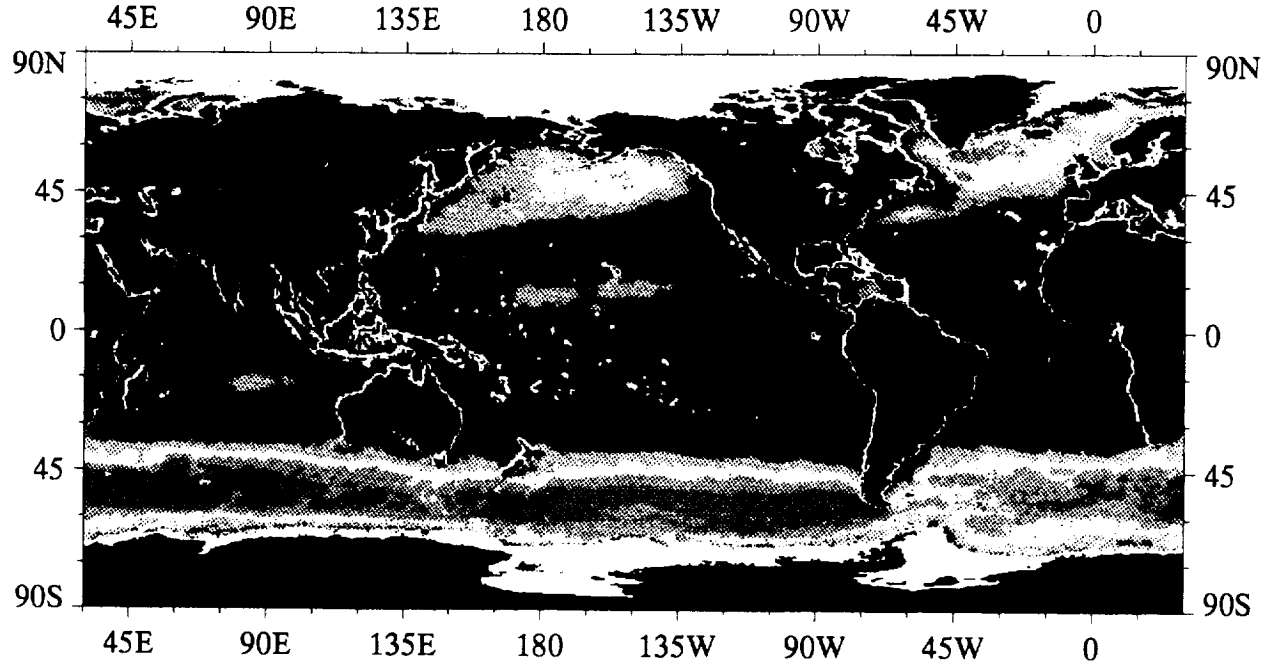

Annual Mean 1988

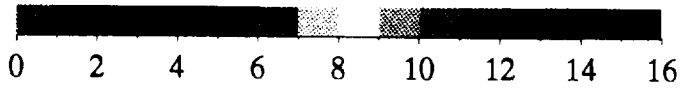

SSMI Wind Speed Referenced to 10 m, m s^{-1}

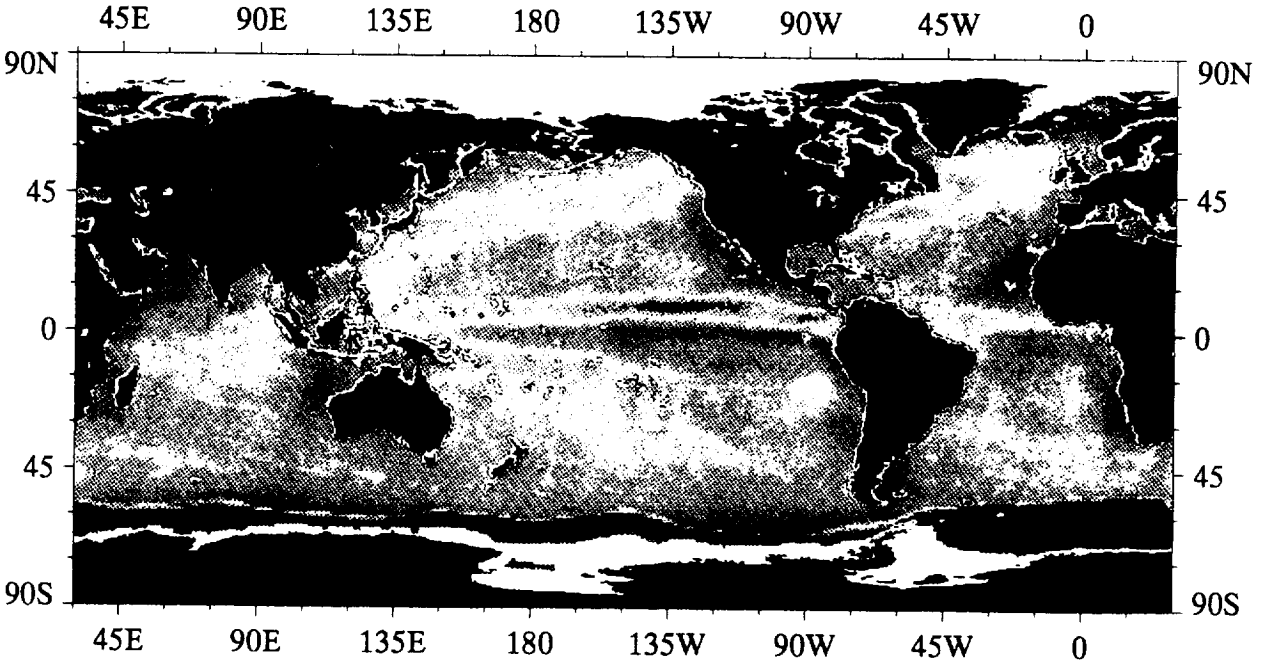

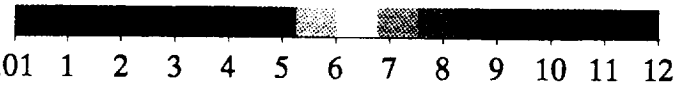

Number x 100 of SSMI Wind Speed Values per Pixel During 1988, max = 1272

A4

Monthly Mean SSMI Surface Wind Speed

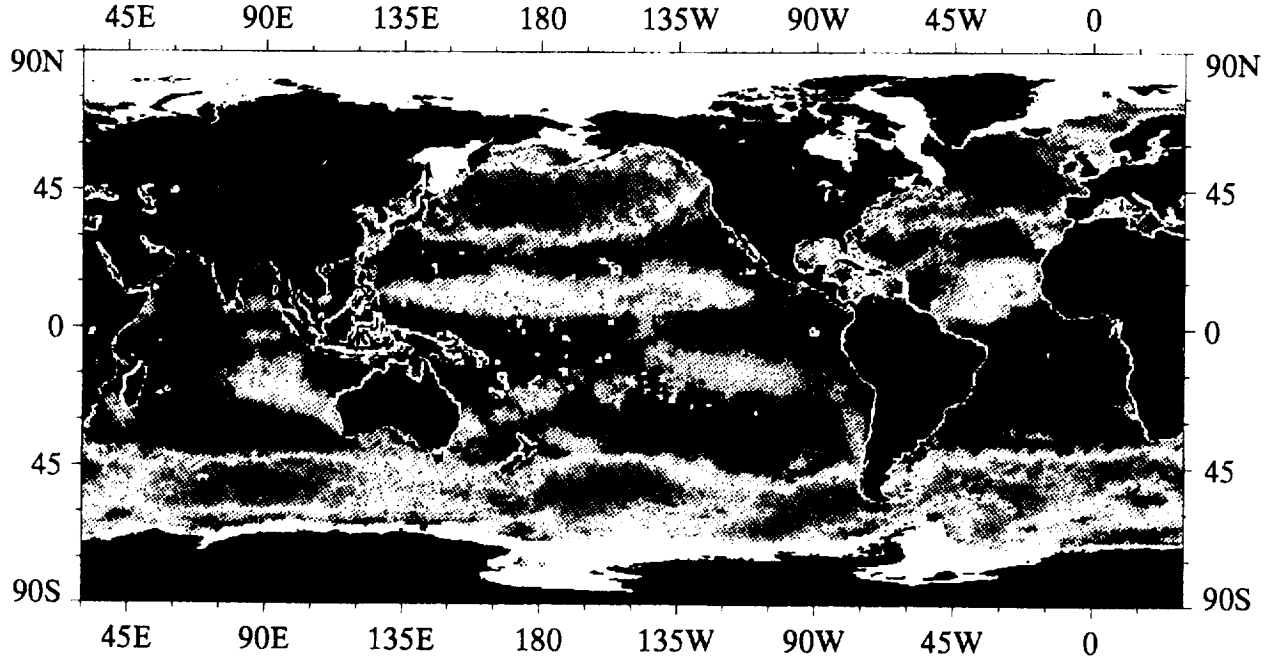

13 - 31 January 1988

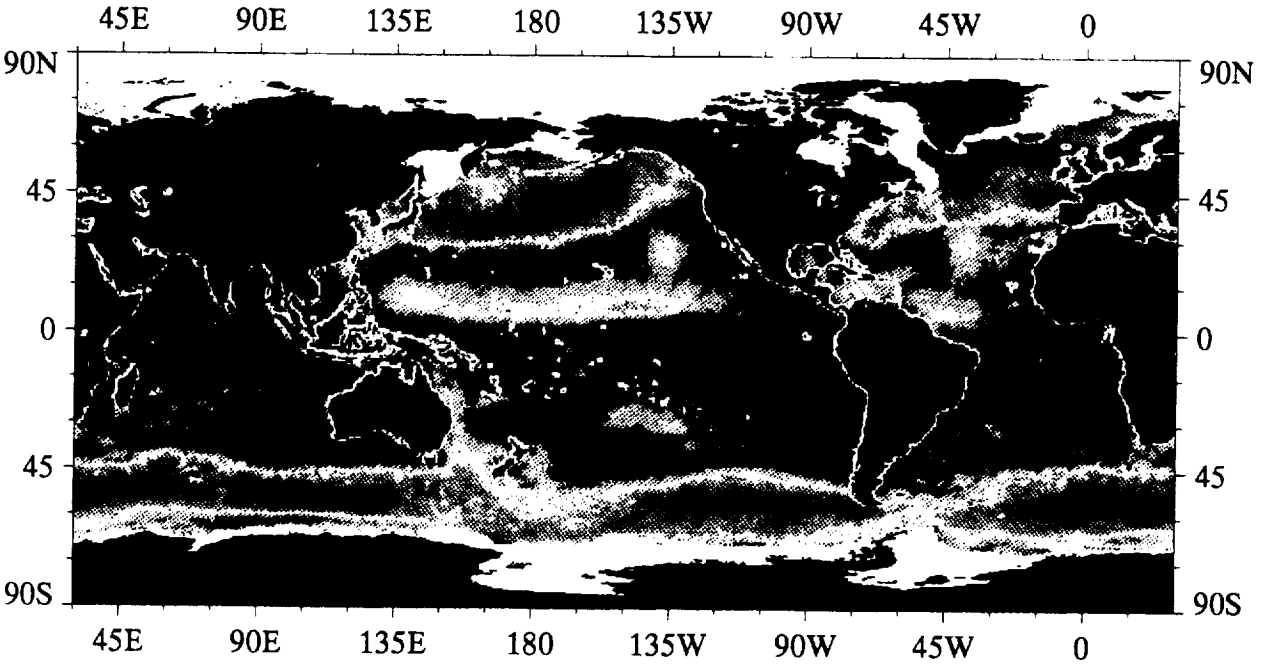

February 1988

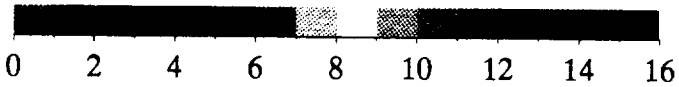

SSMI Wind Speed Referenced to 10 m, m s^{-1}

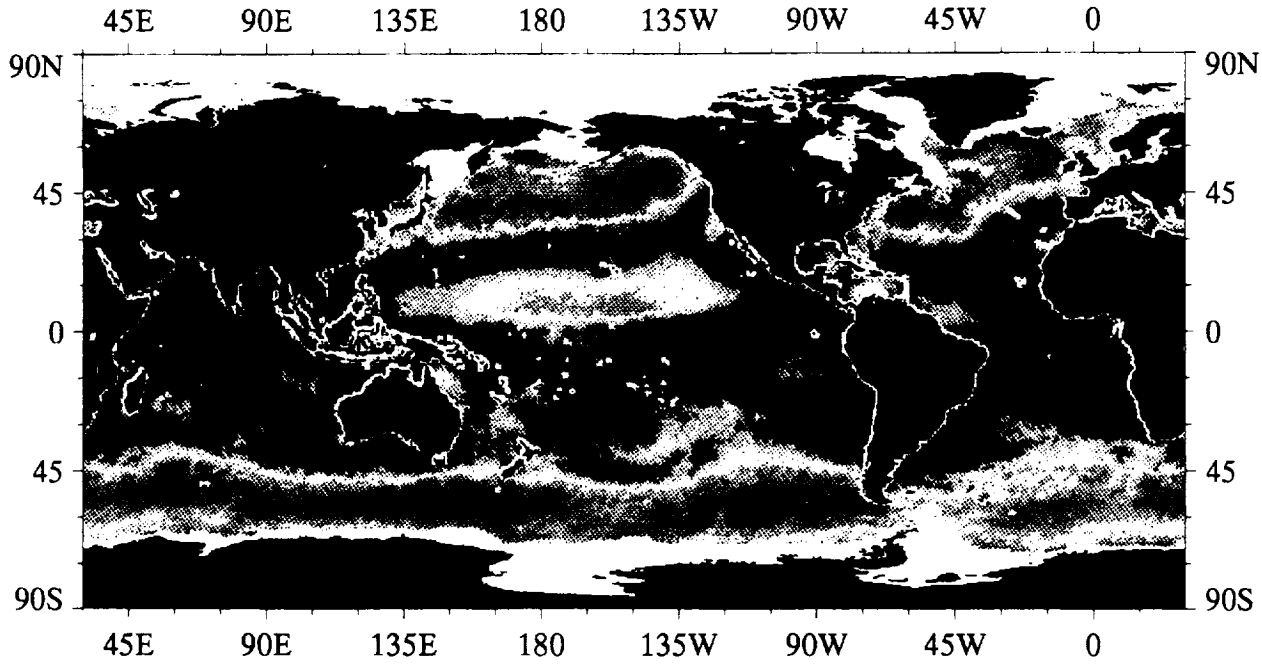

March 1988

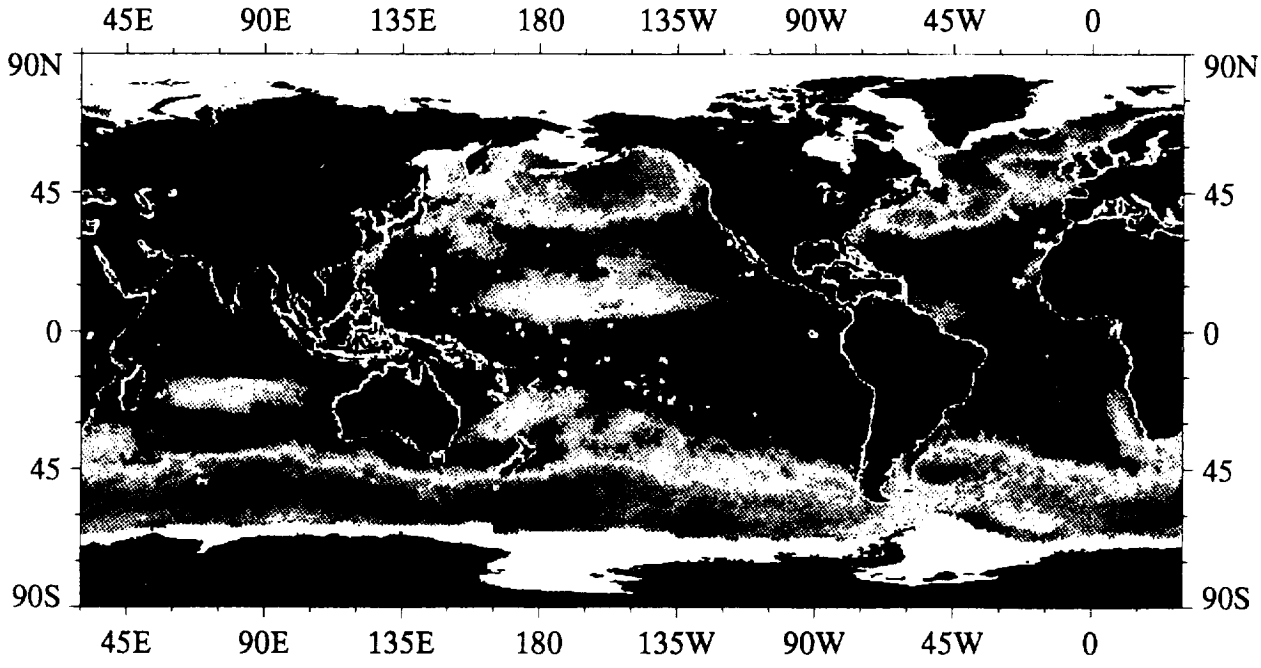

April 1988

SSMI Wind Speed Referenced to 10 m, m s^{-1}

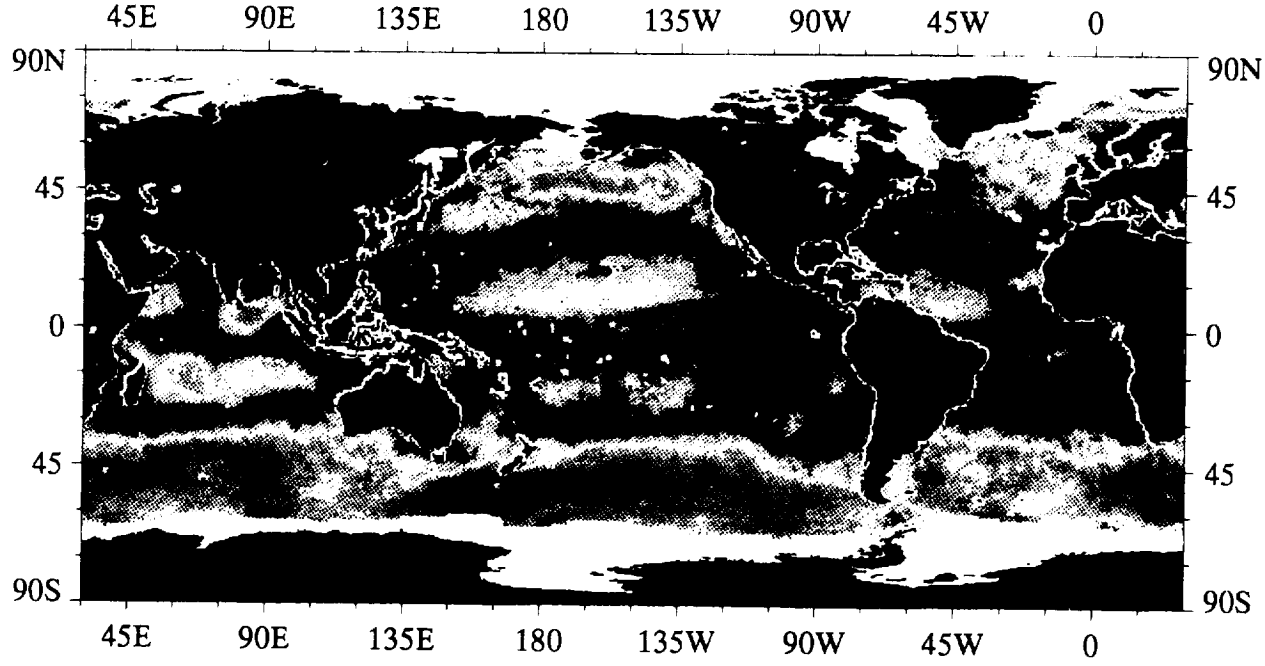

May 1988

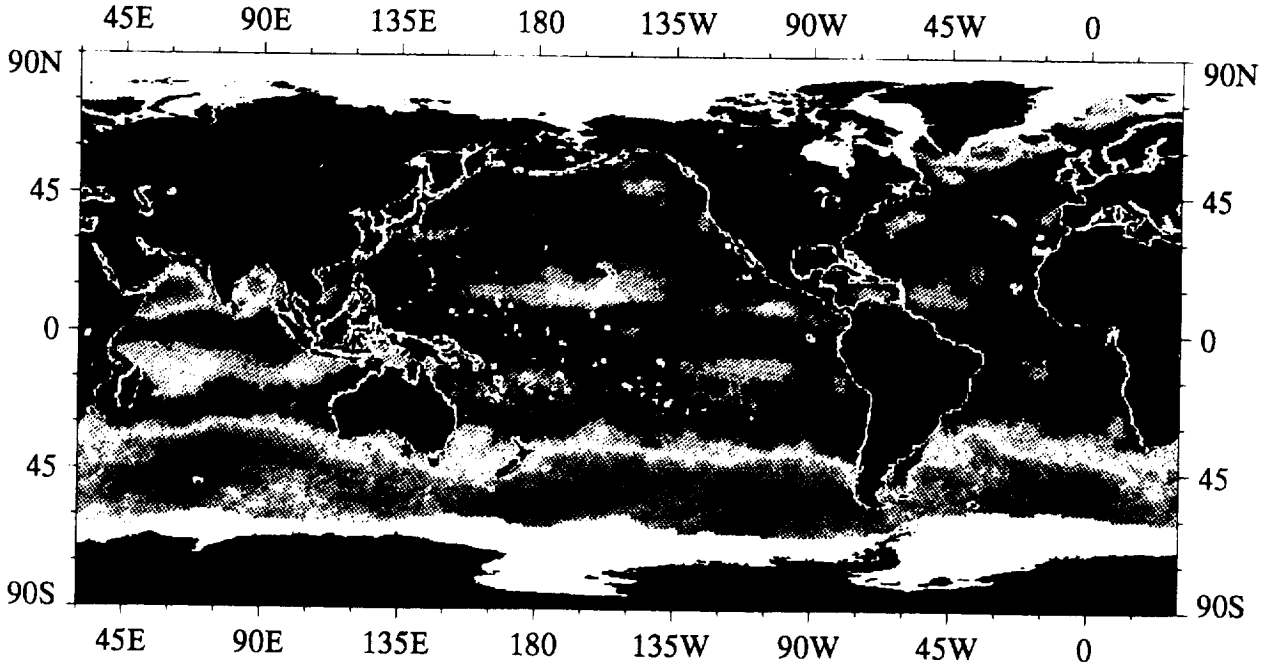

June 1988

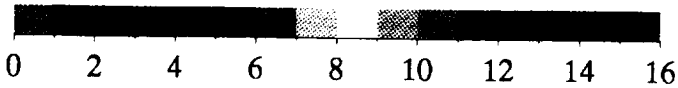

SSMI Wind Speed Referenced to 10 m, m s^{-1}

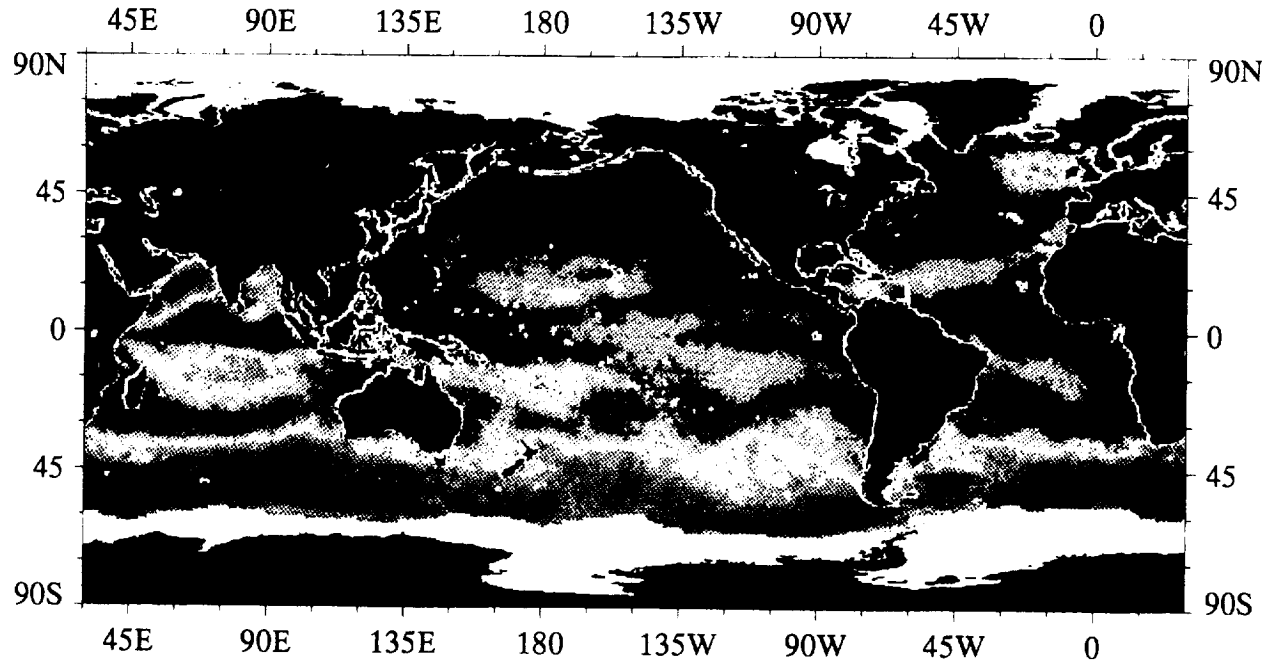

July 1988

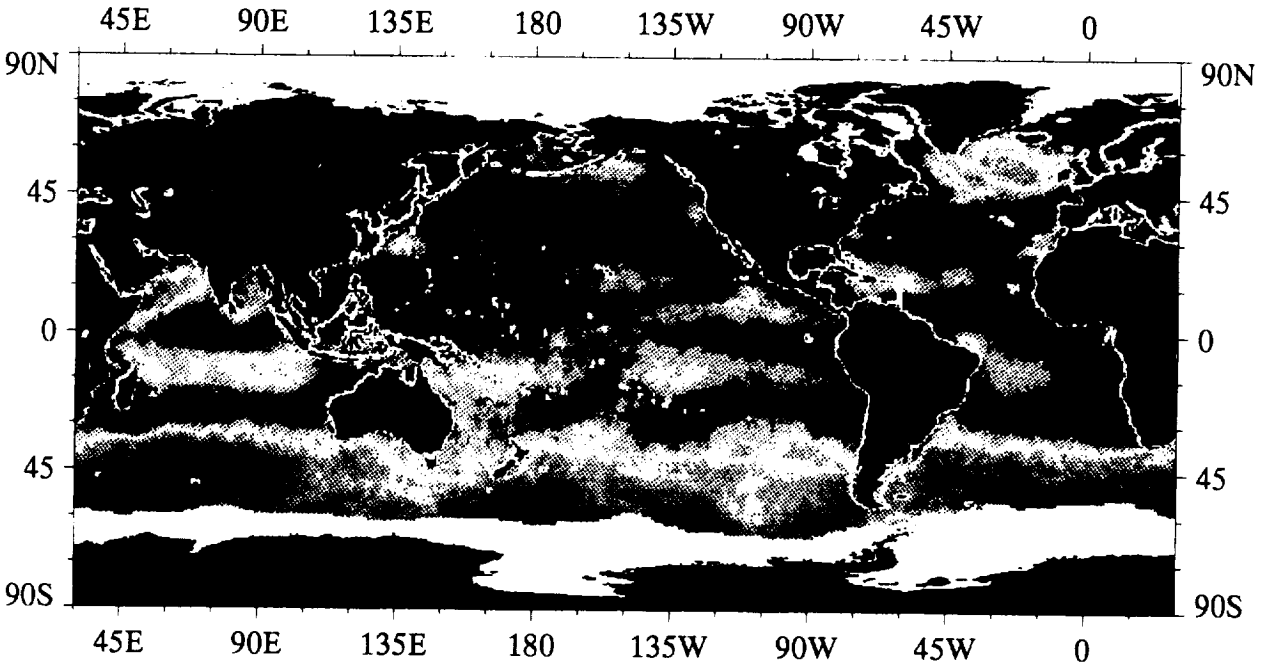

August 1988

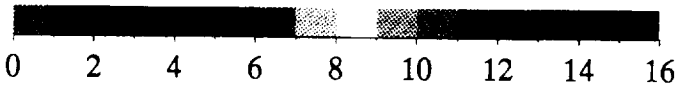

SSMI Wind Speed Referenced to 10 m, m s^{-1}

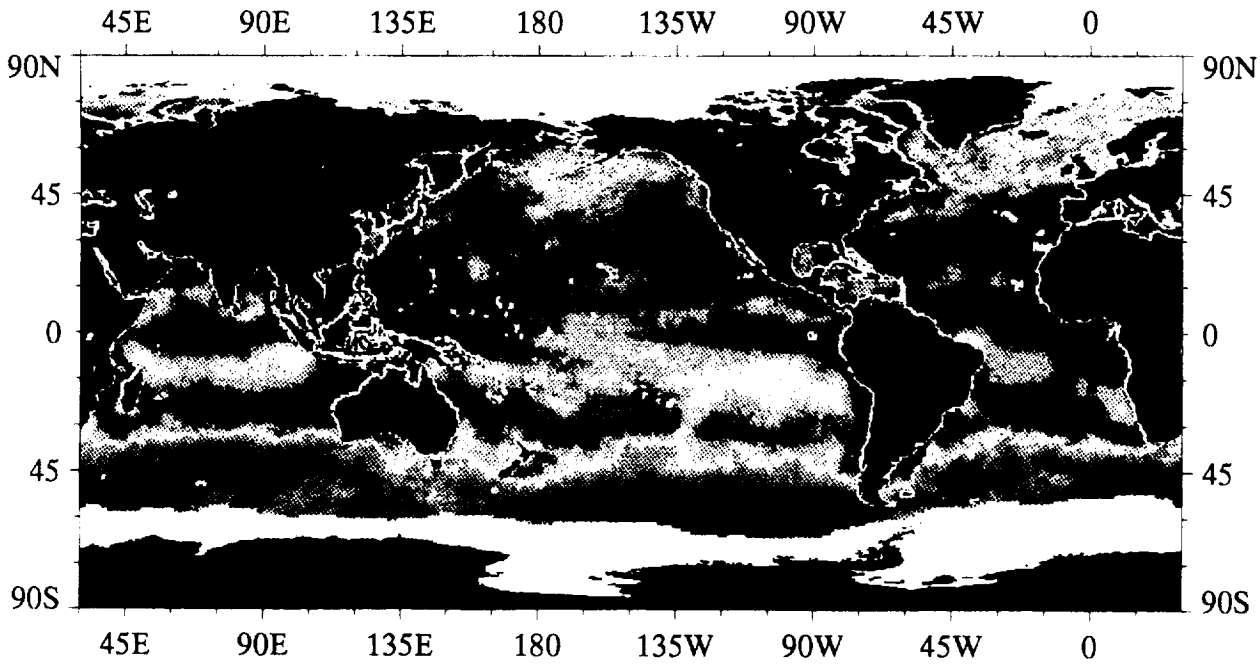

September 1988

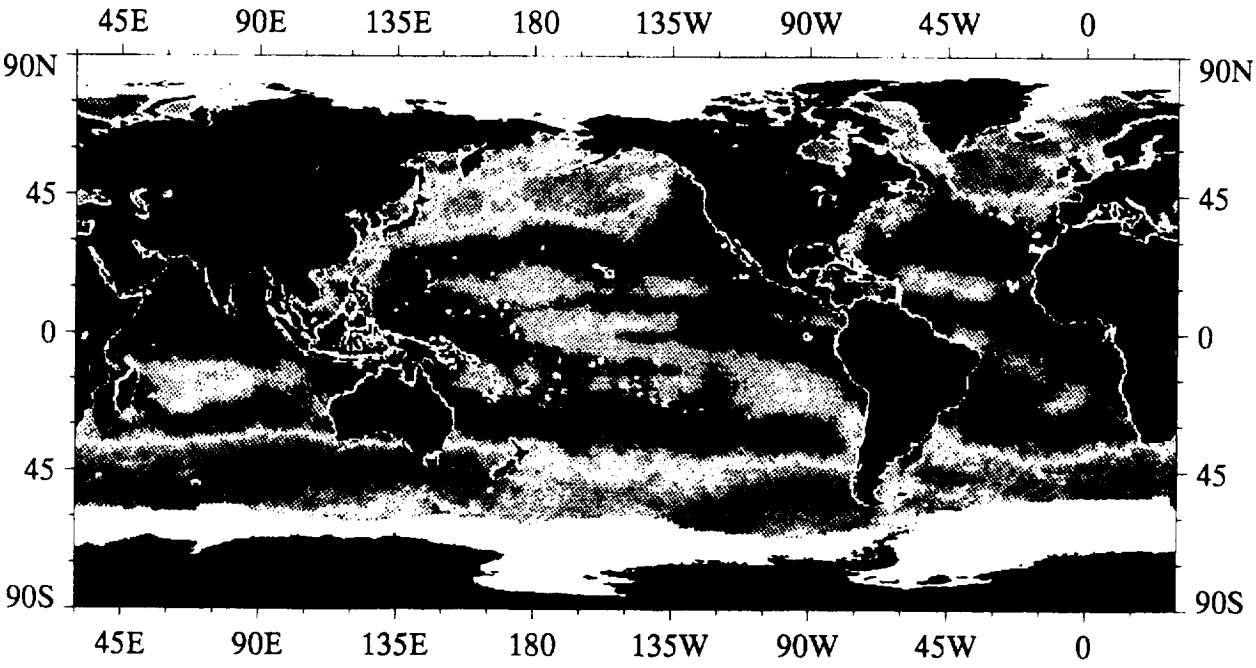

October 1988

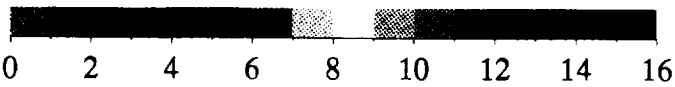

SSMI Wind Speed Referenced to 10 m, m s^{-1}

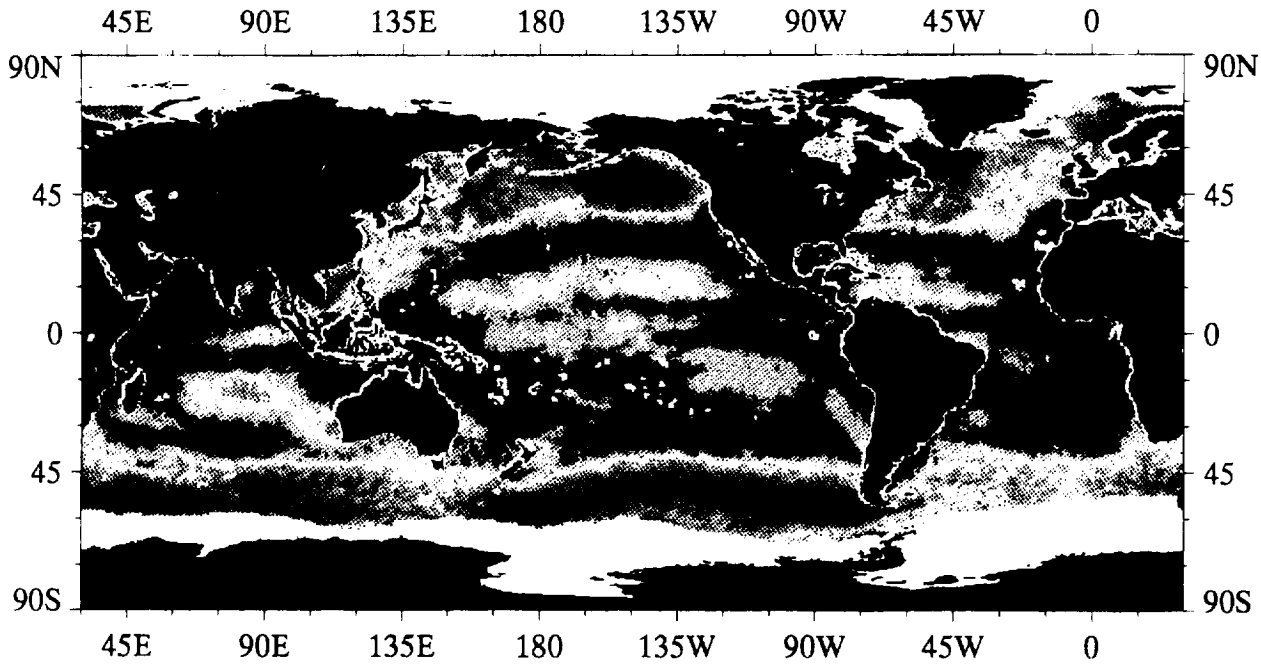

November 1988

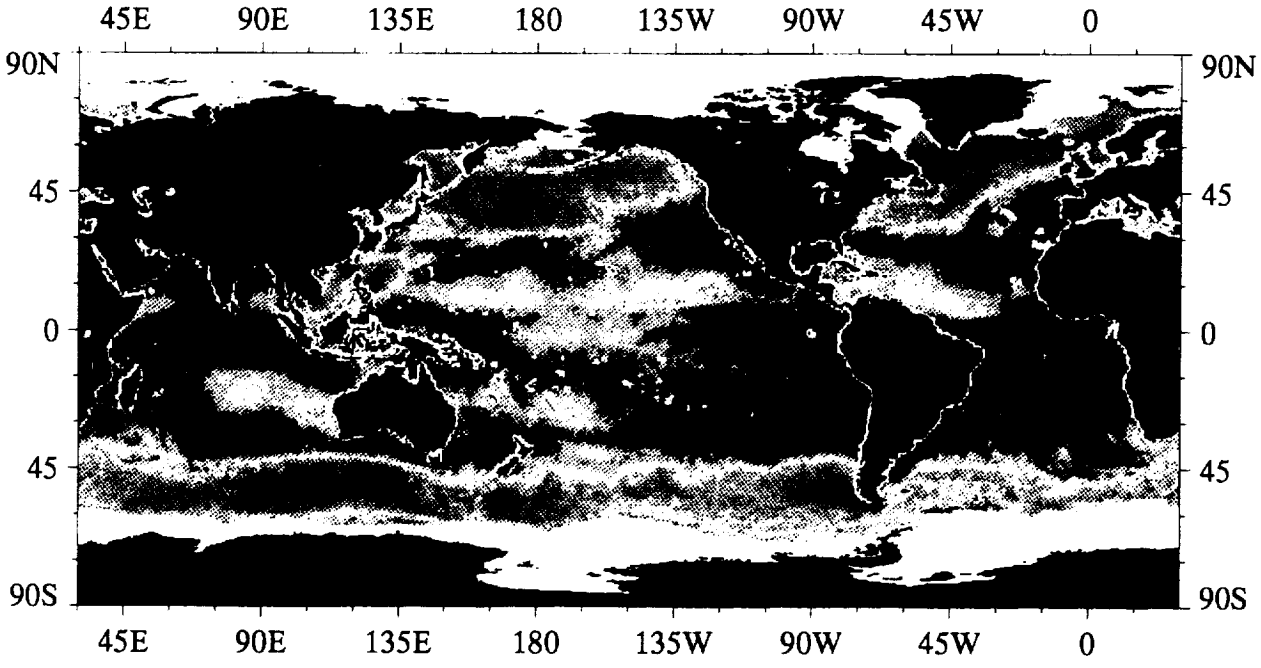

December 1988

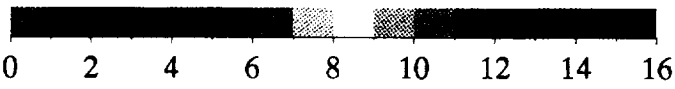

SSMI Wind Speed Referenced to 10 m, m s^{-1}

A5

Monthly SSMI Sampling Distribution

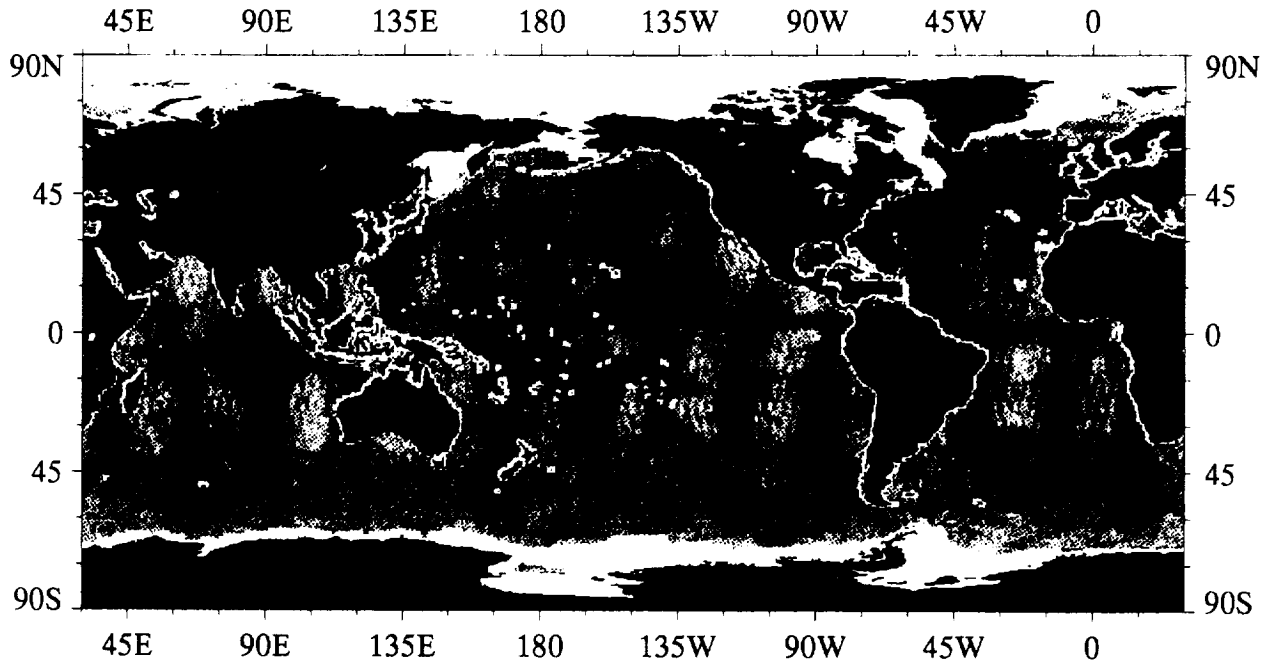

13 - 31 January 1988, max = 86

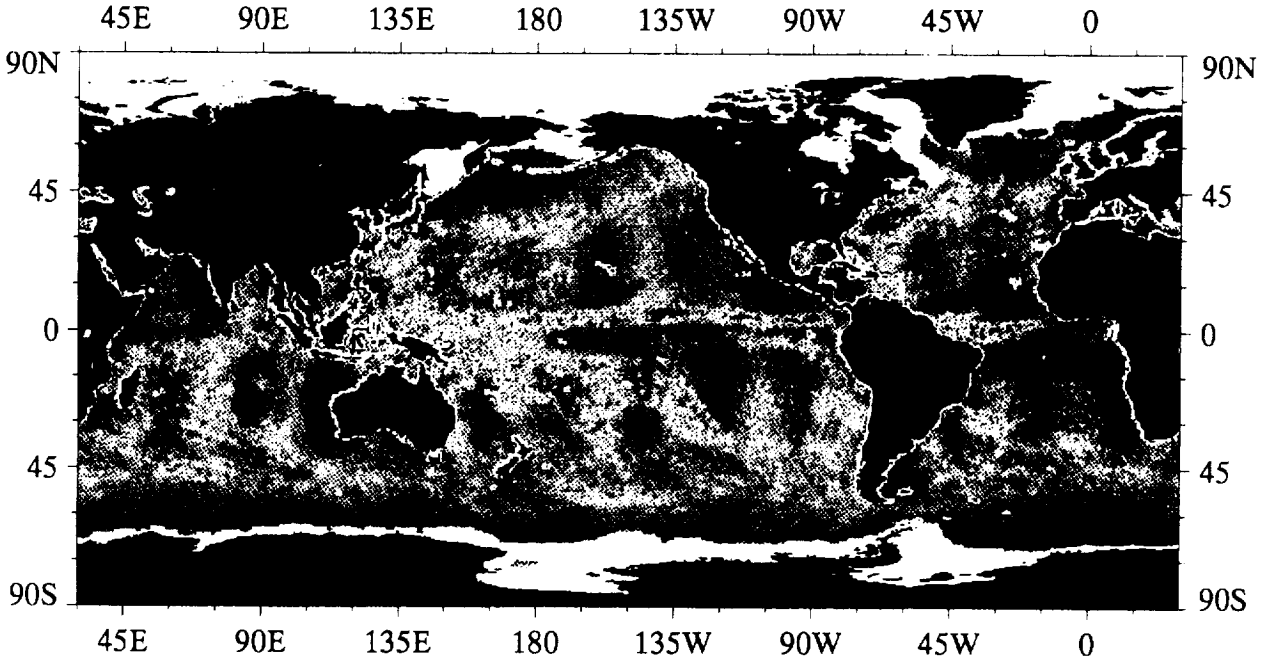

February 1988, max = 143

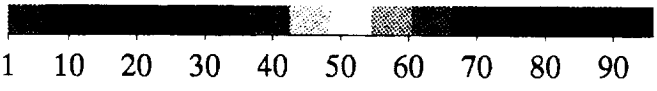

Number of SSMI Wind Speed Values per Pixel

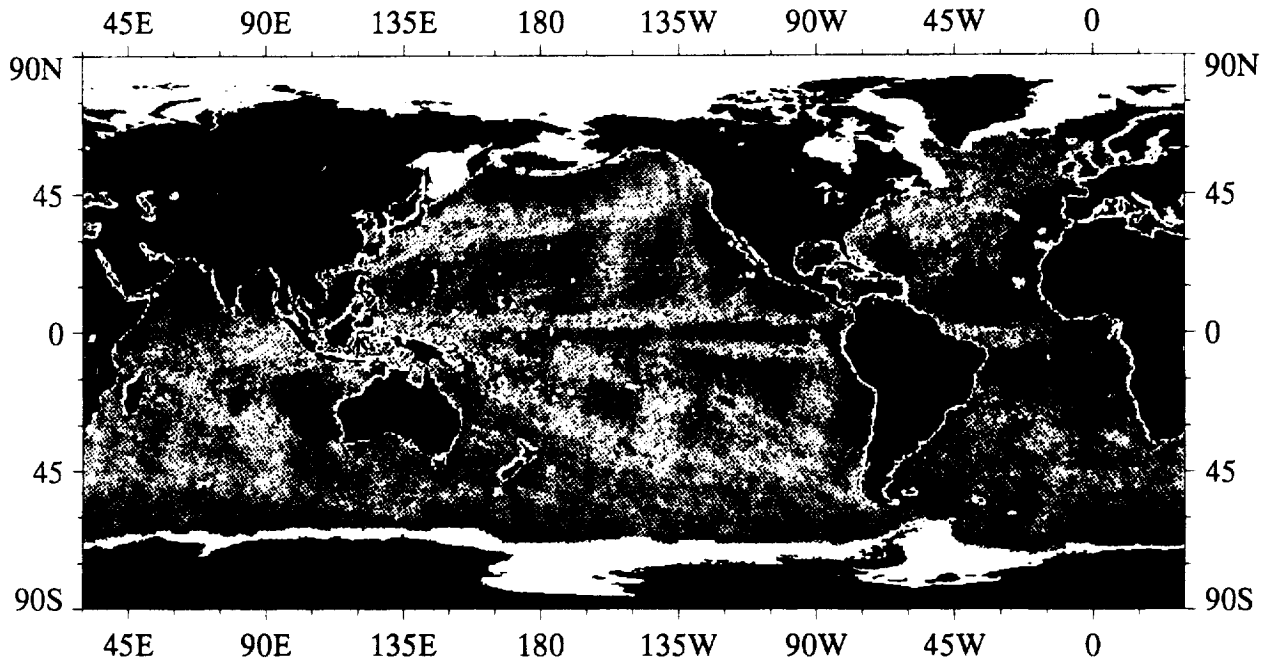

March 1988, max = 144

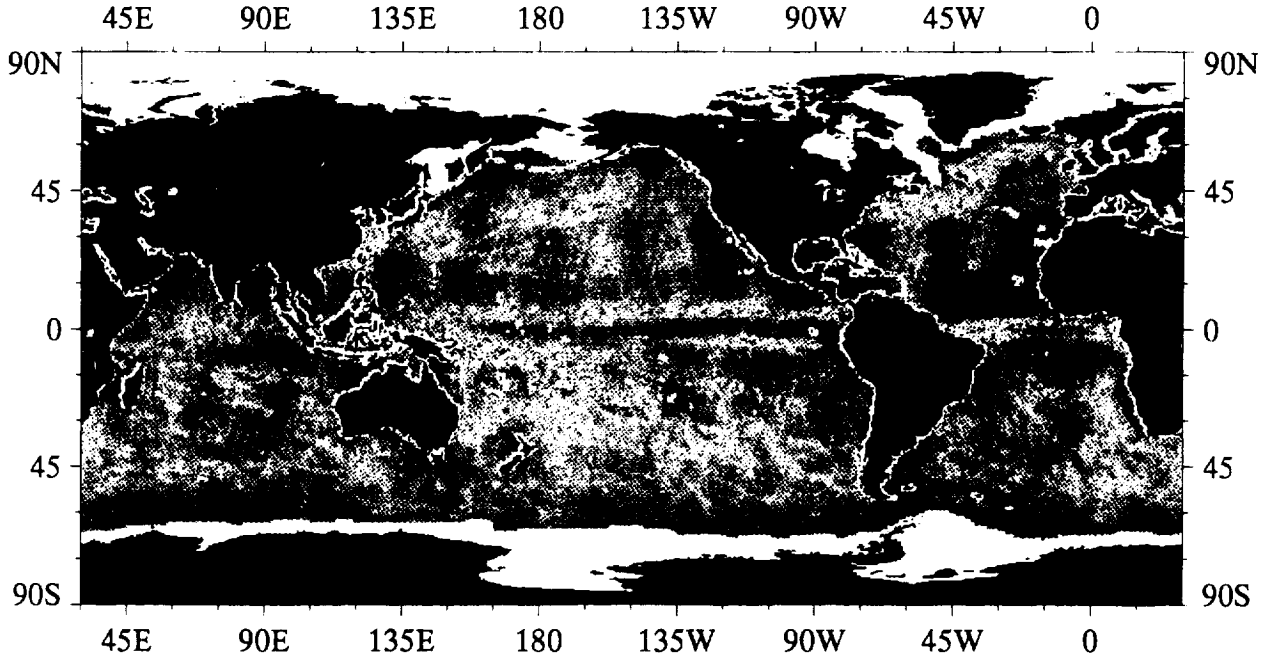

April 1988, max = 127

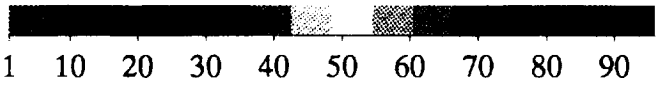

Number of SSMI Wind Speed Values per Pixel

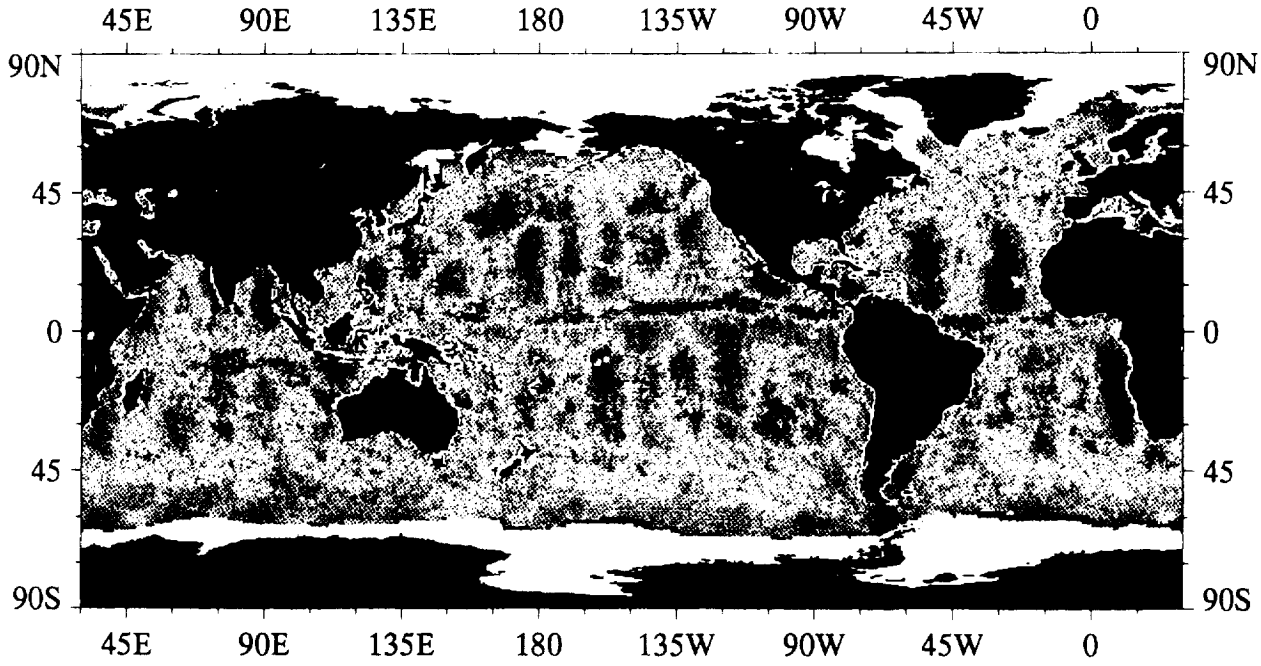

May 1988, max = 116

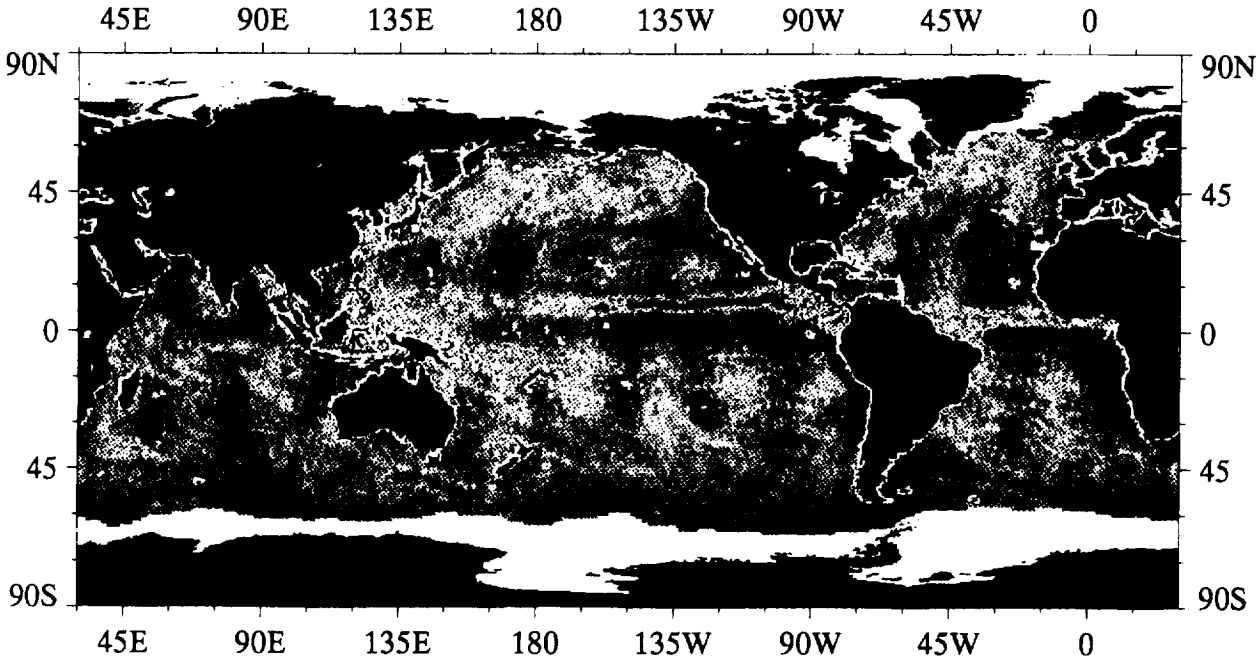

June 1988, max = 124

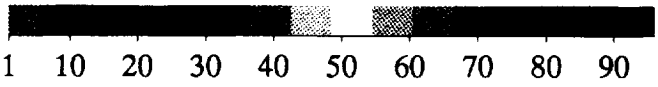

Number of SSMI Wind Speed Values per Pixel

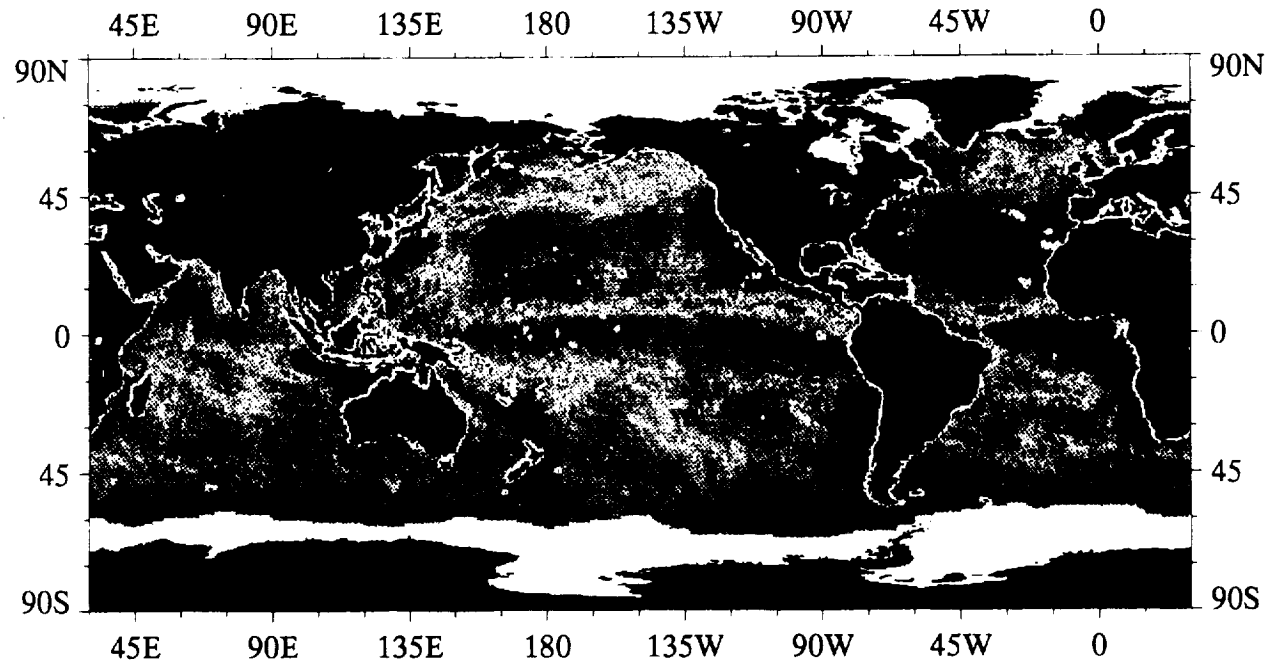

July 1988, max = 137

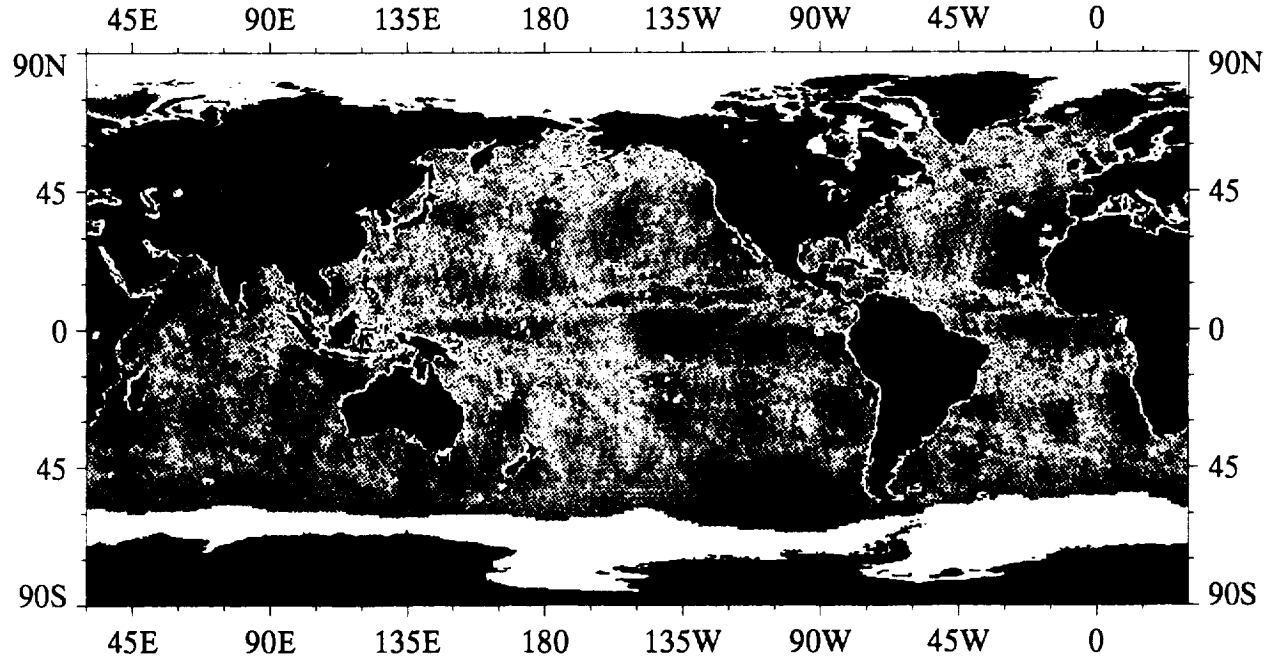

August 1988, max = 131

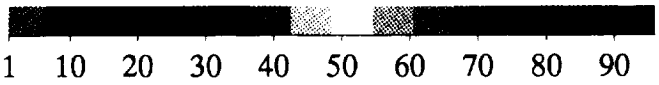

Number of SSMI Wind Speed Values per Pixel

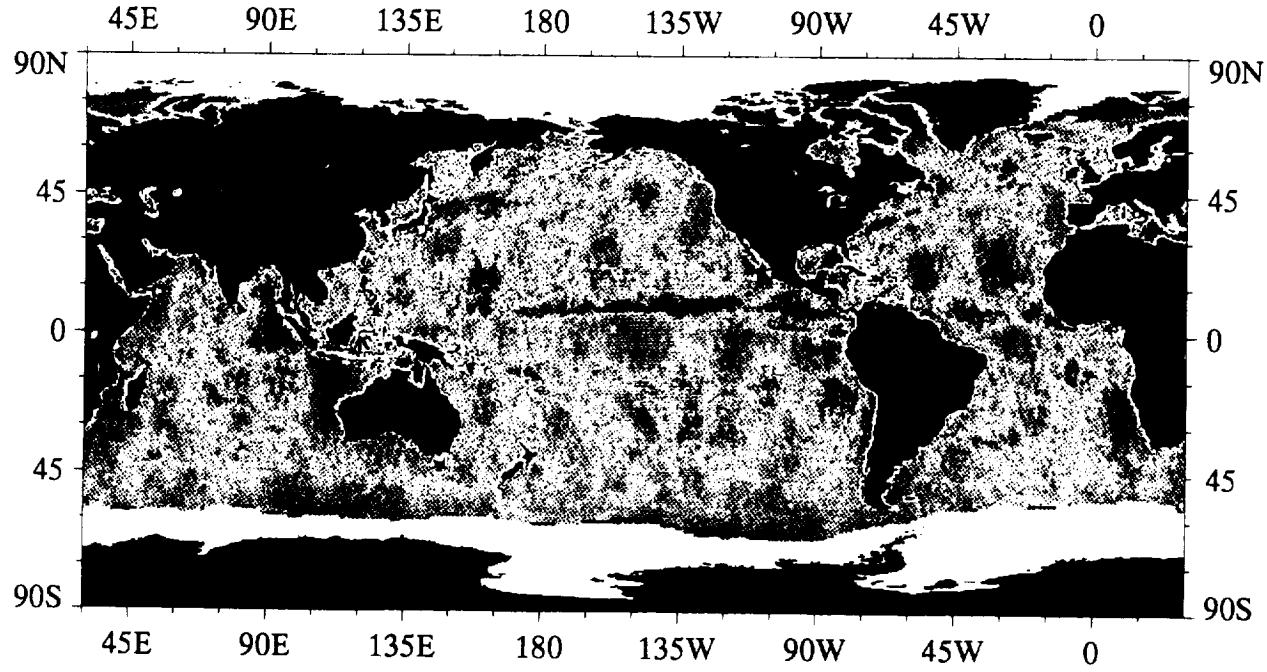

September 1988, max = 120

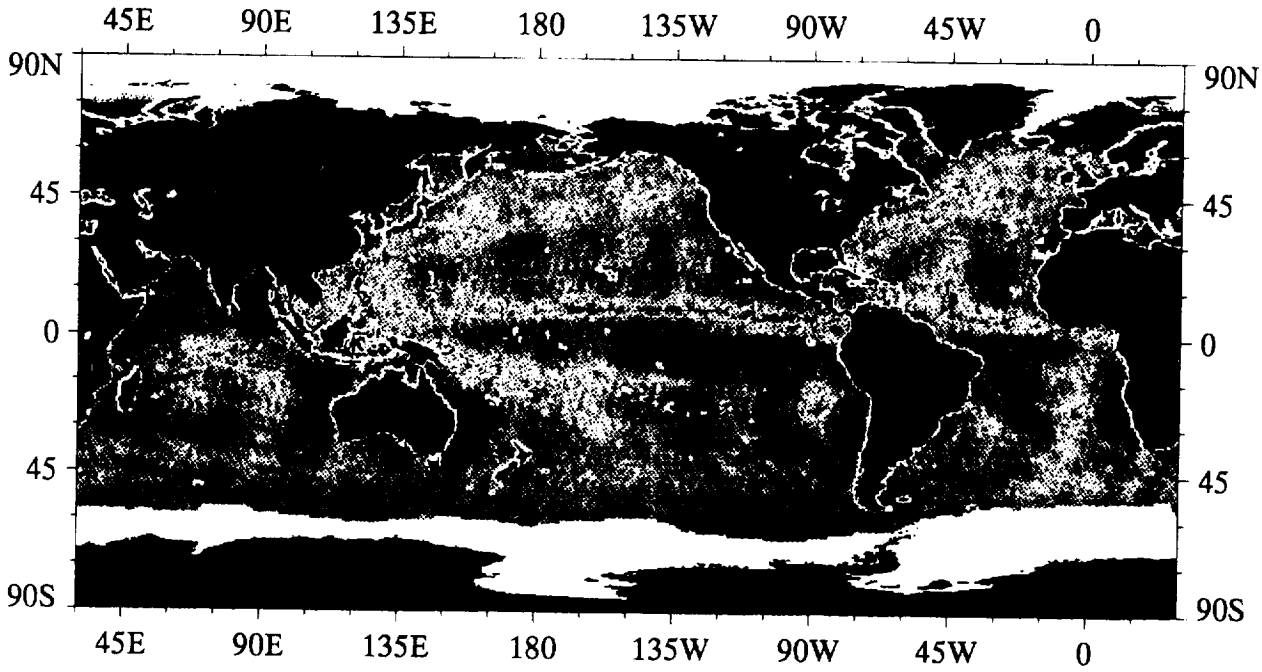

October 1988, max = 144

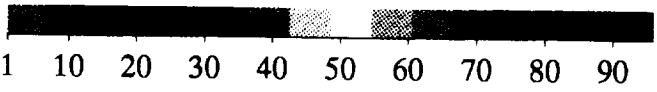

Number of SSMI Wind Speed Values per Pixel

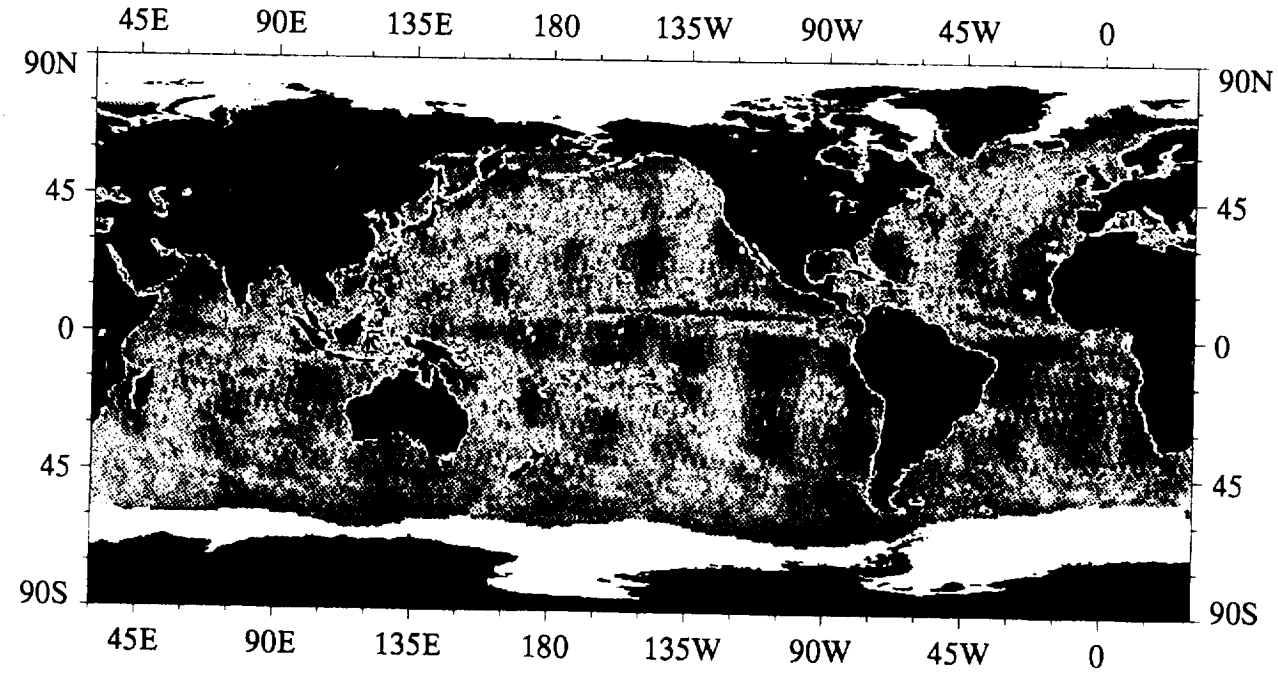

November 1988, max = 126

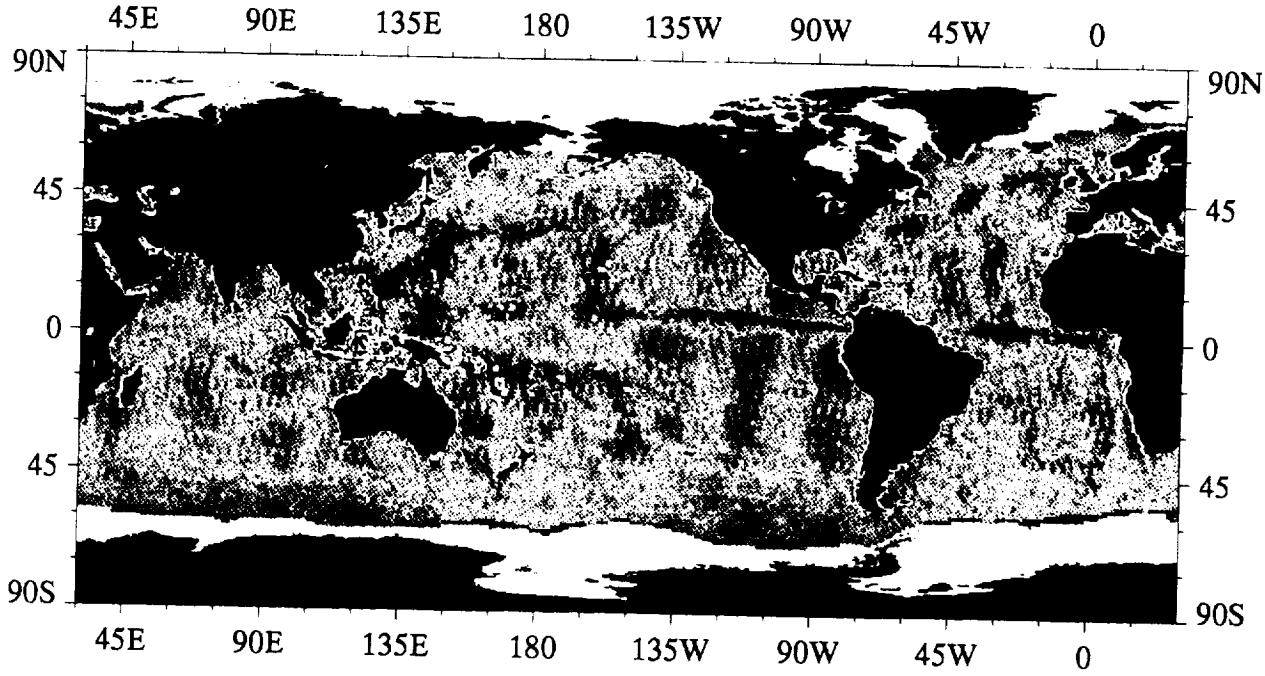

December 1988, max = 110

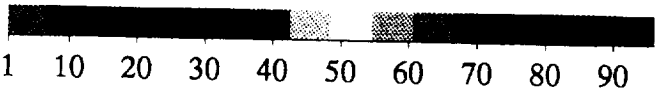

Number of SSMI Wind Speed Values per Pixel

A6

Monthly Standard Deviation of SSMI Surface Wind Speed

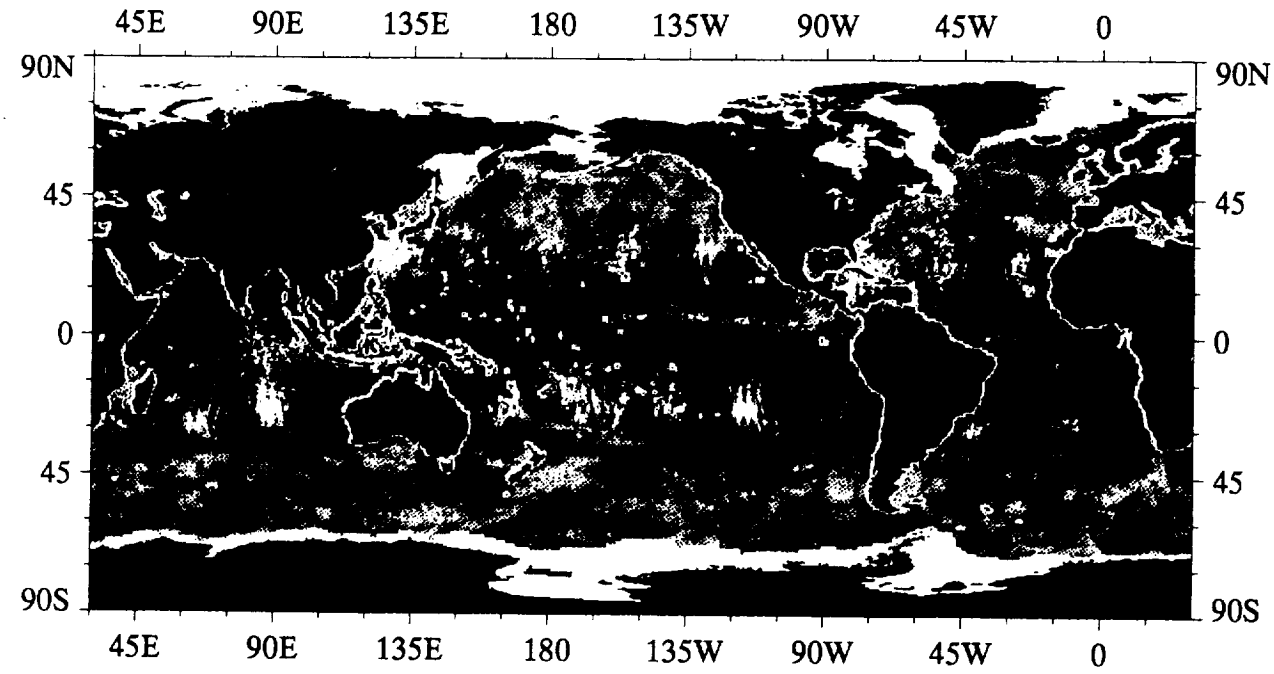

13 - 31 January 1988

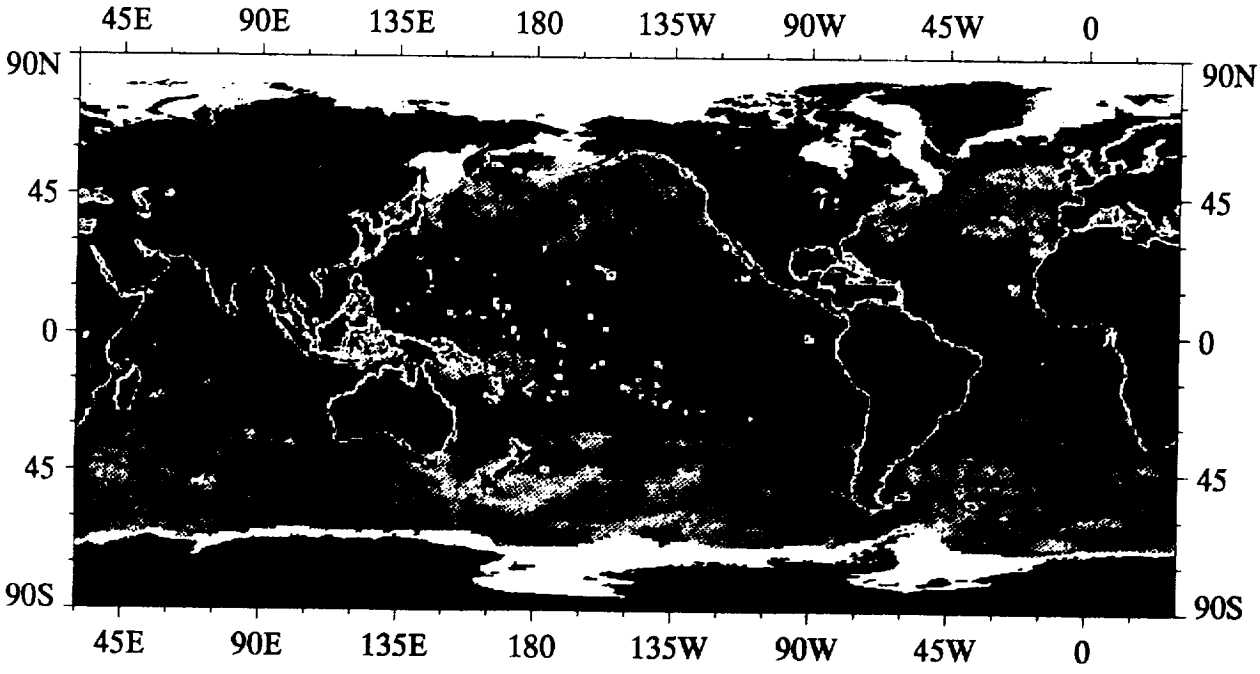

February 1988

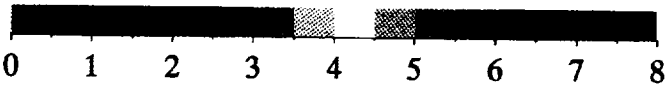

Standard Deviation of SSMI 10 m Wind Speed, m s^{-1}

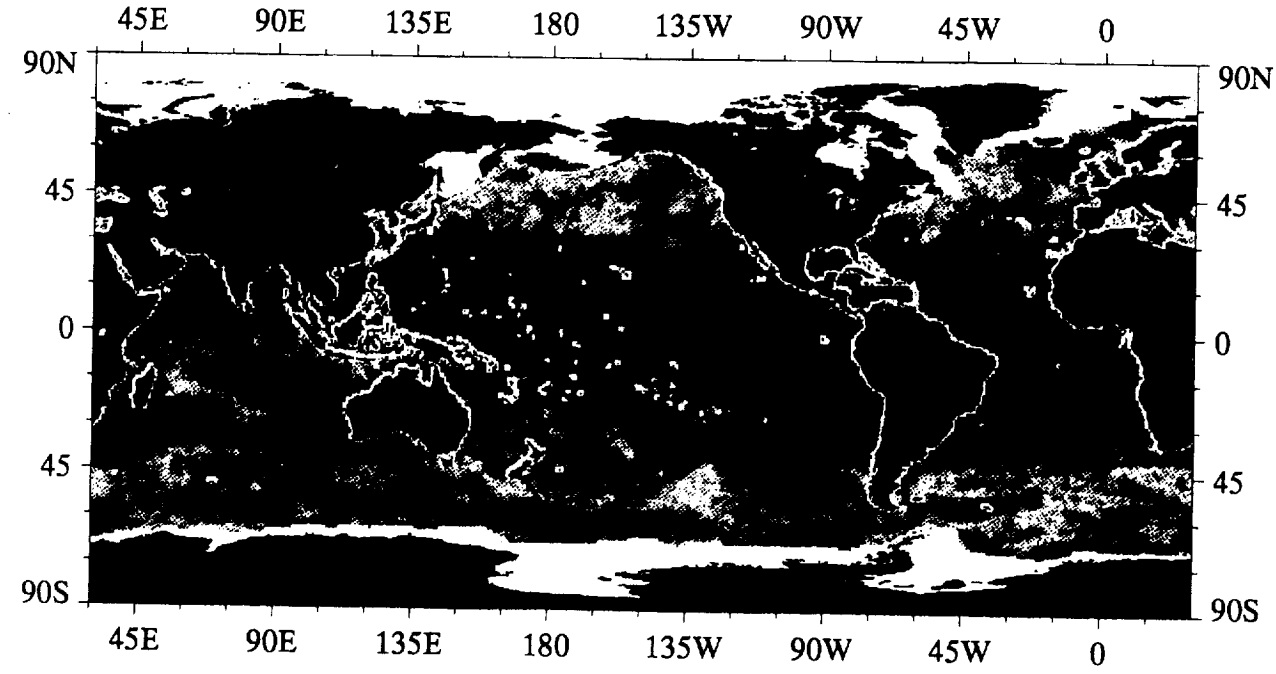

March 1988

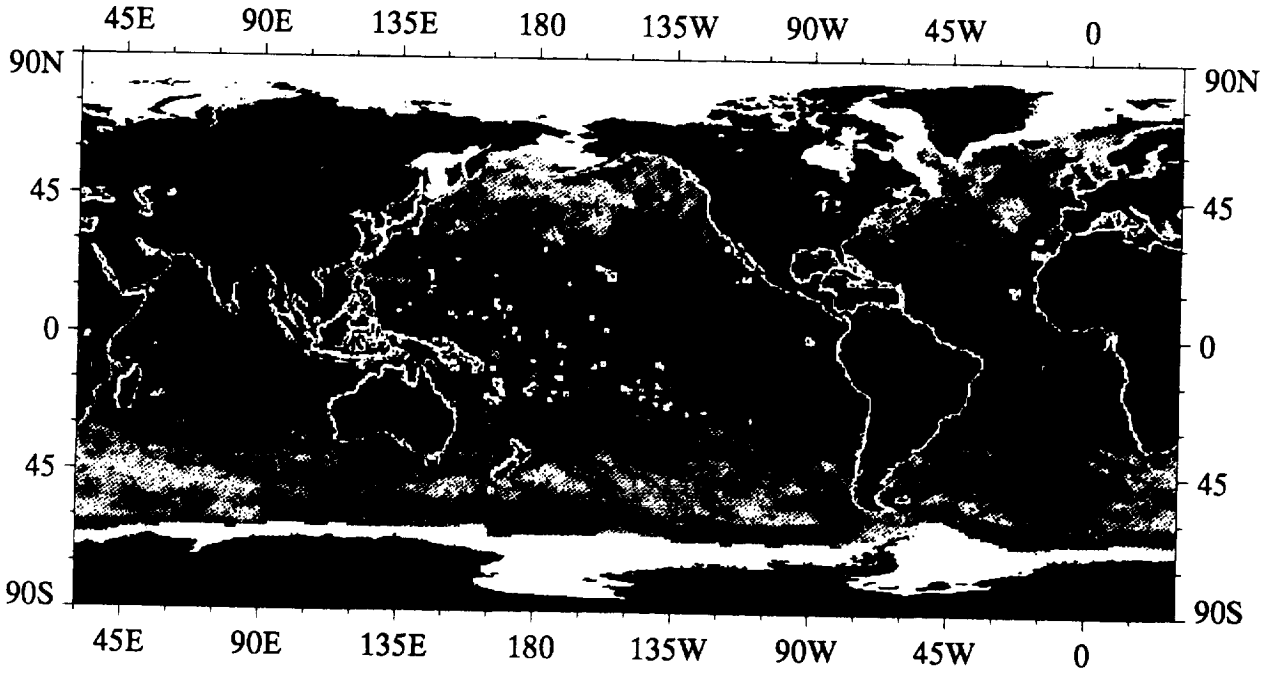

April 1988

Standard Deviation of SSMI 10 m Wind Speed, m s^{-1}

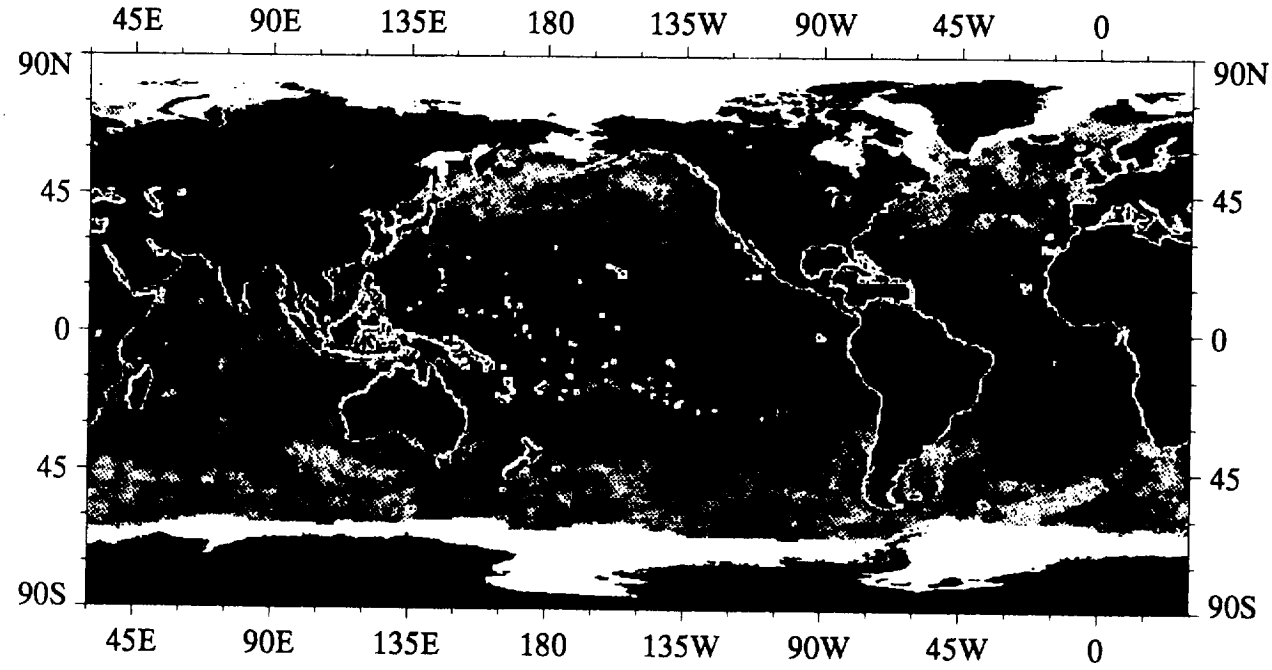

May 1988

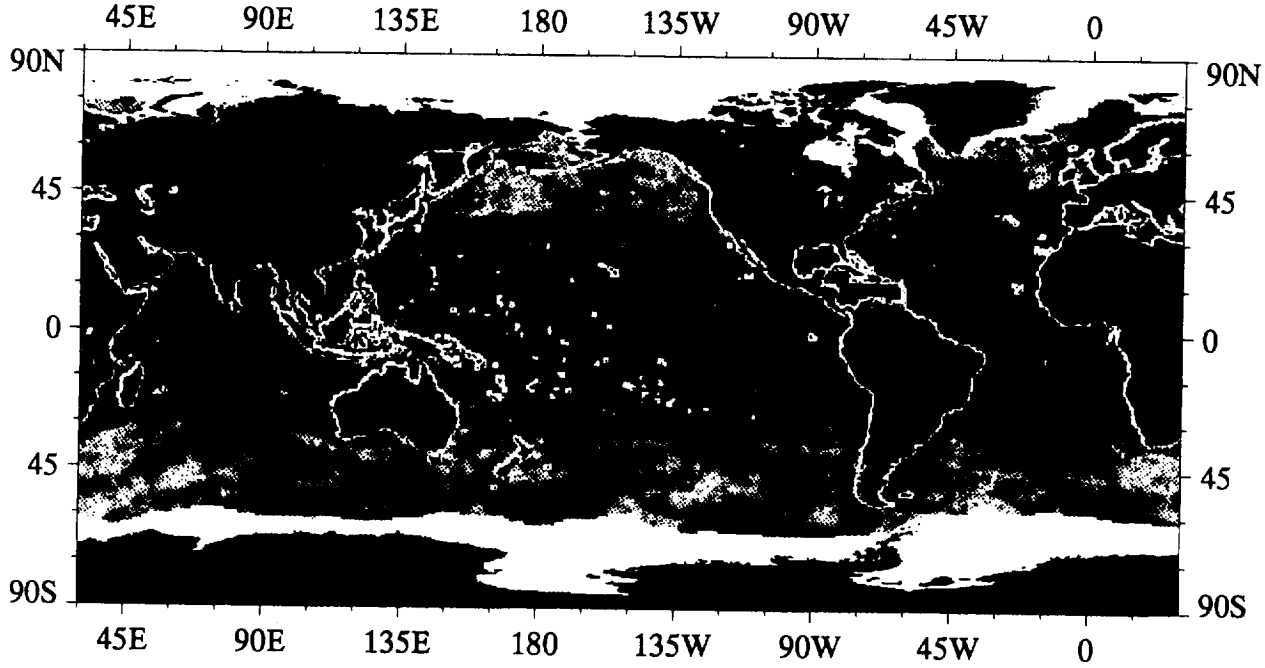

June 1988

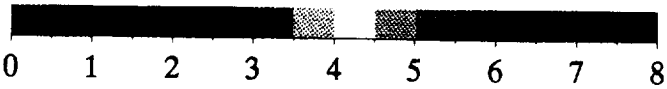

Standard Deviation of SSMI 10 m Wind Speed, m s^{-1}

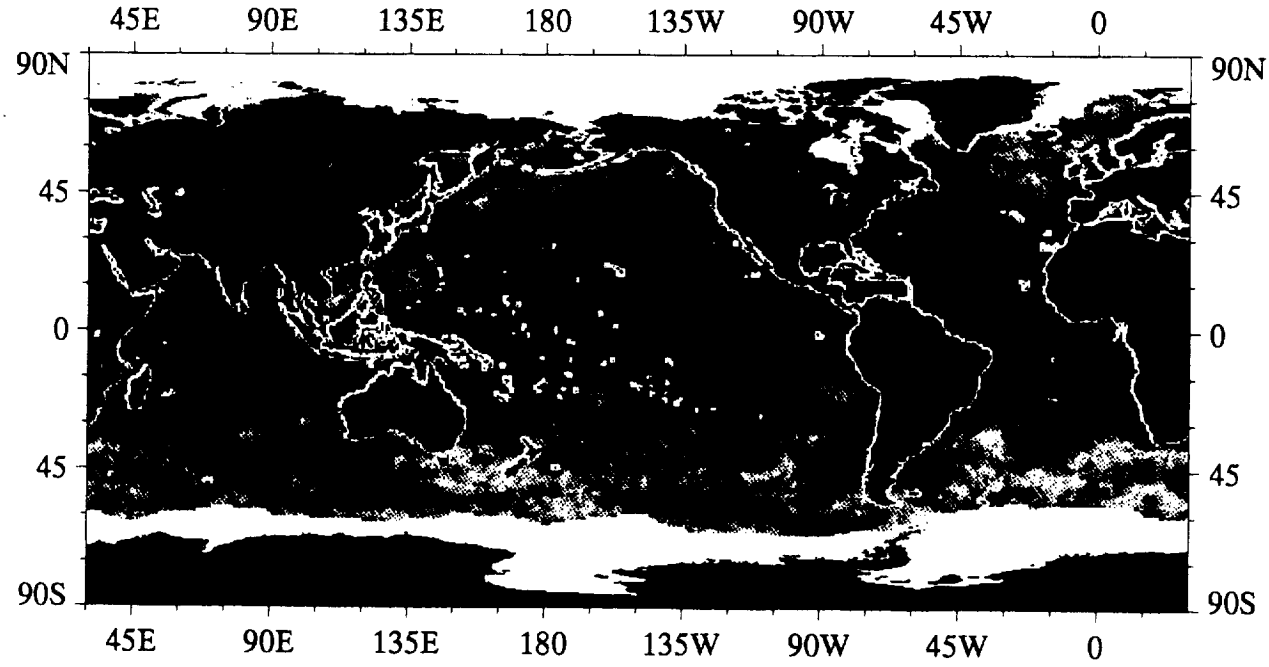

July 1988

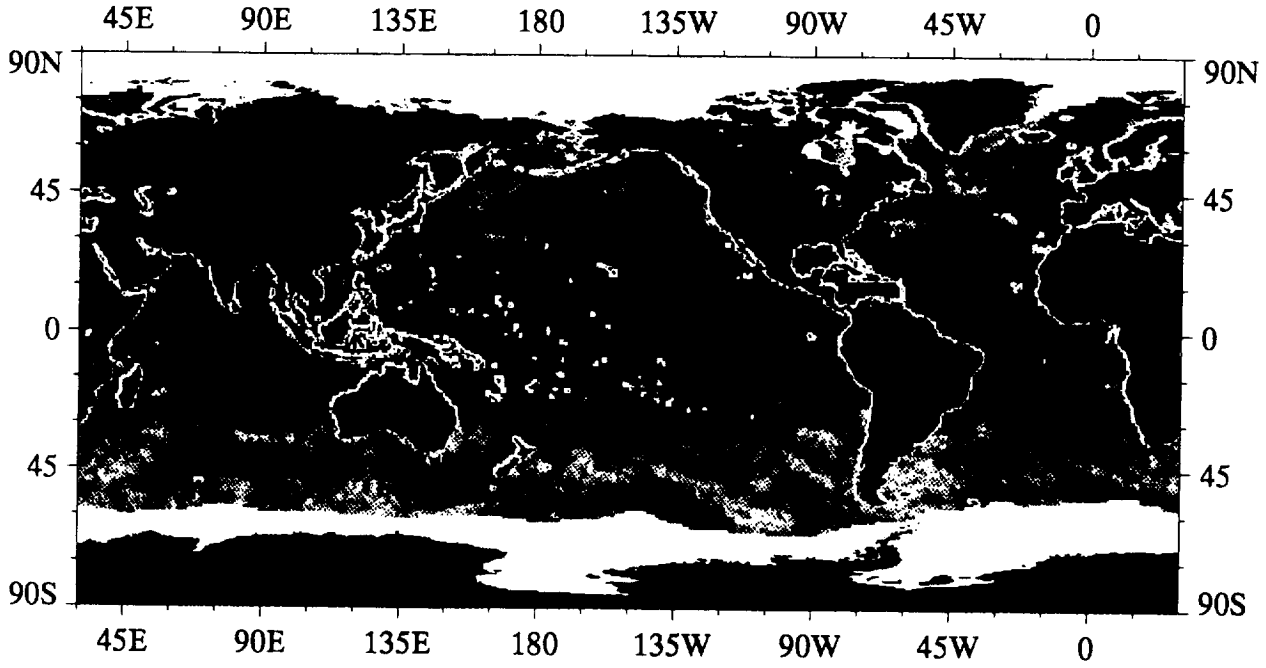

August 1988

Standard Deviation of SSMI 10 m Wind Speed, m s^{-1}

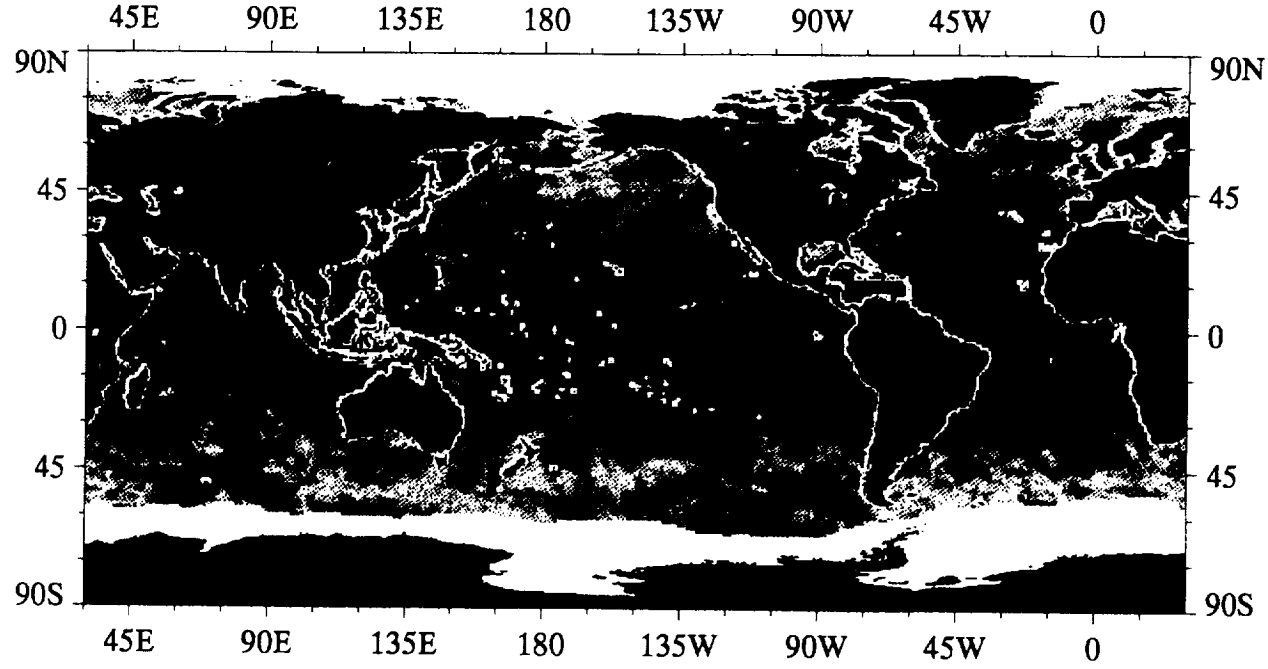

September 1988

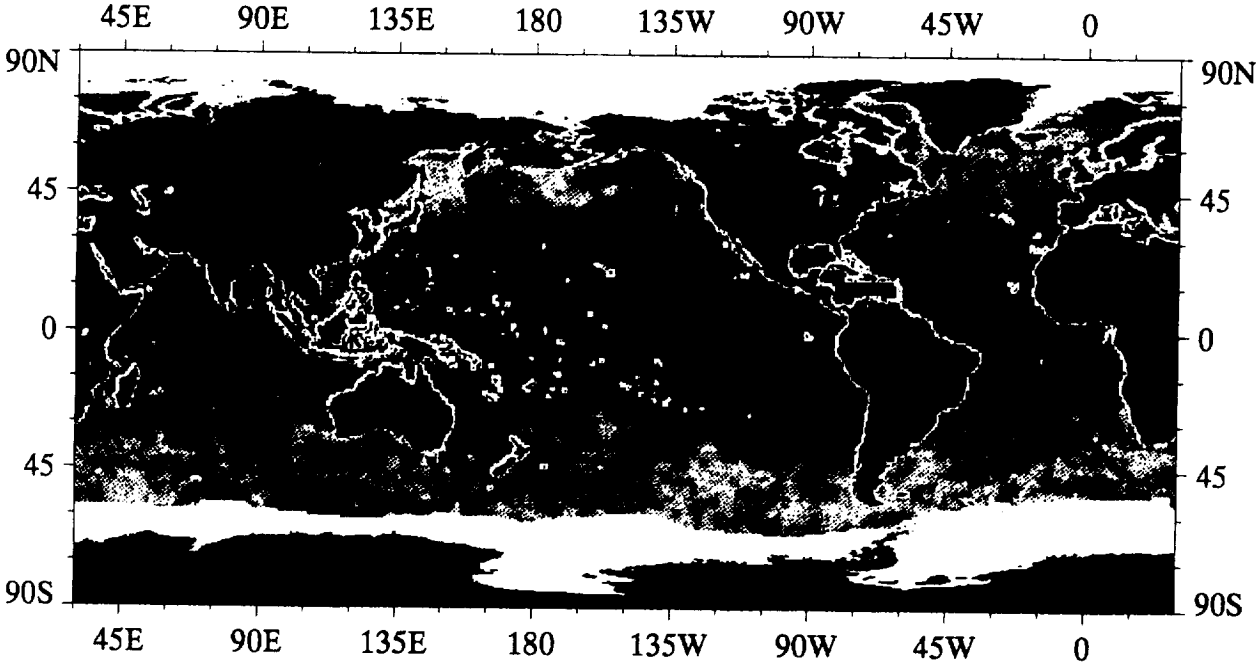

October 1988

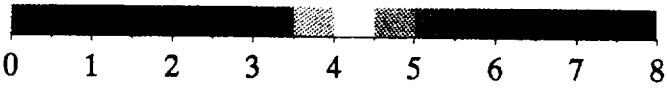

Standard Deviation of SSMI 10 m Wind Speed, m s^{-1}

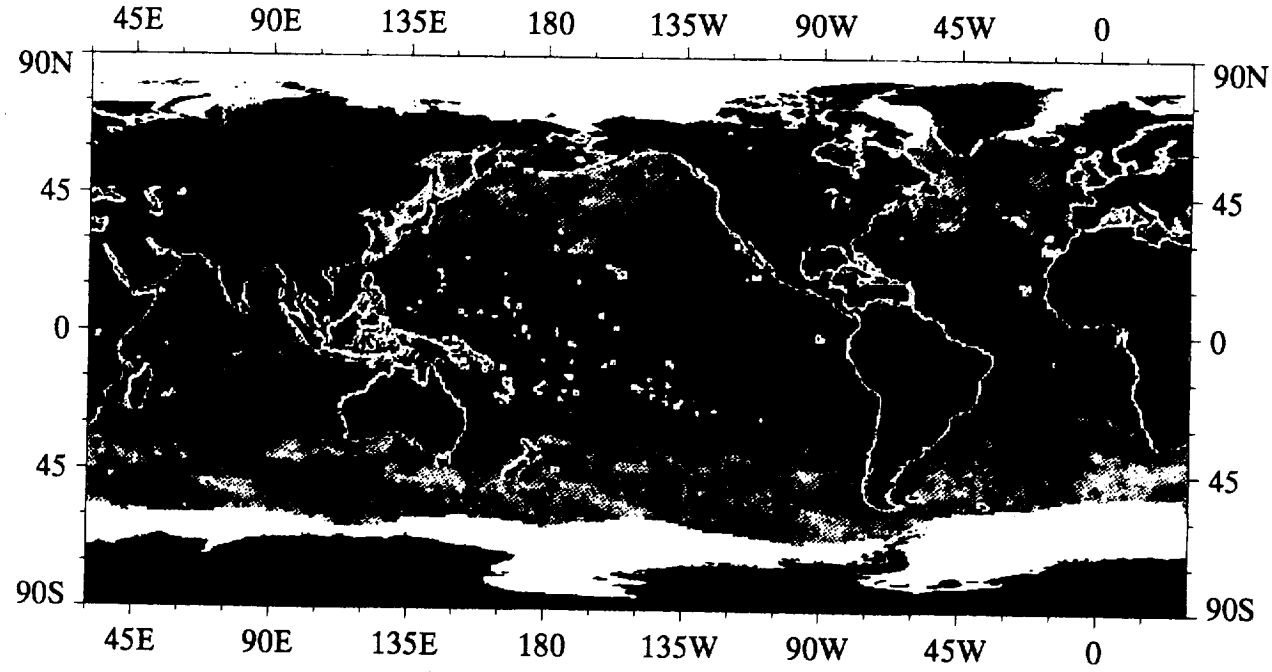

November 1988

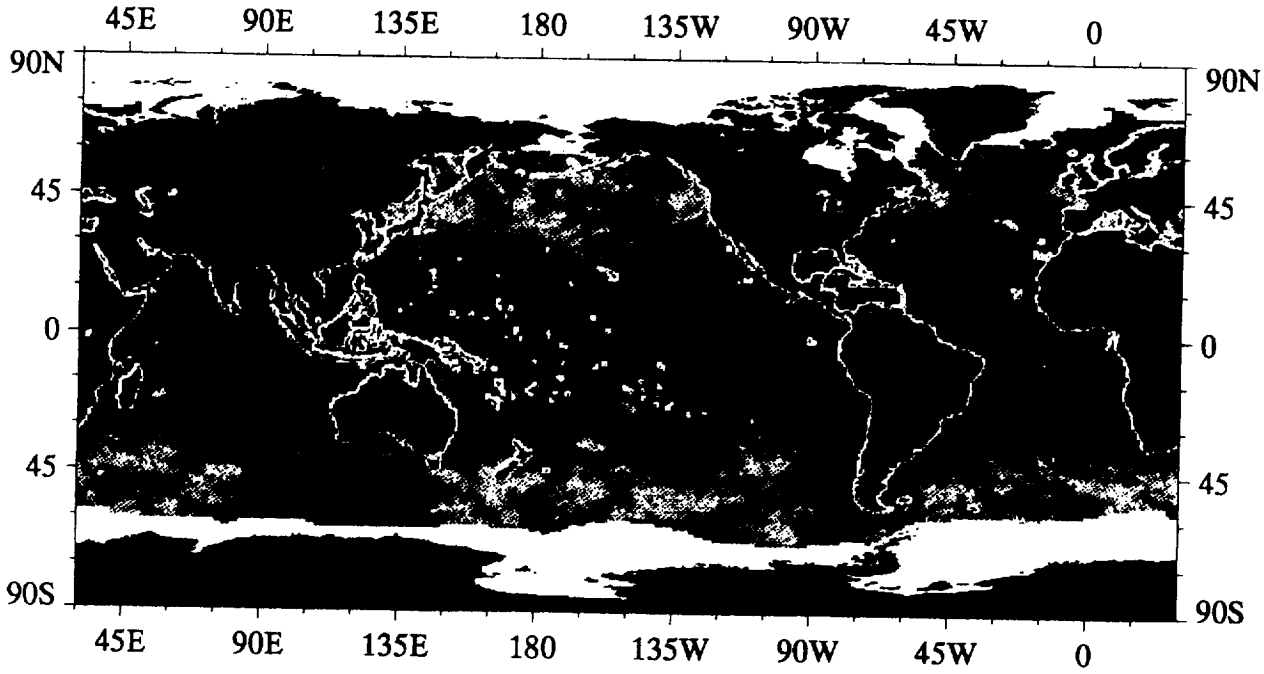

December 1988

Standard Deviation of SSMI 10 m Wind Speed, m s^{-1}

A7

Annual Mean and Sampling Distribution of AVHRR/2 Sea Surface Temperature

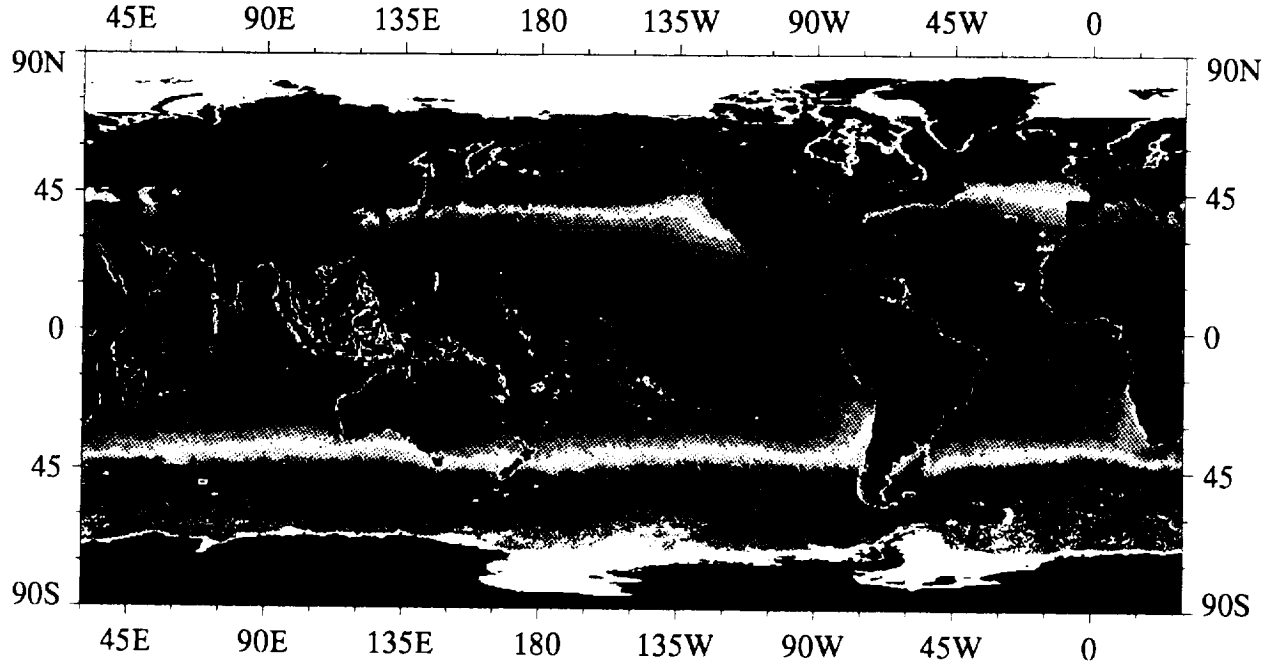

Annual Mean 1988

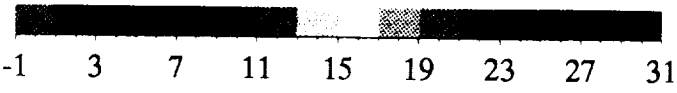

AVHRR Sea Surface Temperature, °C

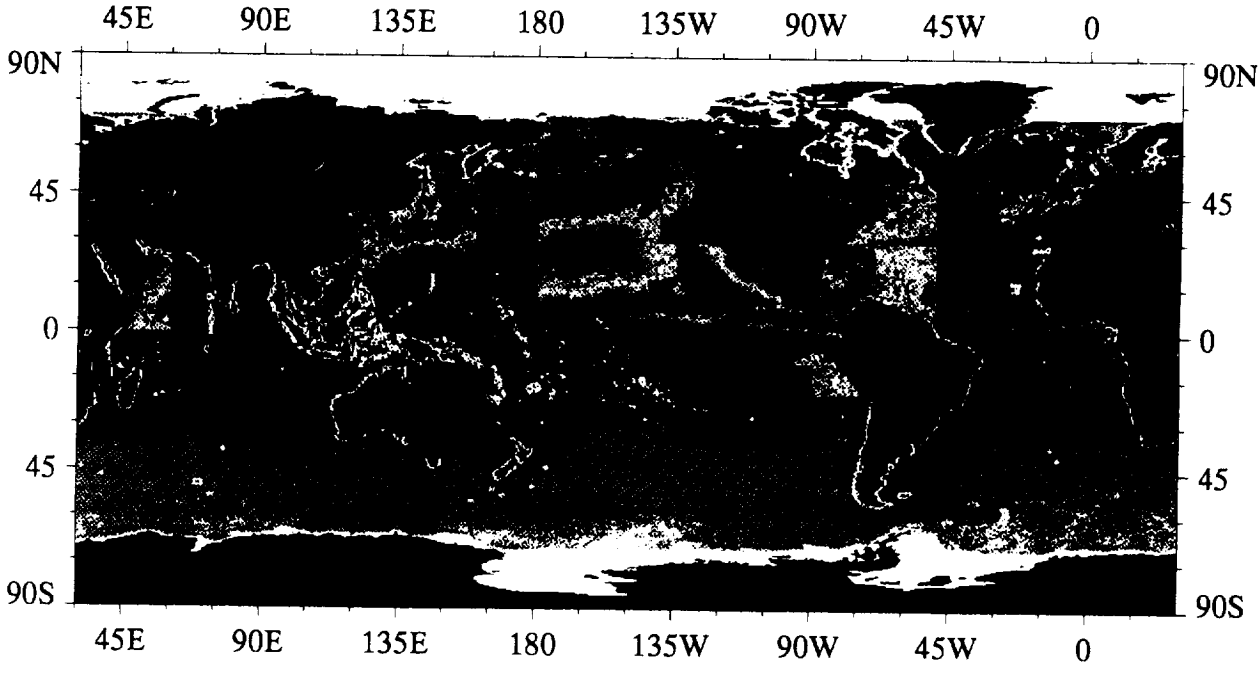

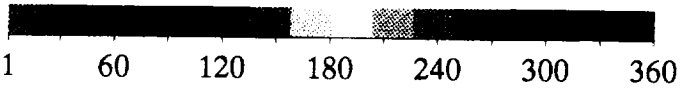

Number of Sea Surface Temperature Values per Pixel During 1988, max = 1929

A8

28-Day Mean AVHRR/2 Sea Surface Temperature

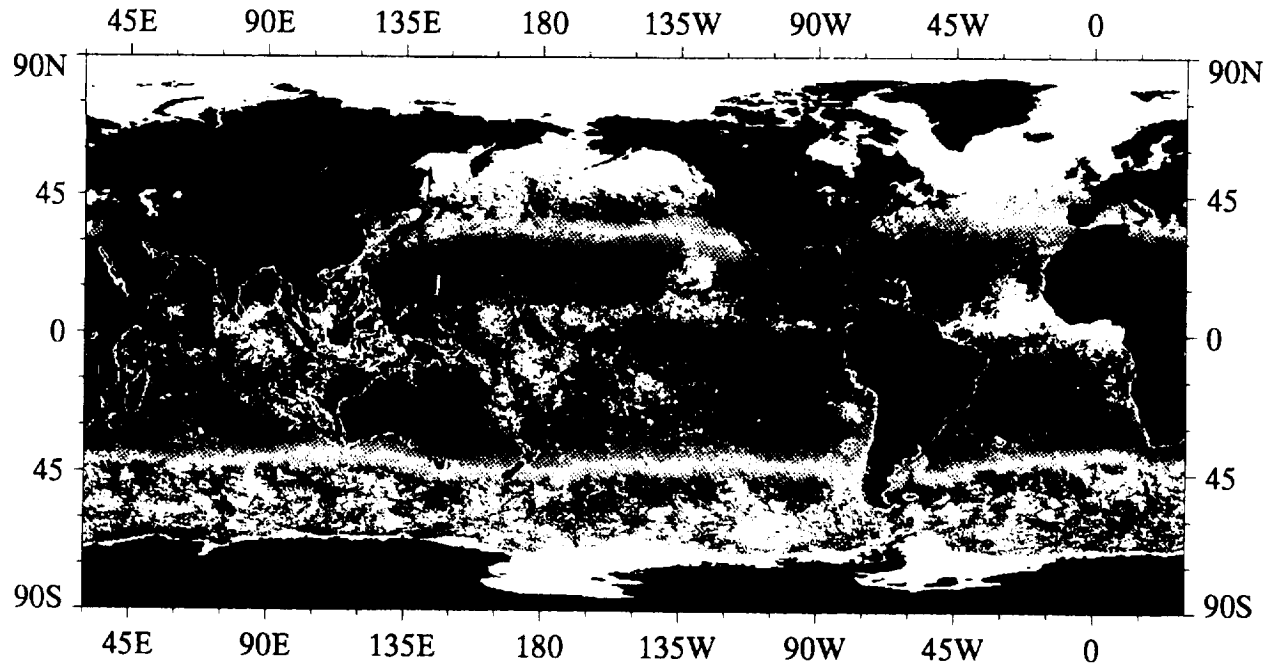

7 January to 3 February 1988

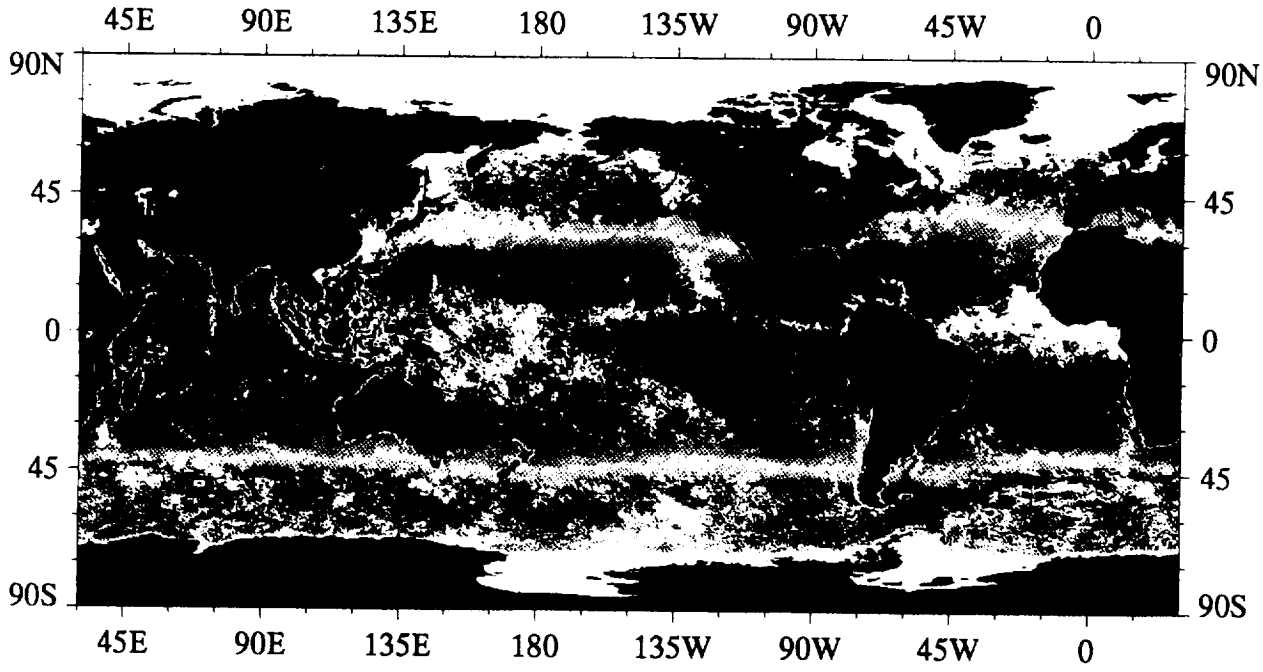

4 February to 2 March 1988

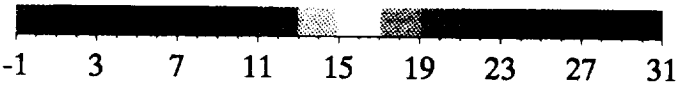

AVHRR Sea Surface Temperature, °C

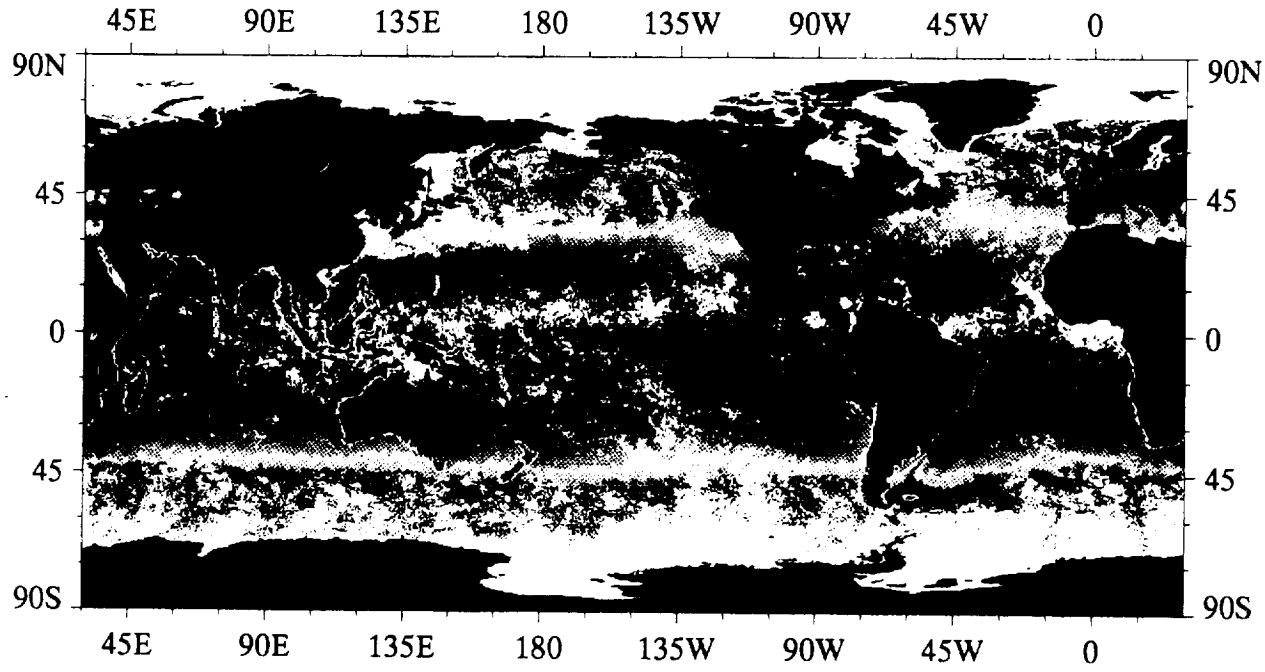

3 March to 30 March 1988

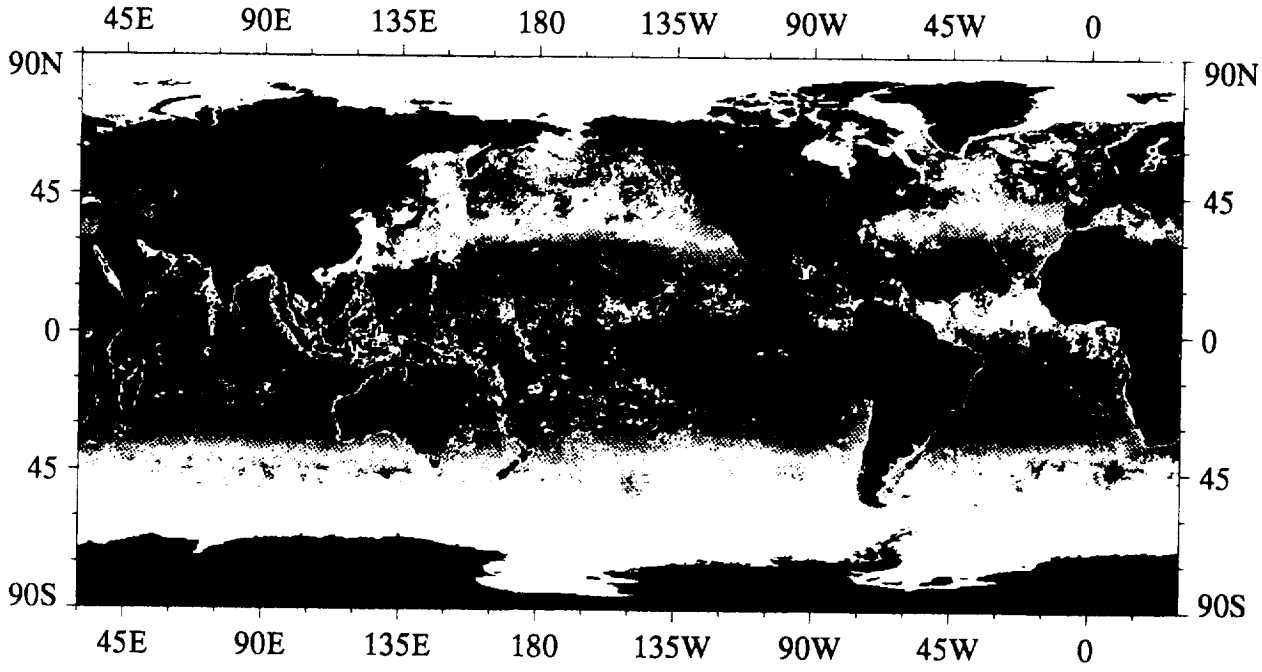

31 March to 27 April 1988

AVHRR Sea Surface Temperature, °C

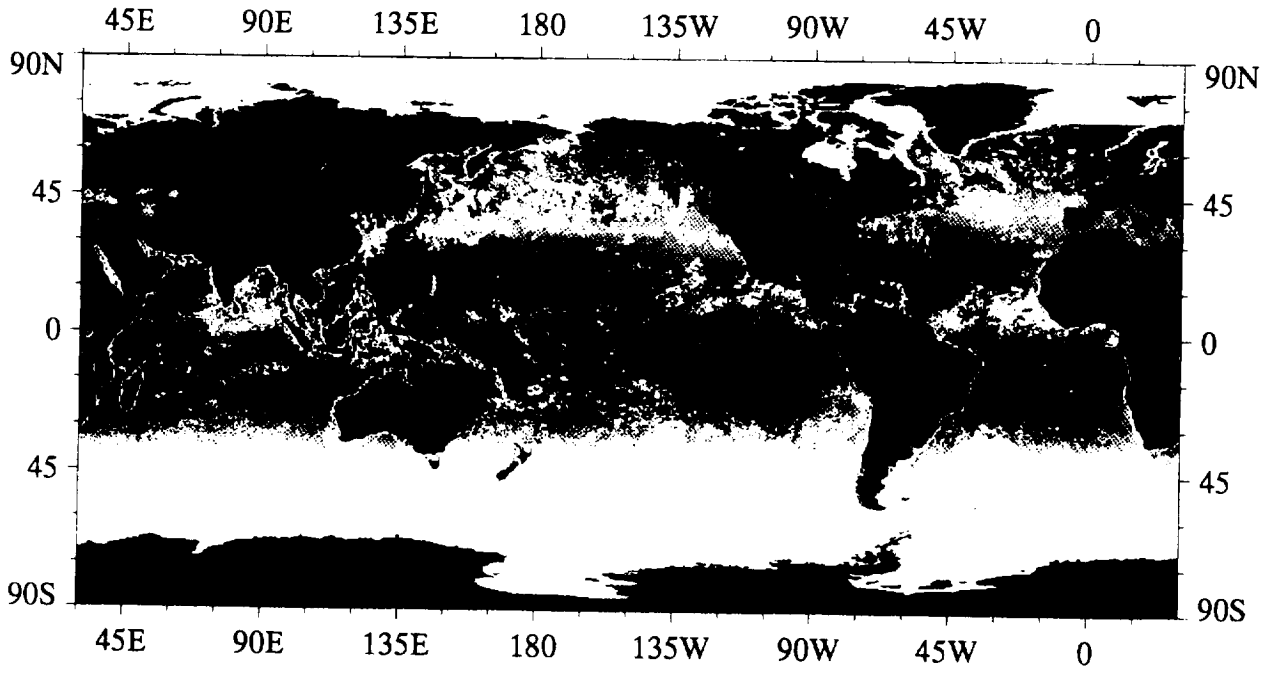

28 April to 25 May 1988

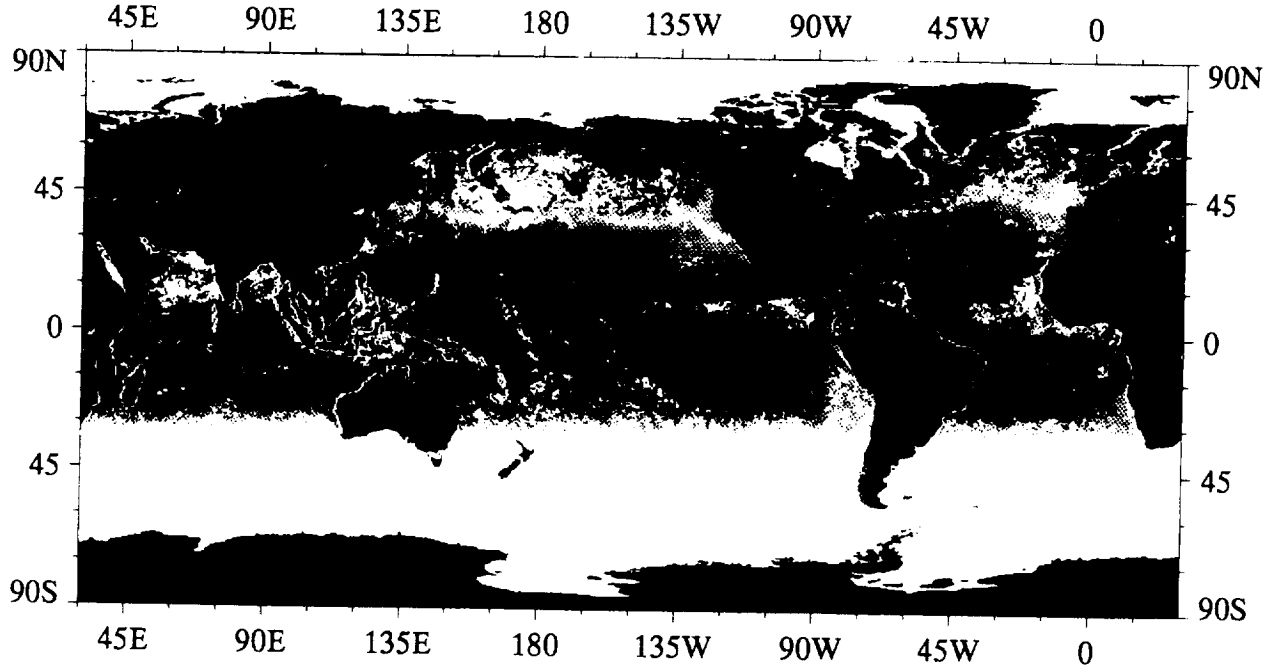

2 June to 29 June 1988

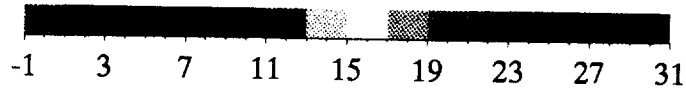

AVHRR Sea Surface Temperature, °C

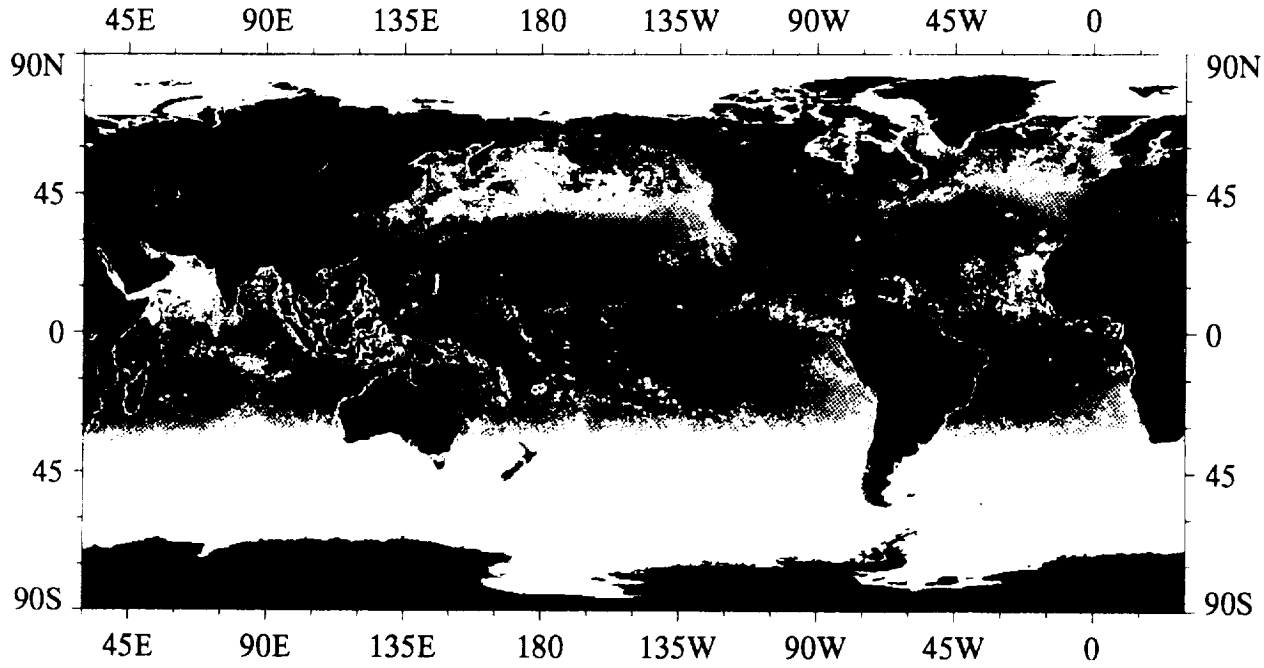

30 June to 27 July 1988

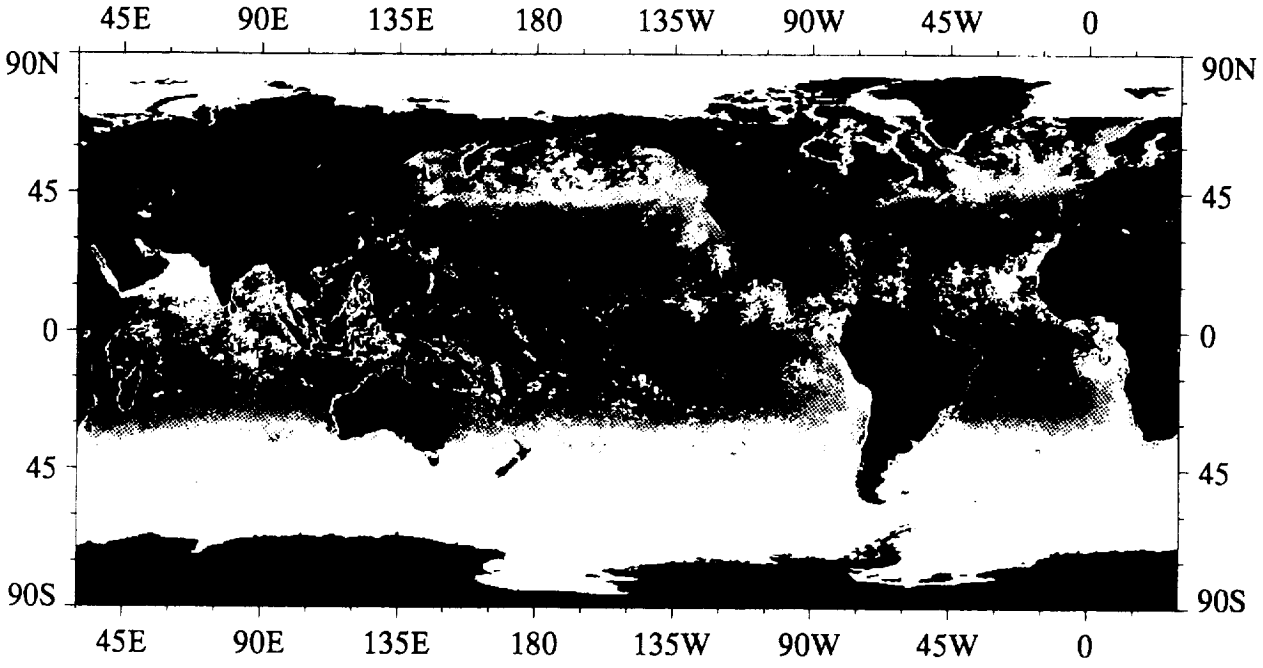

4 August to 31 August 1988

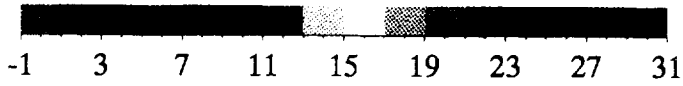

AVHRR Sea Surface Temperature, °C

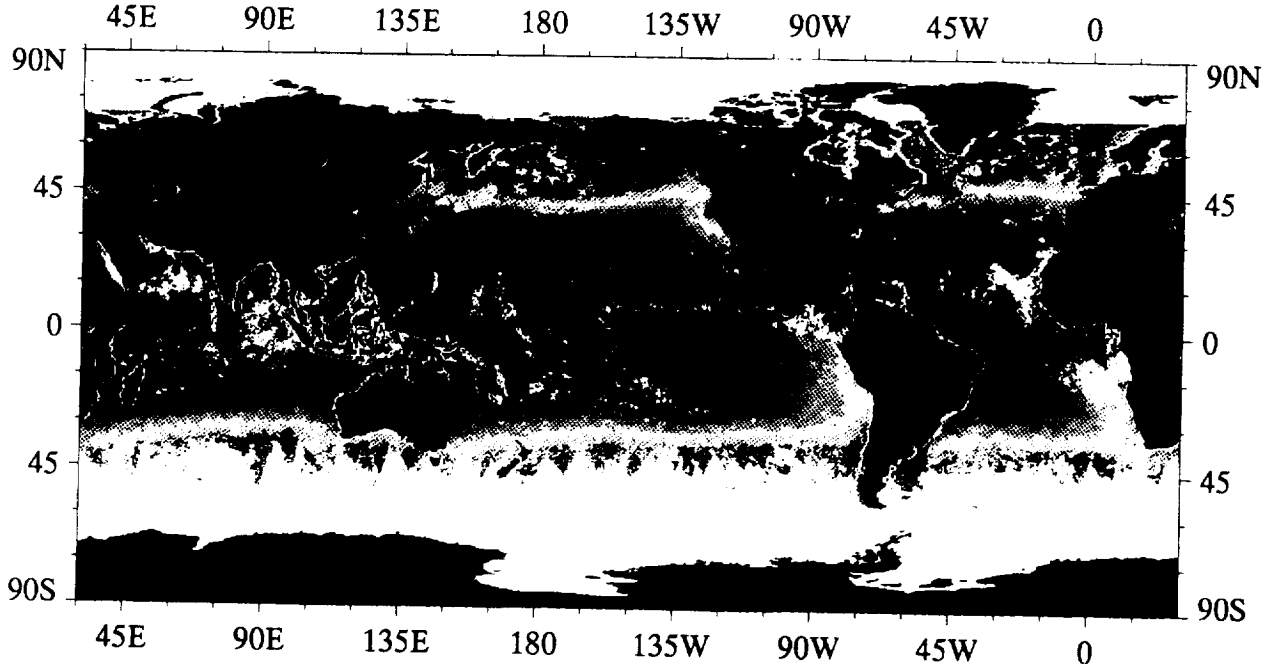

1 September to 28 September 1988

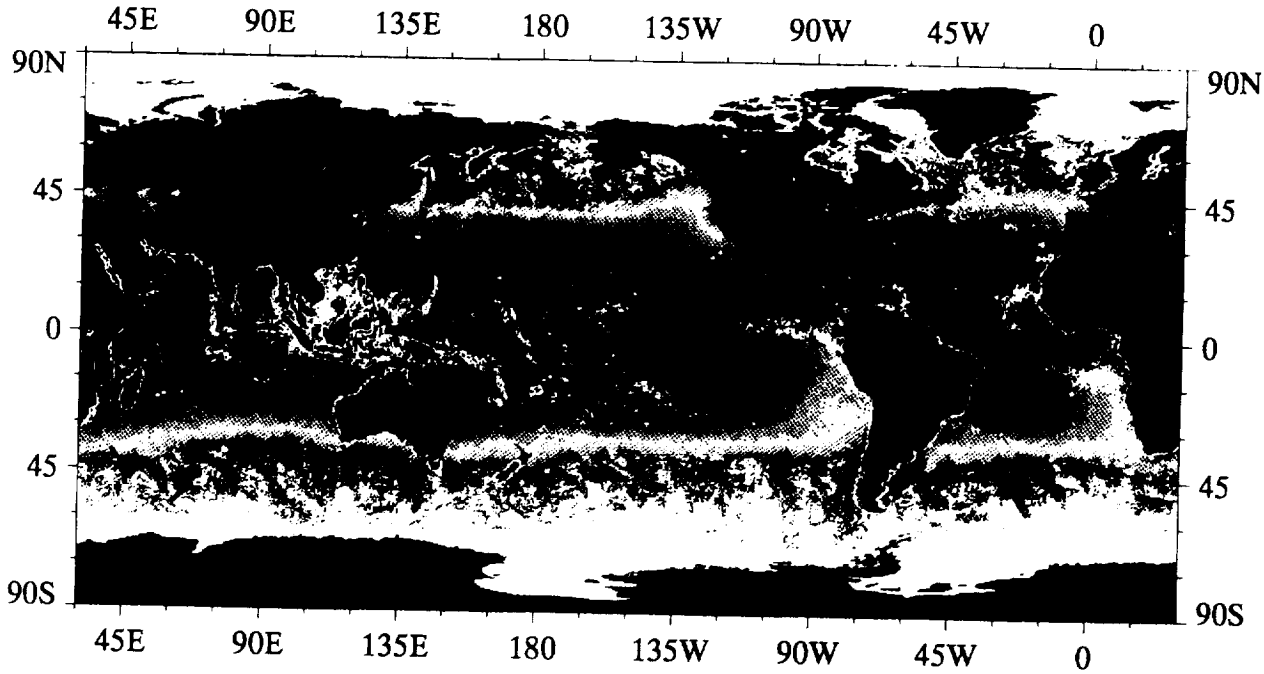

29 September to 26 October 1988

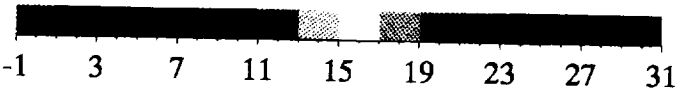

AVHRR Sea Surface Temperature, °C

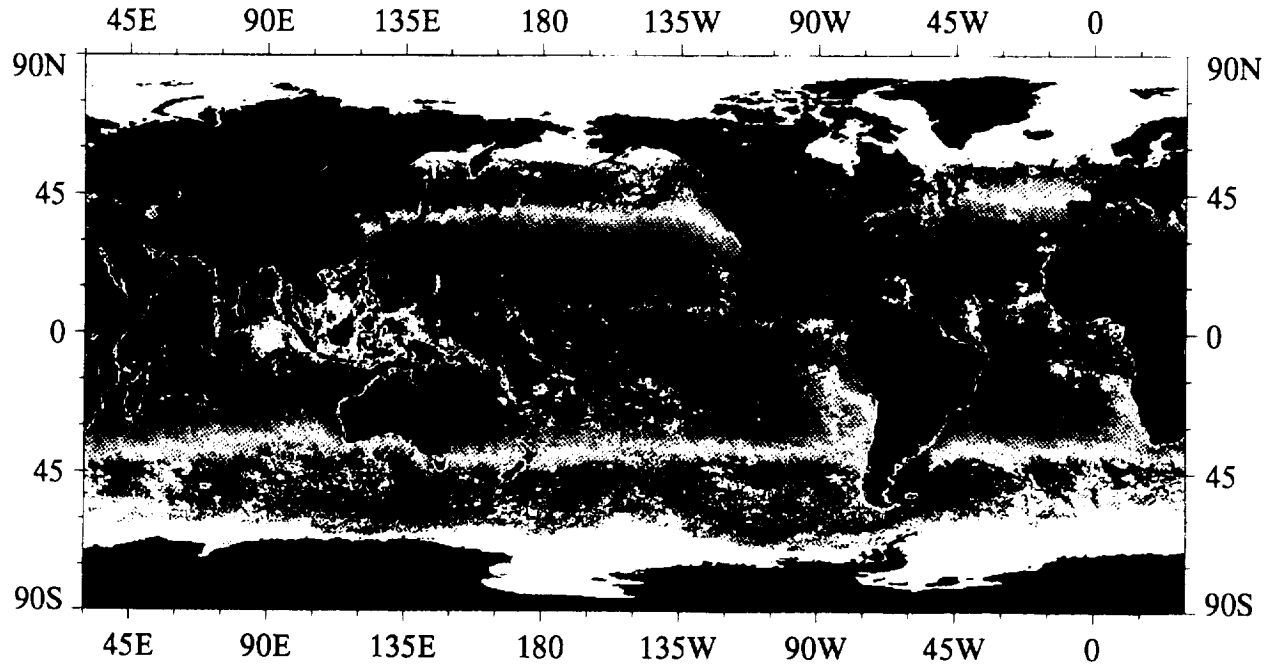

27 October to 23 November 1988

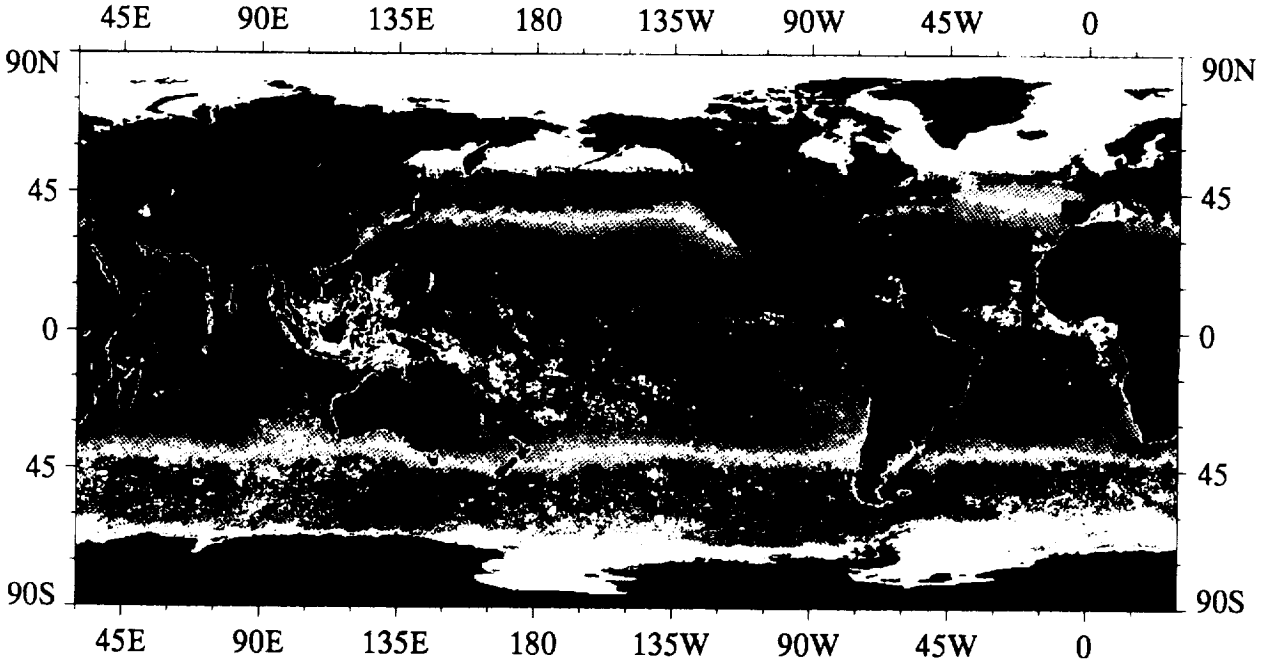

1 December to 28 December 1988

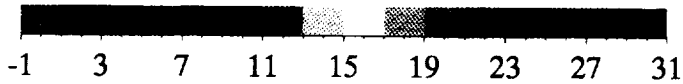

AVHRR Sea Surface Temperature, °C

A9

28-Day AVHRR/2 Sampling Distribution

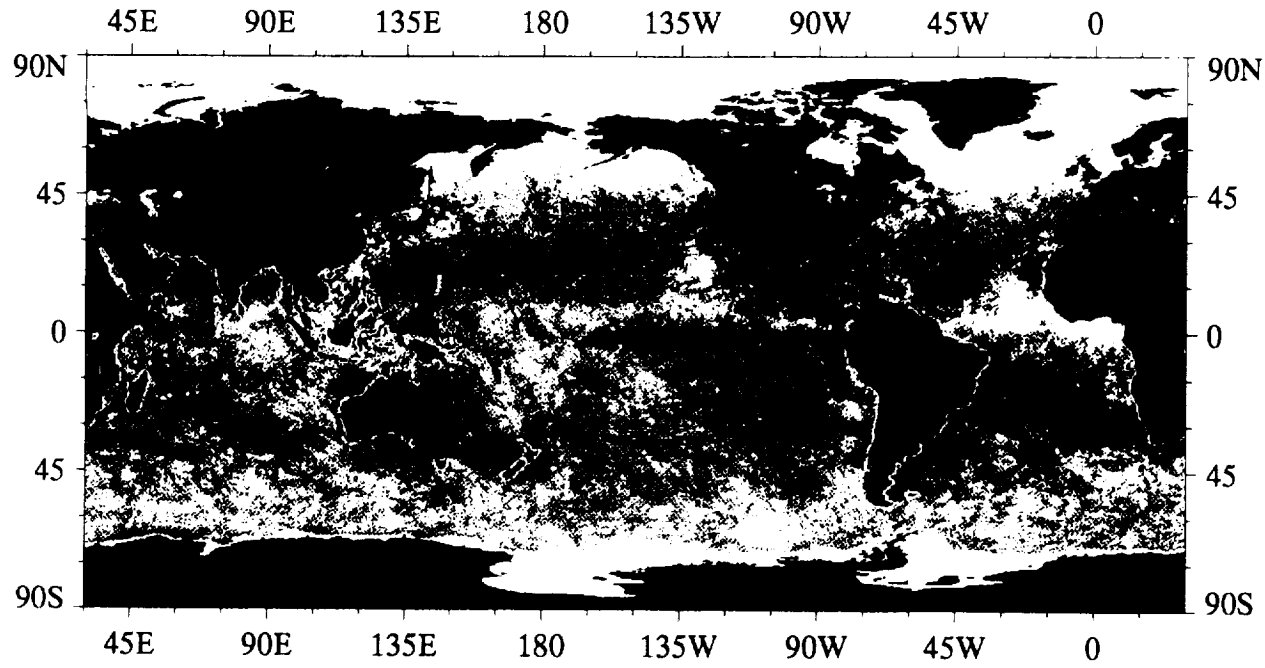

7 January to 3 February 1988, max = 261

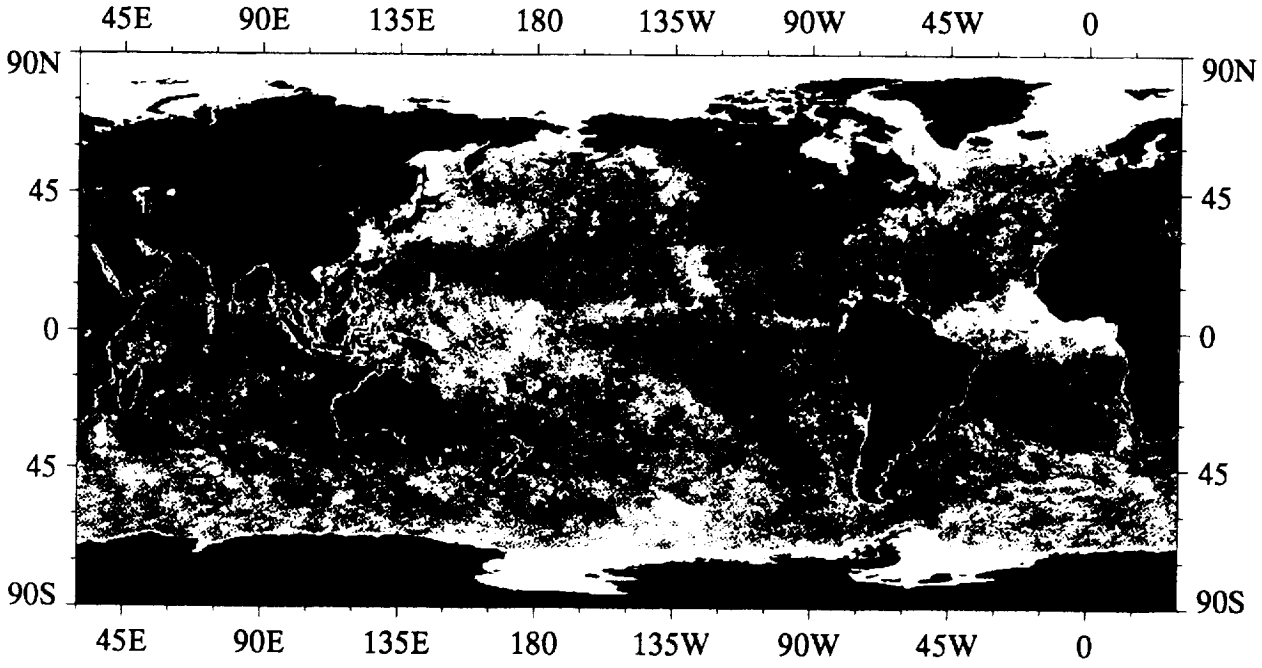

4 February to 2 March 1988, max = 168

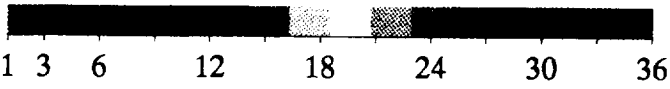

Number of AVHRR Sea Surface Temperature Values per Pixel

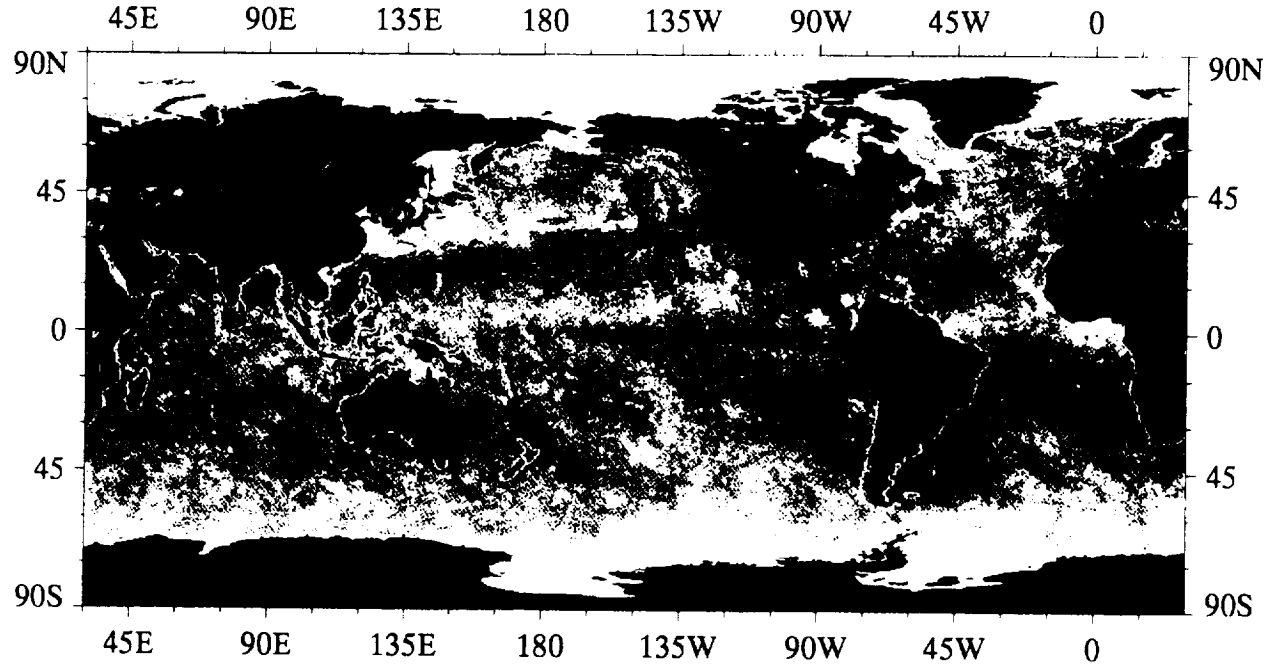

3 March to 30 March 1988, max = 171

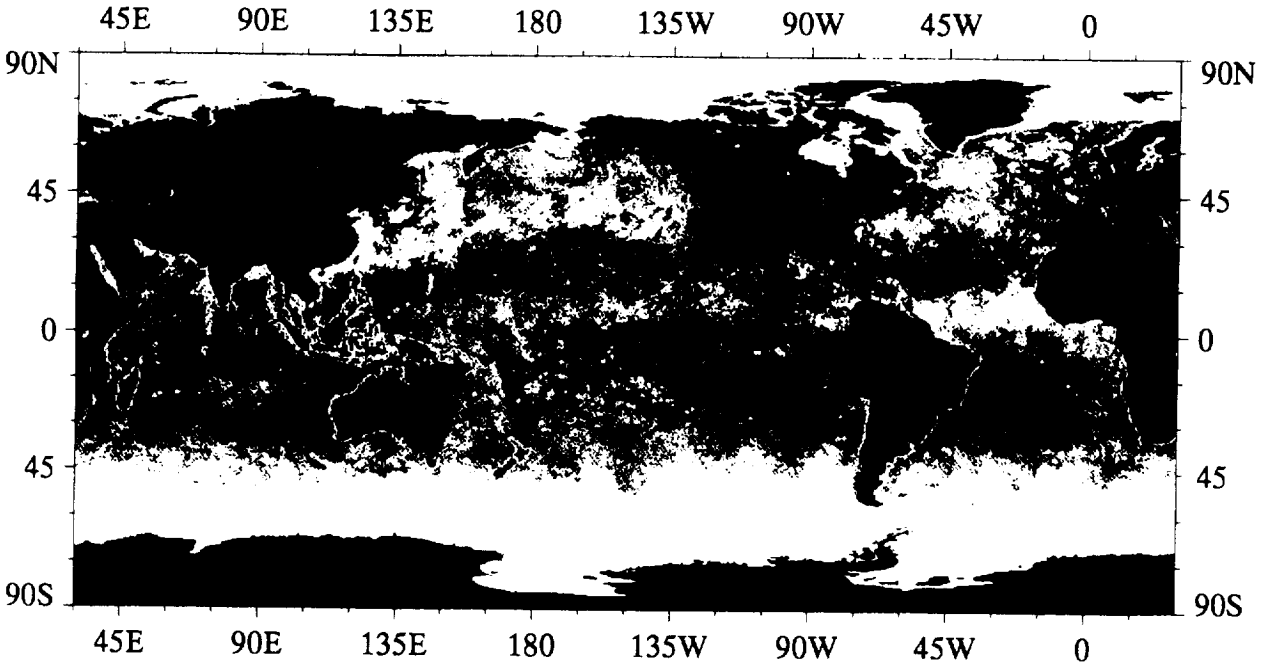

31 March to 27 April 1988, max = 191

Number of AVHRR Sea Surface Temperature Values per Pixel

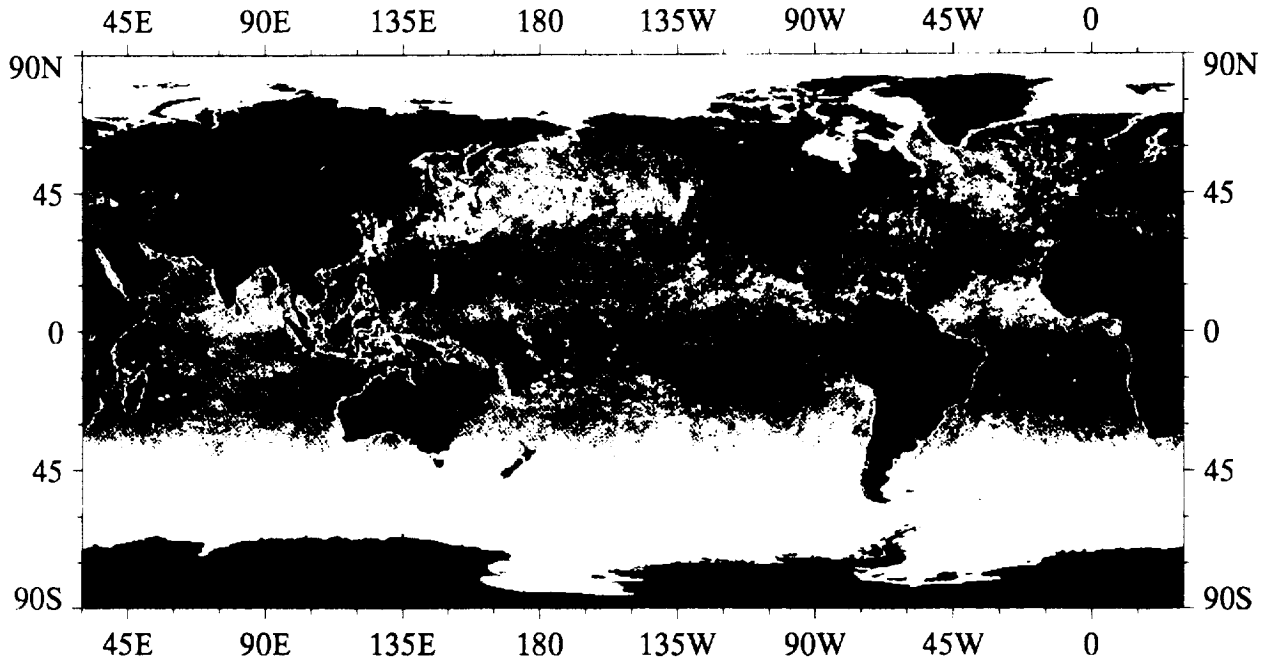

28 April to 25 May 1988, max = 221

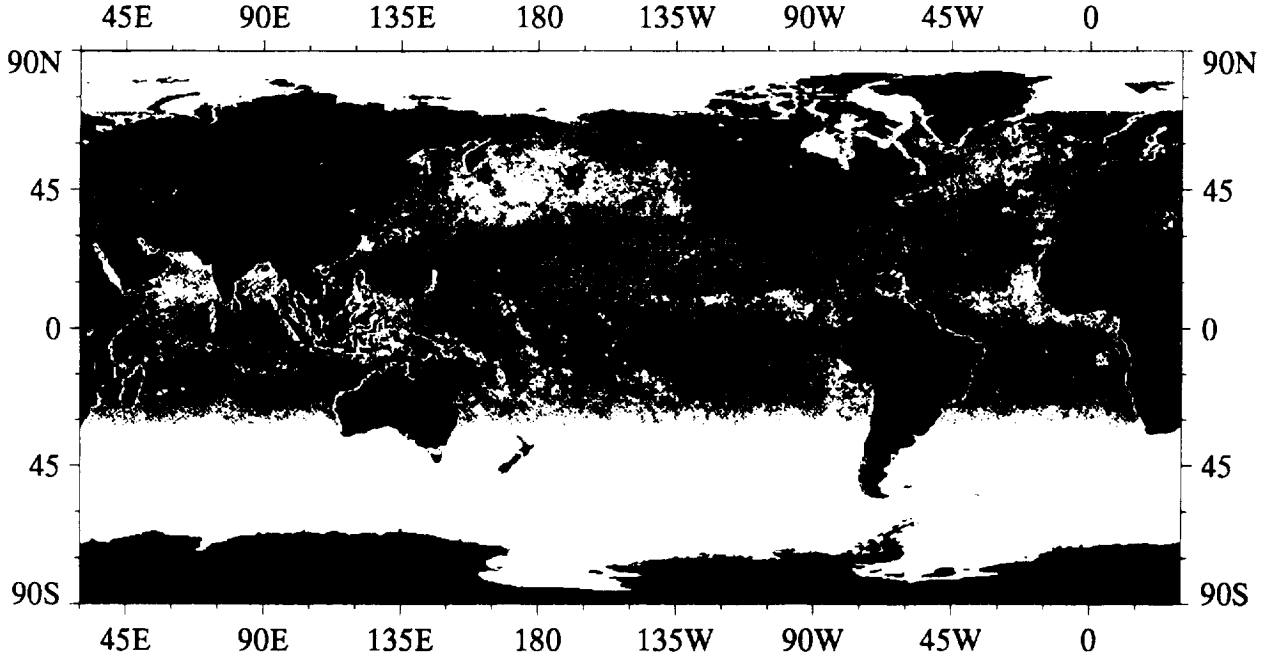

2 June to 29 June 1988, max = 259

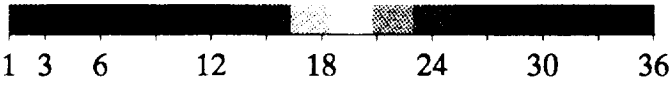

Number of AVHRR Sea Surface Temperature Values per Pixel

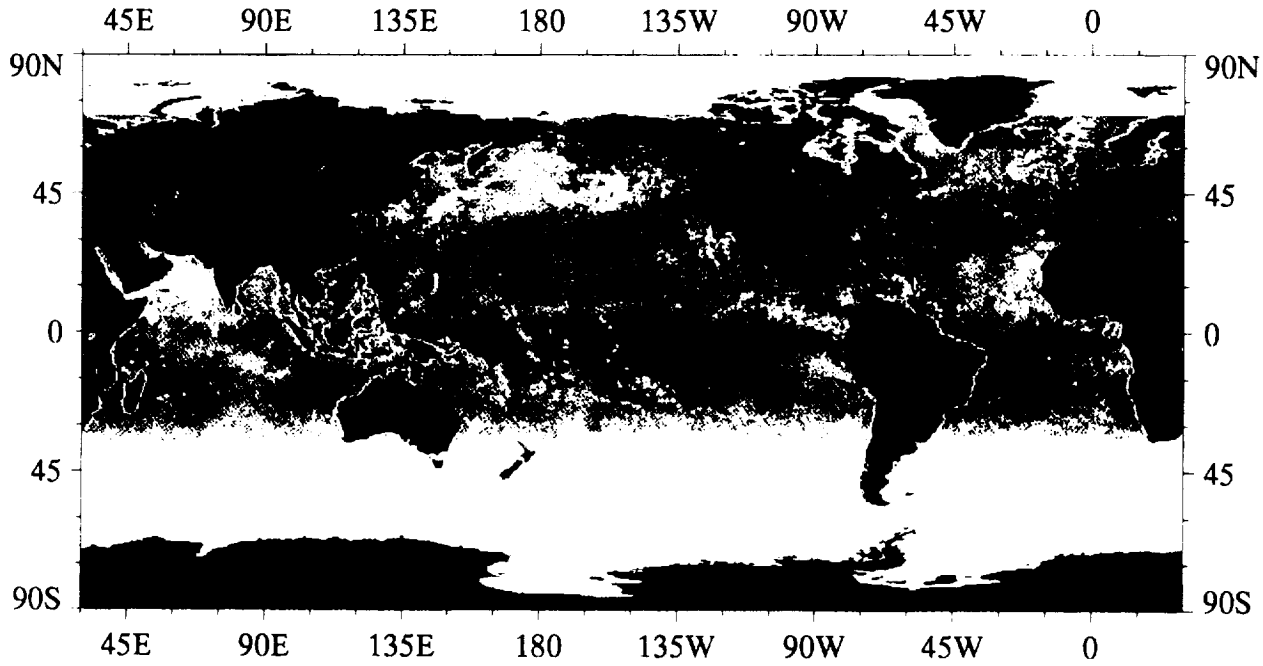

30 June to 27 July 1988, max = 207

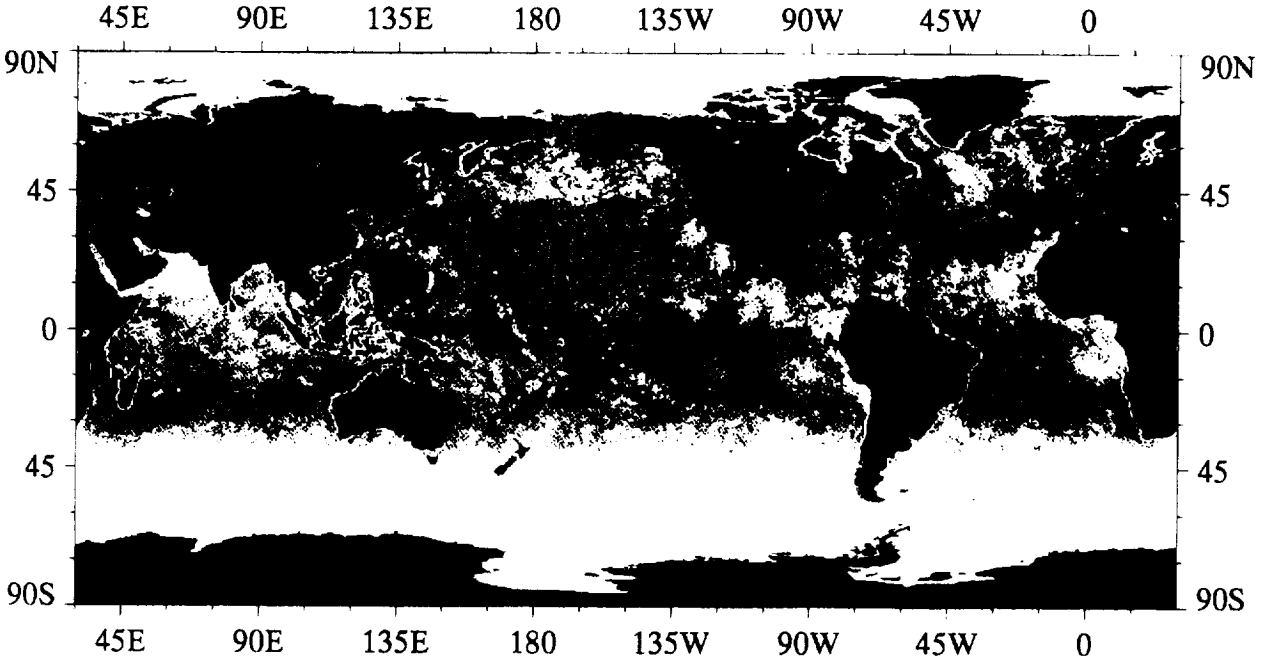

4 August to 31 August 1988, max = 168

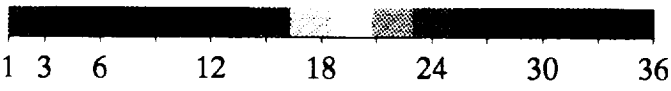

Number of AVHRR Sea Surface Temperature Values per Pixel

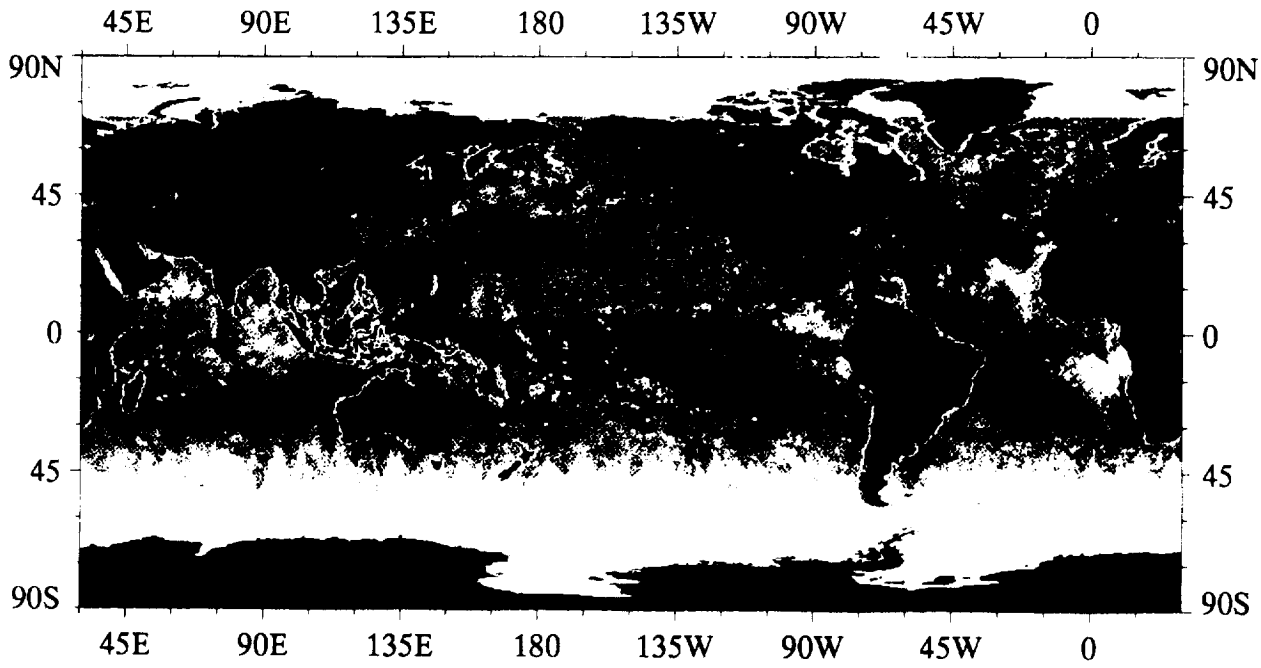

1 September to 28 September 1988, max = 290

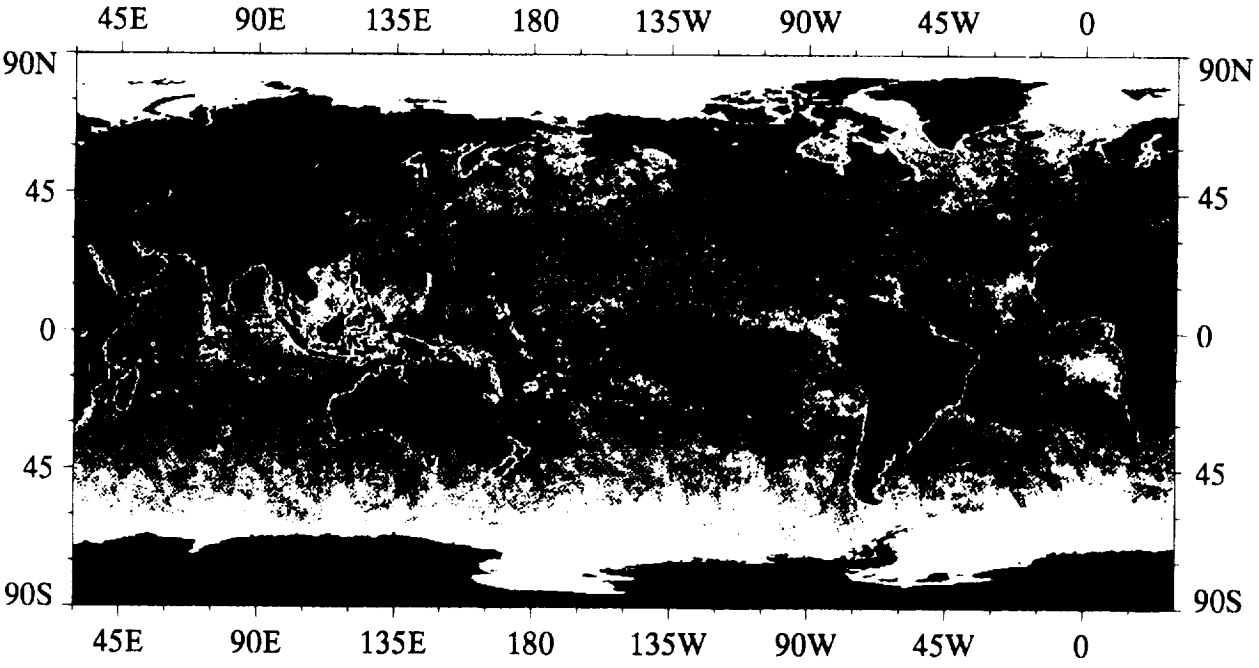

29 September to 26 October 1988, max = 168

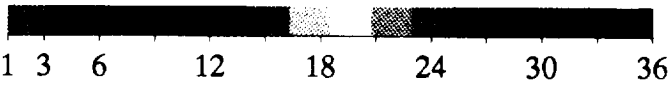

Number of AVHRR Sea Surface Temperature Values per Pixel

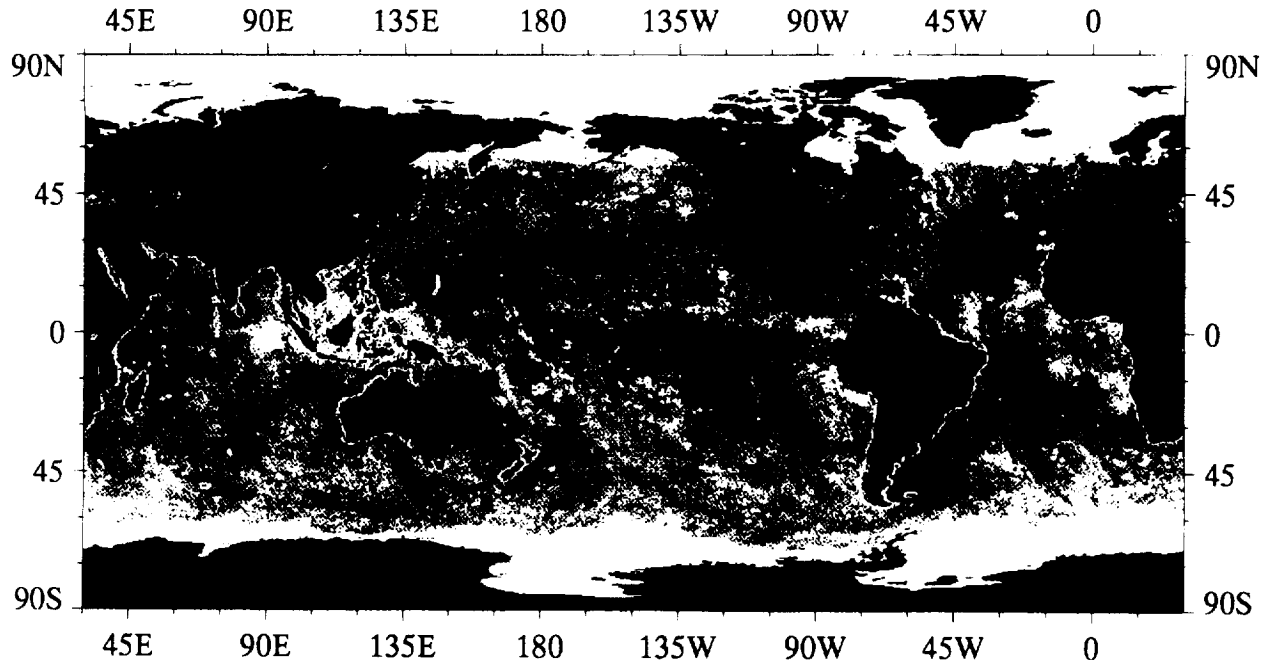

27 October to 23 November 1988, max = 301

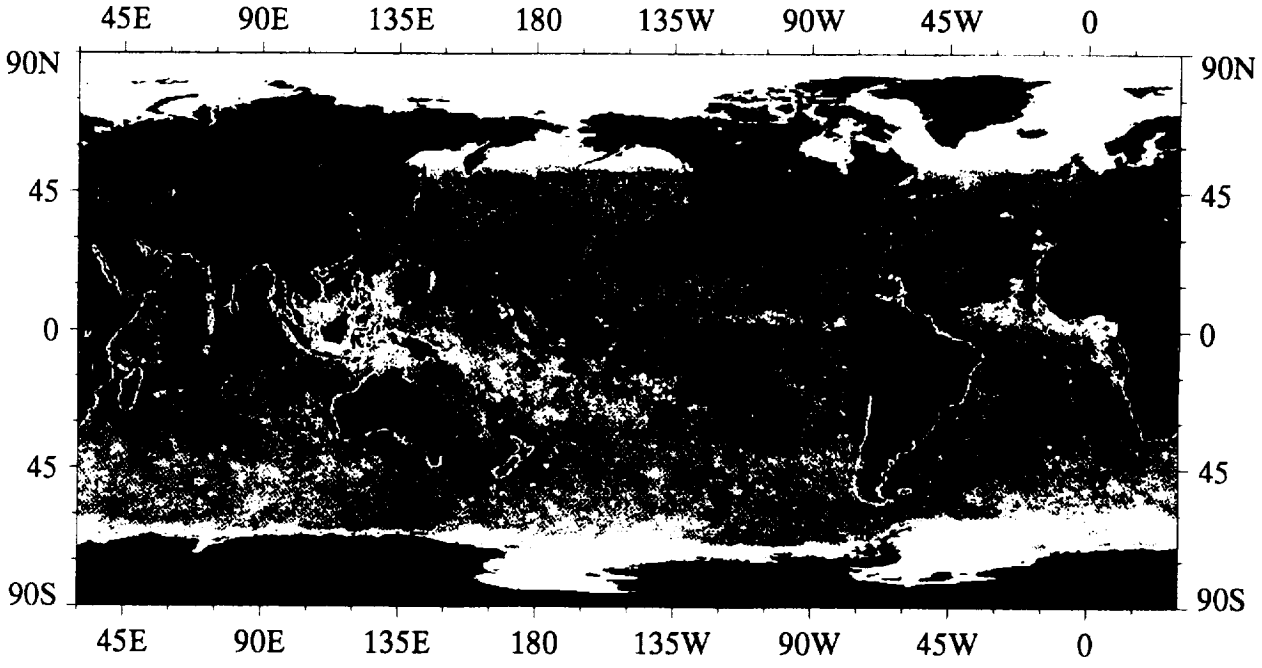

1 December to 28 December 1988, max = 312

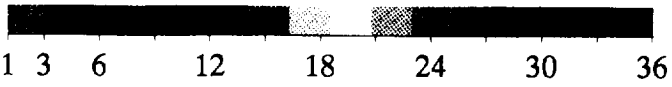

Number of AVHRR Sea Surface Temperature Values per Pixel

A10

Annual Mean ECMWF Surface Wind Components

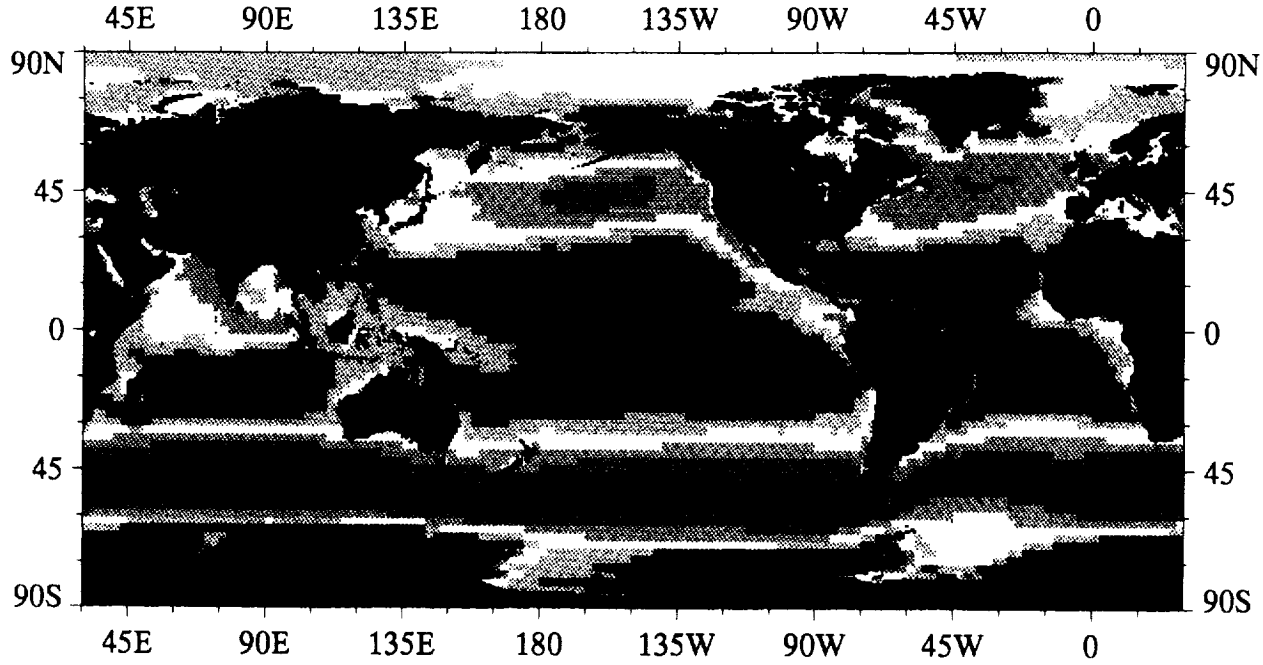

Zonal Wind Speed, Annual Mean 1988

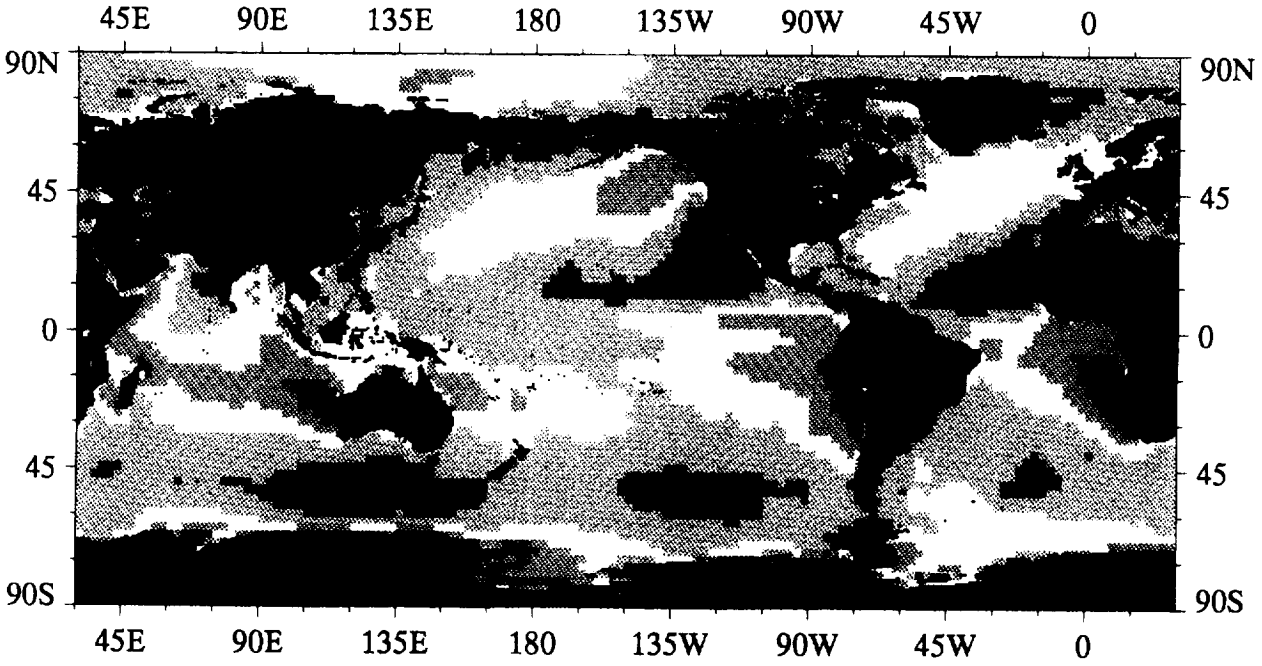

Meridional Wind Speed, Annual Mean 1988

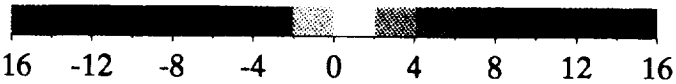

ECMWF 10 m Wind Speed, m s^{-1}

A11

Monthly Mean ECMWF Surface Wind Components

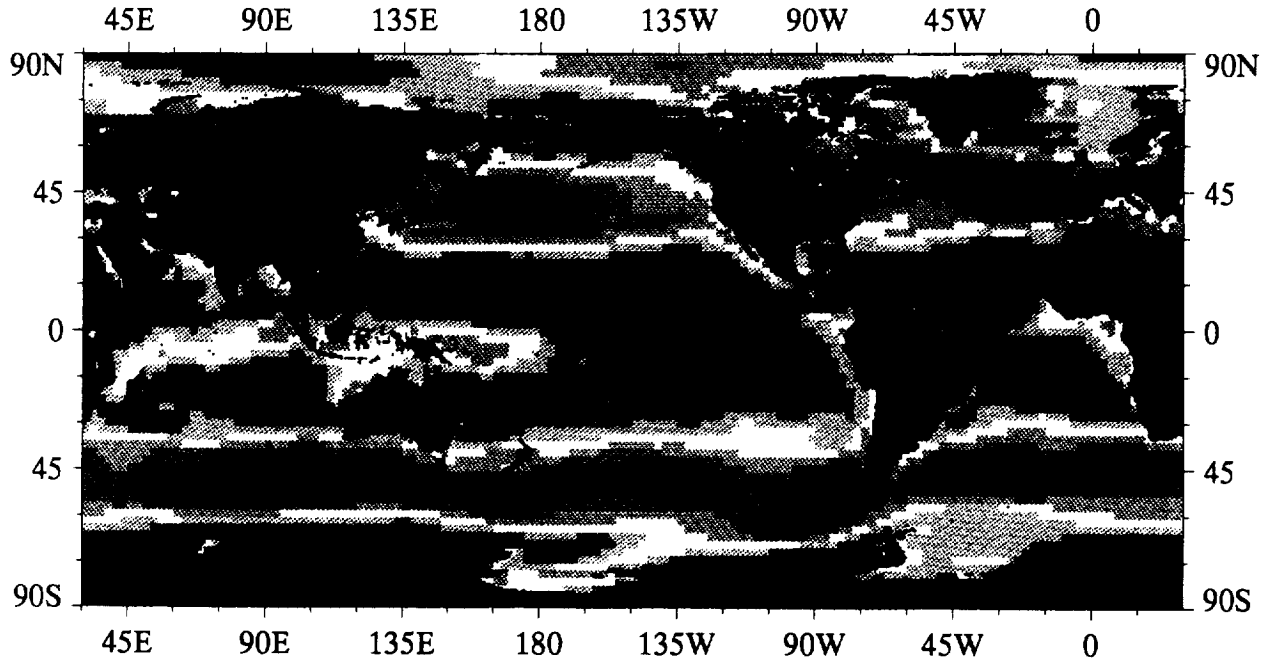

Zonal Wind Speed, January 1988

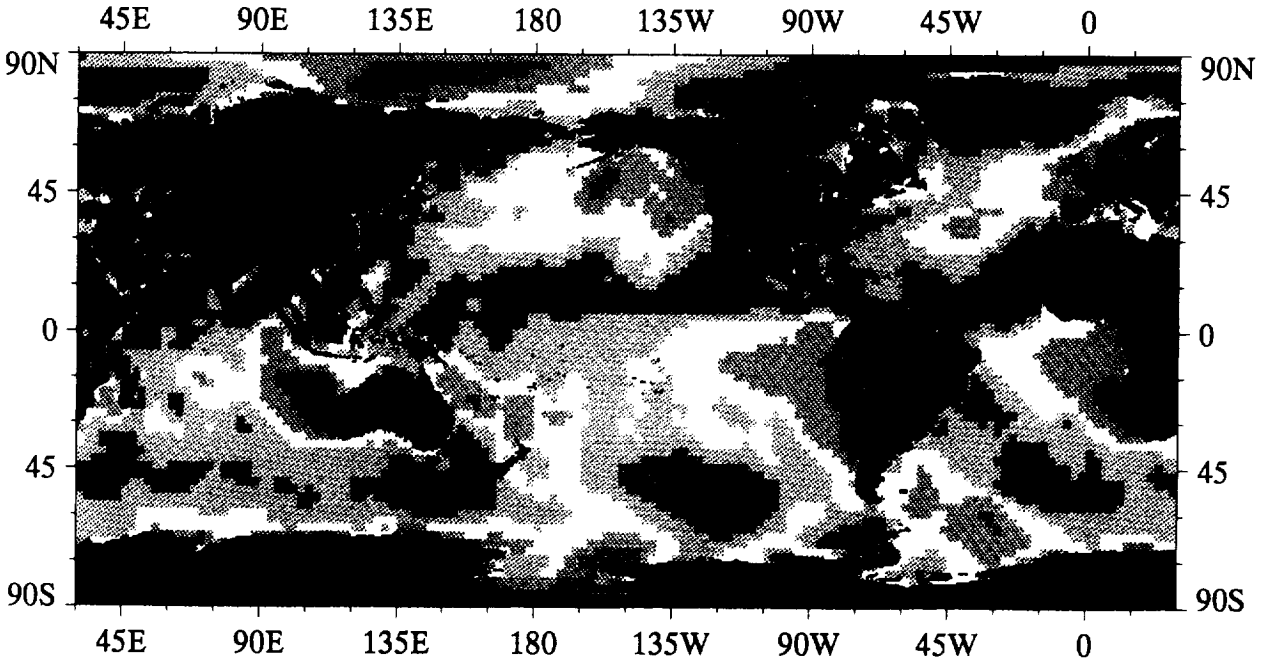

Meridional Wind Speed, January 1988

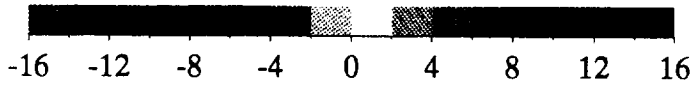

ECMWF 10 m Wind Speed, m s^{-1}

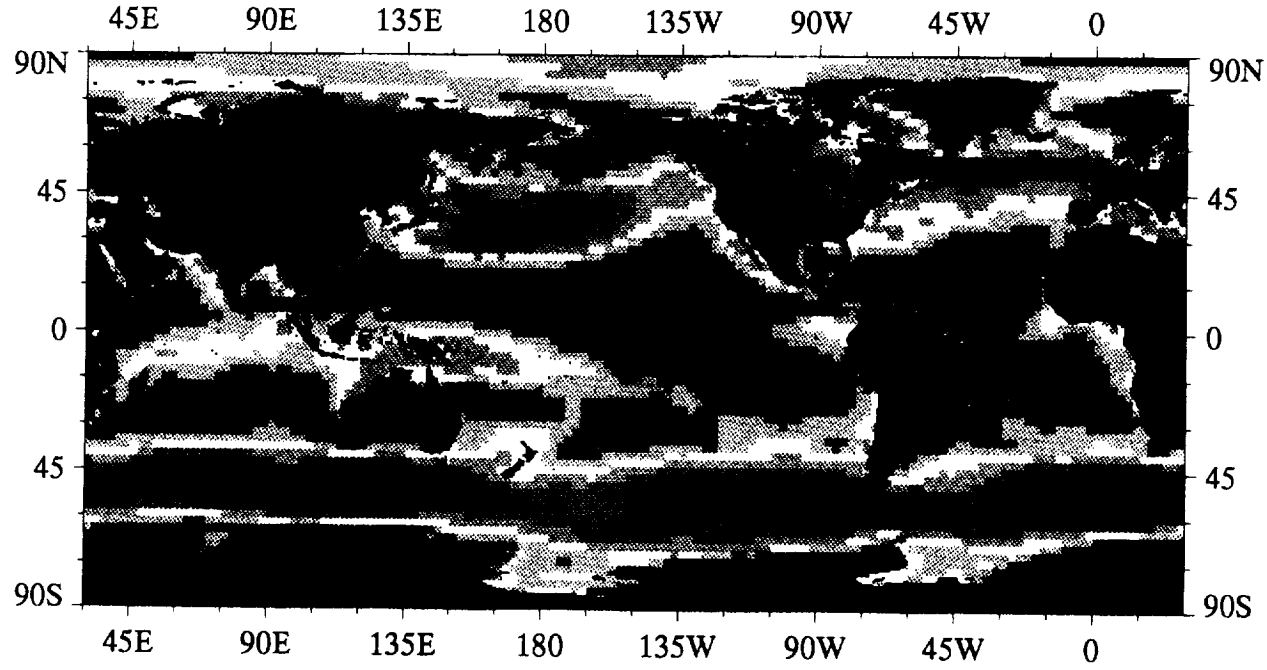

Zonal Wind Speed, February 1988

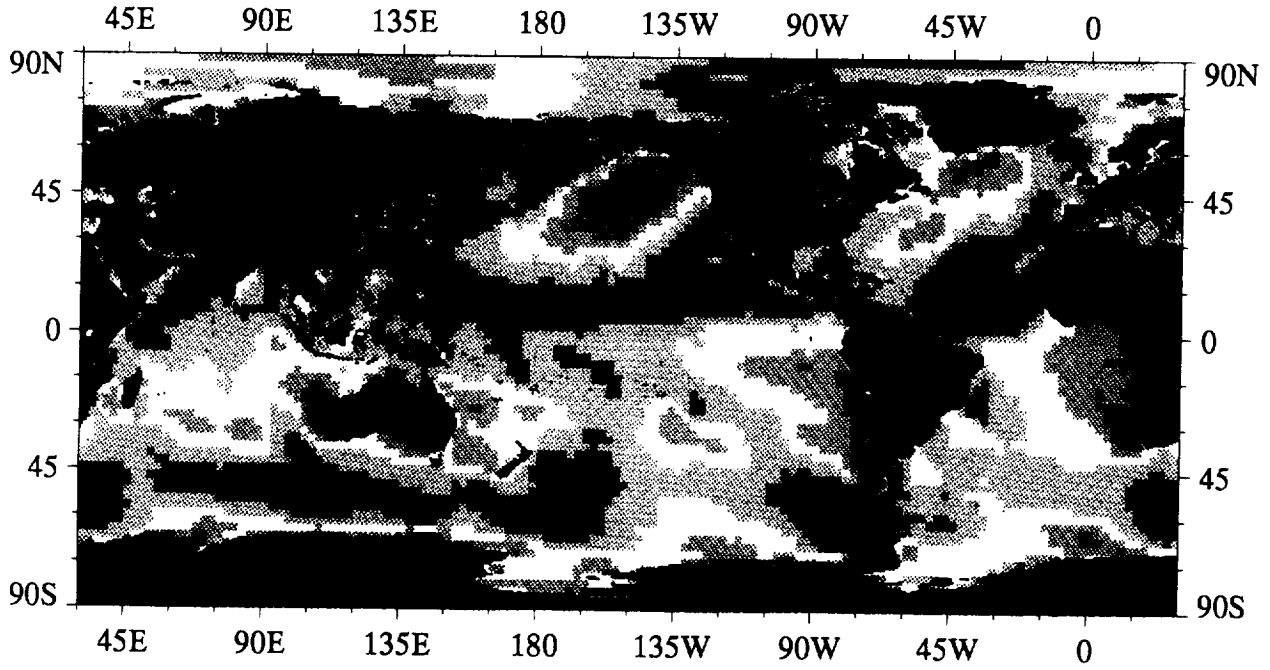

Meridional Wind Speed, February 1988

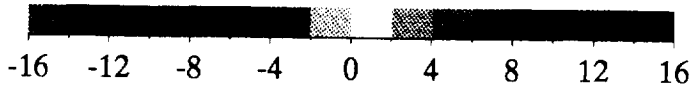

ECMWF 10 m Wind Speed, m s^{-1}

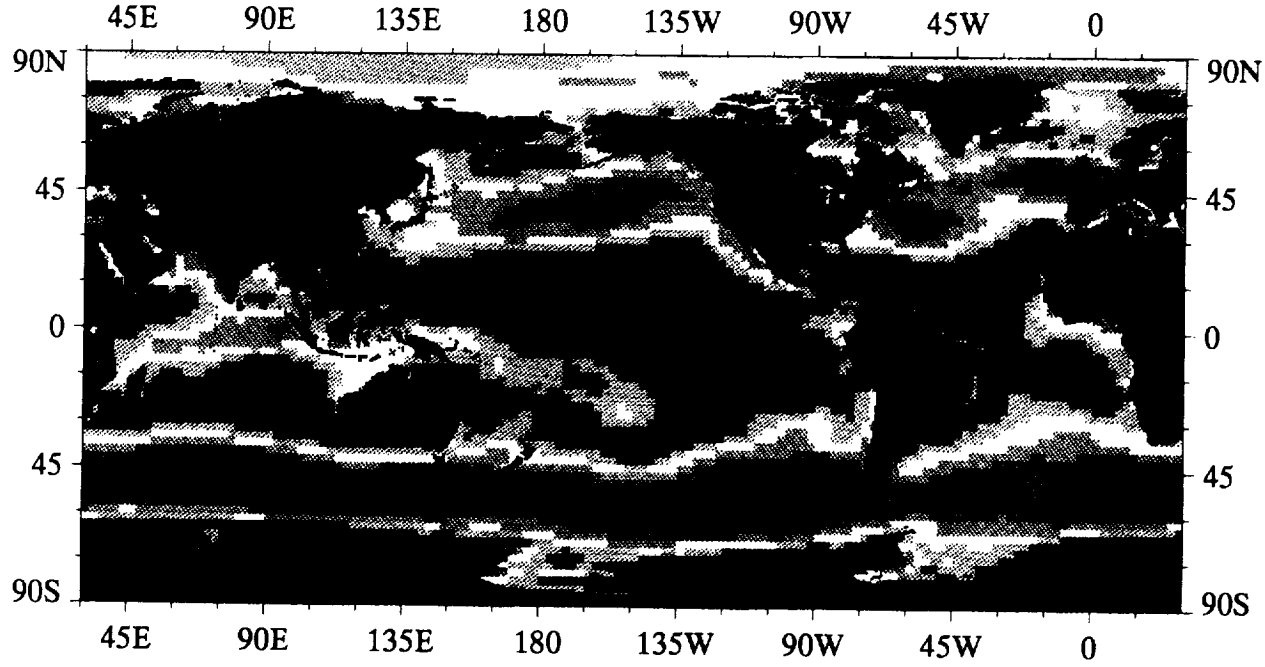

Zonal Wind Speed, March 1988

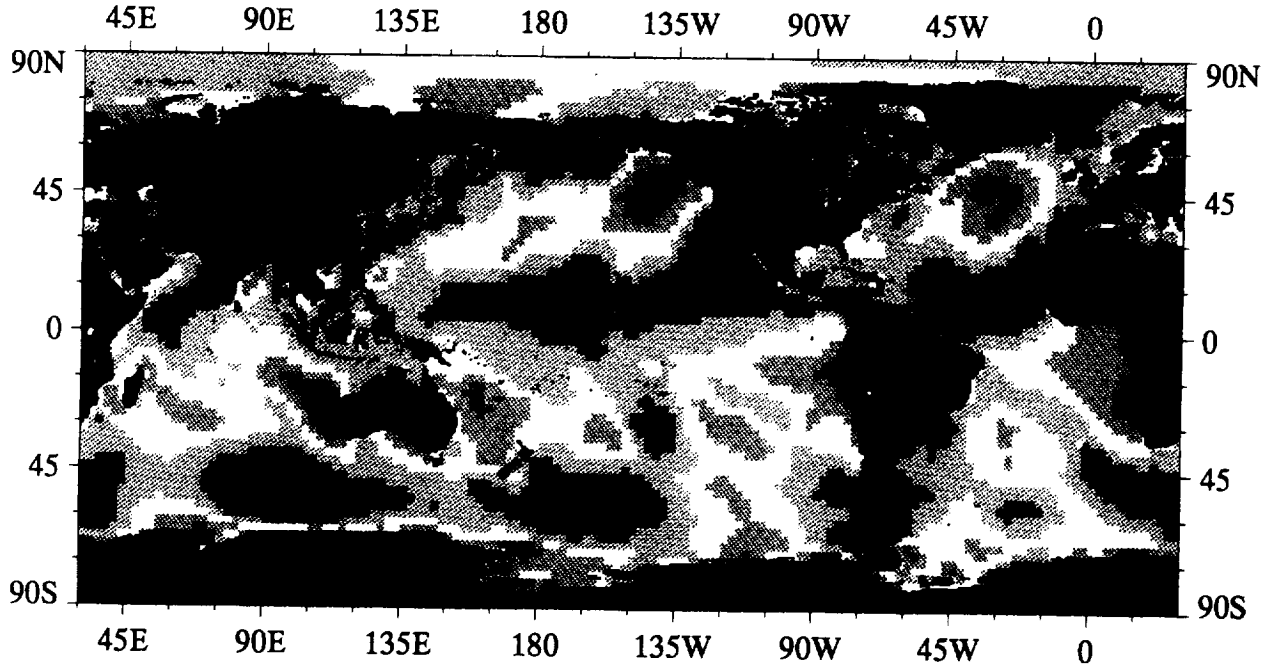

Meridional Wind Speed, March 1988

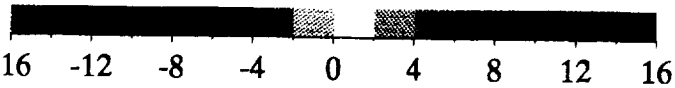

ECMWF 10 m Wind Speed, m s^{-1}

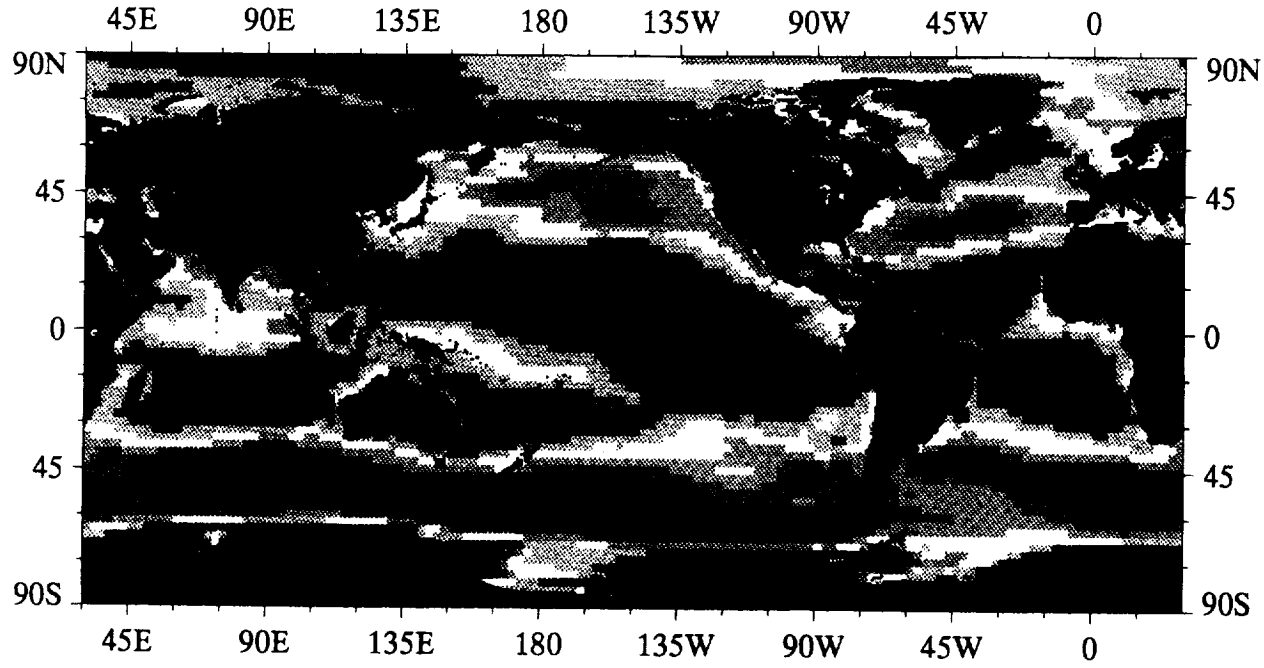

Zonal Wind Speed, April 1988

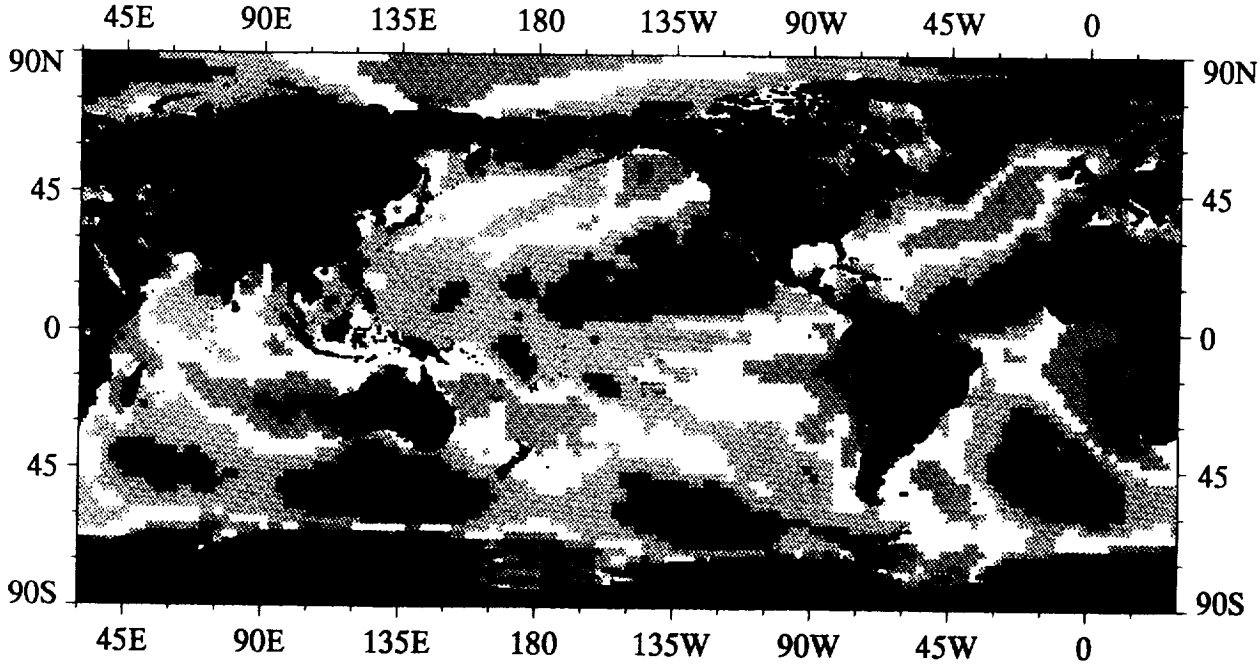

Meridional Wind Speed, April 1988

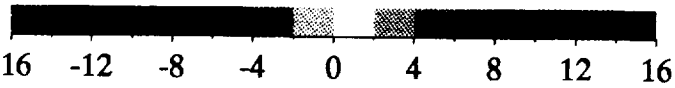

ECMWF 10 m Wind Speed, m s^{-1}

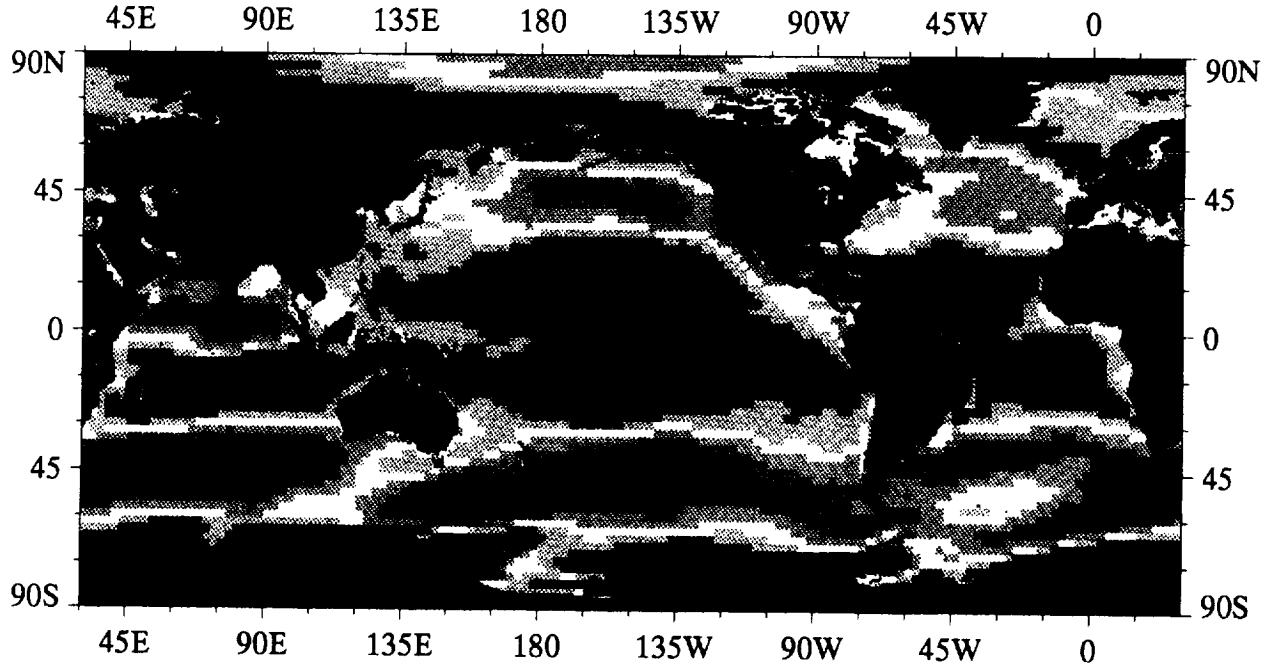

Zonal Wind Speed, May 1988

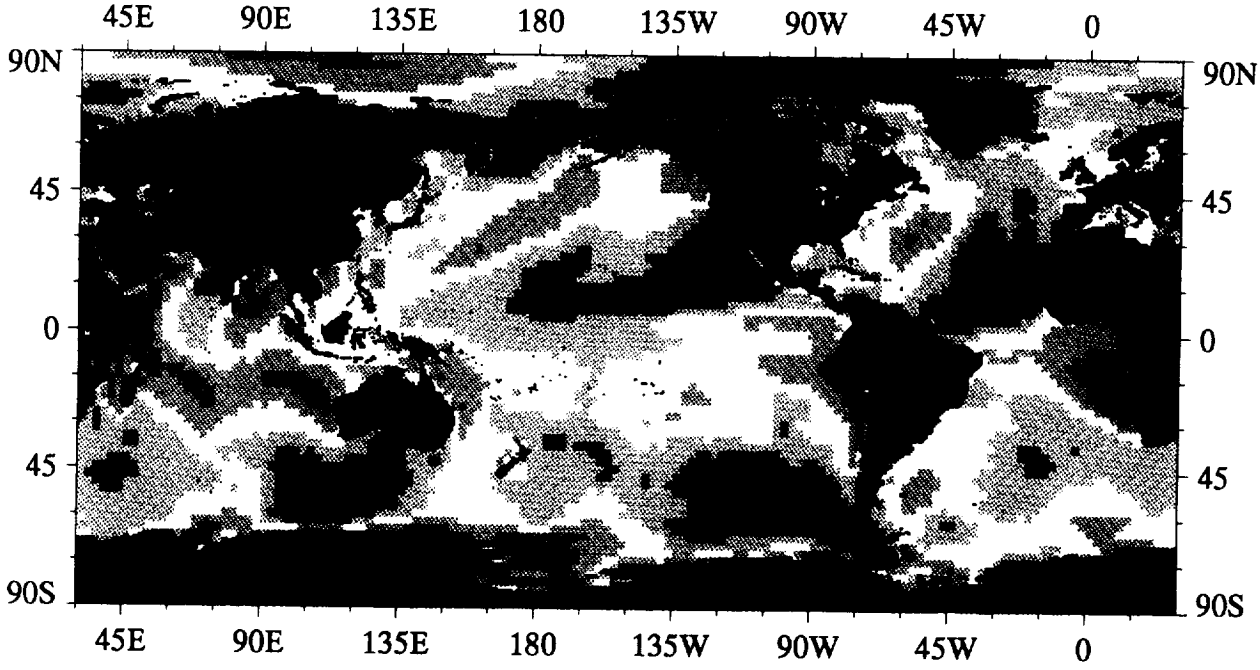

Meridional Wind Speed, May 1988

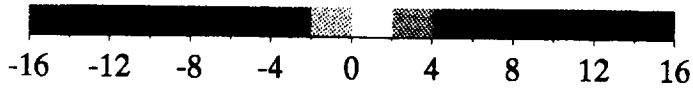

ECMWF 10 m Wind Speed, m s^{-1}

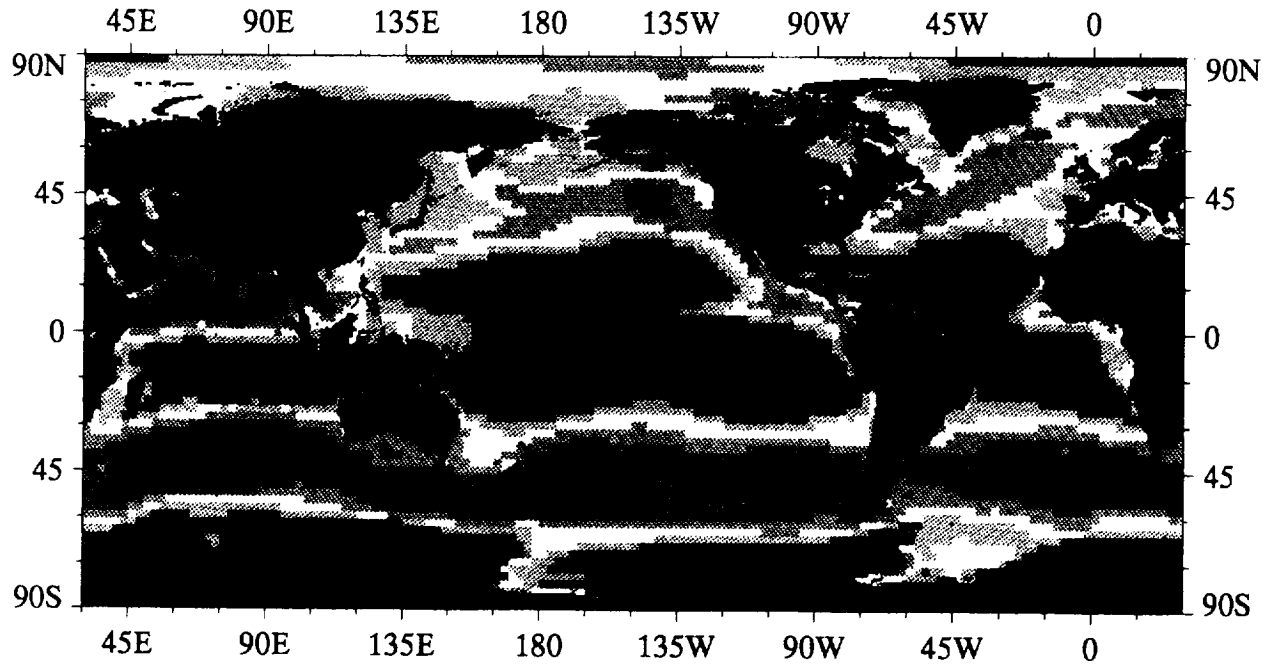

Zonal Wind Speed, June 1988

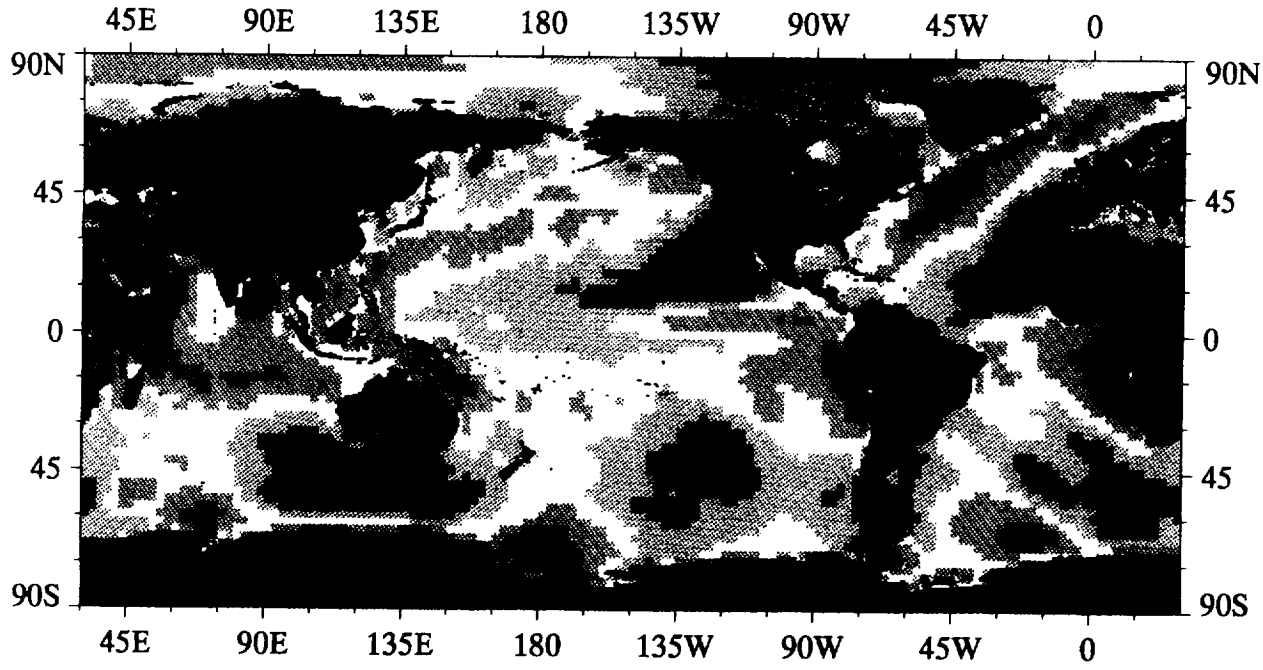

Meridional Wind Speed, June 1988

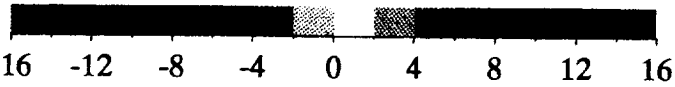

ECMWF 10 m Wind Speed, m s^{-1}

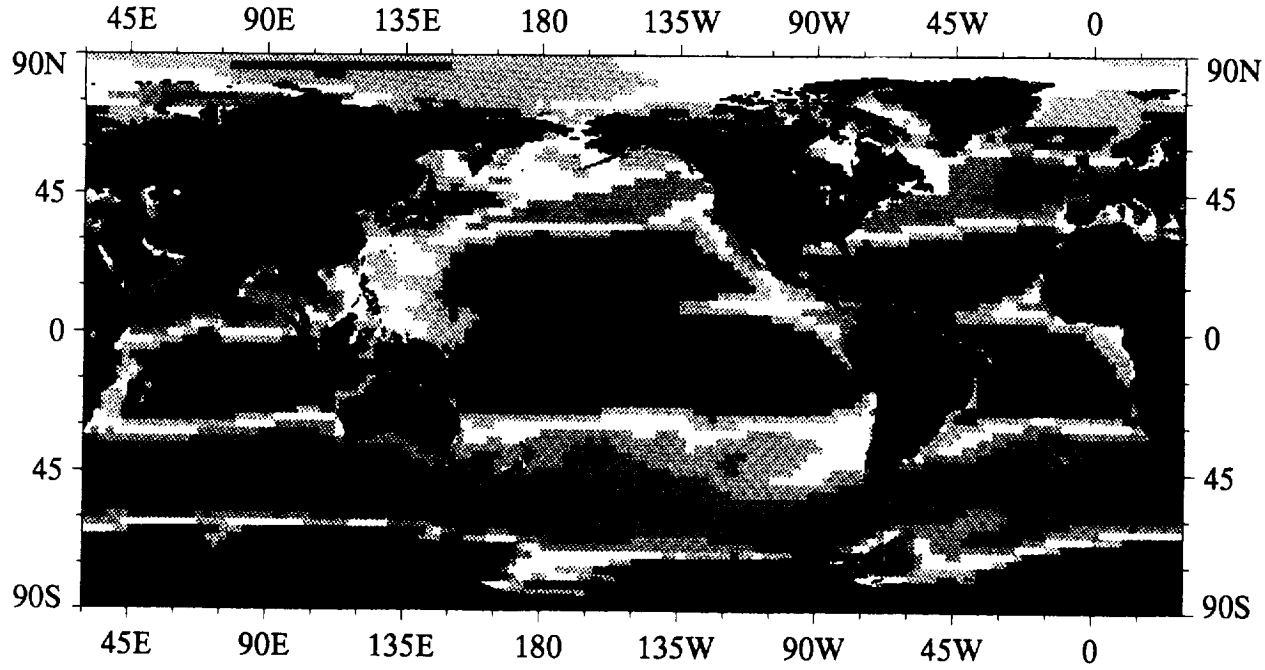

Zonal Wind Speed, July 1988

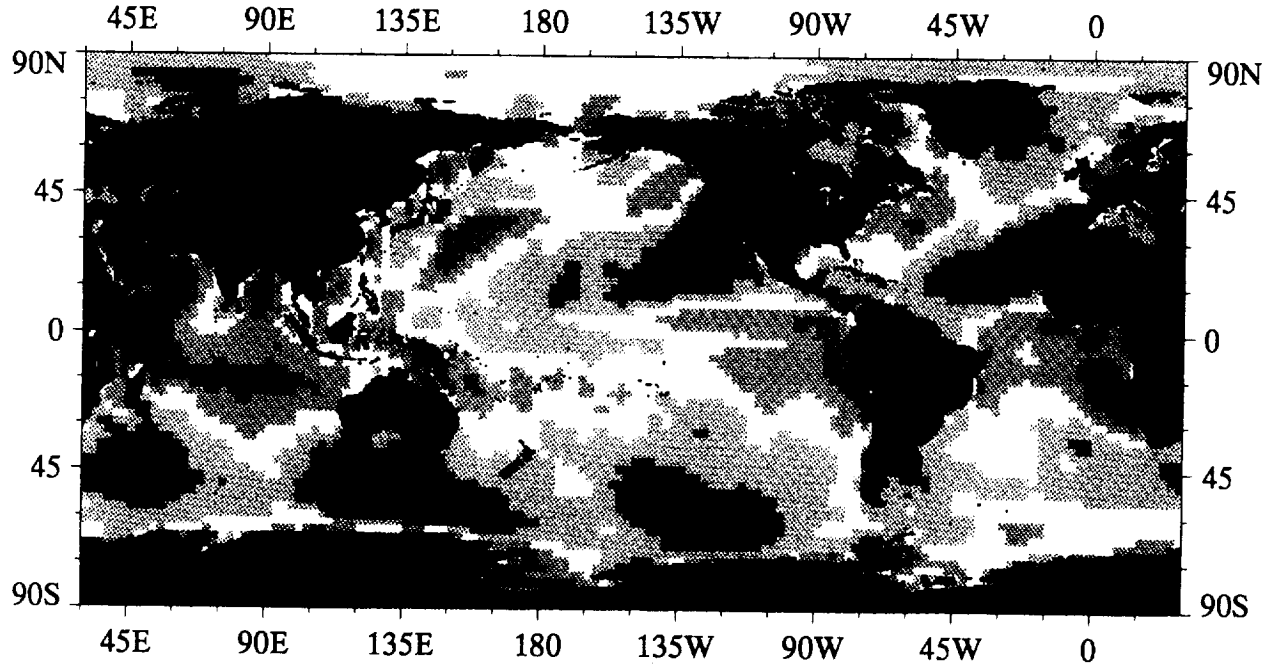

Meridional Wind Speed, July 1988

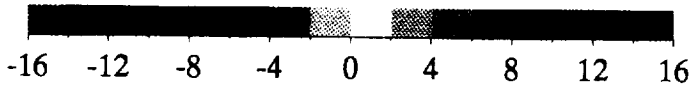

ECMWF 10 m Wind Speed, m s^{-1}

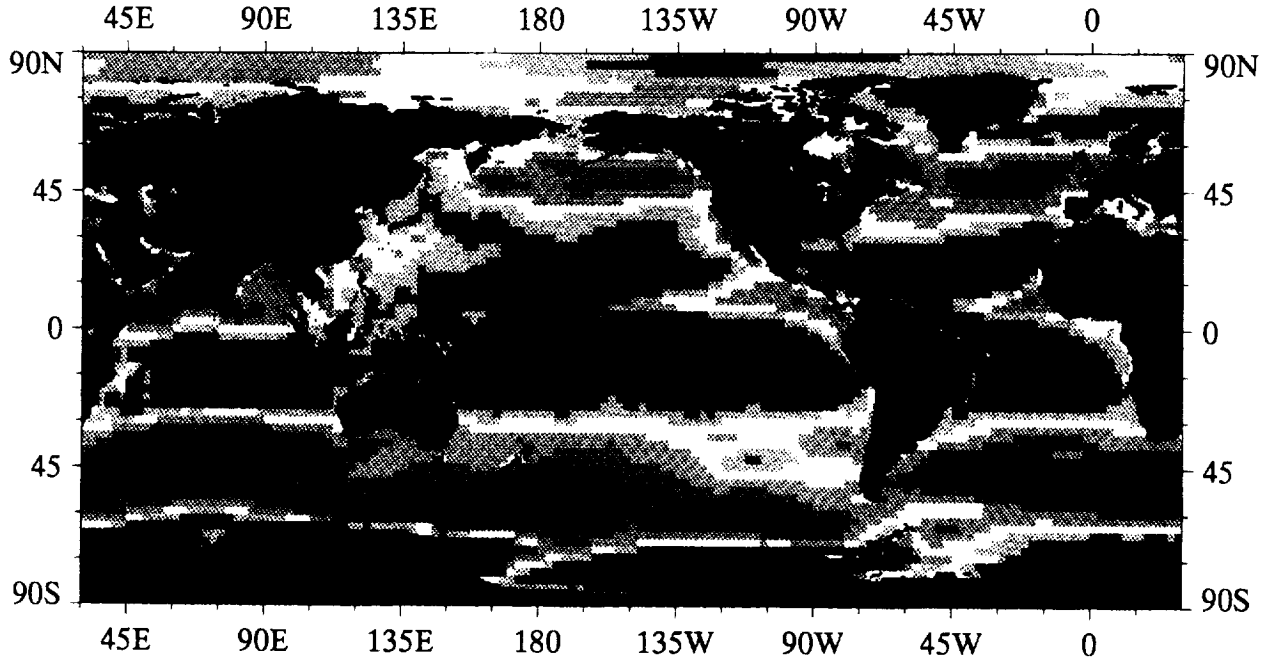

Zonal Wind Speed, August 1988

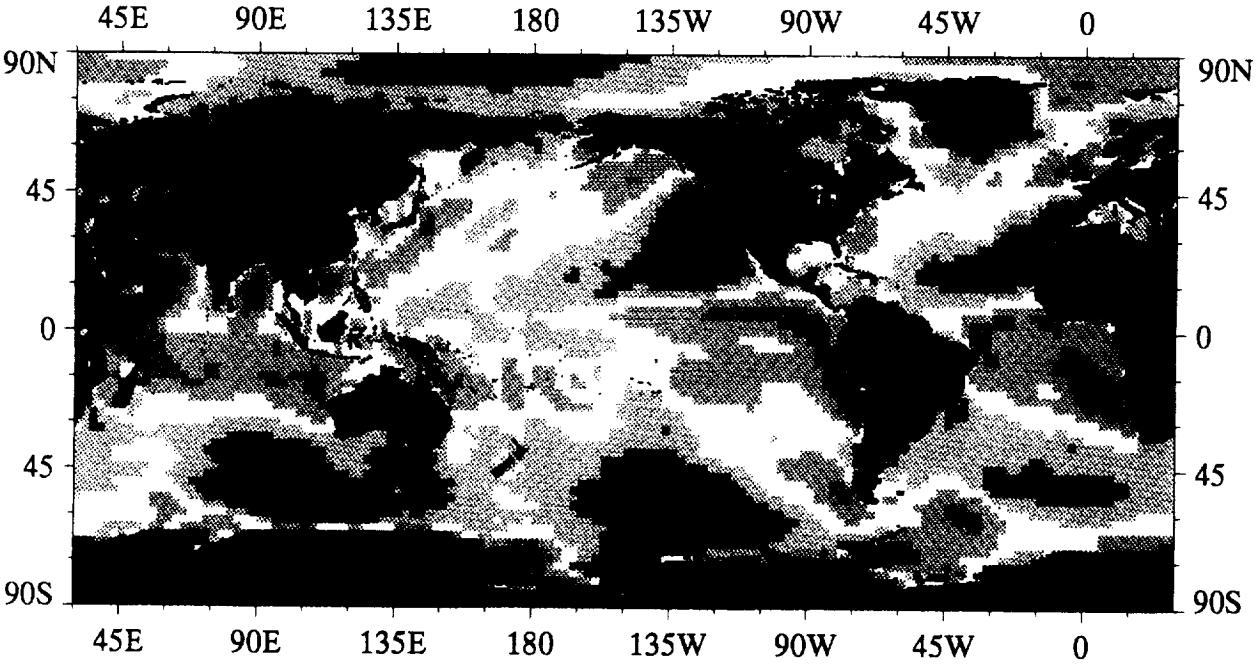

Meridional Wind Speed, August 1988

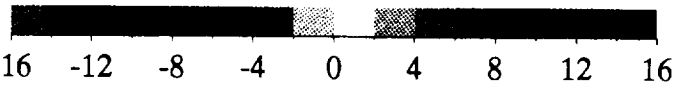

ECMWF 10 m Wind Speed, m s^{-1}

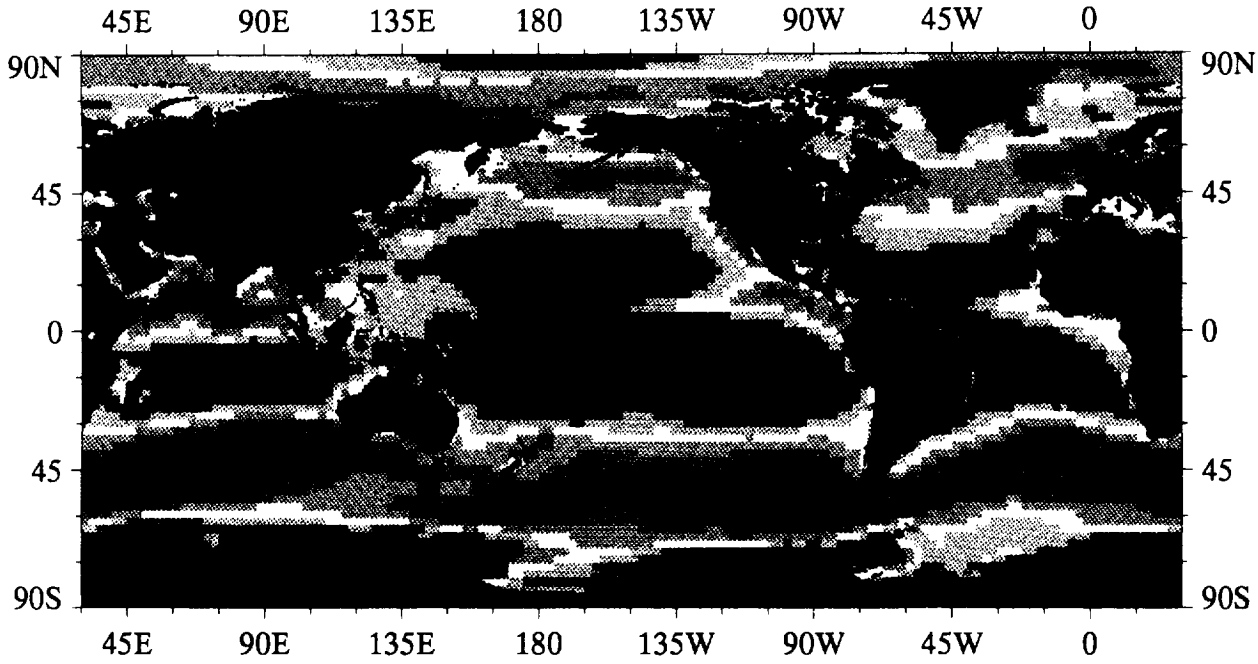

Zonal Wind Speed, September 1988

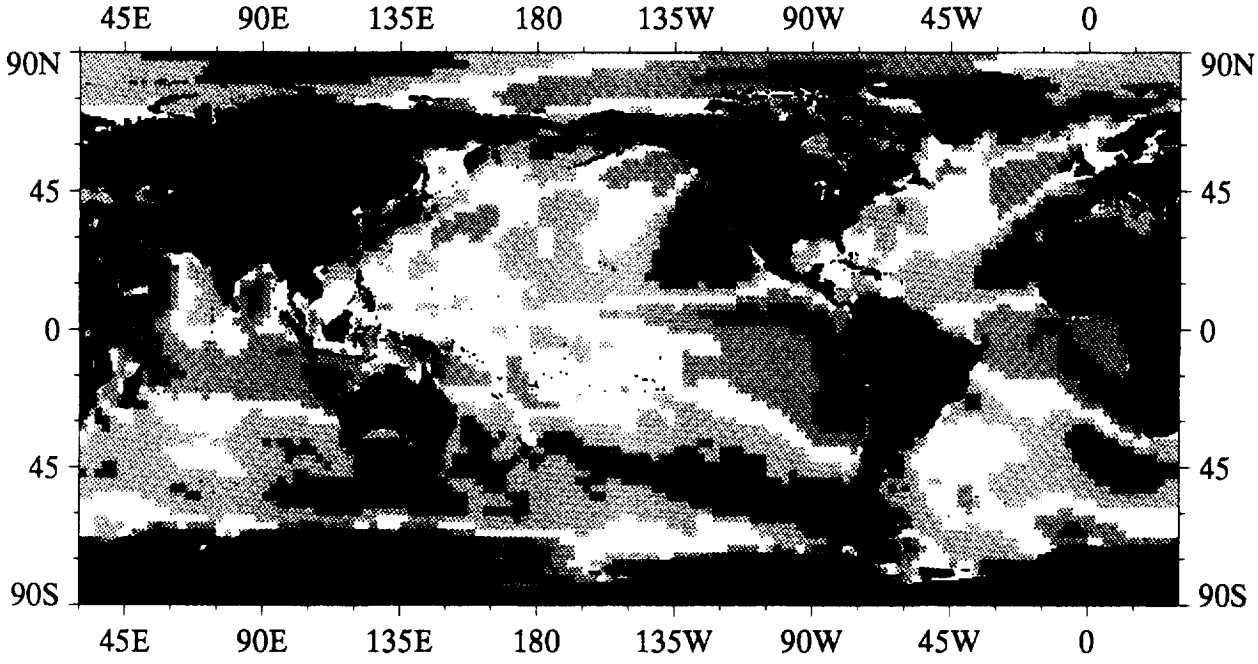

Meridional Wind Speed, September 1988

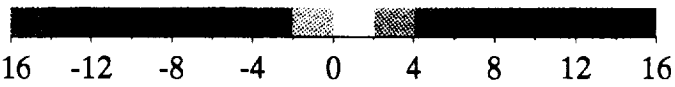

ECMWF 10 m Wind Speed, m s^{-1}

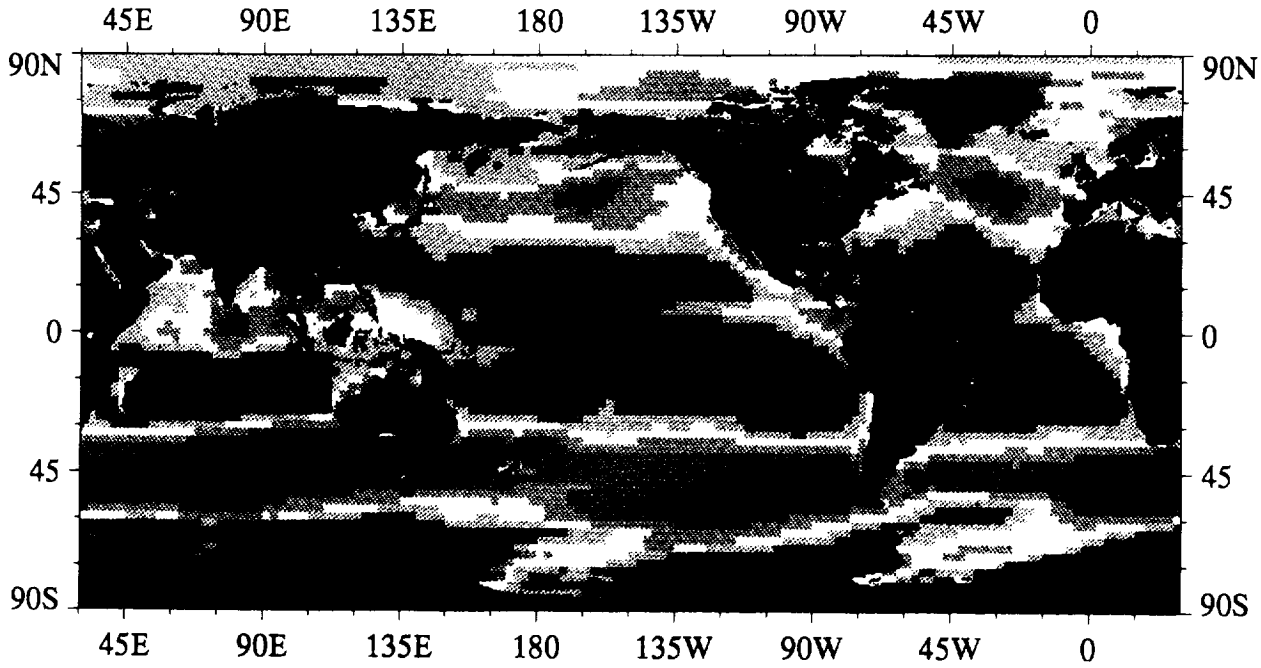

Zonal Wind Speed, October 1988

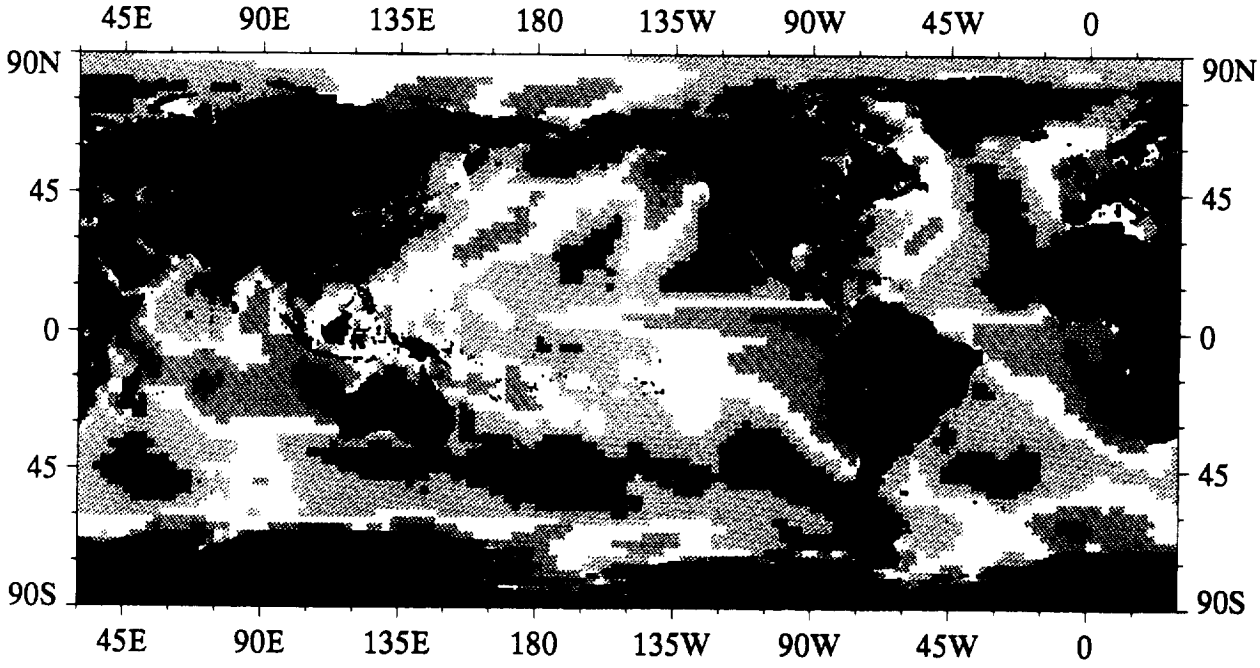

Meridional Wind Speed, October 1988

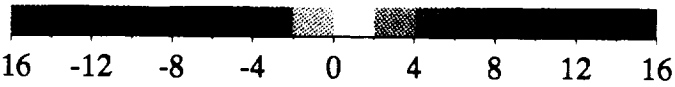

ECMWF 10 m Wind Speed, m s^{-1}

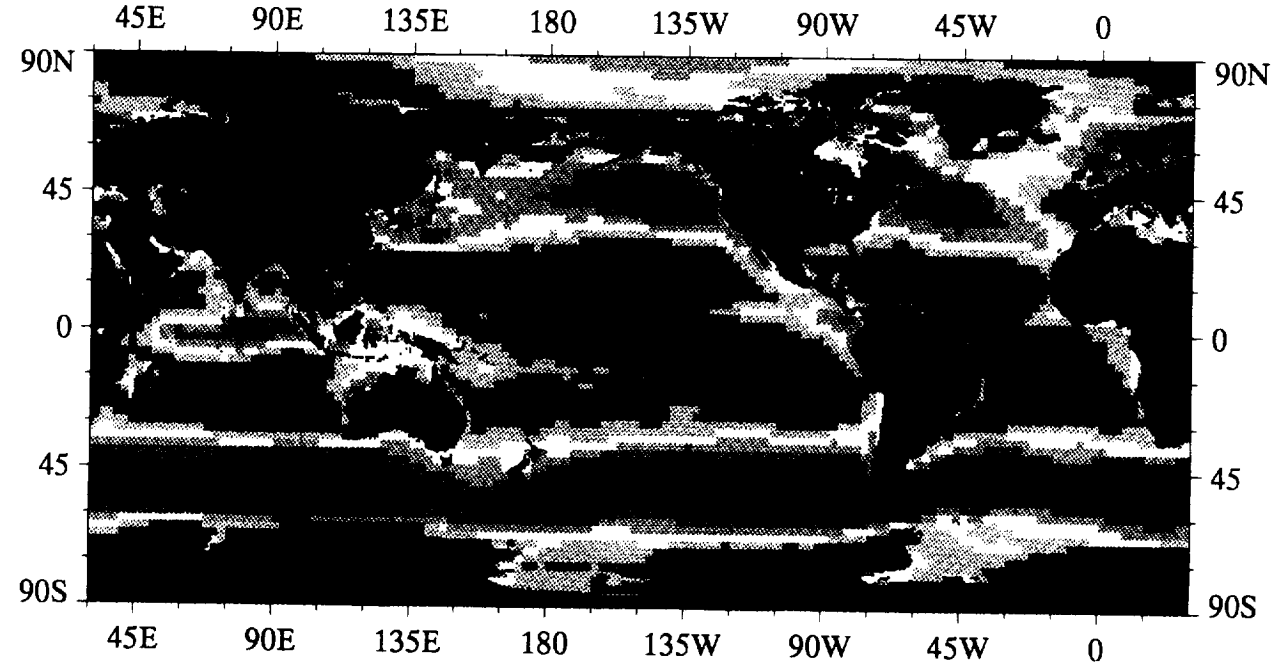

Zonal Wind Speed, November 1988

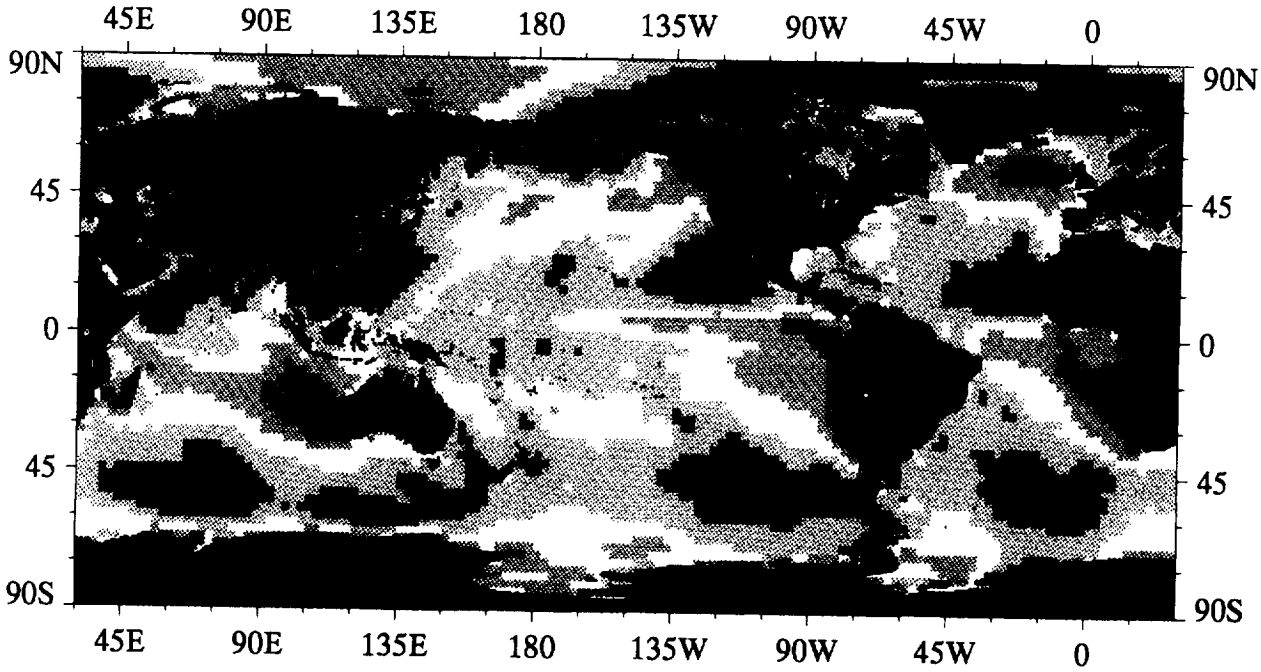

Meridional Wind Speed, November 1988

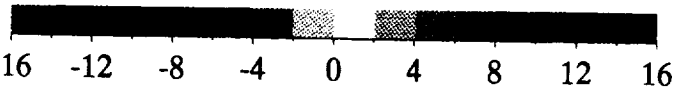

ECMWF 10 m Wind Speed, m s^{-1}

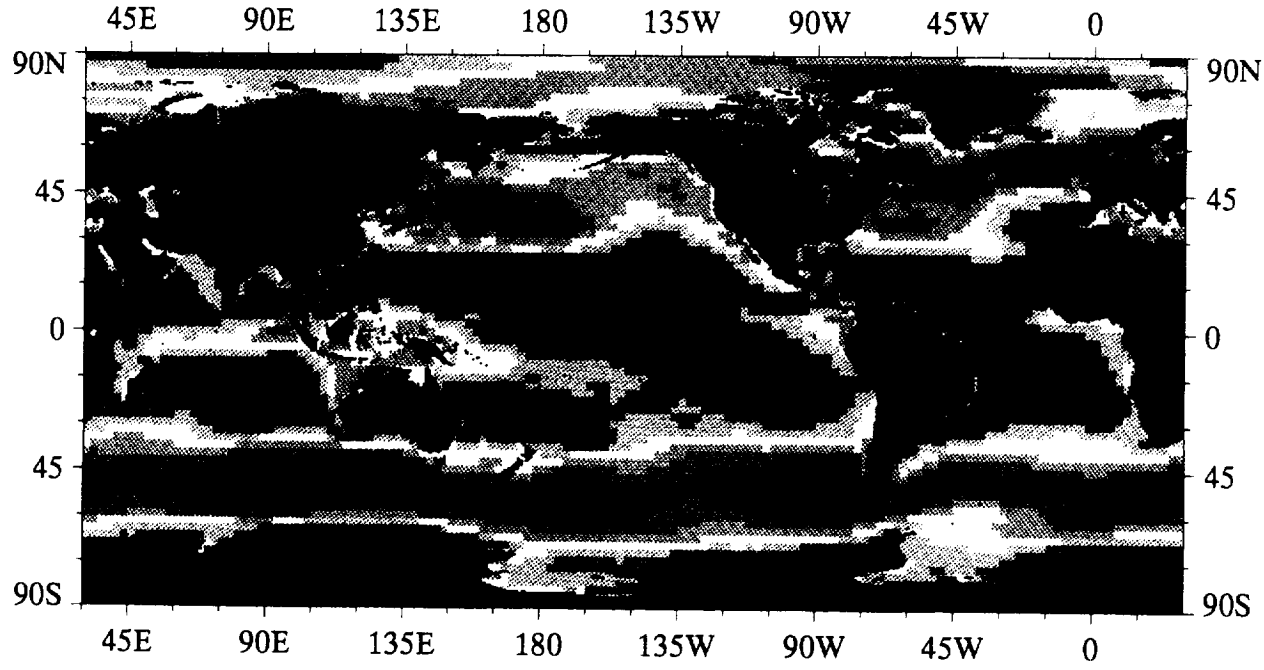

Zonal Wind Speed, December 1988

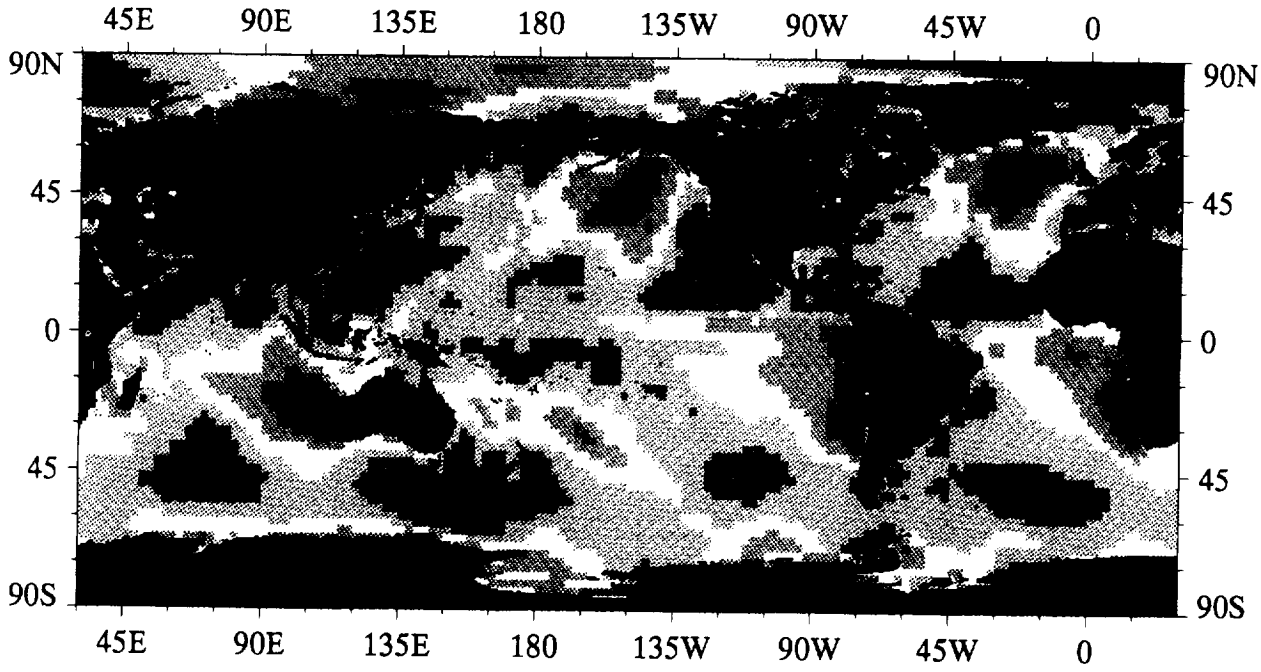

Meridional Wind Speed, December 1988

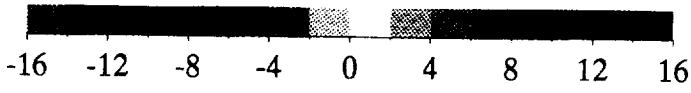

ECMWF 10 m Wind Speed, m s^{-1}

A12

Monthly Standard Deviation of ECMWF Surface Wind Components

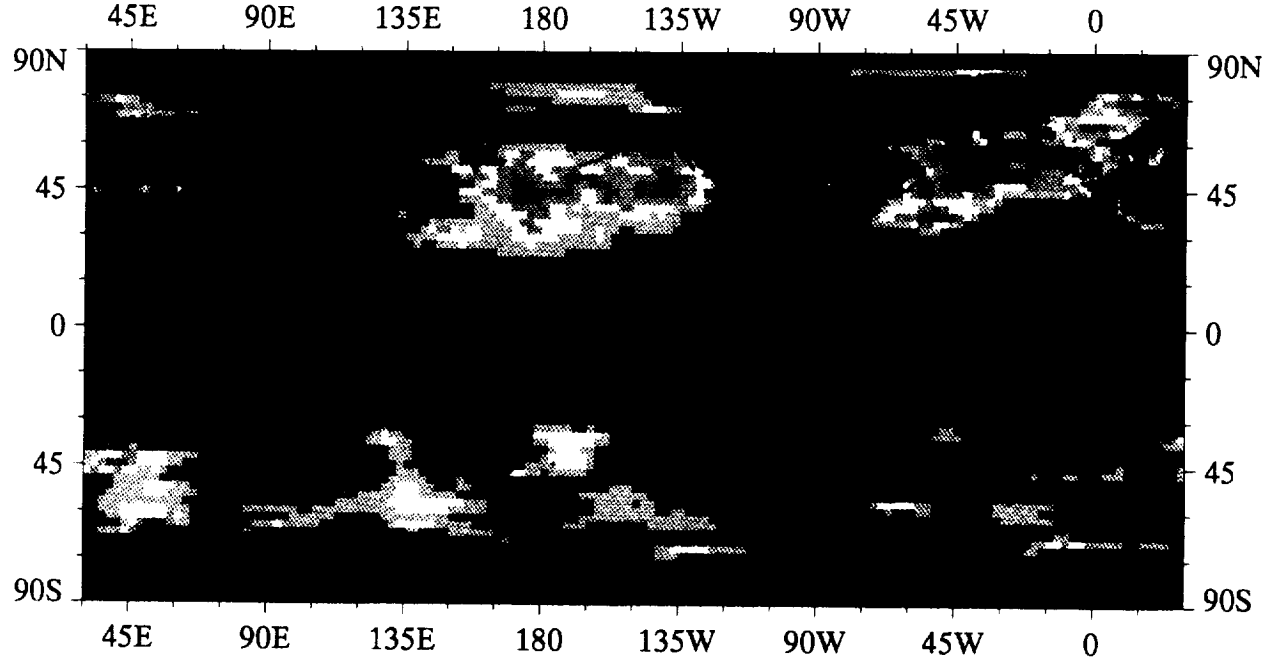

Zonal Wind Speed, January 1988

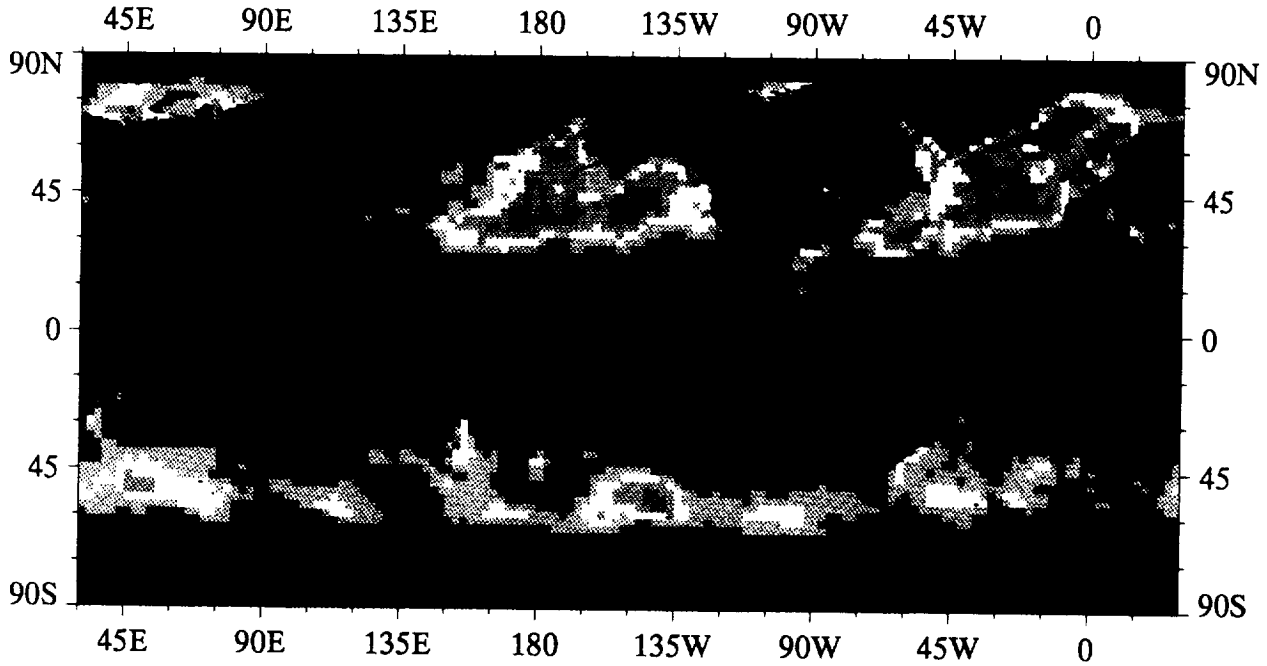

Meridional Wind Speed, January 1988

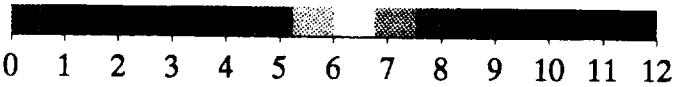

Standard Deviation of ECMWF 10 m Wind Speed, m s^{-1}

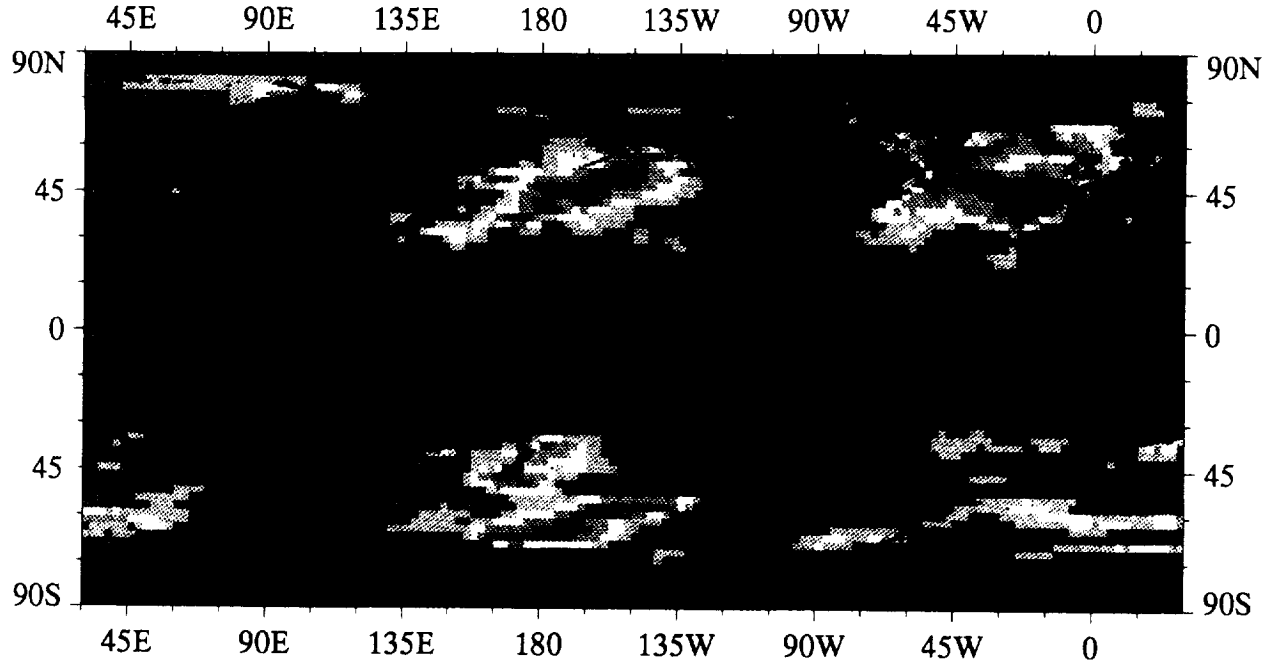

Zonal Wind Speed, February 1988

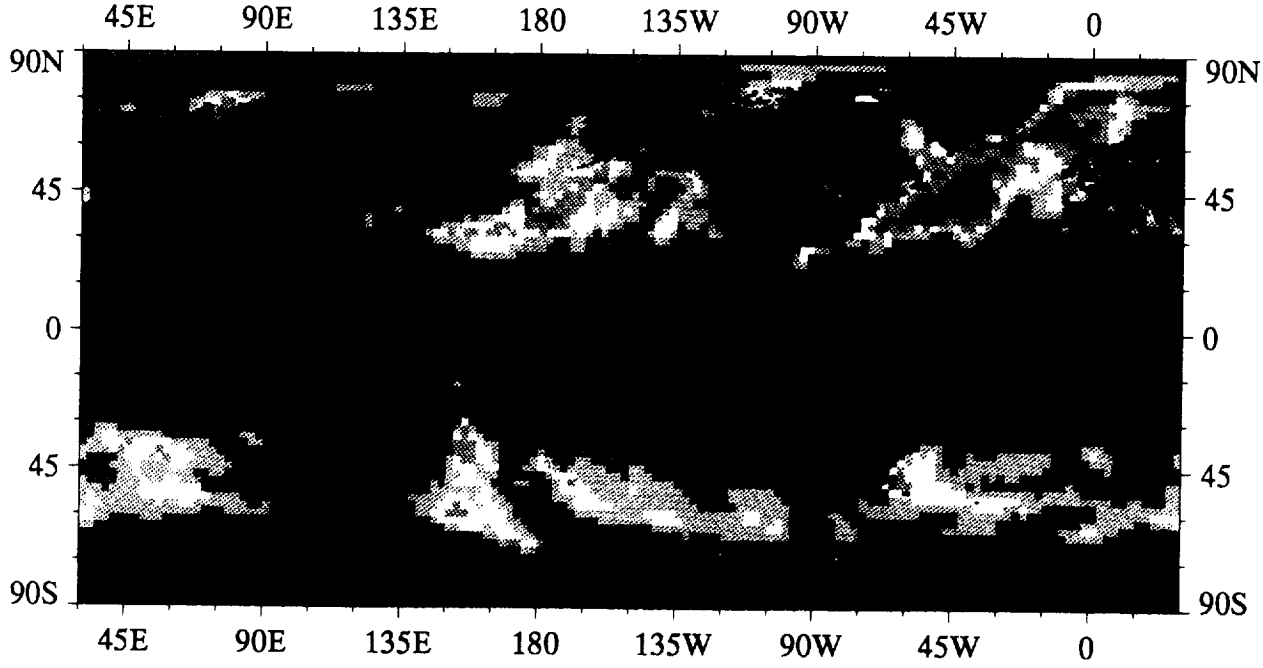

Meridional Wind Speed, February 1988

Standard Deviation of ECMWF 10 m Wind Speed, m s^{-1}

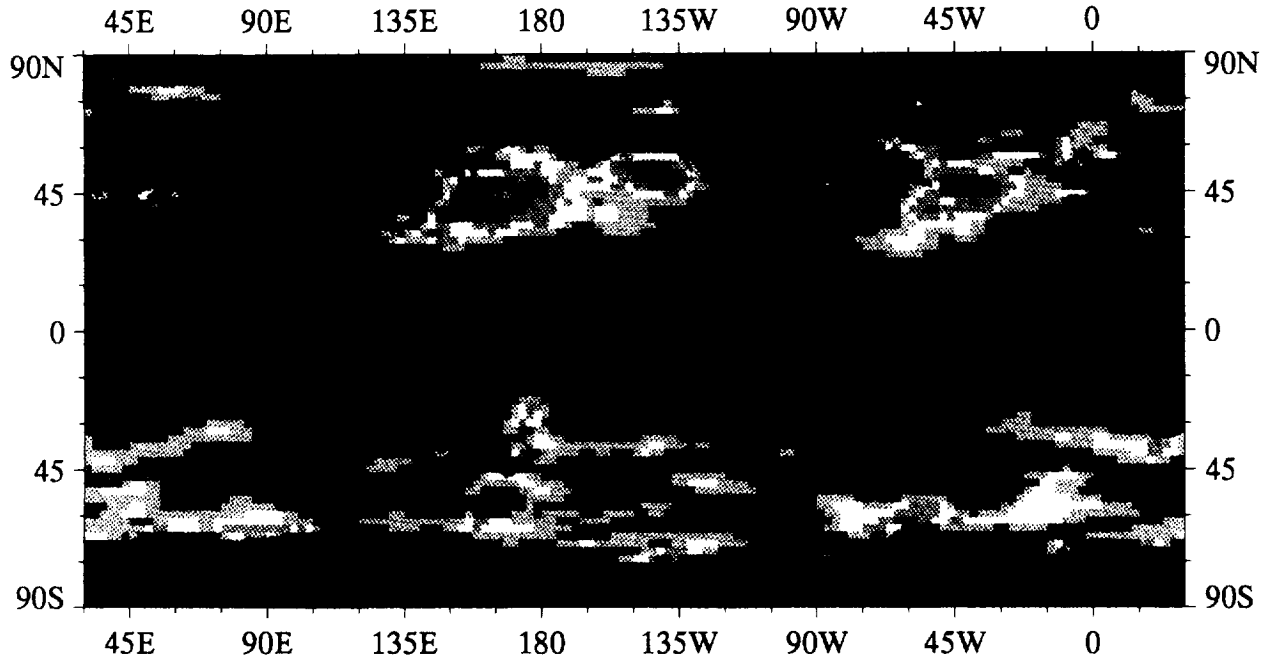

Zonal Wind Speed, March 1988

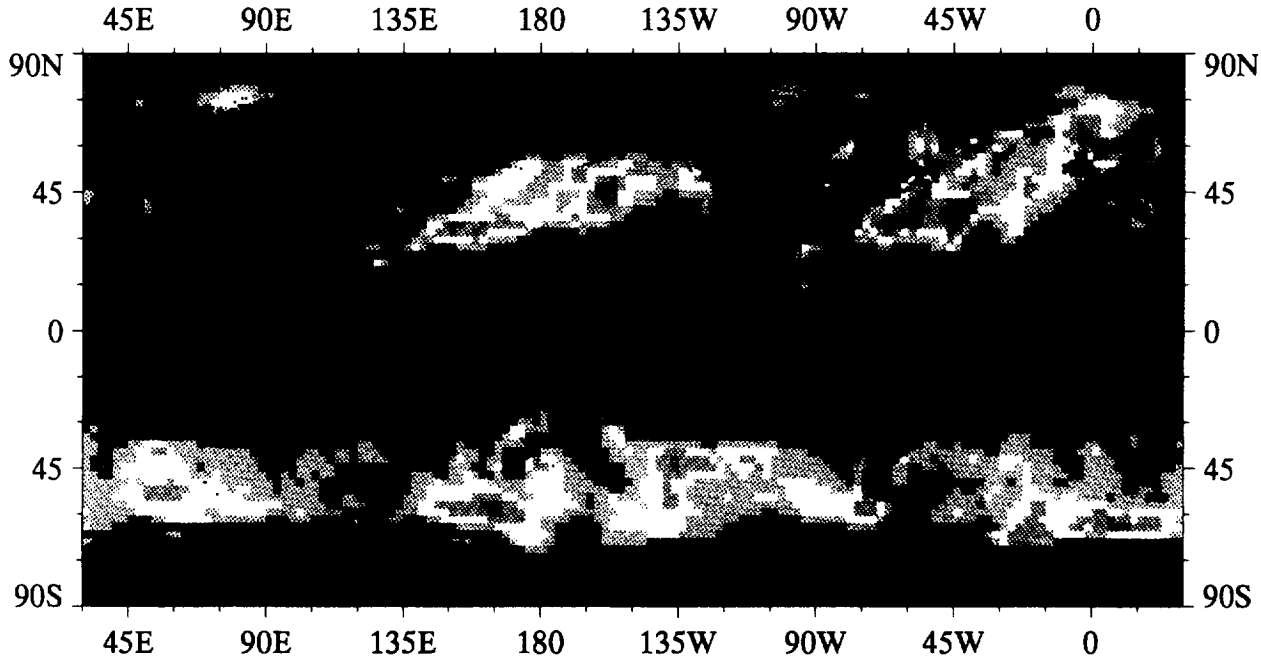

Meridional Wind Speed, March 1988

Standard Deviation of ECMWF 10 m Wind Speed, m s^{-1}

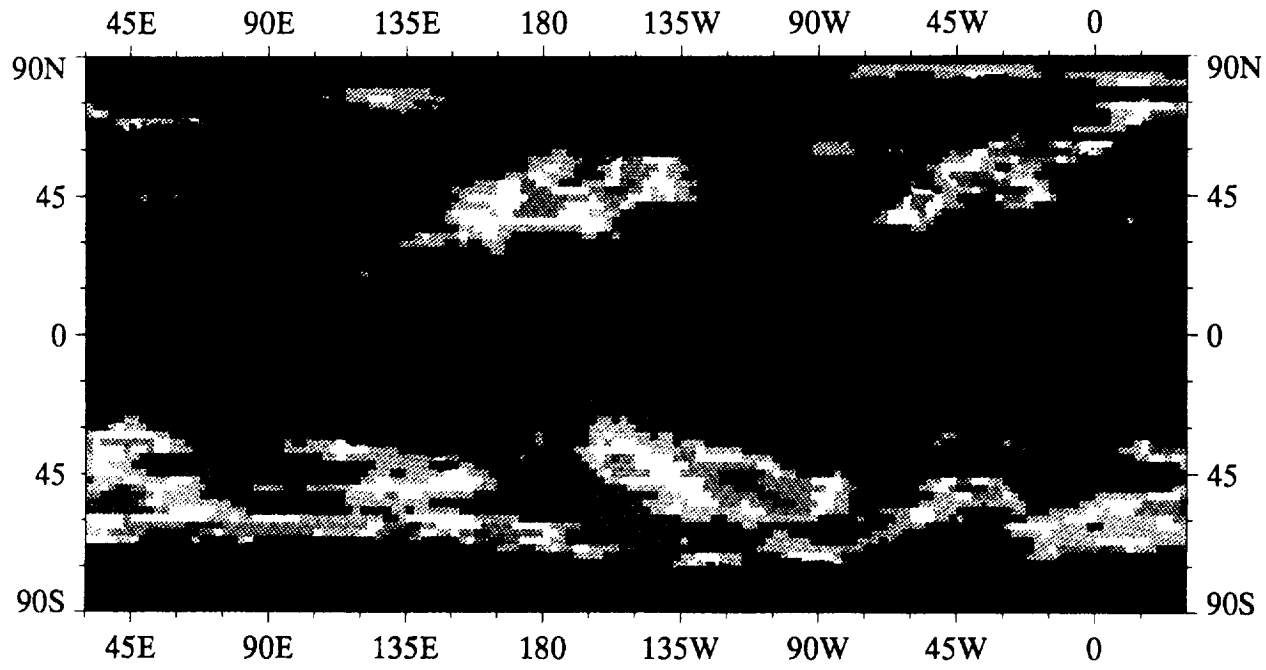

Zonal Wind Speed, April 1988

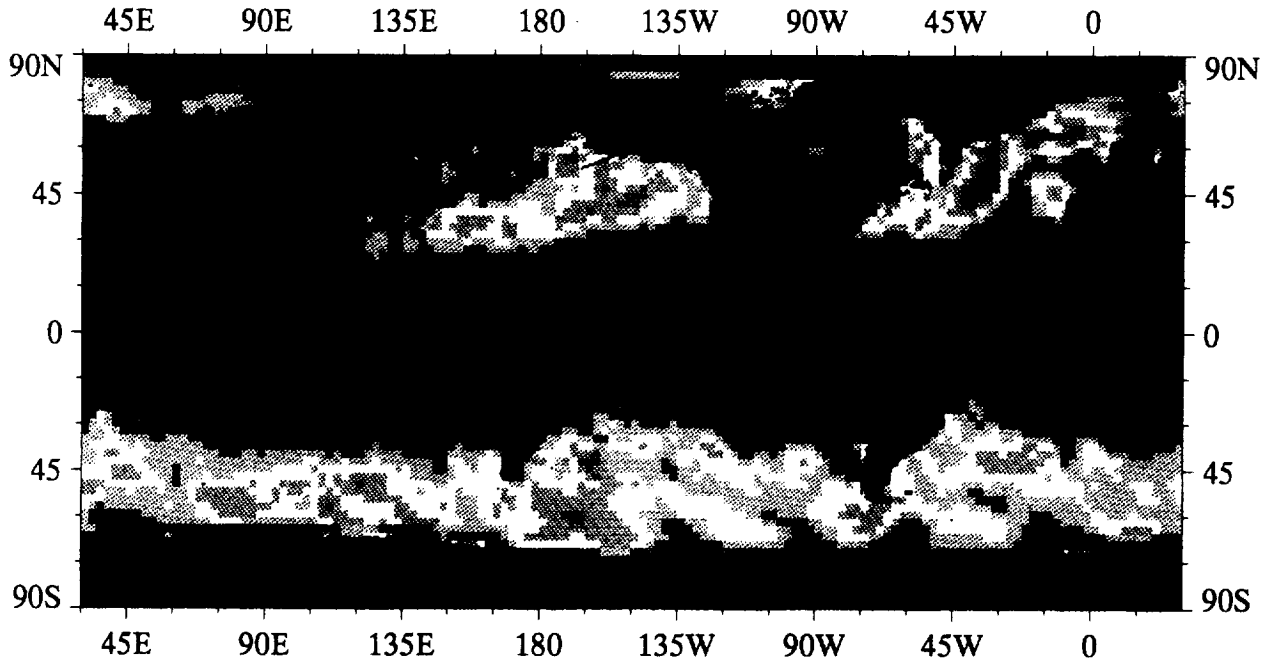

Meridional Wind Speed, April 1988

Standard Deviation of ECMWF 10 m Wind Speed, m s^{-1}

C-2

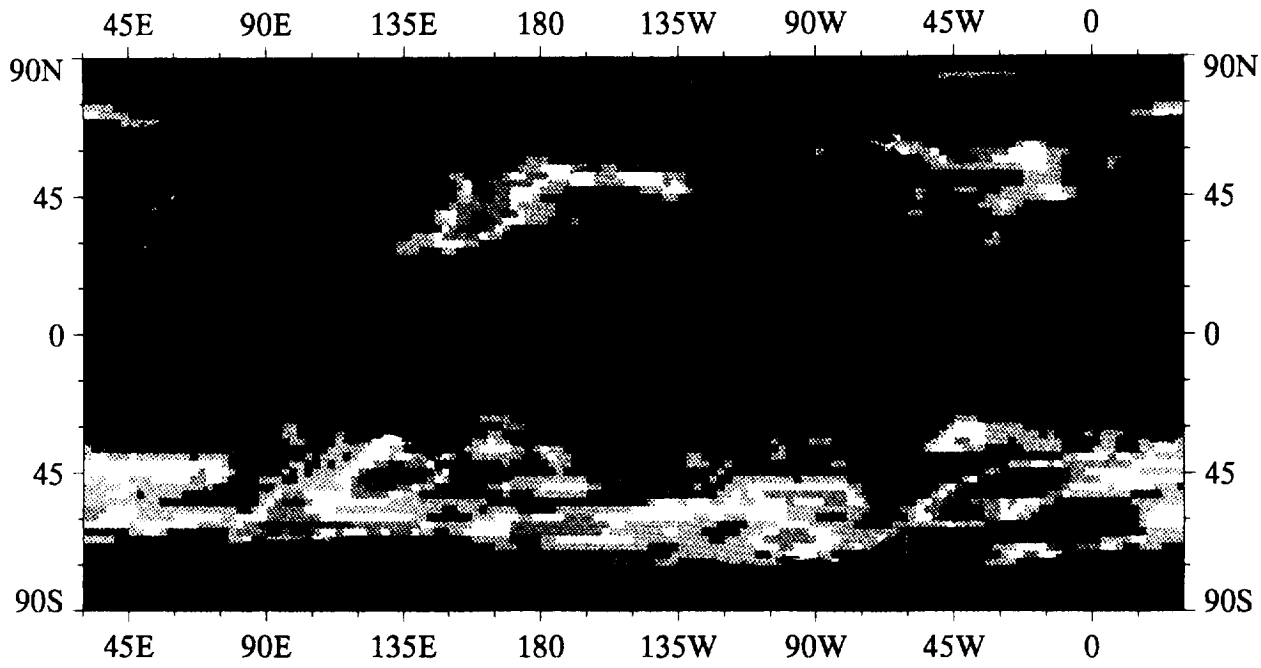

Zonal Wind Speed, May 1988

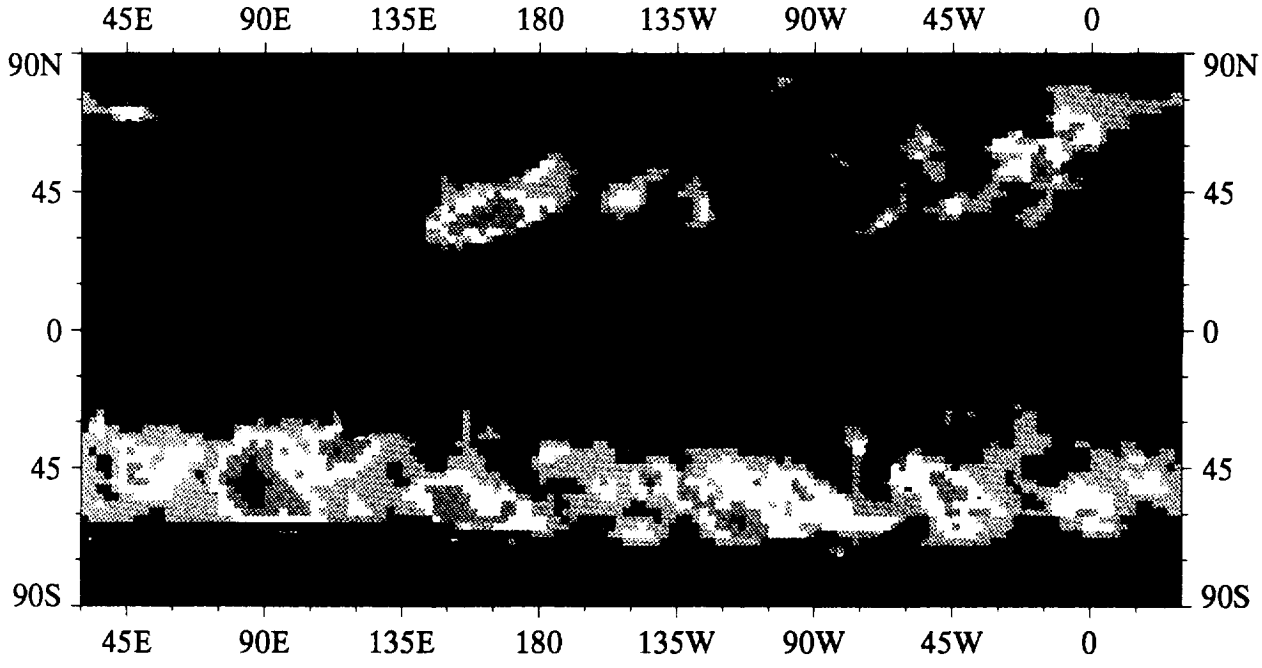

Meridional Wind Speed, May 1988

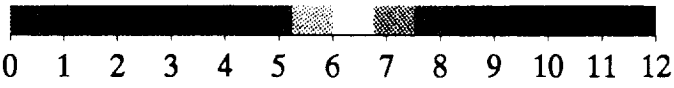

Standard Deviation of ECMWF 10 m Wind Speed, m s^{-1}

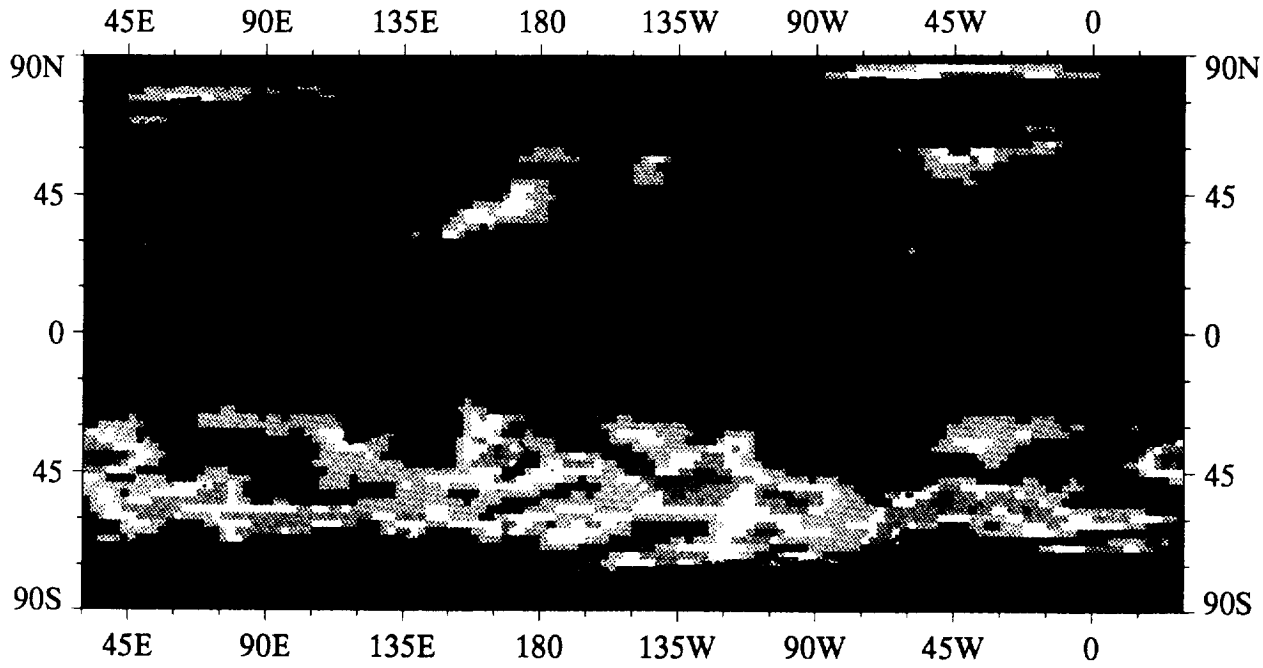

Zonal Wind Speed, June 1988

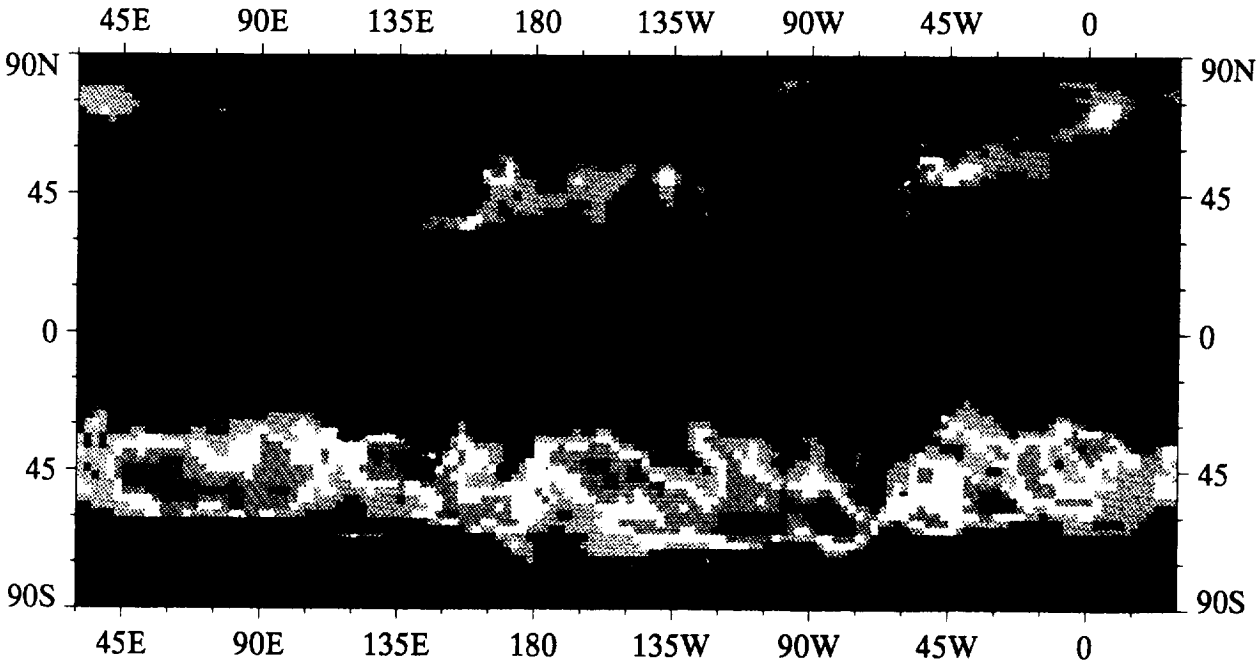

Meridional Wind Speed, June 1988

Standard Deviation of ECMWF 10 m Wind Speed, m s^{-1}

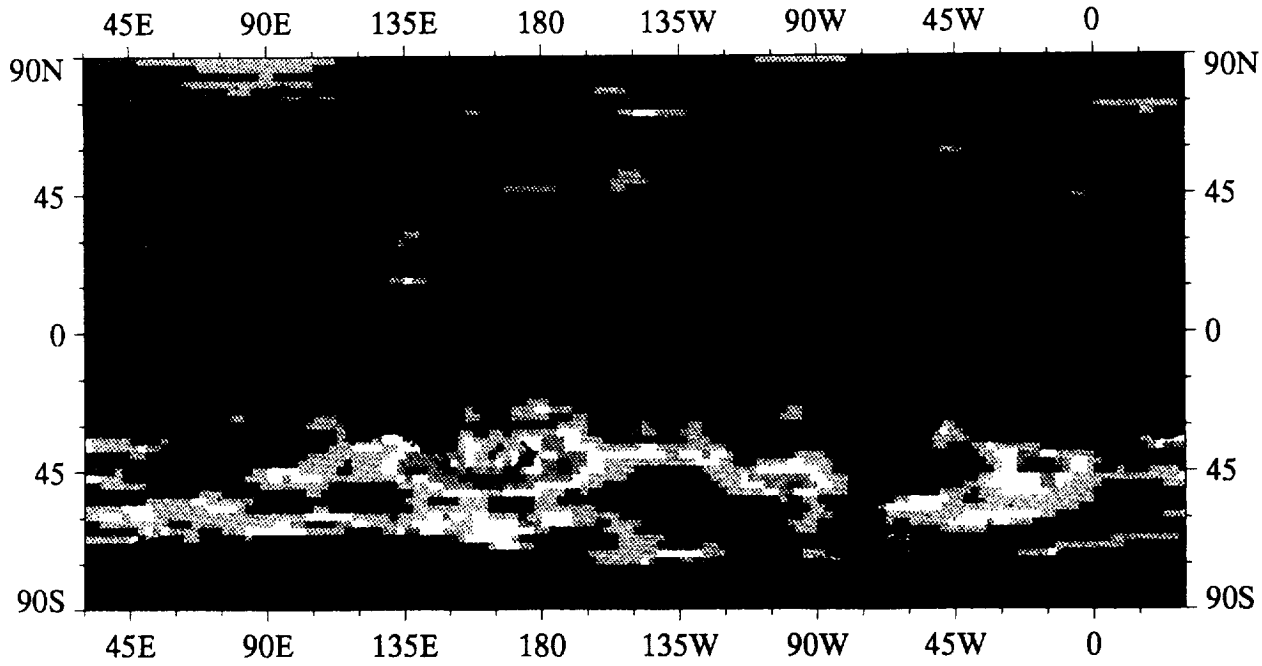

Zonal Wind Speed, July 1988

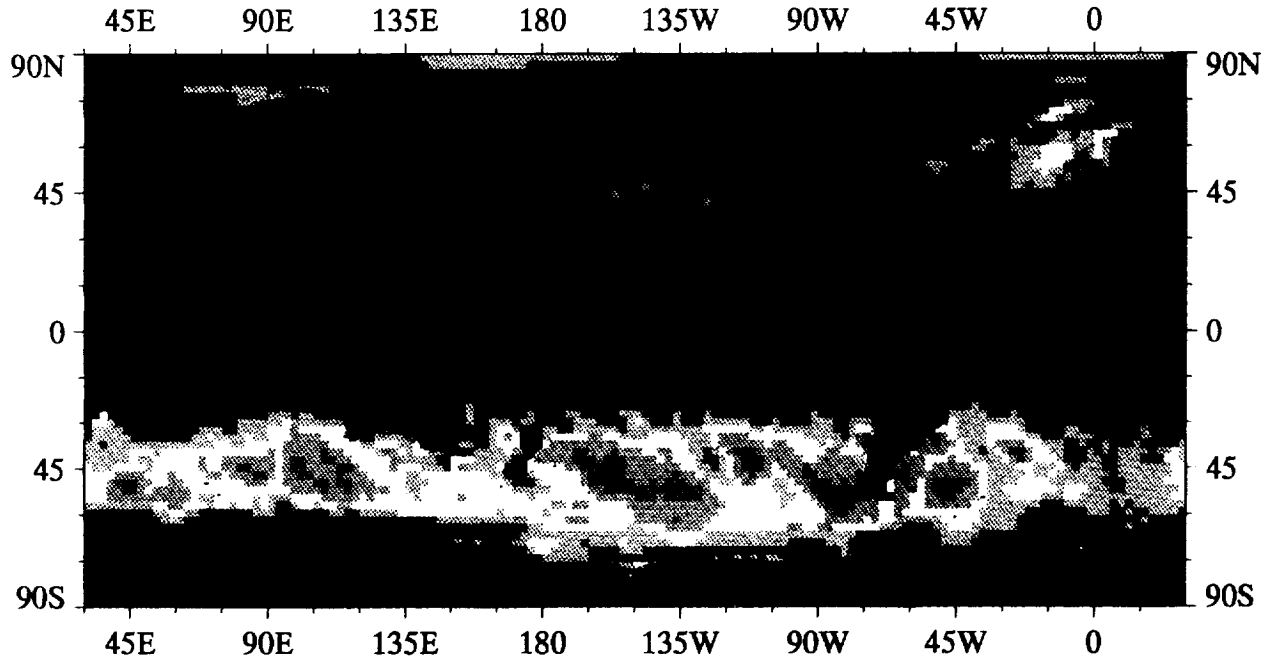

Meridional Wind Speed, July 1988

Standard Deviation of ECMWF 10 m Wind Speed, m s^{-1}

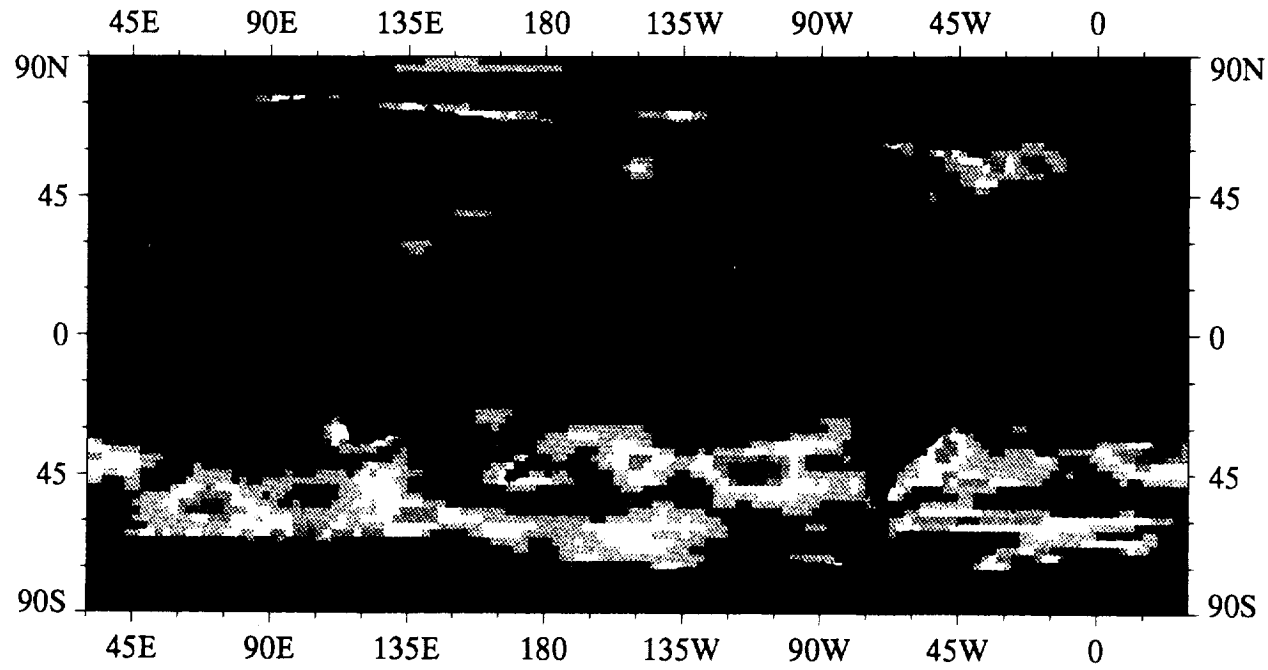

Zonal Wind Speed, August 1988

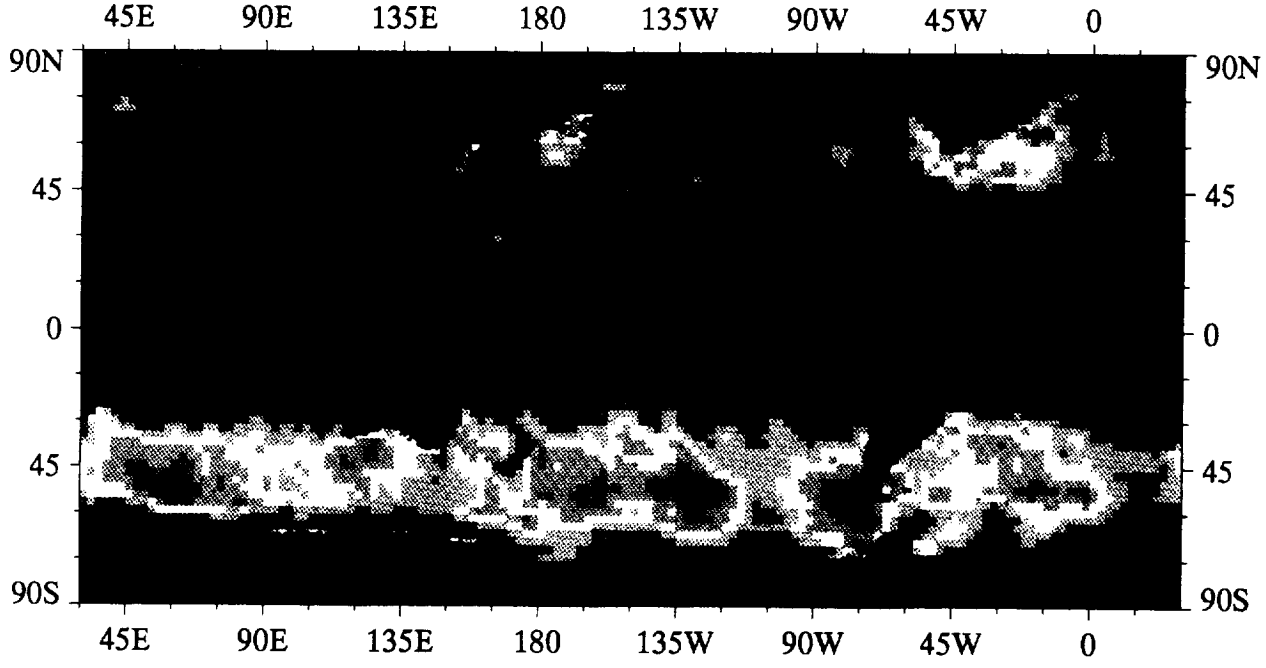

Meridional Wind Speed, August 1988

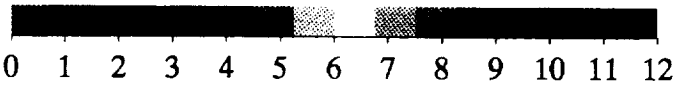

Standard Deviation of ECMWF 10 m Wind Speed, m s^{-1}

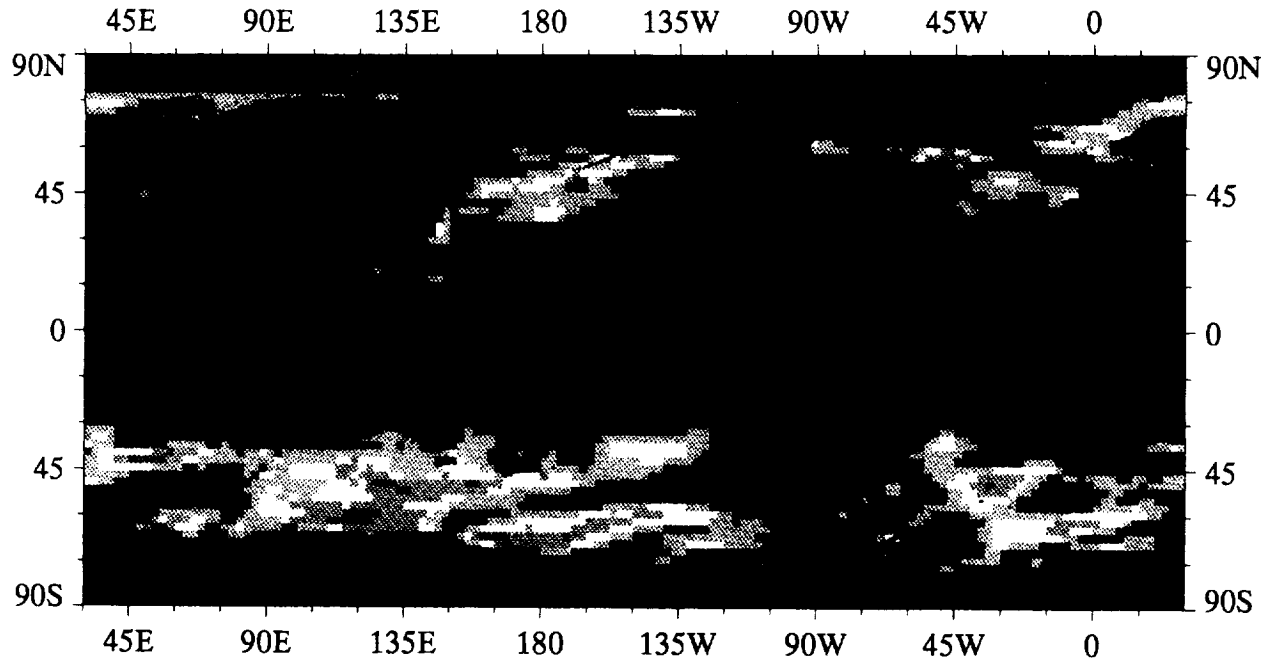

Zonal Wind Speed, September 1988

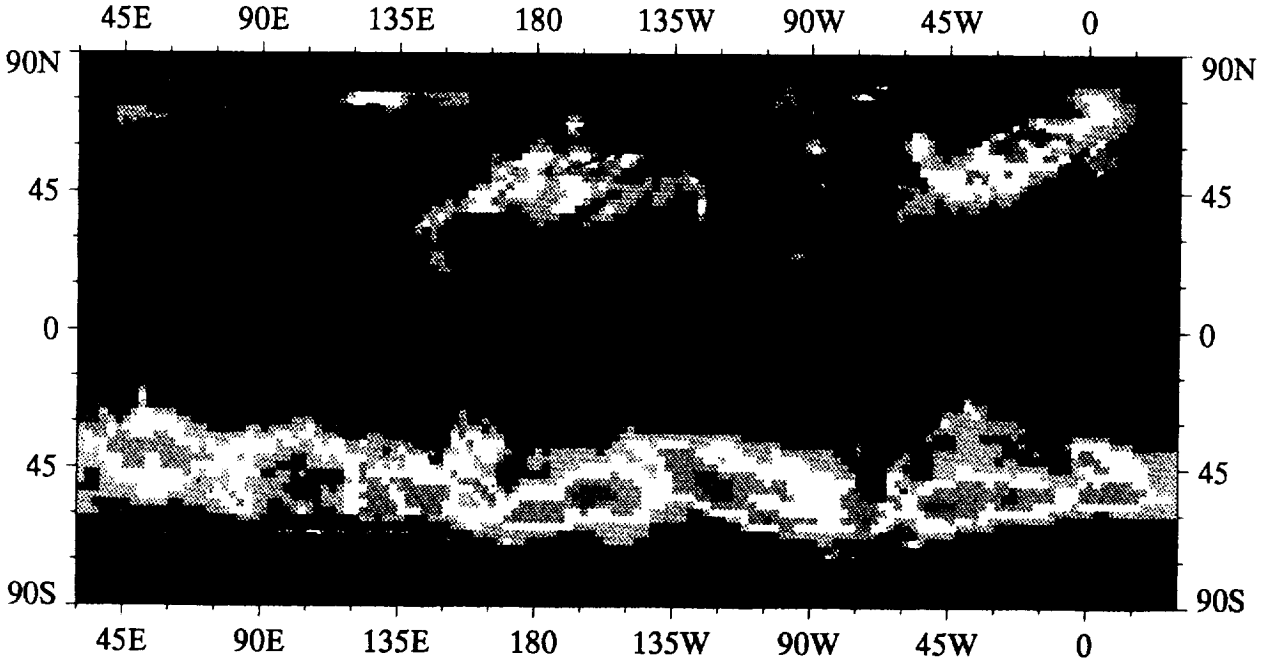

Meridional Wind Speed, September 1988

Standard Deviation of ECMWF 10 m Wind Speed, m s^{-1}

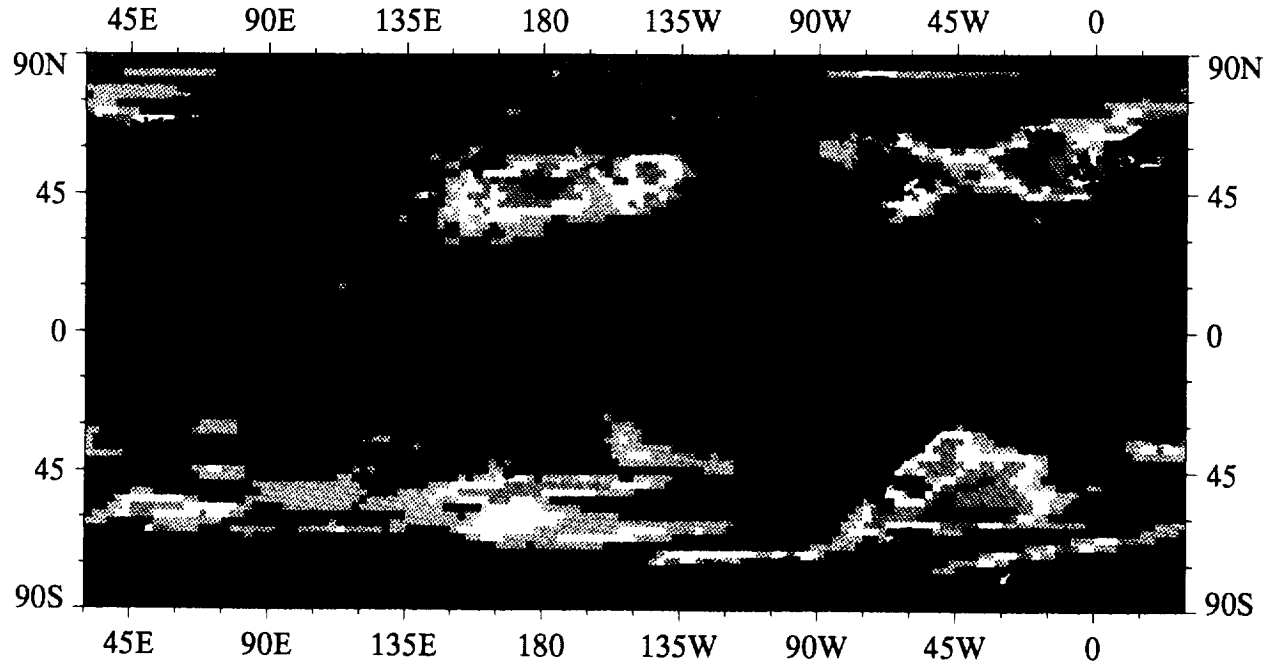

Zonal Wind Speed, October 1988

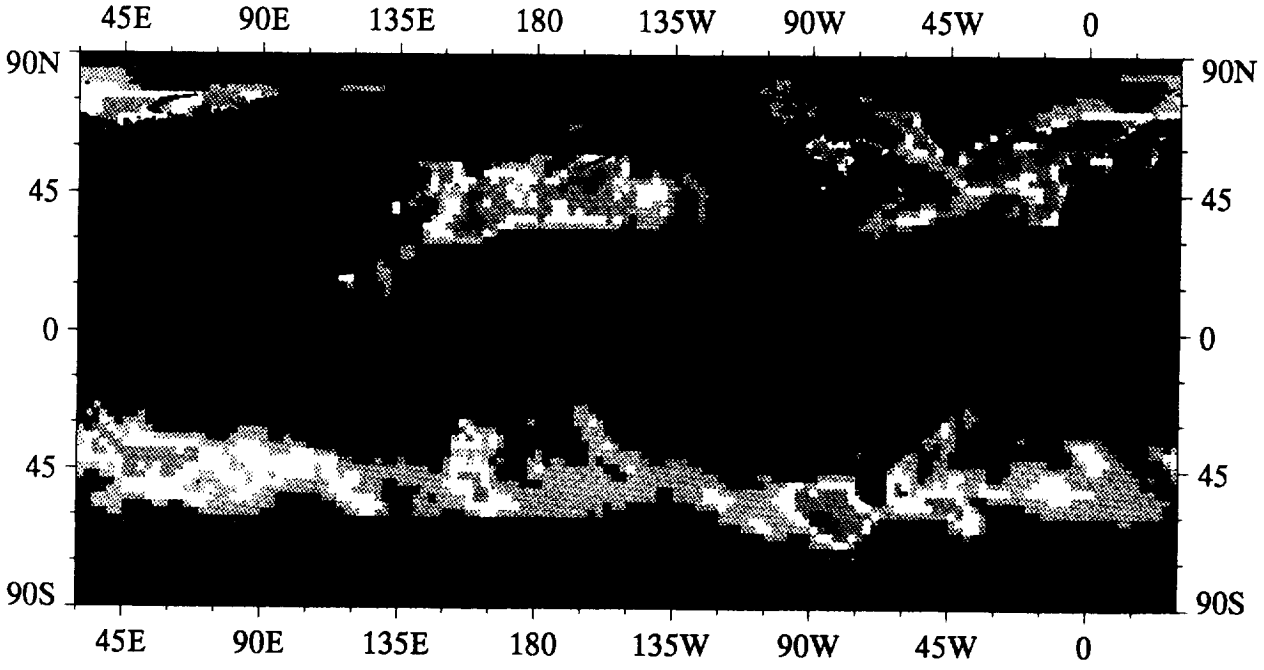

Meridional Wind Speed, October 1988

Standard Deviation of ECMWF 10 m Wind Speed, m s^{-1}

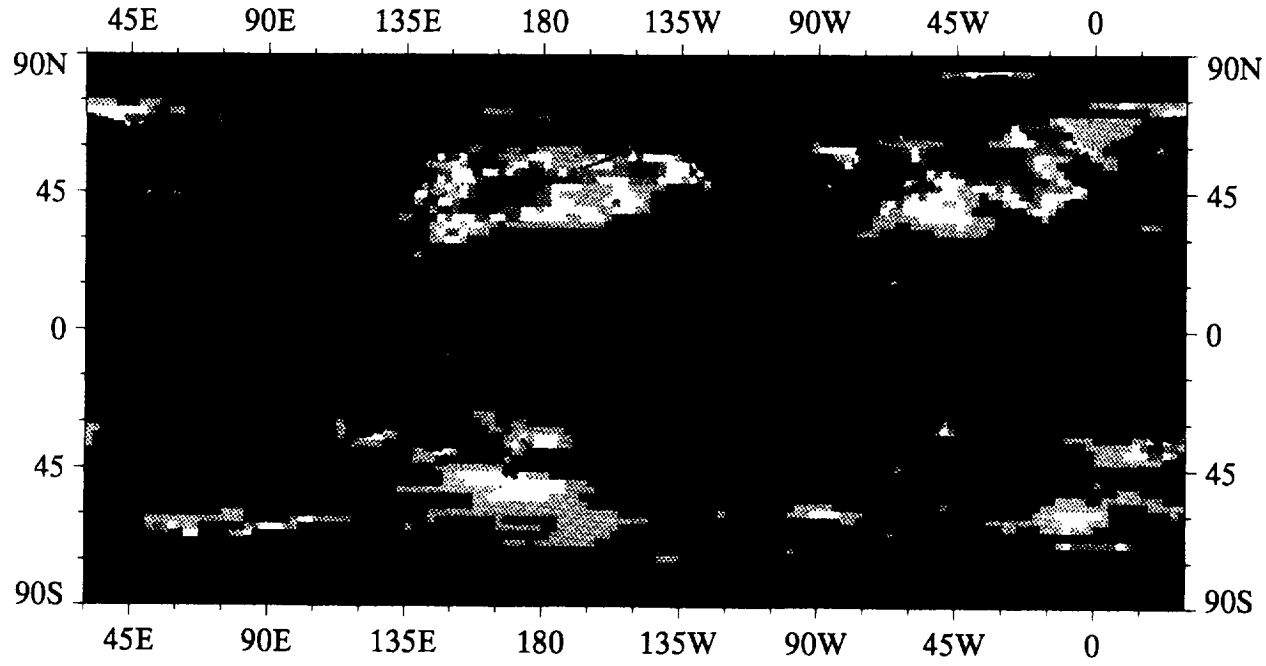

Zonal Wind Speed, November 1988

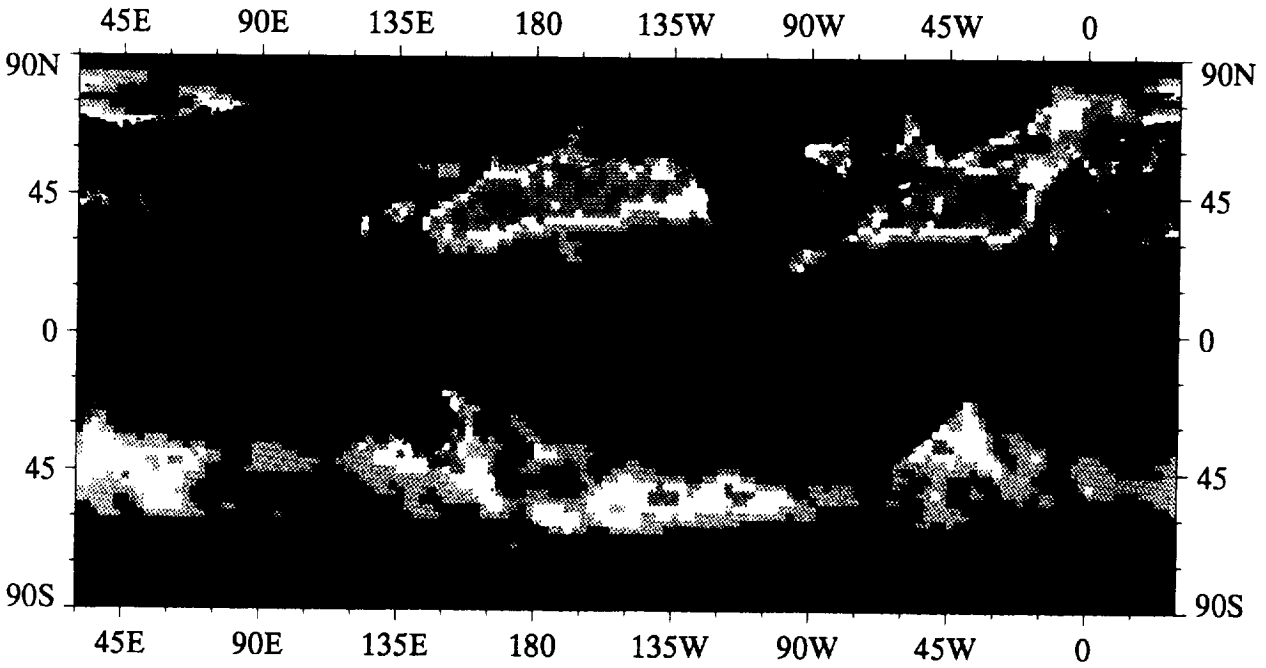

Meridional Wind Speed, November 1988

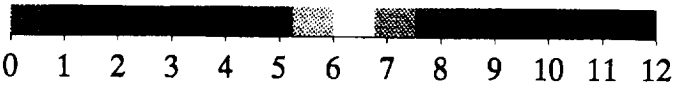

Standard Deviation of ECMWF 10 m Wind Speed, m s^{-1}

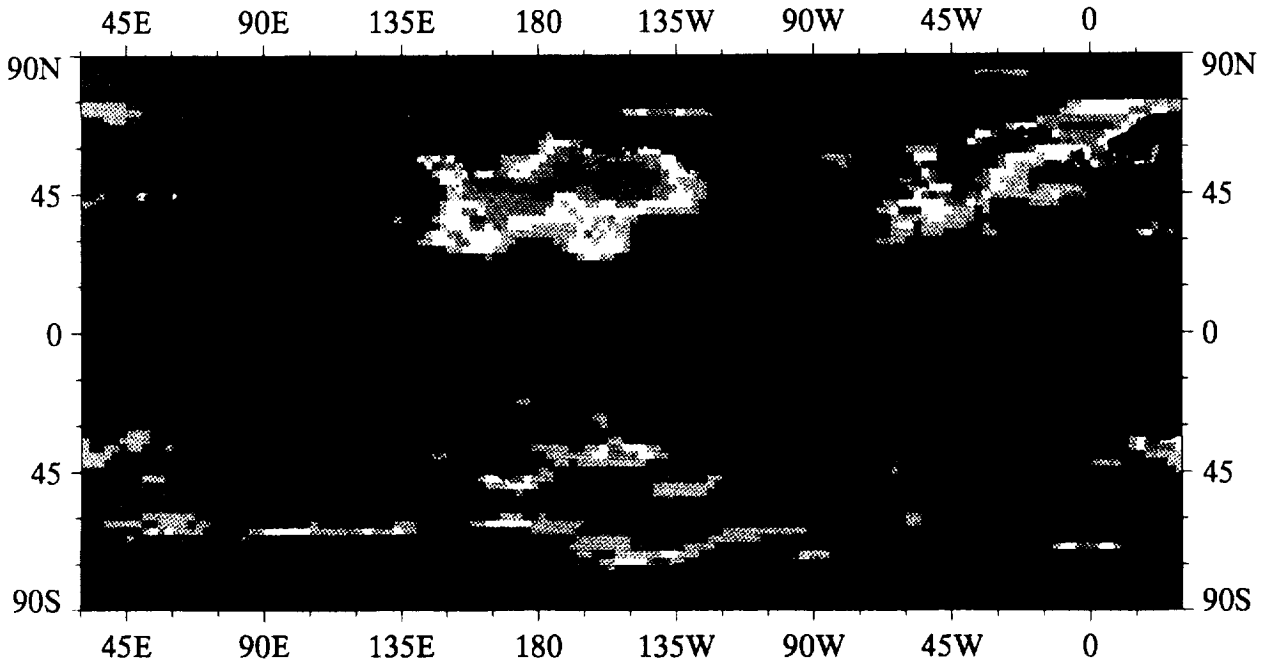

Zonal Wind Speed, December 1988

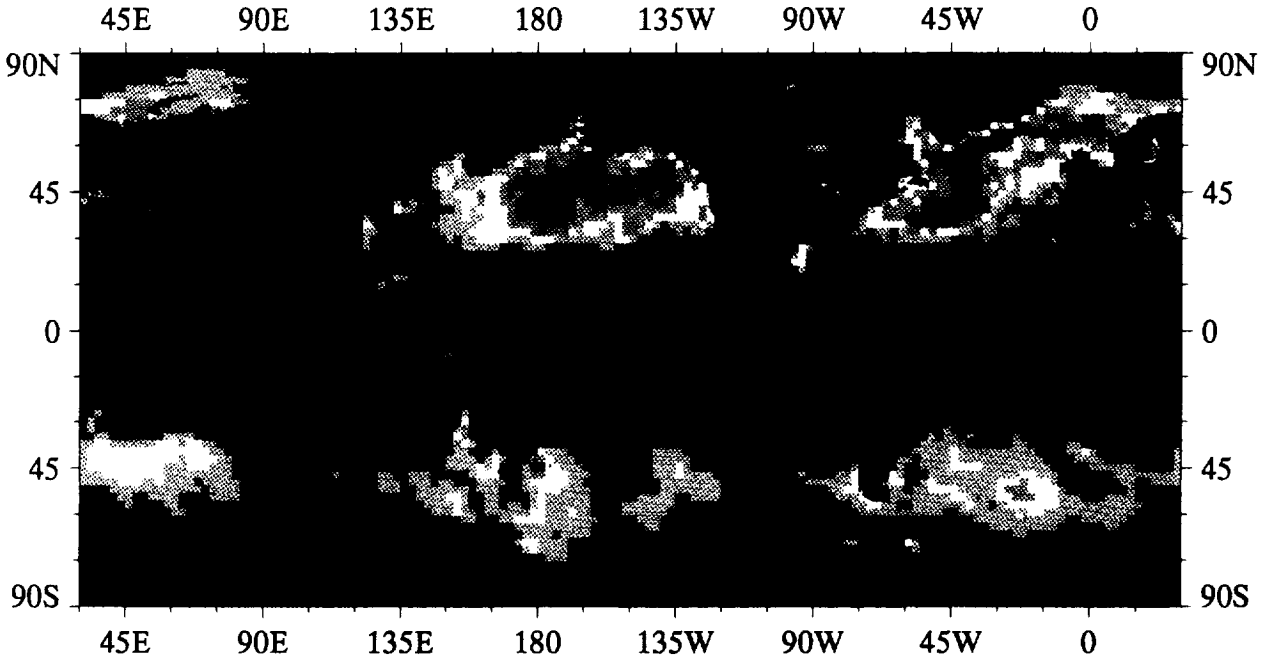

Meridional Wind Speed, December 1988

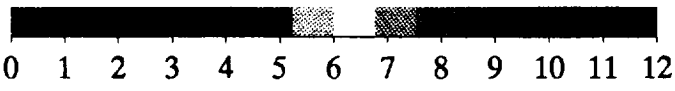

Standard Deviation of ECMWF 10 m Wind Speed, m s^{-1}

A13

Annual Mean ECMWF Surface Wind Speed

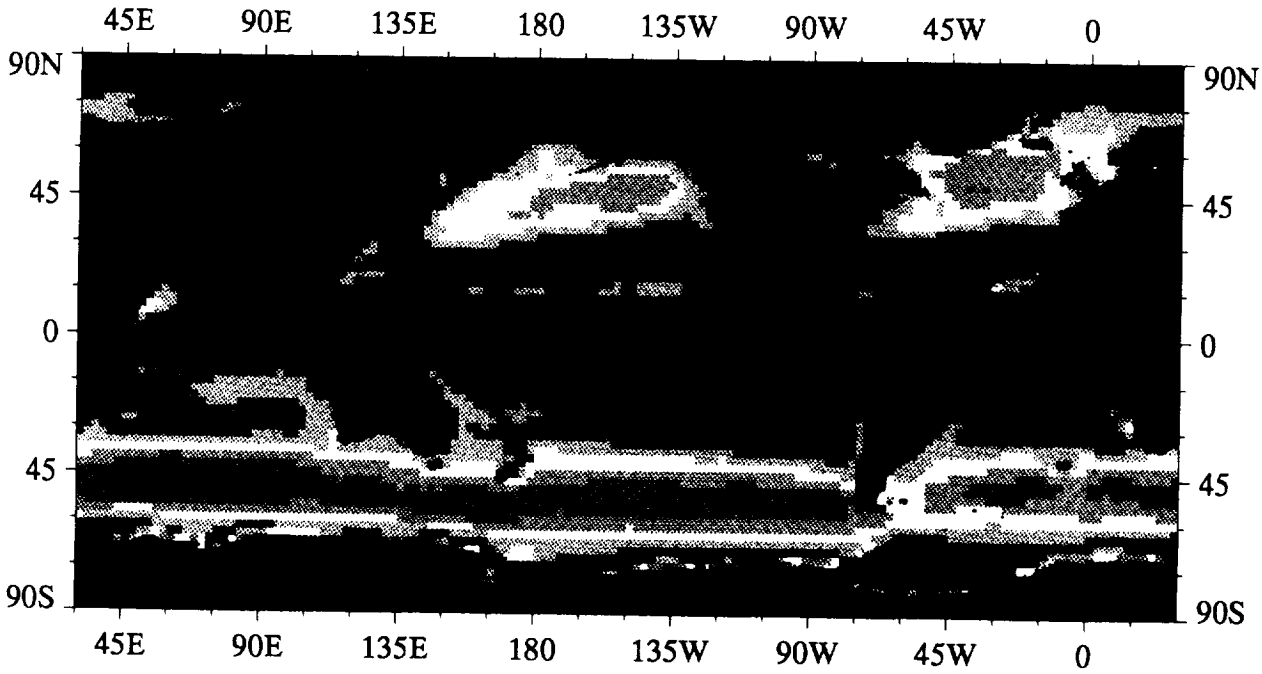

Annual Mean 1988

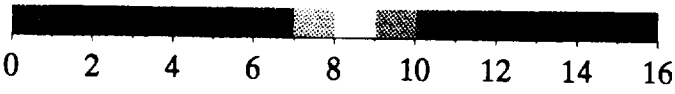

ECMWF 10 m Wind Speed, m s^{-1}

A14

Monthly Mean ECMWF Surface Wind Speed

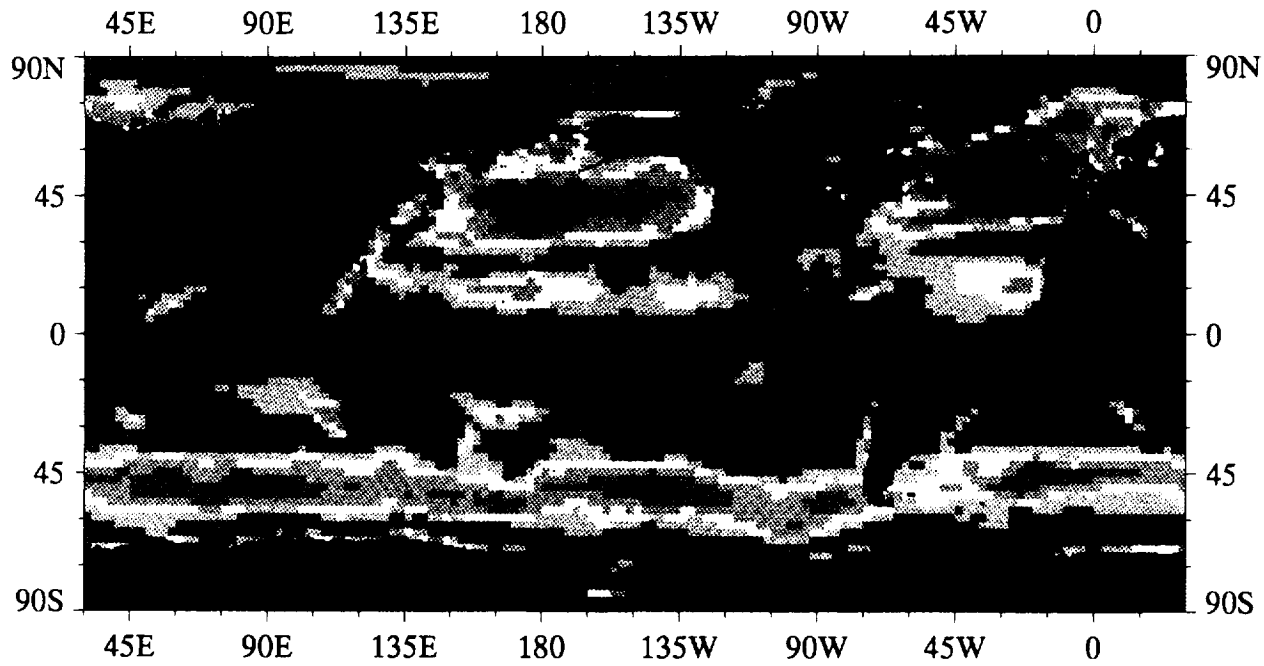

January 1988

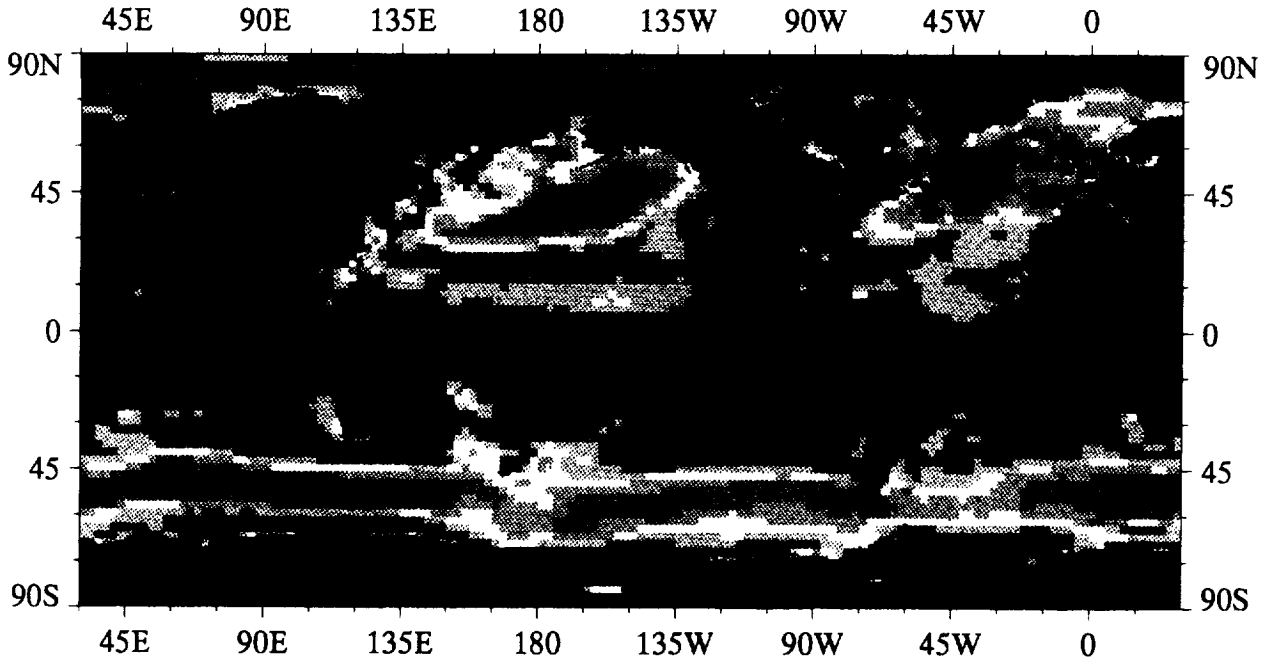

February 1988

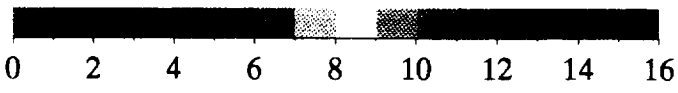

ECMWF 10 m Wind Speed, m s^{-1}

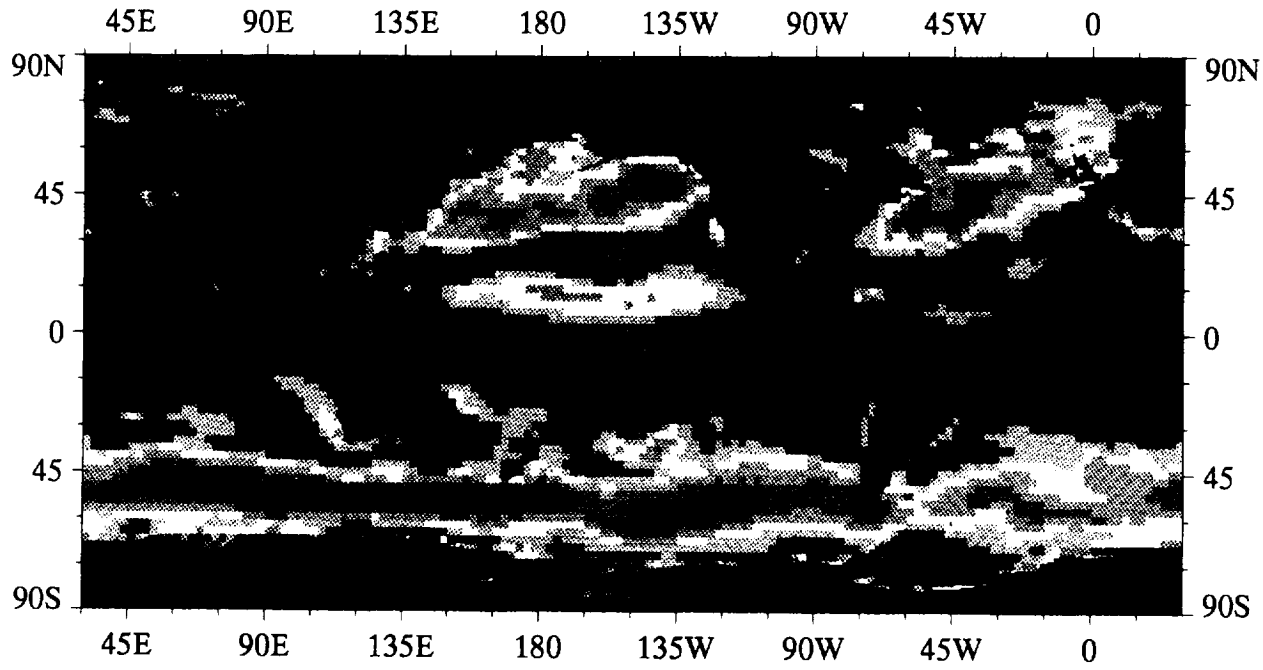

March 1988

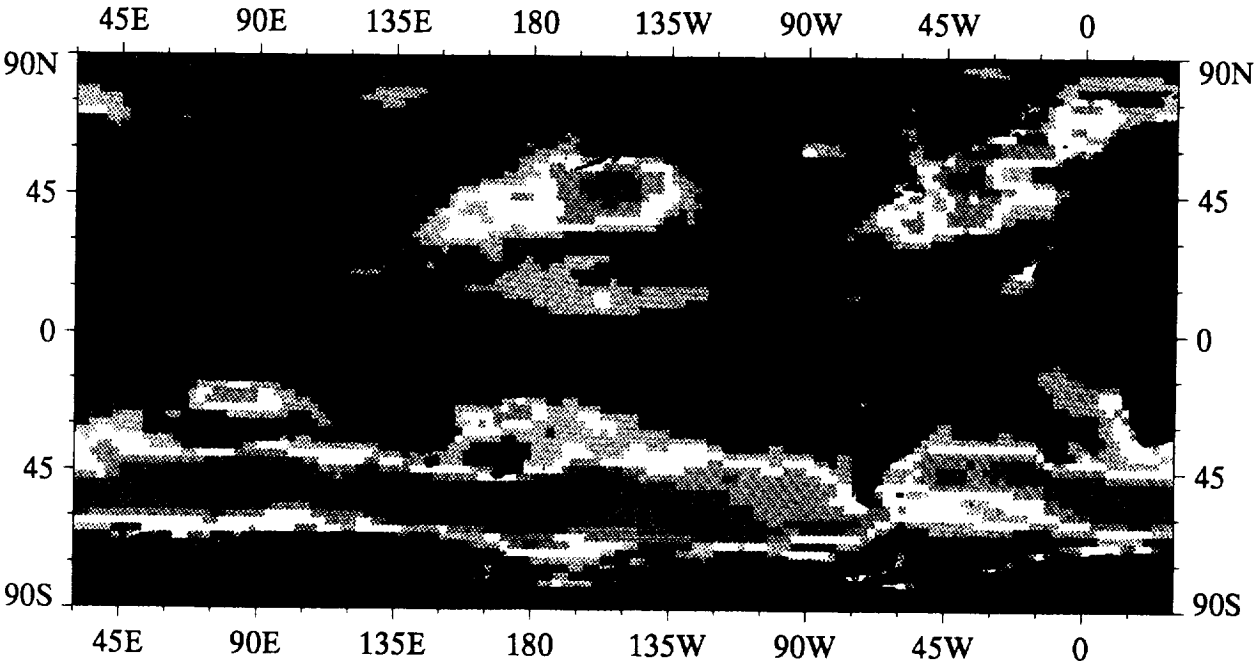

April 1988

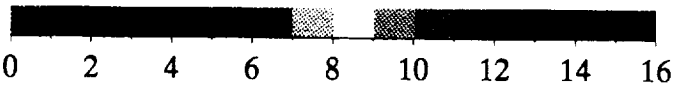

ECMWF 10 m Wind Speed, m s^{-1}

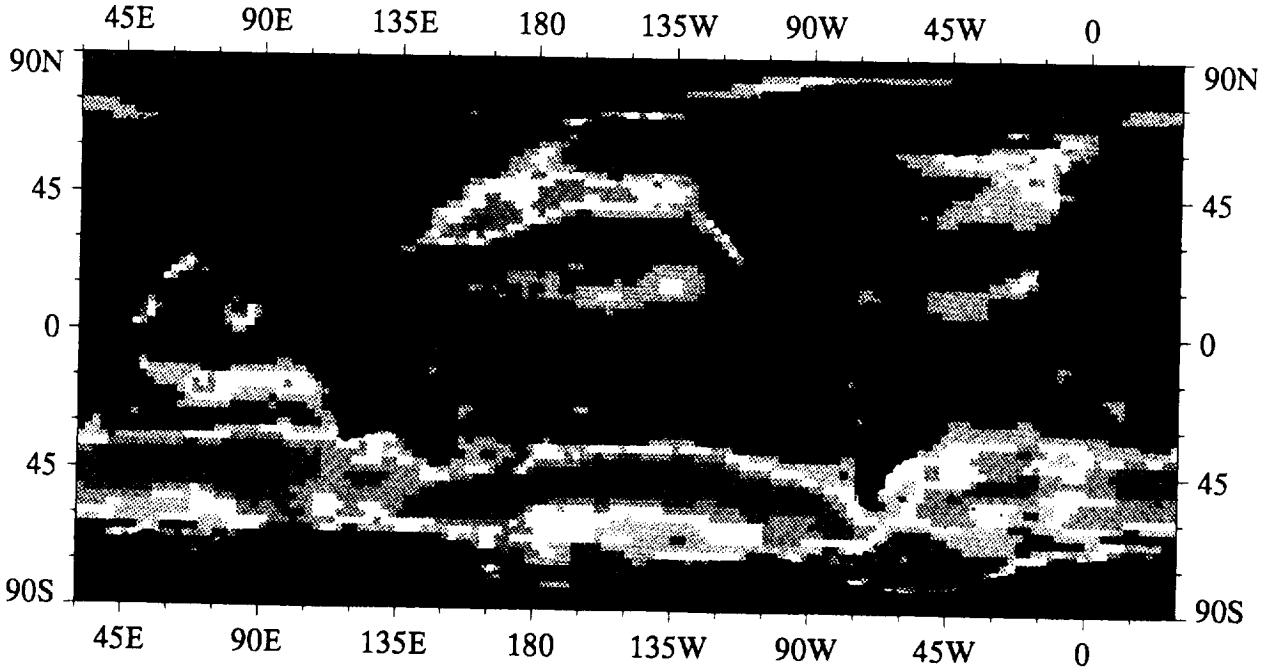

May 1988

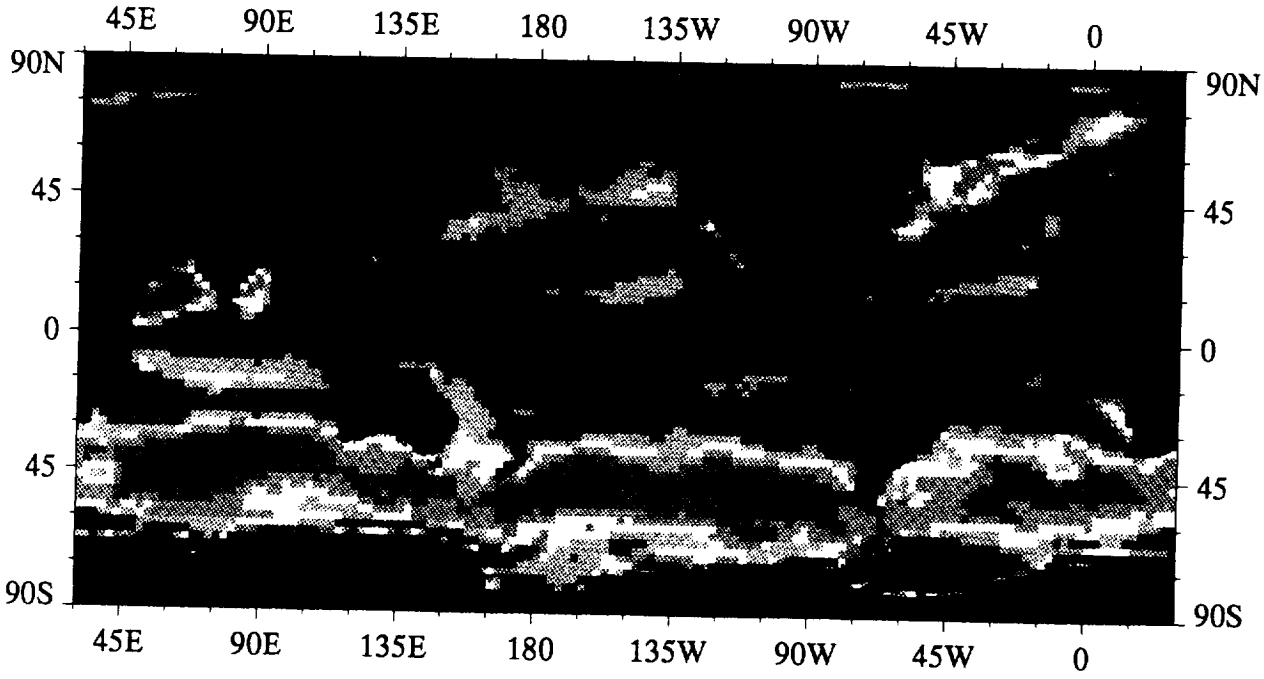

June 1988

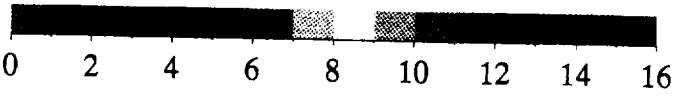

ECMWF 10 m Wind Speed, m s^{-1}

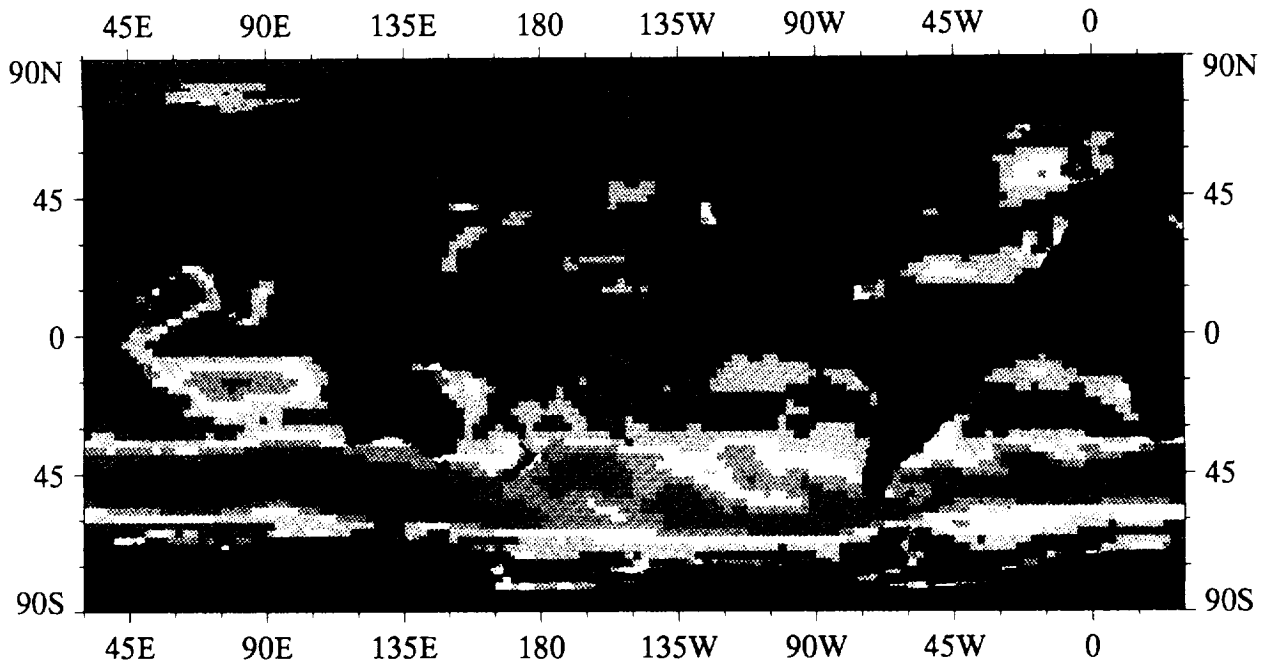

July 1988

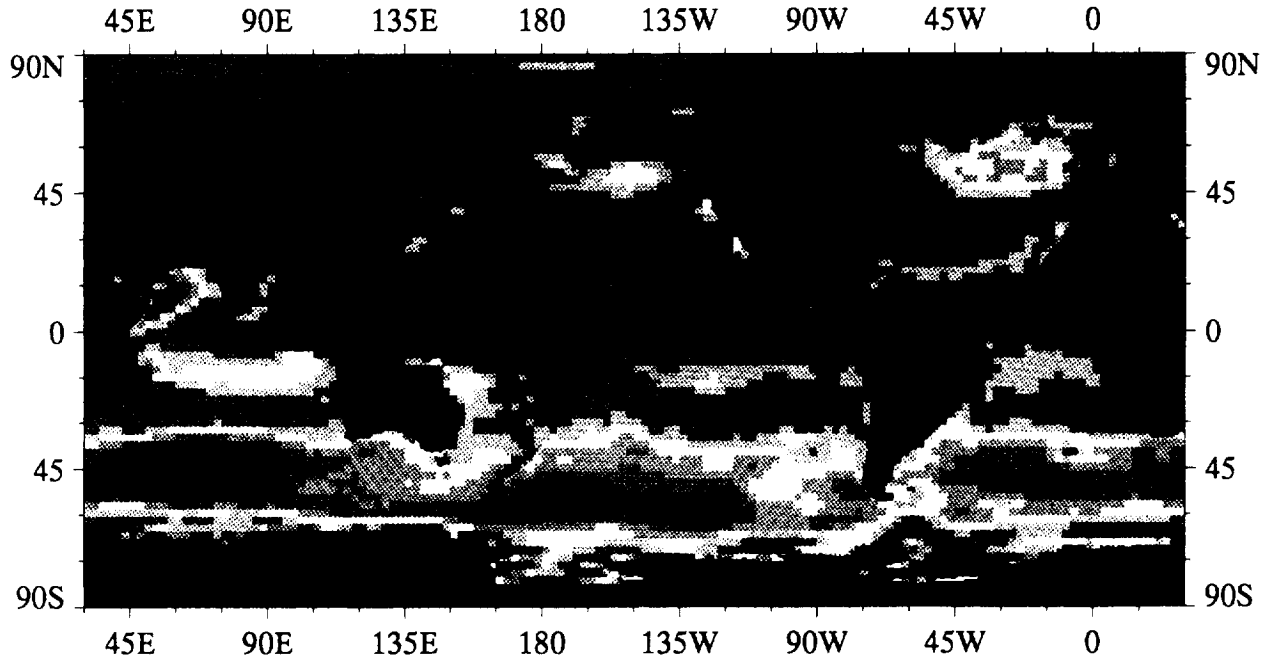

August 1988

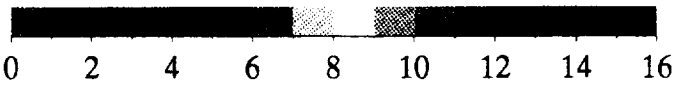

ECMWF 10 m Wind Speed, m s^{-1}

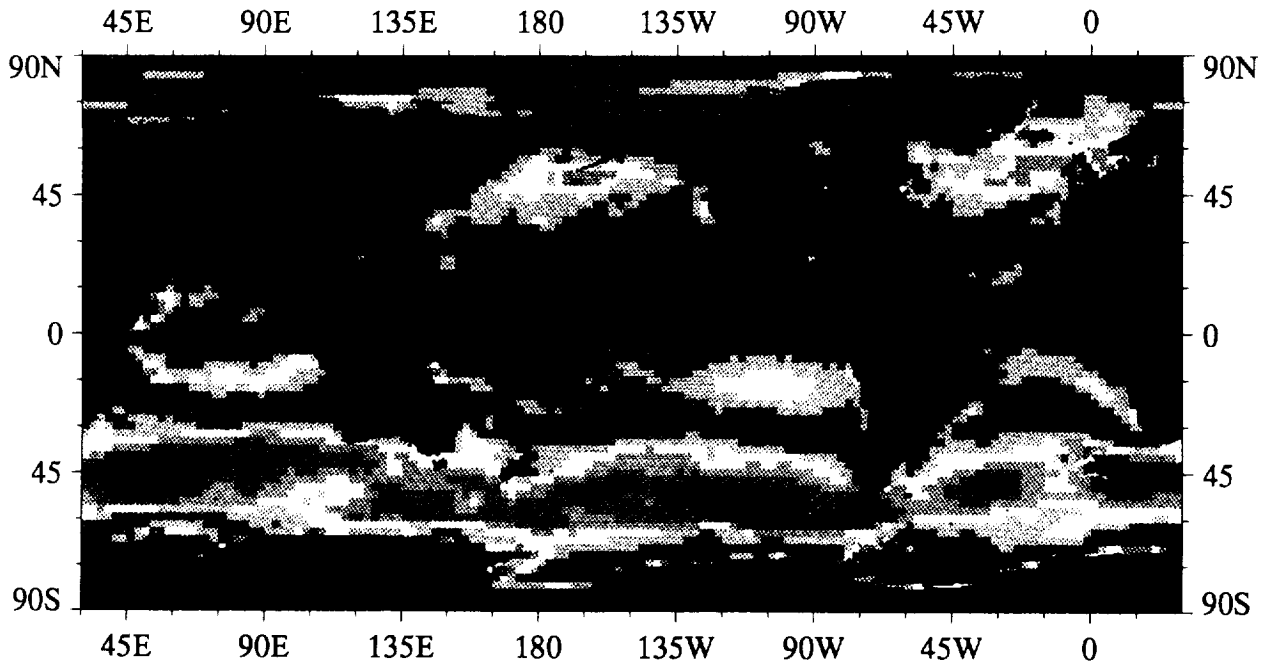

September 1988

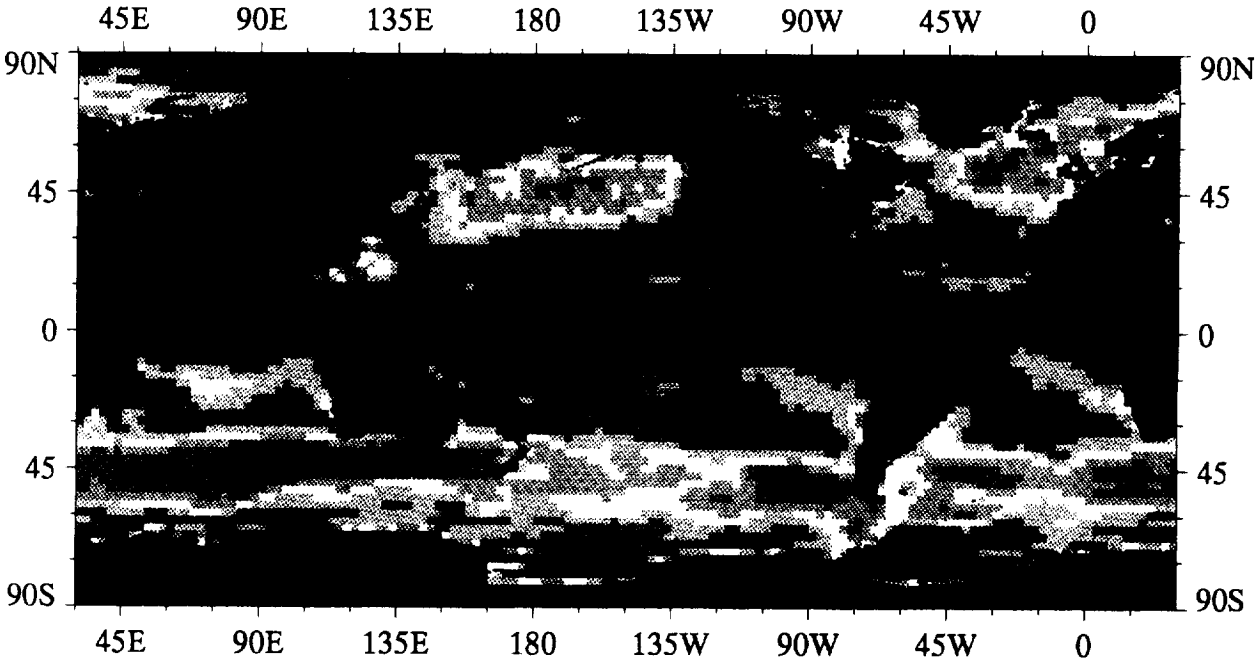

October 1988

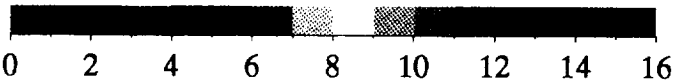

ECMWF 10 m Wind Speed, m s^{-1}

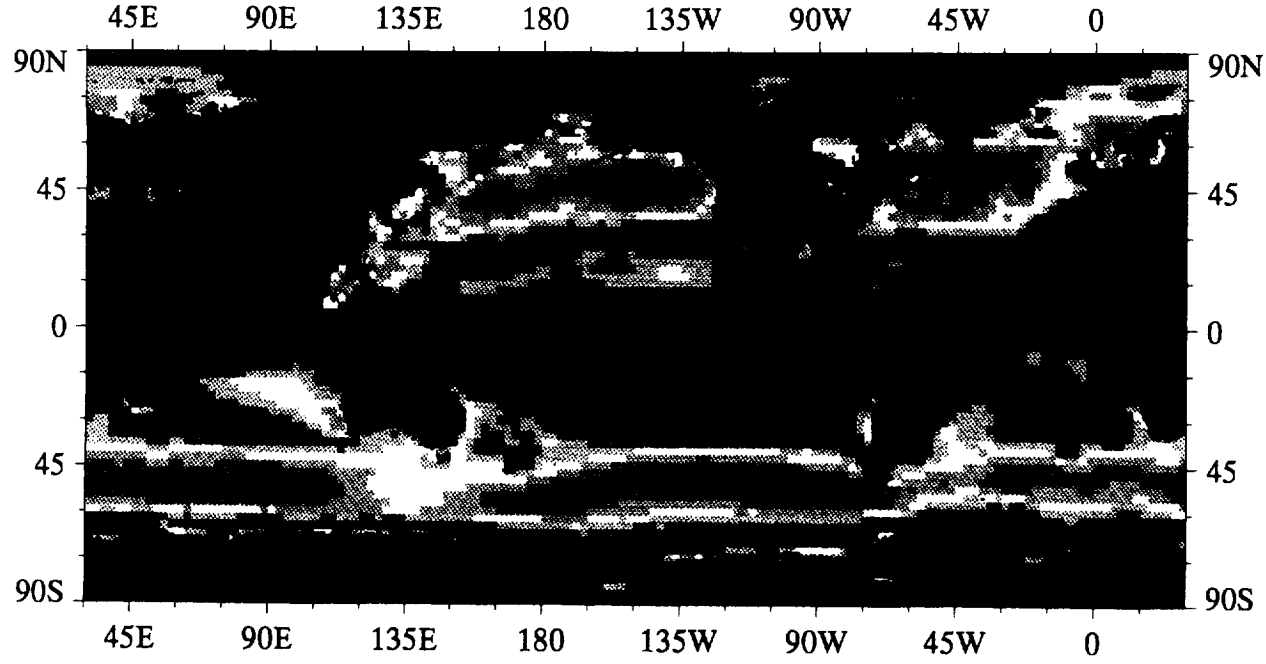

November 1988

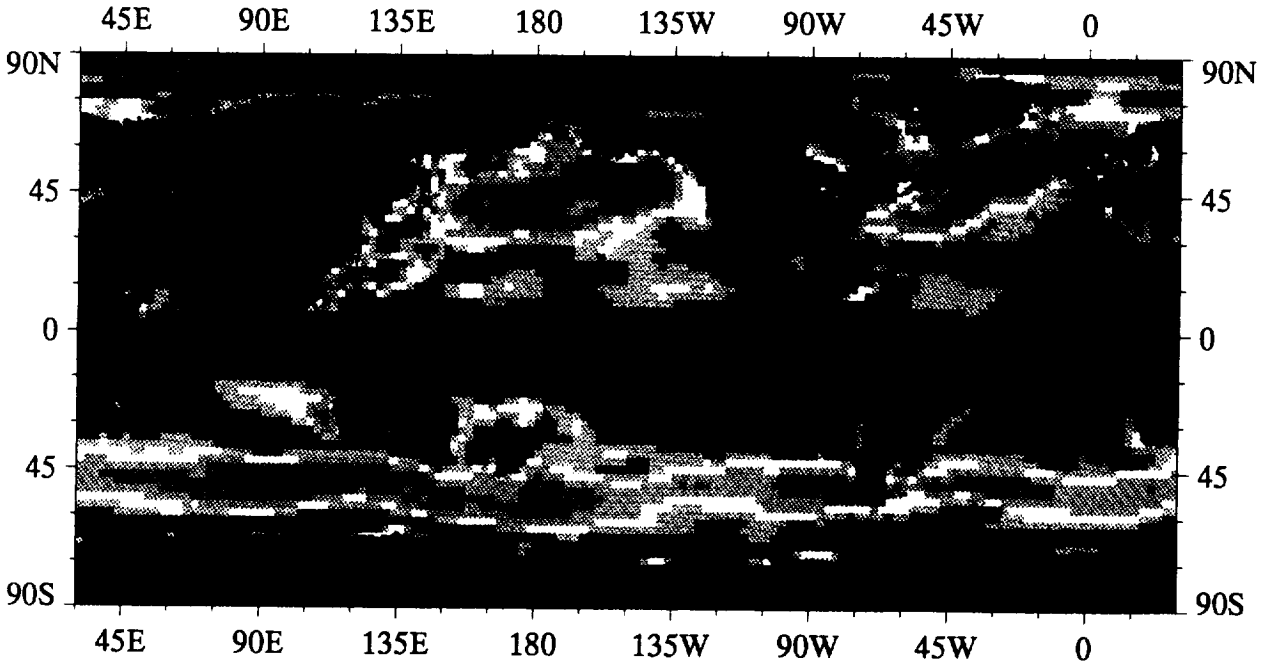

December 1988

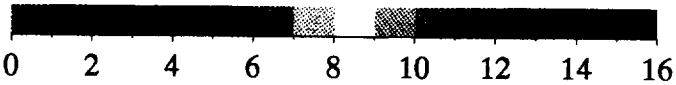

ECMWF 10 m Wind Speed, m s^{-1}

A15

Monthly Standard Deviation of ECMWF Surface Wind Speed

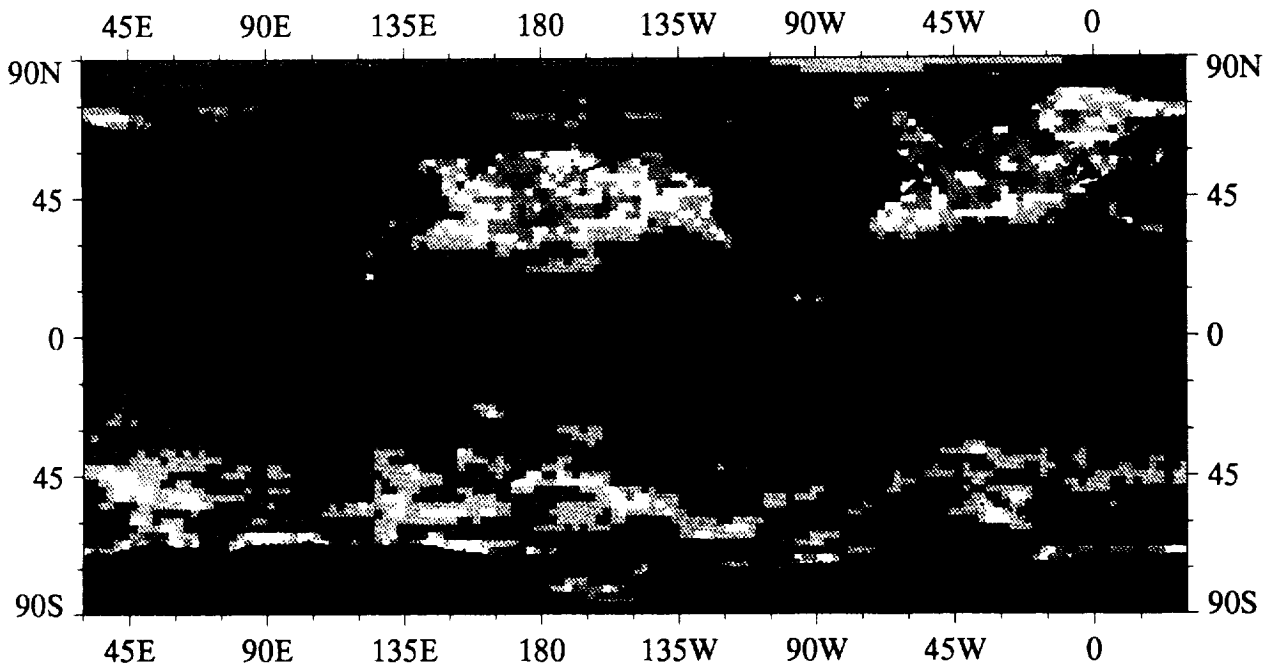

January 1988

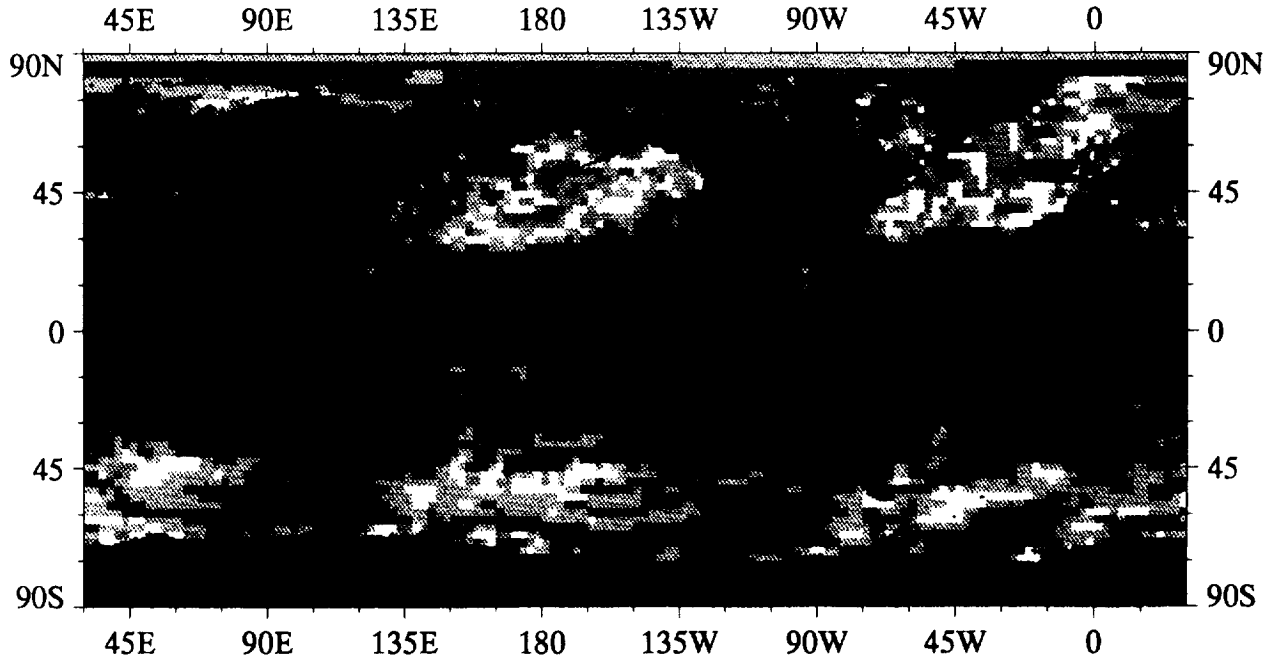

February 1988

Standard Deviation of ECMWF 10 m Wind Speed, m s^{-1}

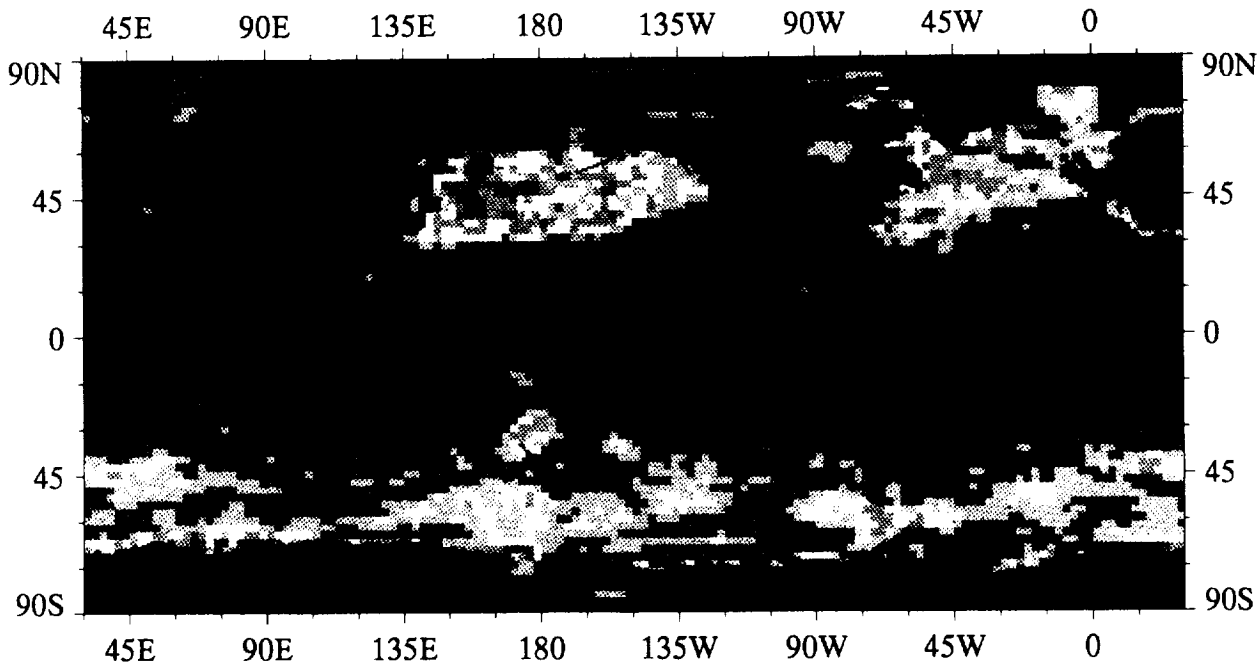

March 1988

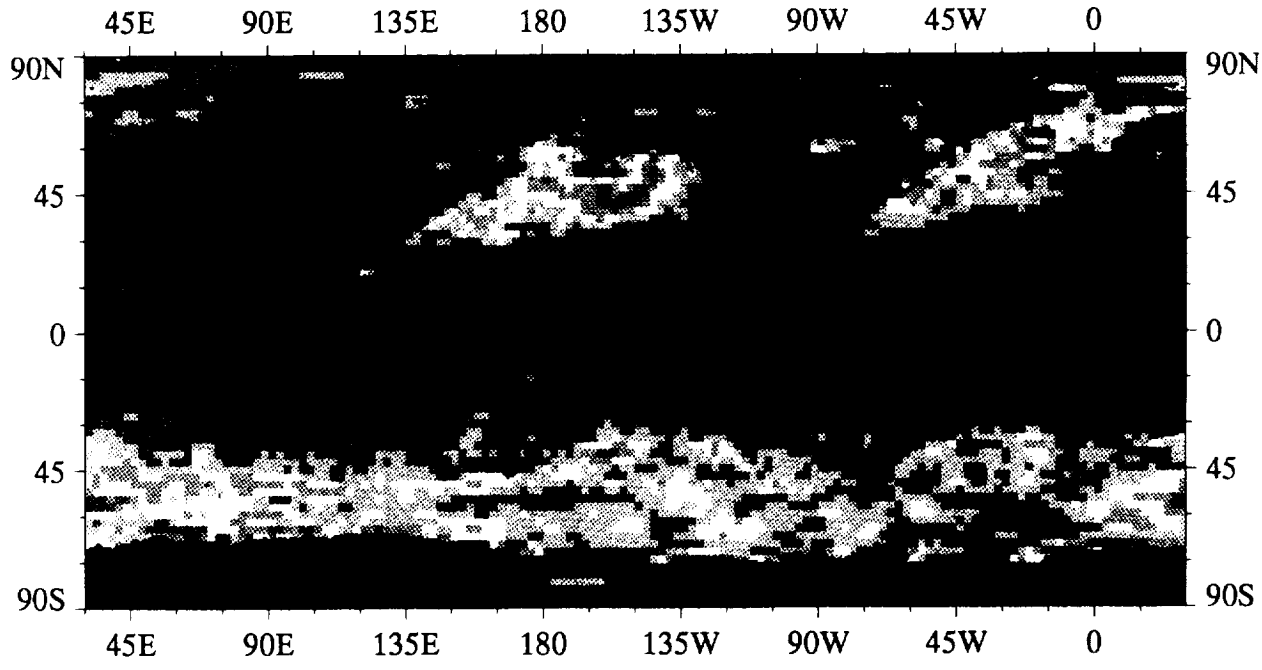

April 1988

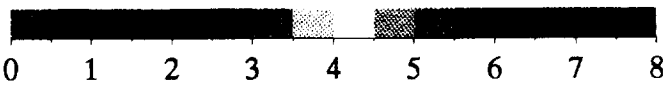

Standard Deviation of ECMWF 10 m Wind Speed, m s^{-1}

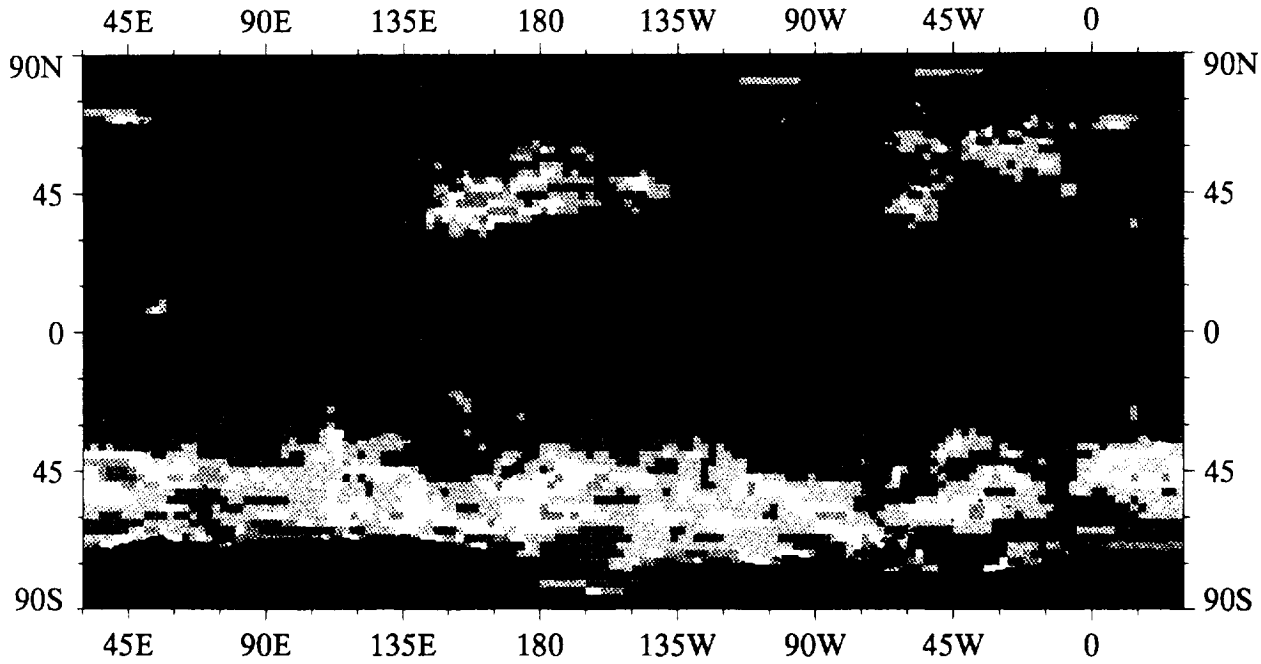

May 1988

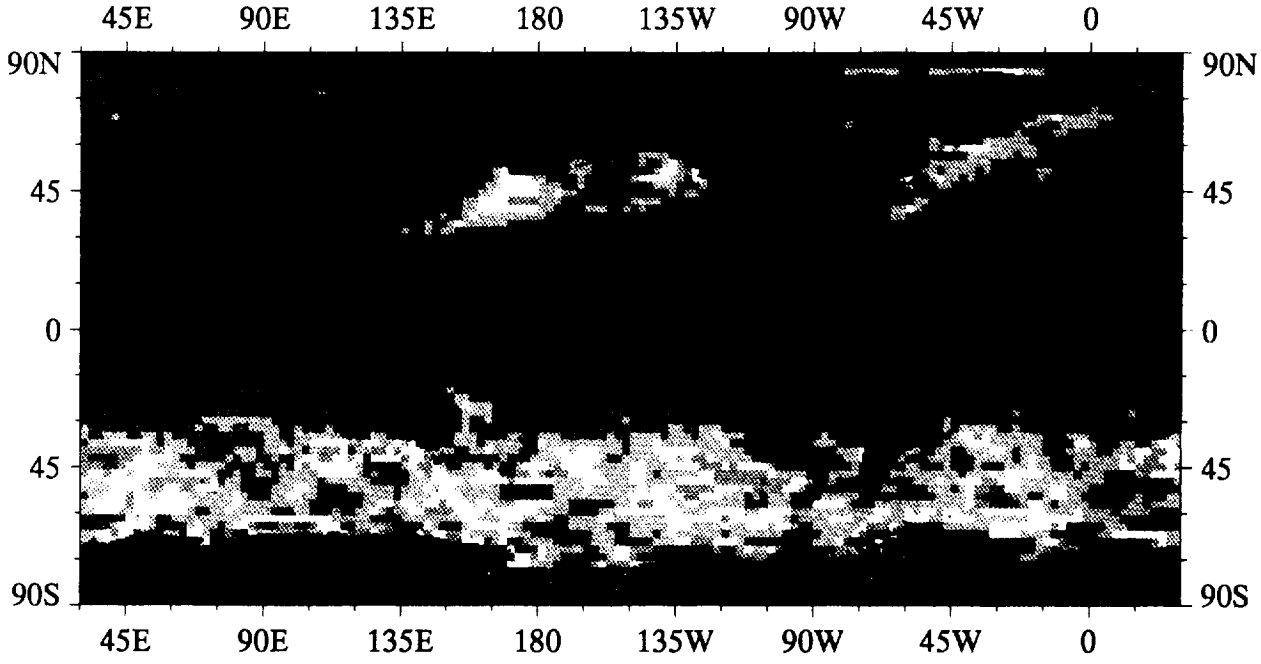

June 1988

Standard Deviation of ECMWF 10 m Wind Speed, m s^{-1}

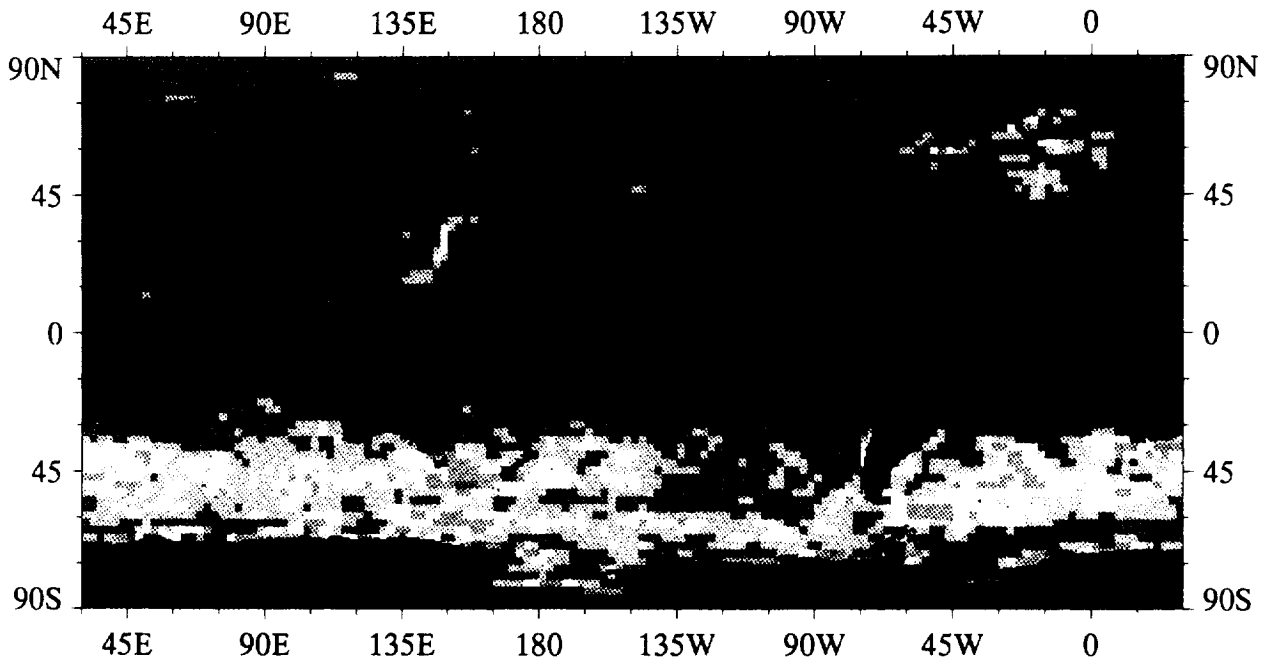

July 1988

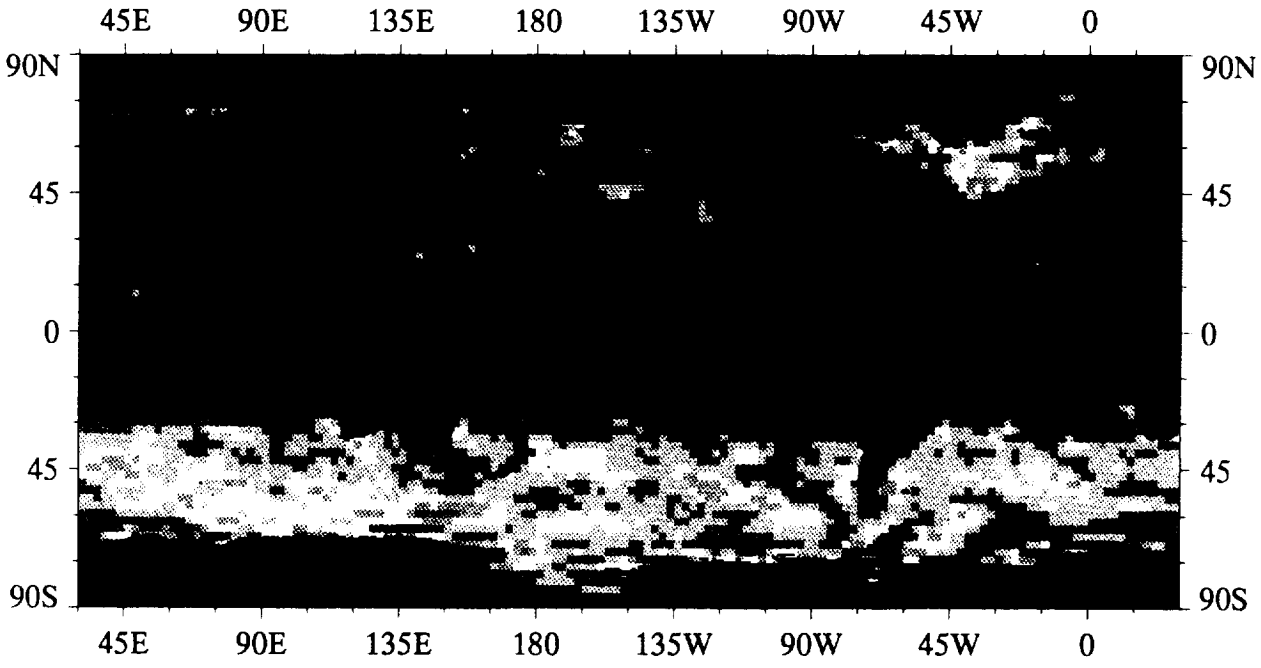

August 1988

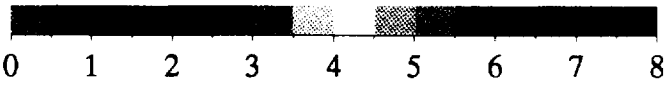

Standard Deviation of ECMWF 10 m Wind Speed, m s^{-1}

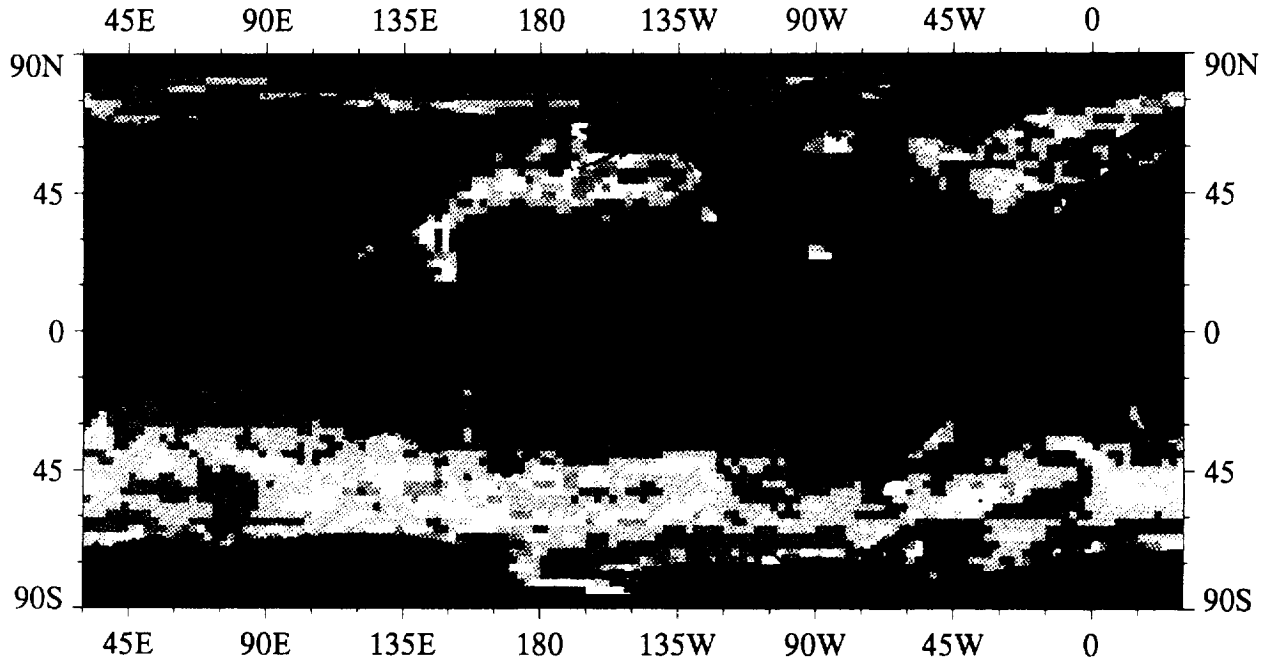

September 1988

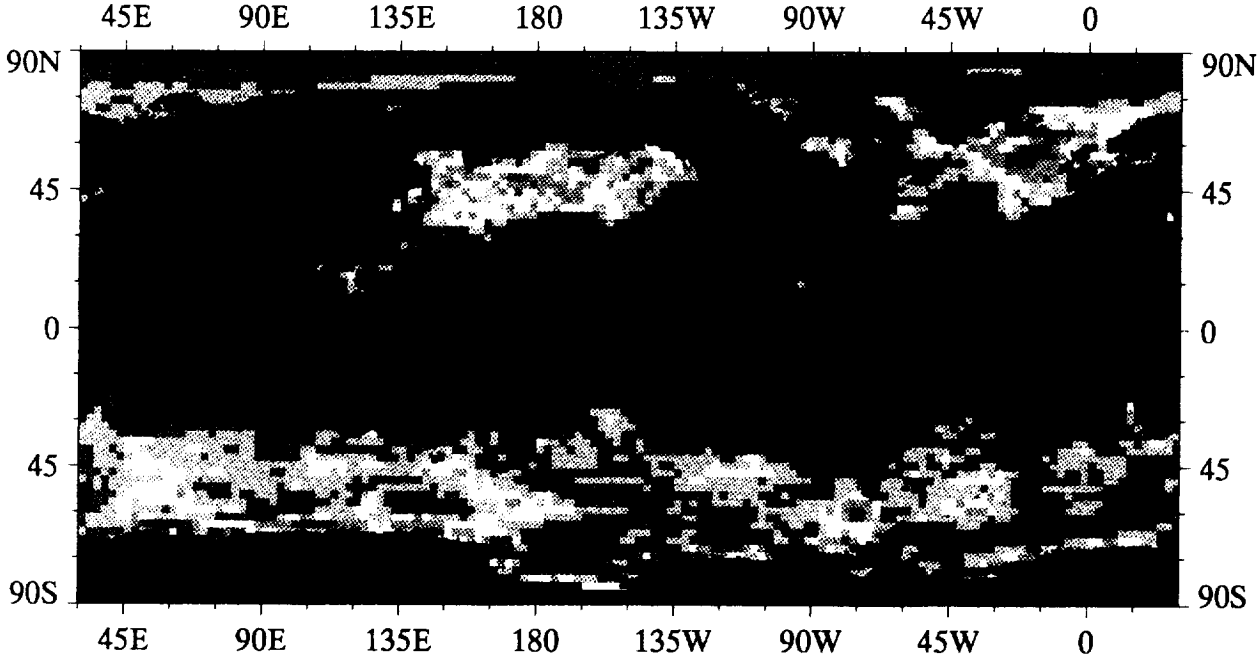

October 1988

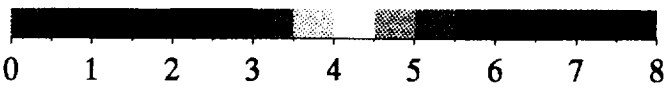

Standard Deviation of ECMWF 10 m Wind Speed, m s^{-1}

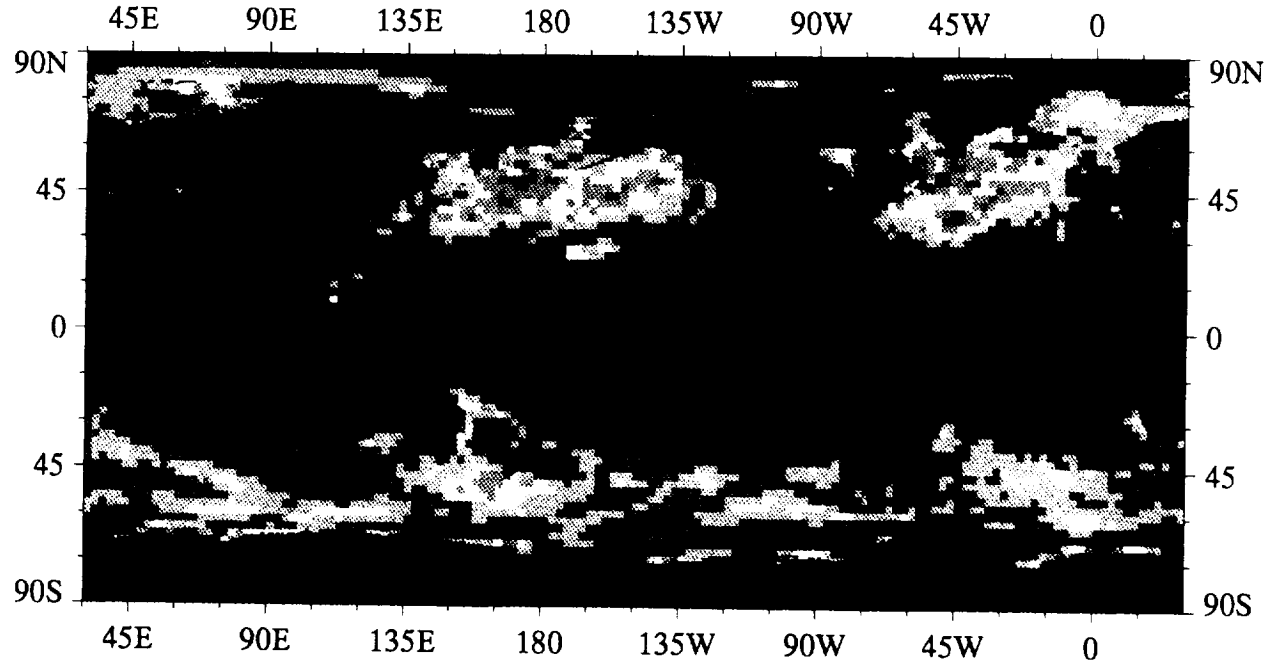

November 1988

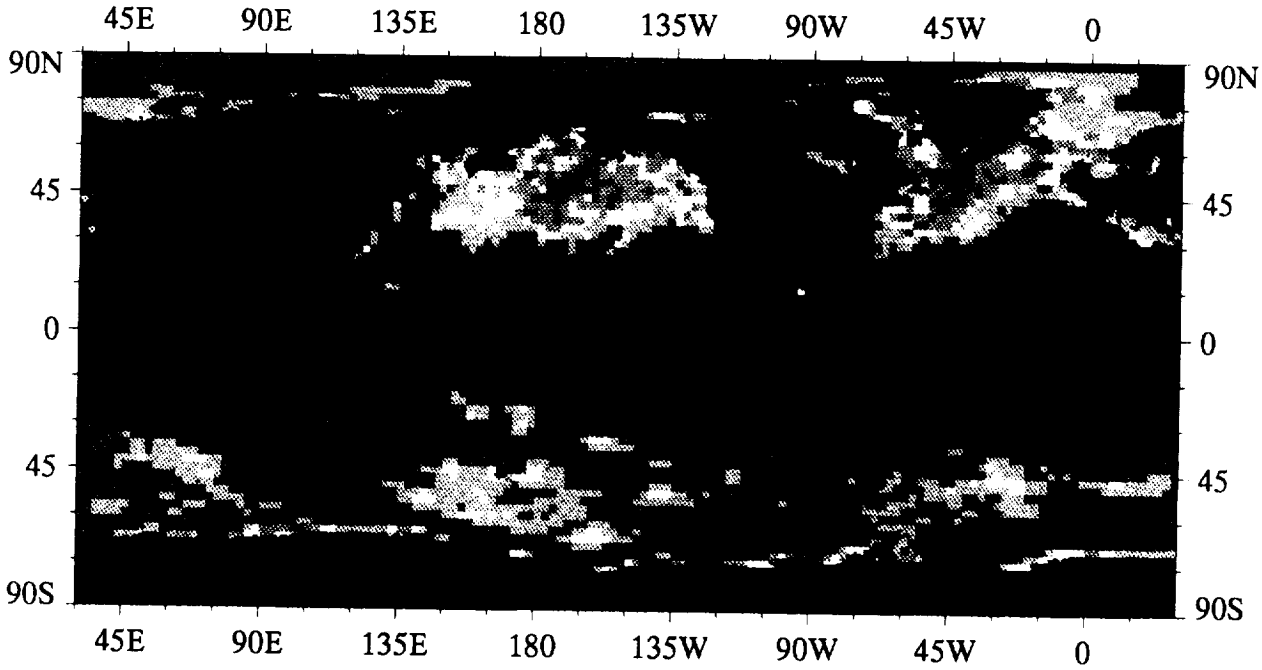

December 1988

Standard Deviation of ECMWF 10 m Wind Speed, m s^{-1}

TECHNICAL REPORT STANDARD TITLE PAGE

1. Report No. 91-8	2. Government Accession No.	3. Recipient's Catalog No.
4. Title and Subtitle An Atlas of Monthly Mean Distributions of GEOSAT Sea Surface Height, SSMI Surface Wind Speed, AVHRR/2 Sea Surface Temperature, and ECMWF Surface Wind Components During 1988		5. Report Date February 1991 6. Performing Organization Code
7. Author(s) D. Halpern, V. Zlotnicki, J. Newman, O. Brown, F. Wentz		8. Performing Organization Report No.
9. Performing Organization Name and Address JET PROPULSION LABORATORY California Institute of Technology 4800 Oak Grove Drive Pasadena, California 91109		10. Work Unit No. 11. Contract or Grant No. NAS7-918 13. Type of Report and Period Covered External Report JPL Publication
12. Sponsoring Agency Name and Address NATIONAL AERONAUTICS AND SPACE ADMINISTRATION Washington, D.C. 20546		14. Sponsoring Agency Code RE4 BP-578-22-26-01-00
15. Supplementary Notes		

16. Abstract

The following monthly mean global distributions for 1988 are presented with a common color scale and geographical map: sea surface height variation estimated from the U.S. Navy geodetic satellite GEOSAT; surface wind speed estimated from the special sensor microwave imager (SSMI) on a U.S. Air Force Defense Meteorological Satellite Program (DMSP) spacecraft; sea surface temperature estimated from the advanced very high resolution radiometer (AVHRR/2) on U.S. National Oceanic and Atmospheric Administration (NOAA) spacecrafts; and the Cartesian components of the 10-m height wind vector computed by the European Center for Medium-Range Weather Forecasting (ECMWF). Charts of monthly mean value, sampling distribution, and standard deviation value are displayed. Annual mean distributions are displayed.

17. Key Words (Selected by Author(s)) Dynamic Oceanography; Meteorology and Climatology; Physical Oceanography	18. Distribution Statement Unclassified; unlimited		
19. Security Classif. (of this report) Unclassified	20. Security Classif. (of this page) Unclassified	21. No. of Pages	22. Price

JPL 0184 R 9/83